



HAL
open science

Stratigraphy and bio-event studies of the Guadalupian - Lopingian boundary in the northern margin of Sanandaj-Sirjan Zone, Central Iran and North-West of Iran

Soheil Hemmati

► **To cite this version:**

Soheil Hemmati. Stratigraphy and bio-event studies of the Guadalupian - Lopingian boundary in the northern margin of Sanandaj-Sirjan Zone, Central Iran and North-West of Iran. Applied geology. Sorbonne Université; Université Ferdowsi de Mashhad (Iran), 2024. English. NNT : 2024SORUS011 . tel-04645846

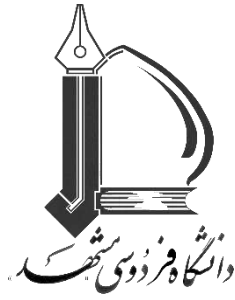
HAL Id: tel-04645846

<https://theses.hal.science/tel-04645846v1>

Submitted on 12 Jul 2024

HAL is a multi-disciplinary open access archive for the deposit and dissemination of scientific research documents, whether they are published or not. The documents may come from teaching and research institutions in France or abroad, or from public or private research centers.

L'archive ouverte pluridisciplinaire **HAL**, est destinée au dépôt et à la diffusion de documents scientifiques de niveau recherche, publiés ou non, émanant des établissements d'enseignement et de recherche français ou étrangers, des laboratoires publics ou privés.



Ferdowsi University of Mashhad & Sorbonne Université

COTUTELLE DOCTORAL THESIS

Stratigraphy and bio-event studies of the Guadalupian - Lopingian boundary in the northern margin of Sanandaj-Sirjan Zone, Central Iran and North-West of Iran.

Études de stratigraphie et d'événements biologiques de la limite Guadalupien - Lopingien sur la marge nord de la zone Sanandaj-Sirjan, centre de l'Iran et nord-ouest de l'Iran.

چینه نگاری و بررسی رخدادهای زیستی گذر گوادالوپین - لوپینگین در شمال پهنه سنندج - سیرجان، ایران مرکزی و شمال باختر ایران

Iranian Supervisor:

Dr. Abbas GHADERI

Author:

Soheil HEMMATI

French Supervisor:

Prof. Sylvie CRASQUIN

*A thesis submitted in fulfillment of the requirements
for the degree of Doctor of Philosophy
in the*

Ferdowsi University of Mashhad & Sorbonne Université

January 2024



Committee Doctoral Thesis Defence Members

Iranian Supervisor

PhD Student

French Supervisor

Dr. Abbas GHADERI

Associate Professor
of Ferdowsi University of Mashhad
Email: aghaderi@um.ac.ir

Soheil HEMMATI

Cotutelle PhD student at
Ferdowsi University of Mashhad
and Sorbonne Université
Email: soheillahemmati@gmail.com

Pr. Sylvie CRASQUIN

Professor form CR2P
Email: sylvie.crasquin@mnhn.fr

Iranian Reviewer

The Juries

French Reviewer

Dr. Mohammad KHANEBAD

Associate Professor
of Ferdowsi University of Mashhad
Email: mkhanebad@um.ac.ir

Pr. Catherine CRONIER

Professor form Université de Lille
Email: catherine.cronier@univ-lille.fr

Iranian Examiner

French Examiner

Dr. Seyed Masoud HOMAM

Associate Professor
of Ferdowsi University of Mashhad
Email: homam@um.ac.ir

Pr. Loïc VILLIER

Professor form CR2P
Email: loic.villier@sorbonne-universite.fr





Ecole Doctorale 398
Géosciences Ressources Naturelles et Environnement
Geosciences, Natural Ressources and Environment

Pr. Loïc Villier
Professeur des Universités
UMR CNRS 7207 Centre de recherche en Paléontologie - Paris (CR2P)
Sorbonne Université et Muséum National d'Histoire Naturelle
Tel. + 33 (0)1 44 27 50 34
Email. loic.villier@sorbonne-universite.fr

To whom it may concern,

As the President of the Doctoral Thesis Defense Committee for Mr. Soheil HEMMATI, a Cotutelle PhD student at Ferdowsi University of Mashhad and Sorbonne Université, I officially announce that he successfully defended his doctoral thesis in the presence of the entire jury committee at 14:00 on January 10th, 2024, in Ferdowsi University of Mashhad (Iran). The members of Mr. HEMMATI's defense committee are as follows:

For the Iran part:

Director of the thesis: Abbas GHADERI, Associate Professor, Department of Geology, Faculty of Science, Ferdowsi University of Mashhad, Mashhad, Iran.

Reporter: Mohammad KHANEHBAD, Associate Professor, Department of Geology, Faculty of Science, Ferdowsi University of Mashhad, Mashhad, Iran.

Examiner: Seyed Masoud HOMAM, Associate Professor, Department of Geology, Faculty of Science, Ferdowsi University of Mashhad, Mashhad, Iran.

For the French part:

Director of the thesis: Sylvie CRASQUIN, Directrice de recherche, CR2P, Campus Pierre et Marie Curie, T.46-56, E.5, 75005 Paris, France.

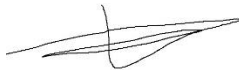
Reporter: Catherine CRONIER, Professeure, Université de Lille, Evo-Eco-Paléo (EEP), Sciences et Technologies, Batiment SN5, 59655 Villeneuve d'Ascq, France.

Examiner: Loïc VILLIER, Professeur, CR2P, Campus Pierre et Marie Curie, T.46-56, E.5, 75005 Paris, France.

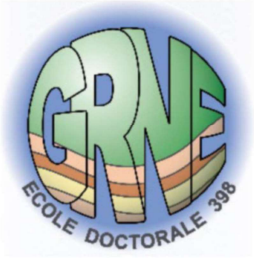
The report of the doctoral defense meeting for Mr. HEMMATI on January 10th, 2024, is presented below:

Mr. Soheil HEMMATI presented his doctoral thesis work for approximately 50 minutes, followed by 70 minutes of constructive scientific discussions and questions. The jury recognizes his excellent level of teaching abilities and skills in emphasizing scientific perspective. The presentation developed the general context and issues of the initial thesis project, justifying the field work and the processing of a large number of samples for micropaleontological and sedimentological research purposes. The context of the Covid-19 health crisis and the absence of conodonts in the samples processed for biostratigraphy led Soheil HEMMATI to revise the objectives, methods and objects of his study during the course of the thesis, which was considerably penalizing. Ultimately, the results acquired deal with the diversity of ostracods and the carbonate sedimentary environments in the Middle Permian on two Iranian sites corresponding, at the time, to distinct tectonic units. The answers to the questions were always very clear, relevant and honest. Soheil HEMMATI expresses himself with confidence and accepts the limits of his results which also offer very interesting perspectives for future work. In particular, he plans to rely on the results obtained on ostracods for one or two future publications as well as for a post-doctoral project which will be submitted in the short term. The jury unanimously agrees to praise the quality of the discussions and congratulates Mr. Soheil HEMMATI for his work and his oral presentation.

Loïc VILLIER



President of the Doctoral
Thesis Defense Committee
of Mr. Soheil HEMMATI



**Ecole Doctorale
Géosciences
Ressources Naturelles et
Environnement
GRNE 398**

Sorbonne Université
Campus Pierre et Marie Curie
Case 72, T46-45 – E2, 4, place Jussieu
75252 Paris Cedex 05

Objet : Soutenance de thèse

Je soussigné, Loïc LABROUSSE, Directeur de l'Ecole Doctorale 398 Géosciences Ressources Naturelles et Environnement de Sorbonne Université, atteste que M. Soheil HEMMATI, inscrit à l'ED GRNE, a soutenu sa thèse le 10/01/2024 à Mashhad, Iran, en présence du jury composé de :

Mme Sylvie CRASQUIN, Directrice de recherche, Sorbonne Université, Directrice de thèse

Mme Catherine CRONIER, Professeure des universités, Université de Lille, Rapporteur

M. Loïc VILLIER, Professeur des universités, Sorbonne Université, Examineur

M. Abbas GHADERI, Maître de conférences, Ferdowsi University of Mashhad, Directeur de thèse

M. Mohammad KHANEBAD, Maître de conférences, Ferdowsi University of Mashhad, Rapporteur

M. Seyed Masoud HOMAM, Maître de conférences, Ferdowsi University of Mashhad, Examineur

Fait à Paris le 11 janvier 2024 pour valoir ce que de droit.

Pr. Loïc LABROUSSE
Directeur de l'Ecole Doctorale GRNE (398)



Loïc LABROUSSE
Directeur Ecole Doctorale
GRNE 398



شماره:

تاریخ: ۱۴۰۲/۱۰/۲۰

صورت جلسه دفاع از رساله دکتری

جلسه دفاع از رساله دکتری آقای سهیل همتی به شماره دانشجویی ۹۵۱۶۳۳۱۰۲۶، رشته زمین شناسی گرایش چینه شناسی و فسیل شناسی در ساعت ۱۴:۰۰ روز چهارشنبه مورخ ۱۴۰۲/۱۰/۲۰ در محل دانشکده علوم (به صورت آنلاین) و با عنوان "چینه نگاری و بررسی رخدادهای زیستی گذر گوادالوپین - لویپنگین در شمال پهنه سنندج - سیرجان، ایران مرکزی و شمال باختری ایران"

با حضور امضاکنندگان ذیل برگزار گردید و بر اساس کیفیت رساله و دستاودهای آن، ارائه دفاعیه و نحوه پاسخ به سئوالات، رای نهایی هیات داوران به شرح ذیل اعلام گردید:

درجه رساله: عالی و با نمره بیست.

استاد(ان) راهنما و مشاور:

- ۱- استاد راهنمای اول ایرانی: دکترعباس قادری (دانشیار گروه زمین شناسی، دانشگاه فردوسی مشهد، ایران)
- ۲- استاد راهنمای دوم ایرانی: دکترعلیرضا عاشوری (استاد تمام بازنشسته گروه زمین شناسی، دانشگاه فردوسی مشهد، ایران)
- ۳- استاد مشاور ایرانی: دکترواچیک هایراپطیان (استادیار گروه زمین شناسی، دانشگاه آزاد اسلامی واحد خوراسگان، ایران)
- ۴- استاد راهنمای فرانسوی: پروفیسور Sylvie CRASQUIN (استاد تمام CNRS، آزمایشگاه CR2P، دانشگاه سوربن، فرانسه)

هیات داوران:

- ۱- داور ایرانی: دکترمحمد خانه باد (دانشیار گروه زمین شناسی، دانشگاه فردوسی مشهد، ایران)
- ۲- داور ایرانی و نماینده تحصیلات تکمیلی دانشگاه فردوسی: دکترسید مسعود همام (دانشیار گروه زمین شناسی، دانشگاه فردوسی مشهد، ایران)
- ۳- داور فرانسوی: پروفیسور Catherine CRONIER (استاد تمام، دانشگاه لیل فرانسه)
- ۴- داور و نماینده تحصیلات تکمیلی دانشگاه سوربن فرانسه: پروفیسور Loïc VILLIER (استاد تمام، آزمایشگاه CR2P، دانشگاه سوربن، فرانسه)

"لازم به ذکر است جزئیات و نحوه نگارش و روند دفاع رساله آقای سهیل همتی، در متن قرارداد نوشته شده بین دانشگاه فردوسی مشهد و دانشگاه سوربن که نسخه اصلی آن در دفتر همکاری های علمی بین المللی دانشگاه موجود بوده و به امضای رئیس محترم وقت دانشگاه، جناب آقای دکتر احد ضابط، و معاونت محترم آموزشی پیشین دانشگاه، جناب آقای دکتر بختیار شعبانی ورکی، نیز رسیده است."

معاون پژوهشی و فناوری دانشکده علوم:
دکتر امیرحسین امیری
۱۴۰۲/۱۰/۲۰
دکتر امیرحسین امیری
معاون پژوهشی دانشکده علوم

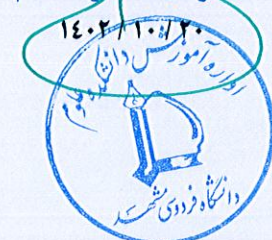
مدیر گروه زمین شناسی:

دکتر فرزین قائمی



نماینده تحصیلات تکمیلی:

دکتر سید مسعود همام



نام و نام خانوادگی دانشجوی: سهیل همتی شماره دانشجویی: ۹۵۱۶۳۳۱۰۲۶ گروه آموزشی: زمین شناسی رشته: زمین شناسی گرایش: چینه شناسی و فسیل شناسی
تاریخ دفاع: ۱۴۰۲ / ۱۰ / ۲۰ عنوان رساله: چینه نگاری و بررسی رخدادهای زیستی گذر گوادالوپین - لوپینگین در شمال پهنه سوندج - سیرجان، ایران مرکزی و شمال باختری ایران

معیارهای ارزشیابی		
پیشینه پژوهش	کیفیت علمی	
ابتکار و نوآوری		
ارزش علمی و یا کاربردی		
جمع بندی نتایج و ارائه پیشنهادات برای ادامه پژوهش		
استفاده از منابع و مآخذ به لحاظ کمی و کیفی (به روز بودن)		
رعایت زمانبندی اجرای پایان نامه		
دستاوردها و ویژگی های خاص		
انسجام در تنظیم و تدوین مطالب، حسن نگارش و رعایت دستورالعمل	کیفیت نگارش	
کیفیت تصویرها، شکل ها و منحنی های استفاده شده	کیفیت ارائه	
تسلط به موضوع و توانایی در پاسخگویی به سوالات در جلسه دفاع		
نحوه ارائه (رعایت زمان، تنظیم موضوع، کیفیت فایل ارائه و ...)	گزارش ها	
تحویل به موقع گزارش ها		
به حروف: بیست تمام	به عدد: ۲۰	نمره نهایی

رساله بر اساس رای اعضای جلسه دفاع:

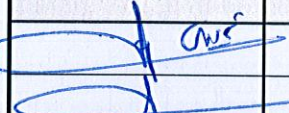
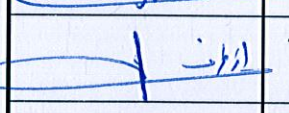
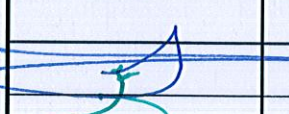
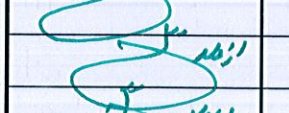
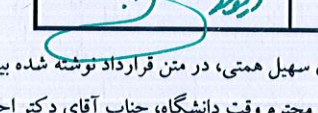
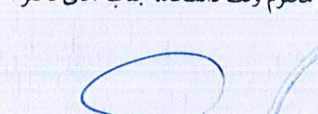
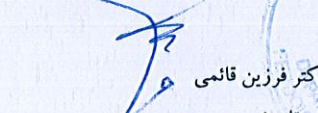
بدون اصلاحات پذیرفته است.

با اصلاحات پذیرفته شد (دانشجو موظف است تا تاریخ / / اصلاحات رساله خود را که به تایید ----- رسیده است به گروه آموزشی تحویل دهد).

مردود شناخته شد.

توضیحات:

عنوان نهایی رساله (در صورت تغییر):

امضا	دانشگاه / دانشکده	مرتبۀ علمی	نام و نام خانوادگی	سمت
	فردوسی / علوم	دانشیار	دکتر عباس قادری	استاد راهنمای اول
	فردوسی / علوم	استاد تمام	دکتر علیرضا عاشوری	استاد راهنمای دوم
	دانشگاه آزاد اسلامی واحد اصفهان (خوراسگان)	استاد یار	دکتر واجیک هایرابطیان	استاد مشاور اول
				استاد مشاور دوم
	فردوسی / علوم	دانشیار	دکتر محمد خانه باد	داور
	فردوسی / علوم	دانشیار	دکتر سید مسعود همام	داور
	دانشگاه لیل فرانسه	استاد تمام	پروفسور کاترین کونیر	داور
	دانشگاه سوربن فرانسه	استاد تمام	پروفسور لوتیک ولیر	داور

نامبرده دانشجوی دکتری مشترک بین دانشگاه فردوسی مشهد و دانشگاه سوربن بوده و جزئیات و نحوه نگارش و روند دفاع رساله آقای سهیل همتی، در متن قرارداد نوشته شده بین دانشگاه فردوسی مشهد و دانشگاه سوربن که نسخه اصلی آن در دفتر همکاری های علمی بین المللی دانشگاه موجود و به امضای رئیس محترم وقت دانشگاه، جناب آقای دکتر احد ضابط، و معاونت محترم آموزشی پیشین دانشگاه، جناب آقای دکتر بختیار شعبانی ورکی، نیز رسیده است، می باشد.

مدیر گروه: دکتر فرزین قائمی
امضا و تاریخ: ۱۴۰۲/۱۰/۲۰

نماینده تحصیلات تکمیلی: دکتر سید مسعود همام
امضا و تاریخ

À REMPLIR PAR LE DOCTORANT:

AUTORISATION ET CHOIX DE DIFFUSION

NOM (S): HEMMATI

Prénom(s): Soheil

Préciser obligatoirement (un seul choix possible):

J'autorise l'établissement à diffuser ma thèse complète directement sur internet.

Attention : ma thèse doit être respectueuse des droits d'auteur.

J'autorise l'établissement à diffuser ma thèse complète sur internet après une période d'embargo.

Durant la période d'embargo, ma thèse est consultable sur l'intranet de Sorbonne Université, conformément à la loi.

6 mois

1 an

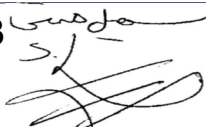
2 ans

Je n'autorise pas l'établissement à diffuser ma thèse complète sur internet, je joins une version incomplète.

Attention : je dois quand même joindre une version complète de la thèse pour son archivage au CINES. Si je coche cette case, la version complète sera consultable sur l'intranet de Sorbonne Université, conformément à la loi. La version incomplète sera diffusée sur internet.

Je n'autorise pas la diffusion du texte intégral de ma thèse sur internet. Ma thèse sera uniquement accessible sur l'intranet de Sorbonne Université, conformément à la loi.

DATE ET SIGNATURE DE L'AUTEUR

20/11/2023 



اصالت نامه رساله دانشگاه فردوسی مشهد

نظر به اتمام تدوین رساله دکتری با عنوان چینه نگاری و بررسی رخدادهای زیستی گذر گوادالوپین - لویینگین در شمال پهنه سنج - سیروجان، ایران مرکزی و شمال باختر ایران و کد ۳/۴۷۱۰۹ موارد ذیل را متعهد می شویم:

- این رساله/ پایان نامه و دستاوردهای آن حاصل پژوهش انجام شده اینجانبان بوده و از صحت و اصالت برخوردار است.
- در استفاده از نتایج سایر پژوهش ها به مرجع مورد استفاده استناد شده است.
- کلیه حقوق مترتب از این اثر شامل مستندات، مقاله، اختراع، دانش فنی، کتاب، نرم افزار، تجهیزات ساخته شده و ... متعلق به دانشگاه فردوسی مشهد می باشد؛ دانشگاه می تواند نسبت به ثبت و نشر آن در هر قالبی، بدون نیاز به کسب اجازه از استادان راهنما و دانشجو و یا پرداخت حق الزحمه، اقدام نماید.
- هر نوع بهره برداری و انتشار دستاوردهای این اثر، واگذاری اطلاعات به دیگران یا چاپ و تکثیر، نسخه برداری، ترجمه و اقتباس از این اثر بدون مجوز معاونت پژوهش و فناوری دانشگاه ممنوع است.
- حقوق مادی و معنوی تمام افرادی که در به دست آمدن نتایج اثر تأثیر گذار بوده اند در بهره برداری و انتشار دستاوردهای آن رعایت می شود.
- در کلیه مراحل انجام این رساله/ پایان نامه، مفاد "منشور و موازین اخلاق پژوهش" رعایت شده و هیچ یک از مصادیق تخلفات پژوهشی مندرج در دستورالعمل "نحوه بررسی تخلفات پژوهشی" و قانون "پیشگیری و مقابله با تقلب در زمینه آثار علمی" رخ نداده است.

اینجانب با آگاهی از اینکه گزارش نهایی رساله/ پایان نامه در مرکز اطلاع رسانی و کتابخانه مرکزی دانشگاه به عنوان سند رسمی بایگانی می گردد و مطابق ضوابط در دسترس مراجعان قرار می گیرد، متعهد می شوم که این گزارش نسخه نهایی بوده و پس از ارسال امکان هیچ گونه تغییری وجود نخواهد داشت.

دانشجو: سهیل همتی

شماره دانشجویی: ۹۵۱۶۳۳۱۰۲۶

گروه: زمین شناسی

۸ بهمن، ۱۴۰۲



رساله/ پایان نامه انجام شده توسط دانشجو مطابق آیین نامه ها و قوانین مصوب فوق الذکر با استفاده از ابزارهای موجود نظیر همانندجویی و سایر جستجوهای عمومی اینترنتی بررسی شد و مورد تایید اینجانبان می باشد.

استاد راهنمای دوم: علیرضا عاشوری

مرتب علمی: استاد گروه زمین شناسی

دانشکده/ دانشگاه: علوم، فردوسی مشهد

۱۲ بهمن، ۱۴۰۲



استاد راهنمای اول: عباس قادری

مرتب علمی: دانشیار گروه زمین شناسی

دانشکده/ دانشگاه: علوم، فردوسی مشهد

۱۲ بهمن، ۱۴۰۲



ACKNOWLEDGMENTS

This thesis was written for my Cotutelle PhD degree in Stratigraphy and Paleontology Sciences with specialization in Micropaleontology at the Ferdowsi University of Mashhad, Iran and Géologie Sciences with specialization in Paléontologie at Sorbonne Université, France and is founded by Ministry of Science Research and Technology of Iran and the French Embassy in Tehran (Bourse du campus Français). The focus of this thesis is on the Bio-event of the Guadalupian and Lopingian Boundaries (GLB) in Iran and attempt to concealment gap information from this period.

After in appreciation of the support I've received from my family, I would like to thank a few people here. I express deep gratitude to my Iranian supervisors, Dr. Abbas GHADERI and Prof. Alireza ASHOURI, for their outstanding intelligence and cutting-edge perspectives at Ferdowsi University of Mashhad. I also appreciate their invaluable assistance in the field.

I convey my sincere appreciation to Prof. Sylvie CRASQUIN, who has been present as my French supervisor throughout the entirety of this thesis. Her perceptive ideas have sparked various dimensions of this project. I am grateful for her valuable guidance, participation in constructive discussions, provision of insightful comments, and offering suggestions that have significantly enriched the trajectory of this work.

I would really appreciate it of Mr. Jean-Christophe BONTÉ from French Embassy in Tehran and Ministry of Science Research and Technology of Iran for organed the Cotutelle PhD scholarship and it was a great privilege to be offered an extraordinary opportunity to follow my dream.

I would like to extend my special thanks to Prof. Loïc LABROUSSE, the director of ED 398, for his exceptional support in managing the academic and administrative aspects of affairs in France. His guidance has been invaluable in navigating the intricacies of academic administration and ensuring a smooth course of proceedings.

I would like to express my sincere advance appreciation to the members of the jury for my PhD Committee Defense. I anticipate with gratitude their high-value recommendations on my doctoral thesis, and I am confident that their valuable comments will contribute significantly to enhancing the overall quality of the thesis.

I would like to express my special gratitude to the staff at both of my universities, particularly acknowledging Mrs. HASSANZADEH from Ferdowsi University of Mashhad, Mrs. ZIZZO from Sorbonne Université, and the exceptional staff at CR2P and MHNN. I would also like to thank all my friends, PhD colleagues and the others for their encouragement and moral support during the entire duration of my work.

I would like to express extend my appreciation to Dr. Frank SENEGAS from CR2P and Matthias RUDEANU for their assistance throughout the entire process of preparing ostracods in the CR2P laboratory in Paris.

I express genuine gratitude for the heartfelt support provided by my friends at Maison des étudiants de l'Asie du Sud-Est. Their kindness played a pivotal role in enabling me to pursue my goal line in France with unwavering energy.

I was fortunate to have these individuals by my side consistently, offering their assistance whenever I required it for my research. Working with them was an incredible experience, as they not only refined my research skills but also imparted insights into real-world dimensions that were previously unfamiliar to me. Their presence and guidance significantly enriched my overall learning journey.

I would like to conclude by repeating a quote attributed to Jalaluddin Mohammad BALKHI (RUMI) "Yesterday I was clever, so I wanted to change the world. Today I am wise, so I am changing myself" and it is my hope that my thesis will give a new perspective on the Iran Permian.

Soheil HEMMATI
January, 2024

TABLE OF CONTENTS

THE LISTS: List of figures, table and plates	IV
ABSTRACT ENGLISH VERSION	VI
ABSTRACT FRENCH VERSION	X
ABSTRACT PERSIAN VERSION	XIV
CHAPTER 1: Introduction and objectives	
1.1. INTRODUCTION	2
1.2. MIDDLE PERMIAN EXTINCTION	3
1.3. OBJECTIVES	8
1.4. CONTENTS OF THE THESIS	9
1.5. REFERENCES	10
CHAPTER 2: Iranian Permian geological setting: overview and selected sections	
2.1. INTRODUCTION	16
2.2. PERMIAN OF IRAN	19
2.3. GLB THEORY IN IRAN	24
2.3.1. STRATIGRAPHIC APPROACH AND CANDIDATE SECTIONS FOR	26
2.3.1.1. ALI-BASHI SECTION	27
2.3.1.1.1. HISTORICAL BACKGROUND	30
2.3.1.1.2. LITHOSTRATIGRAPHY PERSPECTIVE	31
2.3.2.1. BAGH-E-VANG SECTION	39
2.3.2.1.2. HISTORICAL BACKGROUND	41
2.3.2.1.2. LITHOSTRATIGRAPHY PERSPECTIVE	42
2.3.3.1. BAGHUK SECTION	49
2.3.3.1.2. HISTORICAL BACKGROUND	49

2.4 REFERENCES	52
----------------------	----

CHAPTER 3: Material and methods

3.1. INTRODUCTION	62
3.2. EXTRACTION PROCESSING METHODS	62
3.2.1. CONODONT EXTRACTION PROCESSING METHODS	71
3.2.1.1. CH ₂ O ₂ PROTOCOL	72
3.2.1.2. CH ₃ COOH PROTOCOL	72
3.2.1.3. OUTCOMES FROM THE PROTOCOLS	73
3.2.2. OSTRACOD EXTRACTION PROCESSING METHODS	76
3.2.2.1. HOT ACETOLYSIS	77
3.2.2.2. OUTCOMES FROM THE PROTOCOLS	81
3.2.3. RADIOLARIA EXTRACTION PROCESSING METHODS	83
3.2.3.1. OUTCOMES FROM THE PROTOCOLS	84
3.2.4. THIN SECTION PROCESSING METHODS	85
3.3. CONCLUSION	86
3.4. REFERENCES	87

CHAPTER 4: Ostracods: concepts and systematic paleontology

4.1. GENERALITY	90
4.2. HISTORICAL BACKGROUNDS	90
4.3. ELEMENTS OF DESCRIPTION	93
4.4. SYSTEMATICS	95
4.5. CONCLUSION	128
4.6. REFERENCES	141

CHAPTER 5: Facies and palaeoenvironmental analysis

5.1. INTRODUCTION	148
5.2. CARBONATE MICROFACIES OF KHCHIK FORMATION	153
5.2.1. INNER RAMP MICROFACIES ASSEMBLAGES	153
5.2.1.1. LAGOON MICROFACIES	155
5.2.1.1.1. MKL1: NON-FOSSILIFEROUS MUDSTONE	155

5.2.1.1.1.1. INTERPRETATION OF MKL1.....	155
5.2.1.1.2. MKL2	156
5.2.1.1.2.1. MKL2: BIOCLASTIC PACKSTONE.....	156
5.2.1.1.2.2. MKL2-FORAM: FORAMINIFERAL/	156
5.2.1.1.2.3. MKL2-GYMNO: ALGAL BIOCLASTIC	157
5.2.1.1.2.4. INTERPRETATION OF MKL2.....	159
5.2.1.2. RESTRICTED MICROFACIES	160
5.2.1.2.1. MKR1.....	160
5.2.1.2.1.1. MKR1: BIOCLASTIC WACKSTONE.....	160
5.2.1.2.1.2. MKR1-GYMNO: ALGAL BIOCLASTIC	160
5.2.1.2.1.3. MKR1-DOLOM: DOLOMITIZED BIOCLASTIC.....	161
5.2.1.2.1.4. MKR1-FUSUL: FUSULINID BIOCLASTIC.....	161
5.2.1.2.1.5. MKR1-MILIO: MILIOLID BIOCLASTIC	161
5.2.1.2.1.6. INTERPRETATION OF MKR1	162
5.2.1.2.2. MKR2: ALGAL BIOCLASTIC WACKSTONE	162
5.2.1.1.2.1. INTERPRETATION OF MKR2	163
5.2.1.2.3. MKR3.....	163
5.2.1.2.3.1. MKR3: MILIOLID PACKSTONE	163
5.2.1.2.3.2. MKR3-BIOCL: BIOCLASTIC MILIOLID	165
5.2.1.2.3.3. MKR3-FUSUL: FUSULINID MILIOLID.....	165
5.2.1.2.3.4. INTERPRETATION OF MKR3	167
5.2.1.3. OPEN-MARINE MICROFACIES	167
5.2.1.3.1. MKO1	167
5.2.1.3.1.1. MKO1: PELOIDAL PACKSTONE	168
5.2.1.3.1.2. MKO1-BIOCL: BIOCLASTIC PELOID	168
5.2.1.3.1.3. MKO1-PEL/BIO: PELOIDAL/.....	168
5.2.1.3.1.4. INTERPRETATION OF MKO1.....	169
5.2.1.3.2. MKO2: ALGAL BIOCLASTIC PELOID PACKSTONE.....	169
5.2.1.3.2.1. INTERPRETATION OF MKO2.....	170
5.2.1.3.3. MKO3	170
5.2.1.3.3.1. MKO3: BIOCLASTIC WACKSTONE	170
5.2.1.3.3.2. MKO3-CRINO: CRINOID BIOCLASTIC.....	170

5.2.1.3.3.3. INTERPRETATION OF MKO3.....	171
5.2.1.3.4. MKO4	171
5.2.1.3.4.1. MKO4: BIOCLASTIC PACKSTONE	171
5.2.1.3.4.2. MKO4-CRINO: CRINOID BIOCLASTIC.....	173
5.2.1.3.4.3. INTERPRETATION OF MKO4.....	173
5.2.2. MIDDLE RAMP MICROFACIES ASSEMBLAGES	173
5.2.2.1. MKM1	174
5.2.2.1.1. MKM1: PELOIDAL WACKSTONE.....	174
5.2.2.1.2. MKM1-BIOCL: BIOCLASTIC PELOID	174
5.2.2.1.3. MKM1-PEL/BIO: PELOIDAL/.....	175
5.2.2.1.4. INTERPRETATION OF MKM1.....	175
5.2.2.2. MKM2	175
5.2.2.2.1. MKM2: BIOCLASTIC FLOTSTONE	176
5.2.2.2.2. MKM2-BRACH: BRACHIOPOD FLOTSTONE.....	176
5.2.2.2.3. INTERPRETATION OF MKM2.....	176
5.2.2.3. MKM3: BIOCLASTIC WACKSTONE/FLOTSTONE.....	178
5.2.2.3.1. INTERPRETATION OF MKM3.....	178
5.2.3. OUTER RAMP MICROFACIES ASSEMBLAGES.....	178
5.2.3.1. MKT1.....	179
5.2.3.1.1. MKT1: MUDSTONE WITH RARE FOSSILS.....	179
5.2.3.1.2. MKT1-BIOTU: MUDSTONE WITH BIOTU.....	179
5.2.3.1.3. INTERPRETATION OF MKT1	179
5.2.3.2. MKT2.....	180
5.2.3.2.1. MKT2: FOSSILIFEROUS MUDSTONE.....	180
5.2.3.2.2. MKT2-BIOCL: FOSSILIFEROUS MUDSTONE	180
5.2.3.2.3. MKT2-FLOTS: FOSSILIFEROUS MUDSTONE.....	181
5.2.3.2.4. INTERPRETATION OF MKT2	181
5.2.3.3. MKT3: MUDSTONE/BIOCLASTIC WACKSTONE	181
5.2.3.3.1. INTERPRETATION OF MKT3	182
5.3. DEPOSITIONAL MODEL OF KHCHIK FORMATION	186
5.4. CONCLUSION.....	188
5.5. REFERENCES.....	189

CHAPTER 6: Discussion, results and topic suggestions for research

6.1. DISCUSSION.....	192
6.2. RESULTS.....	196
6.2. TOPIC SUGGESTIONS FOR RESEARCH	199
APPENDIX	201

List of figures

CHAPTER 1

Fig. 1.1. List five significant mass extinctions that occurred in the Earth's history 3

Fig. 1.2. Artist's conception of what might have happened in the Paleo-Tethys..... 7

CHAPTER 2

Fig. 2.1. The majority of the plates and terranes discussed in this review are shown..... 17

Fig. 2.2. Major geological subdivisions of Iran modified by [Nezafati \(2006\)](#)..... 18

Fig. 2.3. Plate-tectonic reconstruction of the late Permian (Lopingian). 20

Fig. 2.4. The Middle East region consists of the ... Arabian and Levant plates..... 22

Fig. 2.5. Paleogeographic reconstruction of Pangea undergoing transformation 23

Fig. 2.6. Permian strata in different regions of Iran following [Leven & Gorgij \(2011\)](#) 24

Fig. 2.7. Historical ... of the Guadalupian – Lopingian ... in the northwest of Iran 25

Fig. 2.8. Iran's tectonic ... (adapted from [Angiolini et al. 2007](#) and [Vuolo 2014](#)). 27

Fig. 2.9. A. location ... of the study ... in the northwest of Iran (... [Ghaderi et al. 2016](#)) .. 29

Fig. 2.10. Illustrated comparison of the rock units found in the Khachik Formation 33

Fig. 2.11. Illustrated representation of the lithostratigraphic column 36

Fig. 2.12. In view A-C, a field landscape ... captures the Khachik Formation 37

Fig. 2.13. The lithostratigraphic correlation and ... of lithological characteristics 38

Fig. 2.14. A. location map of the study area in Central Iran (... [Leda et al. 2014](#)). 40

Fig. 2.15. A. The northwestern ... of Kuh-e-Bagh-e-Vang (adapted from [Balini et al.](#)..... 45

Fig. 2.16. An illustrated depiction of the lithostratigraphic column of the 47

Fig. 2.17. In perspectives A-E, a field landscape image captures the sequences..... 48

Fig. 2.18. A. location ... of the study ... in Sanandaj-Sirjan Zone (... [Heuer et al. 2021](#)).... 51

CHAPTER 3

Fig. 3.1. Stratigraphic Recording ... of the Khachik Formation at the Ali-Bashi Section ... 64

Fig. 3.2. Ali-Bashi section in the Julfa region: A) ... limestone of Khachik Formation..... 65

Fig. 3.3. Ali-Bashi section in the Julfa region 66

Fig. 3.4. Stratigraphic Recording ... Jamal Formation at Bagh-e-Vang Section 67

THE LISTS: List of figures, tables and plates V

Fig. 3.5. Field pictures showing of Bagh-e-Vang strata in Tabas region 68

Fig. 3.6. Field pictures showing of Bagh-e-Vang strata in Tabas region: 69

Fig. 3.7. Laboratory images showcasing the preparation of samples from 74

Fig. 3.8. A-B. Depicts a series of laboratory images highlighting the preparation 75

Fig. 3.9. Complete series of laboratory procedures conducted in CR2P 79

Fig. 3.10. Laboratory procedures carried out ... the Ali-Bashi section in France..... 80

Fig. 3.11. Laboratory procedures conducted on both sections in France 81

CHAPTER 4

Fig. 4.1. Stratigraphical timelines of the major ecological radiations of the Ostracoda .. 91

Fig. 4.2. Representative species of some Pennsylvanian ... to Permian ostracods 92

Fig. 4.3. Illustrative instances of selected ostracods from this research include 93

Fig. 4.4. Future and Carapace of the ostracods as seen on lateral, dorsal and ventral ... 94

Fig. 4.5. Stratigraphic log and vertical distribution ... obtained from CH2H2..... 139

Fig. 4.6. Stratigraphic log and vertical distribution ... obtained from hot acetolysis..... 140

CHAPTER 5

Fig. 5.1. Illustration of three significant classifications for the ... of carbonate 148

Fig. 5.2. General distribution of microfacies types on carbonate ramp ([Flügel 2010](#))... 149

Fig. 5.3. SMF types Distribution across Facies Zones (FZ) in the Rimmed 150

Fig. 5.4. Representation of [Wilson's \(1975\)](#) FZs (Facies Belts)..... 151

Fig. 5.5. Illustration of identified skeletal allochems 152

Fig. 5.6. Composite log detailing the carbonate microfacies ... in the Khachik 184

Fig. 5.7. Correlating the general microfacies characteristics of each rock unit..... 185

Fig. 5.8. The depositional pattern of the Khacik Formation in the Ali-Bashi section 187

List of tables

CHAPTER 4

Table 4.1. Taxonomic list of all ostracod species identified from the Ali-bashi sec. 96

CHAPTER 5

Table 5.1. The recognized microfacies ... the Khachik ... the Ali-Bashi section 154

List of plates

CHAPTER 4

PLATE 4.1. SEM micrographs ... Khachik Formation ... extracted by hot acetolysis..... 130
PLATE 4.2. SEM micrographs ... Khachik Formation ... extracted by hot acetolysis..... 132
PLATE 4.3. SEM micrographs ... Khachik Formation ... extracted by hot acetolysis..... 134
PLATE 4.4. SEM micrographs ... Khachik Formation ... extracted by hot acetolysis..... 136
PLATE 4.5. SEM micrographs ... Khachik Formation ... extracted CH₂H₂ and CH₃COOH 137

CHAPTER 5

PLATE 5.1. Illustrations of the identified microfacies: A. Photo of MKL1 revealing 159
PLATE 5.2. Illustrations of microfacies: A. Photo-scan related to MKR1 with 164
PLATE 5.3. Illustrations of the microfacies A. photo-scan MKR2 with 167
PLATE 5.4. Illustrations of the identified microfacies: A. MKO1 with 172
PLATE 5.5. Illustrations of the identified microfacies (all ...): A. MKM1..... 178
PLATE 5.6. Illustrations of the identified microfacies (all ...): A. MKT1 182

ABSTRACT

The Permian era in Iran has continuously interest of the geologists, drawing them into various stratigraphic projects and these attentions have mostly revolved around the Permian-Triassic boundary (PTB) interval. While these efforts have yielded valuable insights, a significant gap in our knowledge remains unexplored: the Guadalupian-Lopingian Boundary (GLB) and its status in the Iranian geological context. The precise location of the Guadalupian-Lopingian Boundary (GLB) has long been a subject of contention among researchers. In rare reports and publications, diverse interpretations have arisen, influenced by lithological criteria rather than biostratigraphic divisions. Both northwestern Iran and central Iran have affected with this issue, each proposing distinct formations. Even in the Tabas region of Central Iran, the GLB has been identified based on infrequent findings of fusulinids, without the presence of zonal marker conodonts. This PhD thesis define to seeking and precisely determine the GLB's location in Iran, considering the different section provided by various regions in Iran.

Between the many sections investigated, three specific regions Julfa (Ali-Bashi section), Tabas (Bagh-e-Vang section), and Abadeh (Baghuk section) have been chosen for focused study in this project. The Ali-Bashi section where sampling and an extensive collection of over 240 rock samples from a measured thickness of 189 meters in the Kachik Formation Khachik Formation (Khachik Beds *sensu* [Stepanov et al. 1969](#)). In the Bagh-e-Vang section a meticulous effort resulted in the collection of more than 160 rock samples from an outcrop measuring 260 meters in thickness in the Jamal Formation. Sampling the Baghuk section, encountered specific obstacles that impeded our progress including: covid-19 pandemic and climatic conditions.

High-detailed lithostratigraphical investigation of the Khachik Formation in the Ali-Bashi section, led to identified 15 distinct rock units within the 4 main members. This discovery has the potential to stimulate the creation of a new lithostratigraphic inventory for these sequences, which can be aligned with the existing background research on the Khachik Formation in this particular section. Furthermore, in the Bagh-e-Vang section, 10 rock units from Jamal Formation strata's belonging to the 3 members have also been identified. Various extraction methods, including cold diluted cold CH_2O_2 , cold and hot (hot acetolysis) CH_3COOH ,

and HF protocols, were tested for the isolation of microfossils such as conodonts, ostracods, and radiolarians from samples collected at the Ali-Bashi and Bagh-e-Vang sections.

After extensive preparation efforts and high-observance to a carefully follow up the protocol for extraction conodont element. A thorough analysis was carried out on over 240 samples obtained from the Khachik Formation at the Ali-Bashi section, was failed and despite applying both the cold diluted CH_2O_2 and CH_3COOH techniques, the anticipated results were unexpected and conodont species were not extracted. In the Bagh-e-Vang section also, the approach of employing the diluted CH_3COOH technique was espoused to investigate conodonts. Protocol test outcomes revealed a compelling confirmation of the absence of conodonts in the second section.

Different extraction methods were applied and tested for ostracod extraction from Ali-Bashi section samples. Hot and cold CH_3COOH ; cold CH_2O_2 acid that led to me to 67 specimens were extracted from over 240 samples of Khachik Formation. Applying the CH_2O_2 method yielded outcomes that enabled me to identify the respective species. These species are: *Bairdia deducta deducta* (Zalanyi, 1974); *Bairdia hungarica* Zalanyi, 1974; *Bairdia* sp.; *Fabalitypris parva* Wang, 1978, *Fabalitypris* sp. 1; *Fabalitypris* sp. 2; *Fabalitypris* sp. 3; *Fabalitypris* sp. 4; *Hollinella* (*Hollinella*) *herrickana* (Girty 1909), *Hollinella* sp., *Sargentina transita* (Kozur 1985) and *Silenites* sp. *Bairdia* sp., *Fabalitypris* sp. 1; *Fabalitypris* sp. 2; *Fabalitypris* sp. 3; *Fabalitypris* sp. 4; *Hollinella* (*Hollinella*) *herrickana* (Girty 1909), *Sargentina transita* (Kozur 1985) and *Silenites* sp. *Bairdia* sp., were obtained exclusively through the diluted CH_2O_2 protocol from the hard dolomitized limestones, while the other cold CH_3COOH procedures were unsuccessful.

The applied of the hot acetolysis preparation method allows to me to identified the these species as follows: *Acratia changxingensis* (Shi, 1987); *Acratia* sp.; *Bairdia deducta deducta* (Zalanyi, 1974); *Bairdia elcapitanensis* Forel 2021; *Bairdia* cf. *fangnianqiao* Crasquin, 2010; *Bairdia grotei* Chitnarin, 2017 *Bairdia hungarica* Zalanyi, 1974; *Bairdia khaokanaensis* Chitnarin, 2017; *Bairdia radlerae* Kellett, 1934; *Bairdia rhomboidalis* Hamilton, 1942; *Bairdia* cf. *songthami* Chitnarin et al. 2017; *Bairdia* sp.30 sensu Chitnarin, 2009; *Bairdia* sp. 1; *Bairdia* sp. 2; *Bairdia* sp. 3; *Bairdia* sp. 4; *Bairdia* sp. 5; *Bairdia* sp. 6; *Bairdia* sp. 7; *Bairdia* sp. 8; *Bairdia* sp. 9; *Bairdia* ? sp.; *Bairdiacypris longirobusta* Chen, 1958; *Bairdiacypris* sp. 6 sensu Zazzali et al., 2015; *Bairdiacypris* sp. B sensu Tarnac et al., 2021; *Bairdiacypris* sp. 1; *Bairdiacypris* sp. 2;

Bairdiacypris sp. 3; *Bairdiacypris* sp. 4; *Bairdiacypris* sp. 5; *Bairdiacypris* sp. 6; *Bairdiacypris* sp. 7; *Bairdiacypris* sp. 8; *Bairdiacypris* sp. 9; *Bairdiacypris* sp.; *Ceratobairdia sexagintaduella* Forel, 2021; *Ceratobairdia?* cf. *crenata* Chen, 1982; *Fabalitypris acetalata* (Coryell & Billings, 1932); *Fabalitypris glennensis* (Harlton, 1927); *Fabalitypris parva* Wang, 1978; *Fabalitypris reniformis* (Chen, 1958) sensu Wang, 1978; *Fabalitypris* sp. 5; *Fabalitypris* sp. 6; *Fabalitypris* sp. 7; *Hollinella* (*Hollinella*) *martensiformis* Crasquin et al., 2010 ; *Hollinella* sp. ; *Indivisia* sp. 1 sensu Forel et al. 2015; *Kempfina qinglaili* (Crasquin, 2008); *Kempfina* sp. 1 ; *Liuzhinia julfensis* Gliwa, 2021; *Praezabythocypris pulchra* Kozur, 1985; *Praezabythocypris* sp. 1; *Pseudacanthoscapha striatula* (Shi, 1982); *Reviya* sp.; *Sargentina minuta* Wang, 1978; *Sargentina* sp.; and *Sulcella sulcata* Coryell & Sample, 1932. Meanwhile, some of the identified species of the *Bairdia*, *Bairdiacypris* and *Fabalitypris* genus genera present promising opportunities for defining new species through further studies. Furthermore, the successful identification of a large volume of ostracod's species from Middle and Upper Permian sequences highlights the significant potential for exploring this fossil-group in Iran. In spite of strict compliance of the recommended protocol, to employ the HF technique in the processing of 12 cherty samples obtained from the Ali-Bashi and 8 cherty samples obtained from Bagh-e-Vang sections yielded a disheartening outcome and none of the radiolarian specimens were discernible in the sediment of either sample set.

Microfacies analysis in the Ali-Bashi section led to identified 28 sub-microfacies which, derived with 15 distinct microfacies. The assemblage of microfacies groups, ranging from MKL1 to MKL2 (lagoonal environment), MKR2 to MKR3 exhibit features characteristic of a restricted inner ramp setting. The MKO1 to MKO4, suggests a confined setting, occurring in the final part of the inner ramp under an open marine environment. Microfacies groups MKM1 to MKM3 are inferred to have been deposited after the open marine environment, within the mid-ramp zones, whereas MKT1 to MKT3 were identified in the initial parts of the outer ramp, corresponding to the Toe-of-slope position in the carbonate shelf setting. Additionally, adhering to the standard microfacies designated by [Flügel \(2010\)](#), the study proposes 10 microfacies of the RMF type, along with their corresponding 4 SMFs for the studied strata. Besides, based on the standard facies zones (FZ) introduced by [Wilson \(1975\)](#), three FZs exhibiting a shallowing-upward trend, namely FZ8, FZ7, and FZ3, have been successfully delineated.

KEYWORDS: Extraction process, Ostracods, CH_2O_2 , CH_3COOH , hot acetolysis, HF, Guadalupian-Lopingian, Khachik Formation, Jamal Formation, Ali-Bashi section, Bagh-e-Vang section, Baghuk section.

RÉSUMÉ

Le Permien d'Iran suscite continuellement l'intérêt des géologues, les entraînant dans divers projets stratigraphiques. Ces efforts se concentrent principalement sur l'intervalle Permien-Trias (PTB). Toutefois, une lacune significative demeure inexplorée : la limite Guadalupien - Lopingien (GLB) et son statut dans le contexte géologique iranien. La localisation précise de la GLB est depuis longtemps un sujet de controverse. Des interprétations diverses ont émergé, basées sur des critères lithologiques plutôt que sur la biostratigraphie, tant dans le nord-ouest que dans le centre de l'Iran. Dans la région de Tabas, dans le centre de l'Iran, la GLB a été identifiée sur la base de rares fusulinidés ; les conodontes marqueurs de zone sont absents. Cette thèse de doctorat vise à rechercher et à déterminer précisément la localisation de la GLB en Iran, en tenant compte des différentes coupes levées dans diverses régions du pays.

Parmi les nombreuses coupes étudiées, trois régions spécifiques, Julfa (coupe d'Ali-Bashi), Tabas (coupe de Bagh-e-Vang) et Abadeh (coupe de Baghuk), ont été choisies pour une étude approfondie. La coupe d'Ali-Bashi a été échantillonnée, avec plus de 240 échantillons de roche sur une épaisseur mesurée de 189 mètres dans la Formation Khachik. Dans la coupe de Bagh-e-Vang, plus de 160 échantillons ont été prélevés sur une épaisseur de 260 mètres dans la Formation Jamal. L'échantillonnage de la coupe de Baghuk a rencontré des obstacles spécifiques, notamment la pandémie de covid-19 et les conditions climatiques.

Une investigation lithostratigraphique détaillée de la Formation Khachik dans la section d'Ali-Bashi a permis d'identifier 15 unités distinctes dans les 4 membres principaux. Cette analyse lithostratigraphique associée aux données bibliographiques met en exergue le haut potentiel de la Formation Khachik dans cette coupe. De plus, dans la section de Bagh-e-Vang, 10 unités rocheuses appartenant à la Formation Jamal ont également été identifiées. Diverses méthodes d'extraction, y compris la technique CH_2O_2 dilué à froid, le CH_3COOH dilué à froid et pur à chaud (acétolyse chaude) et les protocoles HF, ont été testées pour l'extraction de microfossiles tels que les conodontes, les ostracodes et les radiolaires dans les échantillons prélevés dans les sections d'Ali-Bashi et de Bagh-e-Vang.

Malgré des efforts de préparation intensifs et une stricte observance des protocoles d'extraction, une analyse approfondie de plus de 240 échantillons de la Formation Khachik

(coupe d'Ali-Bashi), malgré l'application des techniques CH_2O_2 dilué et CH_3COOH dilué à froid, aucune espèce de conodontes n'a été extraite. Dans la section de Bagh-e-Vang également, l'utilisation de la technique diluée CH_3COOH a confirmé de manière convaincante l'absence de conodontes dans la deuxième section.

Diverses méthodes d'extraction ont été appliquées et testées pour l'extraction des ostracodes à partir des échantillons de la section d'Ali-Bashi. Le CH_3COOH pur à chaud et dilué à froid; l'acide CH_2O_2 à froid a conduit à l'extraction de 67 spécimens parmi plus de 240 échantillons de la Formation Khachik.

L'application de la méthode CH_2O_2 dilué a produit des résultats qui m'ont permis d'identifier les espèces suivantes : *Bairdia deducta deducta* (Zalanyi, 1974); *Bairdia hungarica* Zalanyi, 1974; *Bairdia* sp.; *Fabalitypris parva* Wang, 1978, *Fabalitypris* sp. 1; *Fabalitypris* sp. 2; *Fabalitypris* sp. 3; *Fabalitypris* sp. 4; *Hollinella* (*Hollinella*) *herrickana* (Girty 1909), *Hollinella* sp., *Sargentina transita* (Kozur 1985) et *Silenites* sp.

Bairdia sp., *Fabalitypris* sp. 1; *Fabalitypris* sp. 2; *Fabalitypris* sp. 3; *Fabalitypris* sp. 4; *Hollinella* (*Hollinella*) *herrickana* (Girty 1909), *Sargentina transita* (Kozur 1985) et *Silenites* sp., ont été obtenus exclusivement grâce au protocole CH_2O_2 dilué à partir des calcaires dolomités durs, tandis que les autres procédures à froid avec CH_3COOH ont échoué.

L'application de la méthode de préparation par acétolyse chaude m'a permis d'identifier les espèces: *Acratia changxingensis* (Shi, 1987); *Acratia* sp.; *Bairdia deducta deducta* (Zalanyi, 1974); *Bairdia elcapitanensis* Forel 2021; *Bairdia* cf. *fangnianqiao* Crasquin, 2010; *Bairdia grotei* Chitnarin, 2017 *Bairdia hungarica* Zalanyi, 1974; *Bairdia khaokanaensis* Chitnarin, 2017; *Bairdia radlerae* Kellett, 1934; *Bairdia rhomboidalis* Hamilton, 1942; *Bairdia* cf. *songthami* Chitnarin et al. 2017; *Bairdia* sp.30 sensu Chitnarin, 2009; *Bairdia* sp. 1; *Bairdia* sp. 2; *Bairdia* sp. 3; *Bairdia* sp. 4; *Bairdia* sp. 5; *Bairdia* sp. 6; *Bairdia* sp. 7; *Bairdia* sp. 8; *Bairdia* sp. 9; *Bairdia* ? sp.; *Bairdiacypris longirobusta* Chen, 1958; *Bairdiacypris* sp. 6 sensu Zazzali et al., 2015; *Bairdiacypris* sp. B sensu Tarnac et al., 2021; *Bairdiacypris* sp. 1; *Bairdiacypris* sp. 2; *Bairdiacypris* sp. 3; *Bairdiacypris* sp. 4; *Bairdiacypris* sp. 5; *Bairdiacypris* sp. 6; *Bairdiacypris* sp. 7; *Bairdiacypris* sp. 8; *Bairdiacypris* sp. 9; *Ceratobairdia sexagintaduella* Forel, 2021; *Ceratobairdia?* cf. *crenata* Chen, 1982; *Fabalitypris acetalata* (Coryell & Billings, 1932); *Fabalitypris glennensis* (Harlton, 1927); *Fabalitypris parva* Wang, 1978; *Fabalitypris reniformis* (Chen, 1958) sensu Wang, 1978; *Fabalitypris* sp. 5; *Fabalitypris* sp. 6; *Fabalitypris*

sp. 7; *Hollinella (Hollinella) martensiformis* Crasquin et al., 2010 ; *Hollinella* sp. ; *Indivisia* sp. 1 sensu Forel et al. 2015; *Kempfina qinglaili* (Crasquin, 2008); *Kempfina* sp. 1 ; *Liuzhinia julfensis* Gliwa, 2021; *Praezabythocypris pulchra* Kozur, 1985; *Praezabythocypris* sp. 1; *Praezabythocypris* sp. 2; *Pseudacanthoscapha striatula* (Shi, 1982); *Reviya* sp.; *Sargentina minuta* Wang, 1978; *Sargentina* sp.; et *Sulcella sulcata* Coryell & Sample, 1932. Certaines des espèces identifiées au niveau des genres *Bairdia*, *Bairdiacypris* et *Fabalitypris* présentent des opportunités prometteuses pour définir de nouvelles espèces à travers des études approfondies. De plus, l'identification des espèces d'ostracodes dans les séquences du Permien moyen et supérieur met en lumière le potentiel significatif pour explorer ce groupe fossile en Iran.

En dépit d'une conformité stricte au protocole recommandé, l'utilisation de la technique HF dans le traitement de 12 échantillons cherté d'Ali-Bashi et de 8 échantillons cherté de Baghe-e-Vang a abouti à un résultat décourageant, et aucun spécimen de radiolaire n'était discernable dans le sédiment des deux ensembles d'échantillons.

L'analyse des microfaciès dans la section d'Ali-Bashi a permis d'identifier 28 sub-microfaciès, dérivés de 15 microfaciès distincts. Les groupes de microfaciès, allant de MKL1 à MKL2 (environnement lagunaire), MKR2 à MKR3 présentent des caractéristiques d'un cadre de rampe intérieure restreinte.

Les groupes MKO1 à MKO4 suggèrent un cadre confiné, se produisant dans la partie finale de la rampe intérieure sous un environnement marin ouvert. Les groupes de microfaciès MKM1 à MKM3 sont supposés avoir été déposés après l'environnement marin ouvert, dans les zones de la rampe médiane, tandis que les MKT1 à MKT3 ont été identifiés dans les segments initiaux de la rampe externe, correspondant à la position du pied de pente dans le cadre de la plateforme carbonatée. En outre, conformément aux microfaciès standards désignés par [Flugel \(2010\)](#), l'étude propose 10 microfaciès du type RMF, ainsi que leurs 4 SMF correspondants pour les strates étudiées. De plus, sur la base des zones de faciès standards (FZ) introduites par [Wilson \(1975\)](#), trois FZ présentant une tendance d'abaissement ont été avec succès délimitées, à savoir FZ8, FZ7 et FZ3.

MOTS-CLÉS : Processus d'extraction, Ostracodes, CH_2O_2 , CH_3COOH , acétolyse à chaud, HF, Guadalupien-Lopingien, Formation Khachik, Formation Jamal, section Ali-Bashi, section Baghe-Vang, section Baghuk.

چکیده

پرمین ایران همواره مورد توجه زمین شناسان بوده و عمده این کاوش ها متمرکز با بازه زمانی گذر پرمین-تریاس (PTB)، پیشینه جایگاه دیرینه شناختی آن در پهنه زمین شناختی ایران و همچنین شناخت تاثیر رویداد انقراضی این گذر در پهنه جغرافیایی ایران در این گذر بوده است. با علم به این که پژوهش‌های پرمین ایران منجر به انتشار گزارش‌هایی با ارزش که سبب بازسازی سناریوی های مختلف گذر پرمین-تریاس در ایران گردیده، همچنان یک شکاف مهم و نبود اطلاعاتی د-ر دانش دیرینه شناختی ما درباره پرمین میانی و پسین ایران (گذر گوادالوپین-لوپینگین) و جایگاه زیست چینه نگاری آن در ادبیات زمین‌شناسی ایران به قوت خود باقی مانده است. جایگاه دیرینه شناختی و تعیین دقیق مرز گوادالوپین-لوپینگین (GLB) از جمله موضوعات با سابقه دیرین و مورد اختلاف میان پژوهشگران بوده به طوری که در گزارش‌ها و انتشارات متعدد در ارتباط با این گذر، تفسیرهای متنوعی درباره جایگاه دیرینه شناختی آن ارائه گرفته است که عمده آن ناشی از معیارهای سنگ‌شناسی و نه تقسیمات زیست چینه‌نگاری بوده است. این مهم در هر دو منطقه شمال غربی ایران و ایران مرکزی پررنگ بوده که همین امر موجب پیچیدگی در ساختار دیرینه شناختی این گذر در ایران شده است. این روند در منطقه طبس (ایران مرکزی) با رویکرد دیگری دنبال شده و مکان دقیق گذر GLB با توجه به ریزسنگ‌های کف زی از روزن‌داران به نام فوزولیندها تعیین شده که این گذر بدون حضور کنودونتها به عنوان شاخص‌های زیست پهنه‌بندی این محدوده سنی دارای ابهام آشکارتری نیز است.

با این توضیحات رساله دکتری حال حاضر با هدف تعیین دقیق جایگاه دیرینه شناختی GLB و حوات زیستی رخ داده در آن در ایران تعریف و تلاش گردید تا با توجه به رویکرد زیست چینه نگاری و با تکیه بر گزارش‌های متفاوت ارائه شده از پرمین ایران، از پیچیدگی های ایجاد شده کاسته شود. به همین منظور سه برش چینه شناسی علی‌باشی در جلفا، باغ‌ونگ در طبس و باغوک در آباده که دارای بالاترین پتانسیل دیرینه شناختی برای پی‌جویی گذر یادشده؛ انتخاب و مورد نمونه‌برداری دقیق قرار گرفت. از برش علی‌باشی بیش از ۲۴۰ نمونه سنگی از ۱۸۹ متر سازند خاچیک جمع آوری گردید و در برش باغ‌ونگ نیز ۱۶۰ نمونه سنگی از ۲۶۰ متر سازند جمال با هدف مطالعات ریز دیرینه شناختی برداشت شد. برش باغوک با توجه مواردی نظیر همه‌گیری پاندمی کووید-۱۹ و شرایط آب و هوایی خاص منطقه صورت پذیرفت. ارزیابی سنگ چینه‌نگاری سازند خاچیک در برش علی‌باشی منجر به شناسایی ۱۵ واحد سنگی متمایز چیدمان شده در ۴ عضو اصلی شد که این دستاورد امکان ایجاد یک بروزرسانی نوین با دیدگاه سنگ چینه نگاری برای این توالی‌ها را دارا می‌باشد که از توانایی بسیار خوبی برای هماهنگ شدن با پژوهش‌های پیشین انتشار یافته سازند خاچیک در این برش برخوردار است. علاوه بر این در برش باغ‌ونگ نیز، ۱۰ واحد سنگی از برون‌زدهای سازند جمال در قالب سه عضو اصلی نیز تفکیک گردید.

در این پژوهش، روش‌های آماده‌سازی و استخراج مختلفی همانند، اسید فومیک رقیق سرد (CH_2O_2)، استید استیک رقیق سرد (CH_3COOH)، استولیز داغ (hot acetolysis) و در نهایت (HF) برای بدست آورد ریز سنگواره‌هایی همچون کنودنت‌ها، استراکودها، و همچنین رادیولارپها استفاده شده است. با وجود تلاش‌های گسترده در زمینه آماده‌سازی و پیروی کامل از مراحل آماده‌سازی نمونه‌ها برای تفکیک و شناسایی عناصر کنودونتی، تست و استفاده مستمر و

چندباره از تکنیک‌های CH_2O_2 و CH_3COOH سرد و رقیق بر روی بیش از ۲۴۰ نمونه از سازند خاچیک در برش علی‌باشی، موفقیت آمیز نبوده و ریزسنگواره‌های کنودنتی که به عنوان بازیگر اصلی برای تعیین جایگاه دیرینه‌شناختی GLB شناخته می‌شوند، یافت نگردیدند. همچنین در برش باغ‌ونگ نیز رویکرد استفاده از تکنیک CH_3COOH رقیق شده نیز برای کاوش در مورد کنودونت‌ها انتخاب شد که عدم حضور کنودونت به طور قاطع در برش دوم نیز تثبیت گردید.

در ارتباط با استخراج استراکدها نیز سه روش آماده‌سازی: اسید فرمیک ۱۰٪ (CH_2O_2)، اسید استیک ۱۵٪ (CH_3COOH) سرد و استولیز داغ (CH_3COOH) برای استخراج از نمونه‌های برش چینه‌شناسی علی‌باشی تست شد که حاصل این فرایند شناسایی ۶۷ گونه استراکودی می‌باشد. اعمال روش CH_2O_2 رقیق سرد بر روی نمونه‌های مذکور منجر به شناسایی گونه‌های استراکودی با حفظ شدگی بالا شد که به موجب آن گونه‌های *Bairdia deducta* (Zalanyi, 1974)، *Fabalitypris parva*، *Bairdia sp.*، *Bairdia hungarica* Zalanyi, 1974، *deducta* (Zalanyi, 1974) Wang 1978، *Fabalitypris sp. 1*، *Fabalitypris sp. 2*، *Fabalitypris sp. 3*، *Fabalitypris sp. 4*، *Sargentina transita* (Kozur, 1985)، *Hollinella sp.*، *Hollinella (Hollinella) herrickana* (Girty, 1909) و *Silenites sp.* شناسایی شد. در این میان لازم به ذکر است گونه‌های *Bairdia sp.*، *Fabalitypris sp. 1*، *Hollinella (Hollinella) herrickana*، *Fabalitypris sp. 2*، *Fabalitypris sp. 3*، *Fabalitypris sp. 4*، *Sargentina transita* (Kozur, 1985) (Girty, 1909) و *Silenites sp.* به صورت اختصاصی و تنها با روش CH_2O_2 از سنگ آهک‌های دولومیتی شده استخراج شد و استفاده از روش CH_3COOH رقیق و سرد حاصلی نداشت و منجر به استخراج گونه‌ای با حفظ شدگی بالا از استراکودها نگردید.

روش گرمایی اسیدی اسیتولیز (CH_3COOH خالص و گرم) نیز موفقیت‌آمیز بود و نتایج حاصله منجر به شناسایی تعداد قابل توجهی از گونه‌های استراکودی با حفظ شدگی بالا شد. این گونه‌ها شامل: *Acratia changxingensis* (Shi, 1987)، *Bairdia elcapitanensis* Forel، *Bairdia deducta deducta* (Zalanyi, 1974)، *Bairdia*، *Bairdia grotei* Chitnarin, 2017، *Bairdia cf. fangnianqiao* Crasquin, 2010، *Bairdia radlerae* Kellett، *Bairdia khaokanaensis* Chitnarin, 2017، *hungarica* Zalanyi, 1974، *Bairdia cf. songthami* Chitnarin et al. 2017، *Bairdia rhomboidalis* Hamilton, 1942، 1934، *Bairdia sp. 1*، *Bairdia sp. 2*، *Bairdia sp. 3*، *Bairdia sp. 4*، *Bairdia sp. 30 sensu* Chitnarin, 2009، *Bairdia sp. 5*، *Bairdia sp. 6*، *Bairdia sp. 7*، *Bairdia sp. 8*، *Bairdia sp. 9*، *Bairdia ? sp.*، *Bairdiacypris sp. 6 sensu* Zazzali et al., 2015، *Bairdiacypris longirobusta* Chen, 1958، *Bairdiacypris sp. 1*، *Bairdiacypris sp. B sensu* Tarnac et al., 2021، *Bairdiacypris sp. 3*، *Bairdiacypris sp. 4*، *Bairdiacypris sp. 5*، *Bairdiacypris sp. 6*، *Bairdiacypris sp. 7*، *Ceratobairdia sexagintaduella* Forel, 2021، *Bairdiacypris sp. 8*، *Bairdiacypris sp. 9*، *Fabalitypris acetalata* (Coryell & Billings, 1932)، *Ceratobairdia? cf. crenata* Chen, 1982، *Fabalitypris glennensis* (Harlton, 1927) و *Fabalitypris parva* Wang, 1978.

Fabalitypris، *Fabalitypris* sp. 6، *Fabalitypris* sp. 5، *reniformis* (Chen, 1958) *sensu* Wang, 1978
Hollinella (*Hollinella*)، *Hollinella* (*Hollinella*) *martensiformis* Crasquin et al., 2010، sp. 7
، *Indivisia* sp. 1 *sensu* Forel et al. 2015، *Hollinella* sp.، *martensiformis* Crasquin et al., 2010
، *Liuzhinia julfensis* Gliwa, 2021، *Kempfina* sp. 1، *Kempfina qinglaili* (Crasquin, 2008)
Pseudacanthoscapha، *Praezabythocypris* sp. 1، *Praezabythocypris pulchra* Kozur, 1985
Sulcella، *Sargentina* sp.، *Sargentina minuta* Wang, 1978، *Reviya* sp.، *striatula* (Shi, 1982)
Bairdia sulcata Coryell & Sample, 1932. همزمان با این موارد، برخی از گونه‌های شناسایی شده از جنس‌های *Bairdia*،
، *Fabalitypris* و *Bairdiacypris*، از شاخصه بسیار خوب و نویی را برای تعریف گونه‌های جدید با پژوهش‌های
بیشتری بر روی آنها دارا می‌باشند. علاوه بر این، شناسایی موفق حجم زیادی از گونه‌های استراکودی از توالی‌های پرمین
میان و پرمین بالایی سازند خاچیک در برش چینه شناسی علی‌باشی، حاکی از پتانسیل بالای این ریزسنگواره‌ها در
صورت کاوش دیرینه‌شناختی در ایران را نشان می‌دهد.

با وجود پایبندی دقیق روش توصیه‌شده برای استخراج رادیولارها، تلاش نگارنده و استفاده از تکنیک HF در پردازش
۱۲ نمونه سنگ چرتی از علی‌باشی و ۸ نمونه از برش باغ‌ونگ، به نتیجه‌ای ناامیدکننده منجر شد و متأسفانه هیچ
نمونه رادیولاری در داخل رسوب هیچ یک از نمونه‌های برداشت شده یافت نگردید.

تجزیه و تحلیل ریزرخساره‌ها در برش چینه شناسی علی‌باشی از توالی‌های رسوبی سازند خاچیک منجر به شناسایی
۲۸ زیر ریزرخساره شد که در ۱۵ گروه ریزرخساره از هم متمایز شده‌اند. گروه‌های ریزرخساره‌ای MKL1 تا MKL2 در
ارتباط با پهنه لاگونی بوده، از MKR2 تا MKR3 ویژگی‌هایی رمپ داخلی محدودشده را نشان داده و گروه‌های MKO1
تا MKO4، در قسمت نهایی رمپ داخلی تحت محیط دریایی باز می‌باشند. توالی‌های رسوبی در ارتباط با گروه‌های
ریزرخساره‌ای MKM1 تا MKM3 نیز پس از محیط دریایی باز و در نواحی رمپ میانی نهشته شده‌اند، این در حالی
است که گروه‌های ریزرخساره‌ای MKT1 تا MKT3 در بخش‌های ابتدایی رمپ خارجی شناسایی شده‌اند که با معادل
با Toe-of-slope در شلف کریناته نیز می‌شود. علاوه بر این، با پیروی از ریزرخساره‌های استاندارد مشخص‌شده
توسط [Flugel \(2010\)](#)، ۱۰ ریزرخساره از نوع RMF همراه با ۴ SMF هم تراز آن‌ها برای سازند خاچیک در برش
چینه شناسی علی‌باشی نیز پیشنهاد می‌گردد. علاوه بر این، باتوجه به پهنه رخصاره‌های (FZ) معرفی شده توسط
[Wilson \(1975\)](#)، سه پهنه با روند کم‌عمق به بالا، به نام‌های FZ8، FZ7 و FZ3 در ارتباط با دسته ریزرخساره‌ای
شناسایی شده در برش مذکور از این سازند، نیز گزارش می‌گردد.

کلید واژه: فرآیند استخراج، استراکودها، CH_2O_2 ، CH_3COOH ، اسیتولیز گرمایی، HF، گوادالوپین-لوپینگین، سازند
خاچیک، سازند جمال، برش علی‌باشی، برش باغ‌ونگ، برش باغوک.

CHAPTER 1

Introduction and objectives

1.1. INTRODUCTION.....	2
1.2. MIDDLE PERMIAN EXTINCTION.....	3
1.3. OBJECTIVES.....	8
1.4. CONTENTS OF THE THESIS.....	9
1.5. REFERENCES.....	10

1.1. INTRODUCTION

The widely recognized end-Paleozoic mass extinction, the most severe in the Phanerozoic eon, unfolded as a dual-phased event (Isozaki 2009). The initial pulse marks the boundary between the Capitanian and Wuchiapingian stages (-259.51 \pm 0.21My), referred to as the Guadalupian-Lopingian Boundary (GLB). The second crisis is a major extinction event, known as the Permian-Triassic Boundary (PTB; 251.90 \pm 0.02My). Some authors consider that this event could be considered a major biodiversity crisis of the Phanerozoic (Isozaki, 2009; Day & Rubidge 2021).

Jin et al. (1994) and Stanley and Yang (1994) emphasized that the unadorned decline in diversity among Paleozoic biota during the End Permian Mass Extinction (EPME) was likely a result of the combined impact of two substantial phases or events. These events occurred consecutively within a relatively brief interval of less than 10 million years. This limited timeframe was insufficient for the biosphere and biota to fully recover to the levels observed during the Early-Middle Permian.

The EPME stands out among five significant epochs in deep time, marked by Earth System disruptions that caused profound biodiversity depletion (Gastaldo et al. 2021). This event not only reshaped the course of life but also ushered in a new biological paradigm. Coined by Erwin (1996) as the "Mother of Mass Extinctions," the end-Permian mass extinction represents a pivotal interval in Earth's history. This biotic crisis resulted in the extinction of over 80% of marine species (Stanley 2016) and approximately 75% of terrestrial genera Erwin (2006). However, the impact of this crisis on terrestrial environments exhibited considerable variation, ranging from negligible effects on terrestrial plants to complete devastation of terrestrial ecosystems (Hermann et al. 2011; Elewa & Abdelhady 2020) (fig. 1.1).

The combination of some conditions disrupted the food chain which led to the mass extinction event. For instance, the high temperatures caused an increase in the rate of respiration which depleted the oxygen levels in the water. This hypoxic environment caused many species to die off, and the severe disturbances in the recording of carbon isotopes disrupted the food chain, resulting in a mass extinction event (Shen et al. 2021). Also, the evening of the global climate as a consequence of the end of the late Paleozoic ice age raised global surface temperatures, leading to a warming of the surface waters and thus a diminishing of their capacity to hold oxygen. This poorly oxygenated warm surface water must

have made the global oceanic circulation more sluggish than during ice ages, reducing further what little aeration to the deep ocean it otherwise could have contributed. Therefore, both the low oxygen content of the late Permian atmosphere and the increased surface temperature of its ocean predisposed the Permian world ocean to poor aeration (Sengor & Atayman 2009).

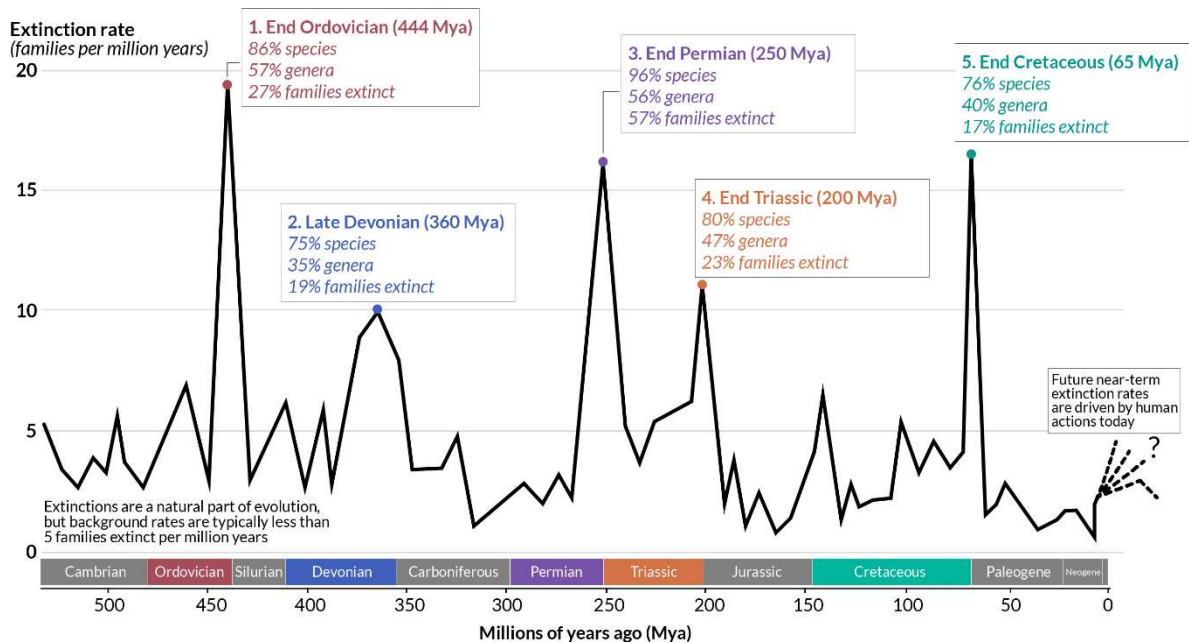


Fig. 1.1. List five significant mass extinctions that occurred in the Earth's history (from Barnosky et al. 2011; McCallum 2015).

The main focus of this PhD thesis is the bio-event occurring in the Middle Permian, with specific attention directed towards the Guadalupian–Lopingian Boundary. Subsequently, the following sections provide a more detailed description of this boundary.

1.2. MIDDLE PERMIAN EXTINCTION

Preceding the mass extinction event at the end of the Permian, there existed another biodiversity crisis during the Middle Permian, specifically at the end of Guadalupian (Capitanian). Despite being overshadowed for an extended period by the prominence of PTB extinction, the mass extinction at the GLB is now recognized as potentially more significant than its successor (Isozaki, 2007a). However, this crisis which is known as a minor extinction event (Elewa & Abdelhady 2020), had a substantial impact on Permian diversity patterns (Jin

et al. 1994). This event, occurring during the mid-Permian (end Guadalupian, approximately 260 million years ago), led to a reduction of over 75% in generic abundance.

Following, higher-resolution paleontological studies and continually upgrading chronological constraints have confirmed that the marine extinctions associated with this event (mid-Permian) may have occurred at different points clustered in the later part of the Capitanian stage, rather than at the boundary between the Guadalupian and Lopingian series (Wignall et al. 2009; Bond et al. 2010, 2015). However, research initiated in the 1990s prompted a reassessment of the importance of this mass extinction occurrence. The contributions of Stanley & Yang (1994), Jin et al. (1994), Shen & Shi (1996), and later Stanley (2016) played a pivotal role in re-evaluating the significance of this event.

The major perspective of the Capitanian scenario is achieved from marine deposits of southern China, where large losses are recorded among fusulinacean, calcareous algae, brachiopods, corals, and ammonoids. However, the extinction has also been tracked by Bond et al. (2015; 2020) in Norway and Canada (outside of former PalaeoTethys). In the last decade, as a consequence of protentional fundamental links to volcanism in the Emeishan Large Igneous Province, the Capitanian biotic crisis (CME) has garnered increasing attention (Wignall et al. 2009; McGhee et al. 2013; Bond & Wignall 2014; Bond & Grasby 2017; Bond et al. 2020). Estimates of its overall severity have varied, depending on the calculations and datasets used, but one of the most recent large-database estimates suggests it may have led to the extinction of 33–35% of marine genera, making it comparable in magnitude to the Cretaceous/Paleogene mass extinction (Stanley 2016; Day & Rubidge 2021).

The Capitanian biotic crisis (CME) has been ranked by some authors as the third largest mass extinction in the Phanerozoic with 40% loss in marine genera (Sepkoski 1996; Bambach et al. 2004). Furthermore, Stanley's later study with Yang Xiangning echoed an earlier conclusion by Heinz Kozur that indeed there were not one but two peaks of extinction in the marine biosphere: one at the end of the Guadalupian and the other at the end of the Changhsingian (Kozur & Mock 1977; Stanley & Yang 1994), with 58% of all marine genera disappearing at the end of the Guadalupian (Stanley & Yang 1994) and anywhere between 83% (Sepkoski 1989, 1990) and 96% (Raup 1991) disappearing at the end of the Changhsingian (Sengor & Atayman 2009).

The groups affected in the Guadalupian extinction were mainly benthic organisms including rugose corals, bryozoans, fusulinid foraminifera, articulated brachiopods, nektobenthic

goniatitid ammonoids, and terrestrial vertebrates (Wei et al. 2020). Insects even suffered terribly (Sengor & Atayman 2009). Besides “the extinctions happened especially in Tethyan, mid-latitude regions; there is very little evidence for the event in northern waters” (Benton 2003). Reevaluation of the ecological severity ranking showed that the end-Guadalupian biotic crisis caused only 25% marine genera loss and is not as severe as previously thought (Payne & Clapham 2012; McGhee et al. 2013). Nevertheless, the end-Guadalupian mass extinction is associated with environmental changes such as carbon, strontium, sulfur isotopic changes, and rapid fluctuations in seawater temperatures (Chen & Shen 2019). Evidence suggests that Emeishan volcanism in southwest China caused or at least largely contributed to the end-Guadalupian mass extinction (Bond et al. 2010; Chen & Xu 2019). Another suggested trigger is the regression due to the largest Paleozoic sea-level fall (Haq & Schutter 2008) that eliminated habitats for faunas that evolved in the epicontinental seas (Chen & Shen 2019).

Moreover, the CME biotic crisis transpired in the marine part, but why terrestrial vertebrates and insects were under suffer. The only thing we can think of is the air they breathe. If that air gets poisoned, they will die. This is something they seem to have shared with their counterparts living in the Paleo-Tethys (Sengor & Atayman 2009). The only mechanism capable of doing this that we know of is volcanism eruption which releases gas (Zhang & Kling 2006, Ryskin 2003 and Kump et al. 2005). If the gases that resulted from anoxia in the ocean end up erupting, they would create a field of devastation around the ocean commensurate with the volume of gas released (fig. 1.2).

Payne et al. (2007) discussed the existence of erosion surfaces on uppermost Permian skeletal limestones in South China, Turkey, and Japan. Their inference, based on sedimentary facies, microfabrics, carbon isotopes, and cements, suggests that this erosion occurred in a submarine setting, possibly due to rapid carbon release from sedimentary reservoirs or the deep ocean. This information corroborates the idea that massive gas release may well have occurred, at least within the Paleo Tethyan and some nearby polluted Panthalassa shelves. This is the only piece of possible direct evidence of gas eruption in the Paleo-Tethys that we are aware of (Sengor & Atayman 2009).

The timing and nature of the extinction event are still being debated. For instance, Kaiho et al. (2005) placed the extinction horizon in the earliest Lopingian in the Laibin area (South China). In contrast, Wignall et al. (2009) and Bond et al. (2010) argued that the extinction

event had occurred earlier, in the middle Capitanian (Late Guadalupian) in South China and both extinction events were associated with significant fluctuations of carbon isotope record (Wang et al. 2004; Kaiho et al. 2005; Wignall et al. 2009). The end-Guadalupian extinction event was accompanied by a significant drop in the carbonate $\delta^{13}\text{C}$ (Wang et al. 2004; Wignall et al. 2009); although Chen et al. (2013) in Nishikane et al. (2014) doubted the global significance of this $\delta^{13}\text{C}$ decrease.

Another event was recorded in the Capitanian of Iwato Formation at the Kamura section, Miyazaki, southwest Japan, which represents a seamount-capping carbonate sequence in the pelagic Panthalassa in the Southern Hemisphere (Isozaki et al. 2007 ab; Kasuya et al. 2012). Isozaki et al. (2007a,b) found a prominent highly positive (more than +5‰) plateau in the $\delta^{13}\text{C}_{\text{carb}}$ values within the Capitanian in the Kamura section. They named this interval the Kamura event and regarded it as a cooling interval.

The Kamura event was also recognized in the Brušane section, Croatia, which was deposited in the European Paleo-Tethys and can be used for global chemostratigraphic correlation (Isozaki et al. 2011). However, no age-diagnostic conodonts have been found in these sections, and the fusulinid biostratigraphy determined the age of the Kamura event.

The absence of conodonts makes this age determination of the Kamura event inconclusive. Afterward the end Guadalupian mass extinction, biodiversity gradually increased until it suddenly dropped at the end Permian.

Rampino & Shen (2021), in the basics of the ecological-impact ranking system, mentioned that the CME crisis involved three Level-2 paleoecological changes: in benthic reef ecosystems, benthic photosymbiotic foraminiferal and bivalve ecosystems, and within nektonic and pelagic ammonoid ecosystems. Additionally, this phenomenon is one of five events in the Phanerozoic with a clear shift from metazoan-dominated reef ecosystems to microbe-dominated reef ecosystems.

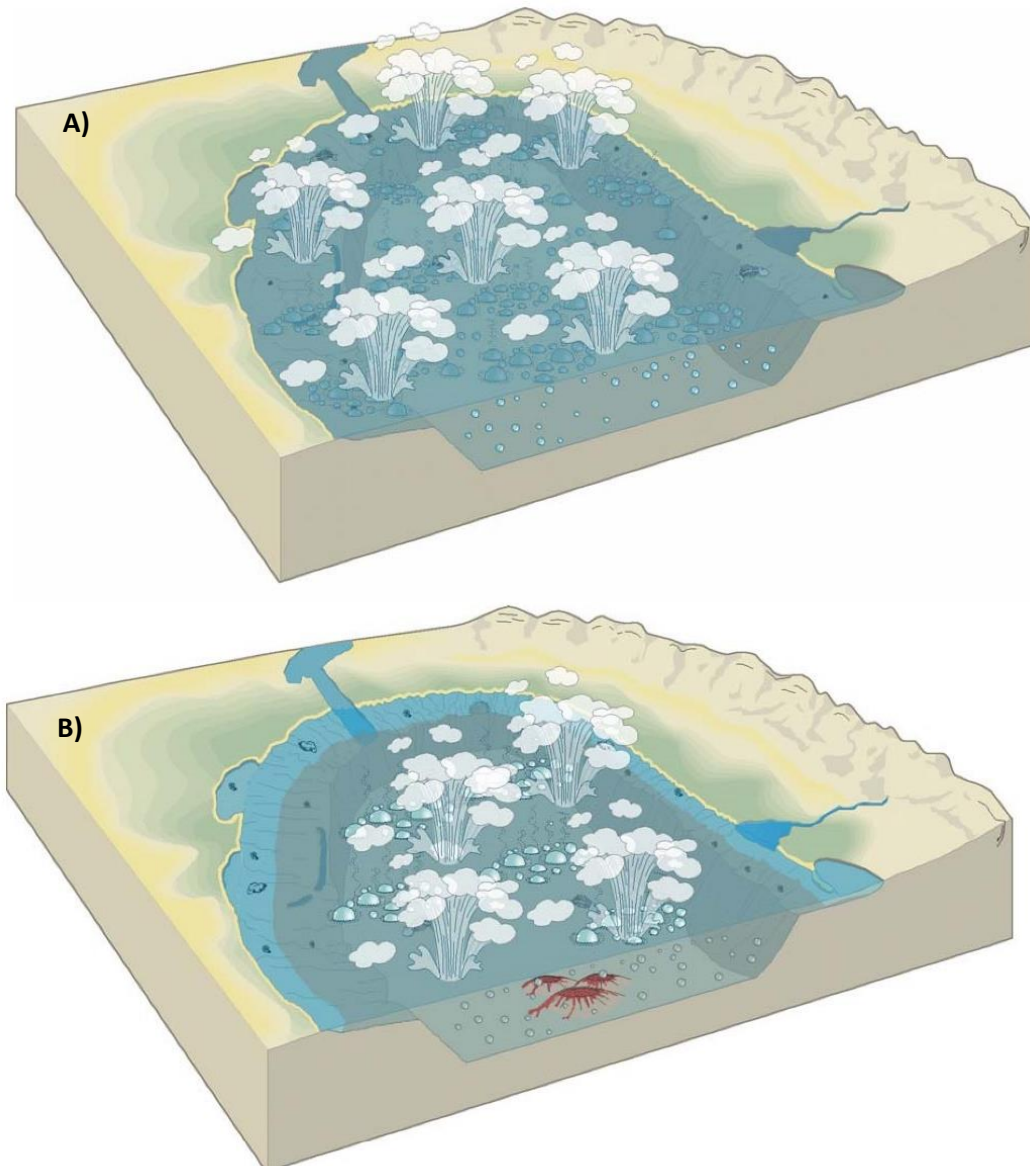


Fig. 1.2. Artist's conception of what might have happened in the Paleo-Tethys during the Permian interval. (A) Changhsingian: Almost all of Paleo-Tethys has turned anoxic. (B) Late Guadalupian: Anoxia has already reached some of the lower shelves. Suboceanic igneous vulcanicity may have triggered a first phase of oceanic gas eruptions. Major gas eruptions may have resulted from oversaturation of the water column by dissolved gases because of millions of years of anoxia and/or further submarine igneous vulcanicity. Widespread death brings the Permian period to a close and with it the Paleozoic era. The Mesozoic begins with a much-impooverished biosphere (Sengor & Atayman 2009).

1.3. OBJECTIVES

The Permian rocks in Iran are extensively exposed, providing a comprehensive display of various marine environments. It is the unknown place to discuss the topic of CME (see Chapter 2).

This thesis mainly aims to explore the bio-event of GLB in Iran, focusing on a designated fossil-rich section located in the northwestern of Iran region, Central Iran, and the Sanandaj-Sirjan Zone. The key questions to be tackled include:

- Is it possible to mark and show a significant lithological bed in Iranian sections or do a lithostratigraphic update for the Middle-Upper Permian boundary interval?
- Could find conodonts from the Middle-Upper Permian boundary interval of the Iranian sections?
- Could the precise location of the GLB be determined and introduced based on the conodont's biozones within these specified stratigraphic sections?
- What are the challenges related to GLB in these sections, and how does the bio-event perspective contribute to understanding this boundary on Iran's part?
- Is it possible to provide a theory regarding the nature of the cherty layers found in these stratigraphic sections?

The investigation will involve meticulous fieldwork, laboratory analyses, and data integration to discern patterns, shifts, and potential correlations in the strata.

The objectives are with more details outlined as follows:

1. Lithostratigraphic investigations of designated sections in diverse Iranian regions: This research endeavors to conduct detailed lithostratigraphic analyses on carefully chosen geological sections located in three distinct regions of Iran: The Northwest, Central Iran, and the Sanandaj-Sirjan Zone. The purpose of these investigations is to gain an in-depth understanding of the geological formations present in these regions, thereby contributing to the broader comprehension of their geological history.
2. Integration of biostratigraphic concepts with zonal marker microfossils, conodonts: in the selected sections, a crucial objective is to establish and integrate biostratigraphic concepts

using zonal marker microfossils, particularly conodonts. The systematic examination and analysis of these microfossils were undertaken.

3. Thorough systematic micropaleontological investigations: This part is devoted to the identification and analysis of extracted microfossils, such as Ostracods.

3. Examination and tacking of the GLB in Iran. By precisely identifying this boundary, the research aims to shed light on significant geological events and changes that occurred during that transitional period, thus contributing to our comprehension of global geological and paleontological transformations.

1.5. CONTENTS OF THE THESIS

As a consequence, this thesis can be categorized as follows:

To begin with, the initial part of **Chapter 2** provides an overview of the general geology and stratigraphy of Iran, along with an introduction to the Permian strata relevant to this research. Following this, the final section of the chapter elaborates on the specifics of the study sections.

Moving on, the second aspect involves outlining the general methodology and techniques used for extracting microfossil targets in this project. Subsequently, the protocols employed in the study sections are detailed, accompanied by a discussion of these methodologies in the concluding section of **Chapter 3**.

The third is an approach to the paleontology of the ostracod group and the first analysis of the ostracod is contained in **Chapter 4**.

Chapter 5 is dedicated to the analysis of microfacies and the patterns of paleoenvironments within the study sections.

Lastly, **Chapter 6** draws upon the results gathered from the preceding chapters, offering discussions and conclusions that encompass all the aforementioned aspects.

1.5. REFERENCES

- Bambach, R.K., Knoll, A.H. and Wang, S.C., 2004. Origination, extinction, and mass depletions of marine diversity. *Paleobiology*, 30(4), pp.522-542.
- Benton, M.J. and Twitchett, R.J., 2003. How to kill (almost) all life: the end-Permian extinction event. *Trends in Ecology & Evolution*, 18(7), pp.358-365.
- Bond, D.P. and Grasby, S.E., 2017. On the causes of mass extinctions. *Palaeogeography, Palaeoclimatology, Palaeoecology*, 478, pp.3-29.
- Bond, D.P., Hilton, J., Wignall, P.B., Ali, J.R., Stevens, L.G., Sun, Y. and Lai, X., 2010. The Middle Permian (Capitanian) mass extinction on land and in the oceans. *Earth-Science Reviews*, 102(1-2), pp.100-116.
- Bond, D.P., Wignall, P.B. and Grasby, S.E., 2020. The Capitanian (Guadalupian, Middle Permian) mass extinction in NW Pangea (Borup Fiord, Arctic Canada): A global crisis driven by volcanism and anoxia. *GSA Bulletin*, 132(5-6), pp.931-942.
- Bond, D.P., Wignall, P.B., Joachimski, M.M., Sun, Y., Savov, I., Grasby, S.E., Beauchamp, B. and Blomeier, D.P., 2015. An abrupt extinction in the Middle Permian (Capitanian) of the Boreal Realm (Spitsbergen) and its link to anoxia and acidification. *Bulletin*, 127(9-10), pp.1411-1421.
- Bond, D.P., Wignall, P.B., Keller, G. and Kerr, A.C., 2014. Large igneous provinces and mass extinctions: an update. *Volcanism, impacts, and mass extinctions: causes and effects*, 505, pp.29-55.
- Barnosky, A.D., Matzke, N., Tomiya, S., Wogan, G.O., Swartz, B., Quental, T.B., Marshall, C., McGuire, J.L., Lindsey, E.L., Maguire, K.C. and Mersey, B., 2011. Has the Earth's sixth mass extinction already arrived? *Nature*, 471(7336), pp.51-57.
- Chen, B., Joachimski, M.M., Shen, S.Z., Lambert, L.L., Lai, X.L., Wang, X.D., Chen, J. and Yuan, D.X., 2013. Permian ice volume and palaeoclimate history: Oxygen isotope proxies revisited. *Gondwana Research*, 24(1), pp.77-89.
- Day, M.O. and Rubidge, B.S., 2021. The Late Capitanian mass extinction of terrestrial vertebrates in the Karoo Basin of South Africa. *Frontiers in Earth Science*, 9, p.631198.
- Day, M.O., Benson, R.B., Kammerer, C.F. and Rubidge, B.S., 2018. Evolutionary rates of mid-Permian tetrapods from South Africa and the role of temporal resolution in turnover reconstruction. *Paleobiology*, 44(3), pp.347-367.
- Elewa, A.M. and Abdelhady, A.A., 2008. Cenomanian/Turonian mass extinction of macroinvertebrates in the context of Paleogeology; A case study from North Wadi Qena, Eastern Desert, Egypt. *Mass Extinction*, pp.103-127.

- Elewa, A.M. and Abdelhady, A.A., 2020. Past, present, and future mass extinctions. *Journal of African Earth Sciences*, 162, p.103678.
- Erwin, D.H., 2006. Dates and rates: temporal resolution in the deep time stratigraphic record. *Annu. Rev. Earth Planet. Sci.*, 34, pp.569-590.
- Gastaldo, R.A., Kamo, S.L., Neveling, J., Geissman, J.W., Bamford, M. and Looy, C.V., 2015. Is the vertebrate-defined Permian-Triassic boundary in the Karoo Basin, South Africa, the terrestrial expression of the end-Permian marine event? *Geology*, 43(10), pp.939-942.
- Gastaldo, R.A., Kamo, S.L., Neveling, J., Geissman, J.W., Looy, C.V. and Martini, A.M., 2020. The base of the Lystrosaurus Assemblage Zone, Karoo Basin, predates the end-Permian marine extinction. *Nature Communications*, 11(1), p.1428.
- Gastaldo, R.A., Isozaki, Y., Kustatscher, E., Reisz, R., and Shen, S., 2021. Editorial: Permian Extinctions. *Front. Earth Sci.* 9:772688. doi: 10.3389/feart.2021.772688
- Gradstein, F.M., Ogg, J.G., Schmitz, M.D. and Ogg, G.M. eds., 2020. *Geologic time scale 2020*. Elsevier.
- Haq, B.U. and Schutter, S.R., 2008. A chronology of Paleozoic sea-level changes. *Science*, 322(5898), pp.64-68.
- Hermann, E., Hochuli, P.A., Bucher, H., Brühwiler, T., Hautmann, M., Ware, D. and Roohi, G., 2011. Terrestrial ecosystems on North Gondwana following the end-Permian mass extinction. *Gondwana Research*, 20(2-3), pp.630-637.
- Isozaki, Y., 2007a. Guadalupian–Lopingian boundary event in mid-Panthalassa: correlation of accreted deep-sea chert and mid-oceanic atoll carbonates. In: Wong, T. (Ed.), *Proceedings of the XVth Int. Congress of Carboniferous and Permian Stratigraphy*, Royal Netherlands Academy of Arts and Sciences, Special Publication, Amsterdam, pp. 111–124.
- Isozaki, Y., 2007b. Plume winter scenario for biospheric catastrophe: the Permo-Triassic boundary case. In: Yuen, D., Maruyama, S., Karato, S., Windley, B.F. (Eds.), *Superplume: Beyond Plate Tectonics*. Springer, Dordrecht, pp. 409–440.
- Isozaki, Y., 2009. Illawarra Reversal: The fingerprint of a superplume that triggered Pangean breakup and the end-Guadalupian (Permian) mass extinction. *Gondwana Research*, 15(3-4), pp.421-432.
- Isozaki, Y., Aljinović, D. and Kawahata, H., 2011. The Guadalupian (Permian) Kamura event in European Tethys. *Palaeogeography, Palaeoclimatology, Palaeoecology*, 308(1-2), pp.12-21.
- Jin, S., Tiefel, T.H., McCormack, M., Fastnacht, R.A., Ramesh, R. and Chen, L.H., 1994. Thousandfold change in resistivity in magnetoresistive La-Ca-Mn-O films. *Science*, 264(5157), pp.413-415.
- Kaiho, K., Chen, Z.Q., Ohashi, T., Arinobu, T., Sawada, K. and Cramer, B.S., 2005. A negative carbon isotope anomaly associated with the earliest Lopingian (Late Permian) mass extinction. *Palaeogeography, Palaeoclimatology, Palaeoecology*, 223(1-2), pp.172-180.

- Kasuya, A., Isozaki, Y. and Igo, H., 2012. Constraining paleo-latitude of a biogeographic boundary in mid-Panthalassa: Fusuline province shift on the Late Guadalupian (Permian) migrating seamount. *Gondwana Research*, 21(2-3), pp.611-623.
- Kozur, H. and Mock, R., 1977. Conodonts and Holothurian sclerites from the Upper Permian and Triassic of the Bükk mountains (North Hungary). *Acta Mineralogica Petrographica, Szeged*, 23(1), pp.109-126.
- Kump, L.R., Pavlov, A. and Arthur, M.A., 2005. Massive release of hydrogen sulfide to the surface ocean and atmosphere during intervals of oceanic anoxia. *Geology*, 33(5), pp.397-400.
- McCallum, M.L., 2015. Vertebrate biodiversity losses point to a sixth mass extinction. *Biodiversity and Conservation*, 24(10), pp.2497-2519.
- McGhee Jr, G.R., Clapham, M.E., Sheehan, P.M., Bottjer, D.J. and Droser, M.L., 2013. A new ecological-severity ranking of major Phanerozoic biodiversity crises. *Palaeogeography, Palaeoclimatology, Palaeoecology*, 370, pp.260-270.
- Nishikane, Y., Kaiho, K., Henderson, C.M., Takahashi, S. and Suzuki, N., 2014. Guadalupian–Lopingian conodont and carbon isotope stratigraphies of a deep chert sequence in Japan. *Palaeogeography, Palaeoclimatology, Palaeoecology*, 403, pp.16-29.
- Payne, J.L. and Clapham, M.E., 2012. End-Permian mass extinction in the oceans: an ancient analog for the twenty-first century? *Annual Review of Earth and Planetary Sciences*, 40, pp.89-111.
- Payne, J.L. and Finnegan, S., 2007. The effect of geographic range on extinction risk during background and mass extinction. *Proceedings of the National Academy of Sciences*, 104(25), pp.10506-10511.
- Rampino, M.R. and Shen, S.Z., 2021. The end-Guadalupian (259.8 Ma) biodiversity crisis: the sixth major mass extinction? *Historical Biology*, 33(5), pp.716-722.
- Raup, D.M. and Sepkoski Jr, J.J., 1982. Mass extinctions in the marine fossil record. *Science*, 215(4539), pp.1501-1503.
- Raup, D.M., 1986. Biological extinction in Earth history. *Science*, 231(4745), pp.1528-1533.
- Raup, D.M., 1994. The role of extinction in evolution. *Proceedings of the National Academy of Sciences*, 91(15), pp.6758-6763.
- Ryskin, G., 2003. Methane-driven oceanic eruptions and mass extinctions. *Geology*, 31(9), pp.741-744.
- Şengör, A.C. and Atayman, S., 2009. The Permian extinction and the Tethys: an exercise in global geology.
- Sepkoski Jr, J.J., 1989. Periodicity in extinction and the problem of catastrophism in the history of life. *Journal of the Geological Society*, 146(1), pp.7-19.
- Sepkoski Jr, J.J., 1990. The taxonomic structure of periodic extinction. *Geological Society of America Special Paper*, 247, pp.33-44.

- Sepkoski Jr, J.J., 1996. Patterns of Phanerozoic extinction: a perspective from global databases. In *Global Events and Event Stratigraphy in the Phanerozoic: Results of the International Interdisciplinary Cooperation in the IGCP-Project 216 "Global Biological Events in Earth History"* (pp. 35-51). Berlin, Heidelberg: Springer Berlin Heidelberg.
- Shen, J., Chen, J., Algeo, T.J., Feng, Q., Yu, J., Xu, Y.G., Xu, G., Lei, Y., Planavsky, N.J. and Xie, S., 2021. Mercury fluxes record regional volcanism in the South China craton prior to the end-Permian mass extinction. *Geology*, 49(4), pp.452-456.
- Shen, S. and Shi, G.R., 1996. Diversity and extinction patterns of Permian Brachiopoda of South China. *Historical Biology*, 12(2), pp.93-110.
- Shen, S.Z., Crowley, J.L., Wang, Y., Bowring, S.A., Erwin, D.H., Sadler, P.M., Cao, C.Q., Rothman, D.H., Henderson, C.M., Ramezani, J. and Zhang, H., 2011. Calibrating the end-Permian mass extinction. *Science*, 334(6061), pp.1367-1372.
- Shen, S.Z., Xie, J.F., Zhang, H. and Shi, G.R., 2009. Roadian–Wordian (Guadalupian, middle Permian) global palaeobiogeography of brachiopods. *Global and Planetary Change*, 65(3-4), pp.166-181.
- Stanley, S.M. and Yang, X., 1994. A double mass extinction at the end of the Paleozoic Era. *Science*, 266(5189), pp.1340-1344.
- Stanley, S.M., 2016. Estimates of the magnitudes of major marine mass extinctions in Earth history. *Proceedings of the National Academy of Sciences*, 113(42), pp. E6325-E6334.
- Tennant, J.P., Mannion, P.D., Upchurch, P., Sutton, M.D. and Price, G.D., 2017. Biotic and environmental dynamics through the Late Jurassic–Early Cretaceous transition: evidence for protracted faunal and ecological turnover. *Biological Reviews*, 92(2), pp.776-814.
- Twitchett, R.J., Looy, C.V., Morante, R., Visscher, H. and Wignall, P.B., 2001. Rapid and synchronous collapse of marine and terrestrial ecosystems during the end-Permian biotic crisis. *Geology*, 29(4), pp.351-354.
- Wang, W., Cao, C. and Wang, Y., 2004. The carbon isotope excursion on GSSP candidate section of Lopingian–Guadalupian boundary. *Earth and Planetary Science Letters*, 220(1-2), pp.57-67.
- Ward, P.D., Botha, J., Buick, R., De Kock, M.O., Erwin, D.H., Garrison, G.H., Kirschvink, J.L. and Smith, R., 2005. Abrupt and gradual extinction among Late Permian land vertebrates in the Karoo Basin, South Africa. *Science*, 307(5710), pp.709-714.
- Wei, H., Tang, Z., Qiu, Z., Yan, D. and Bai, M., 2020. Formation of large carbonate concretions in black cherts in the Gufeng Formation (Guadalupian) at Enshi, South China. *Geobiology*, 18(1), pp.14-30.
- Wignall, P.B., 2015. *The Worst of Times: How life on Earth survived eighty million years of extinctions*. Princeton University Press.

Wignall, P.B., Sun, Y., Bond, D.P., Izon, G., Newton, R.J., Védérine, S., Widdowson, M., Ali, J.R., Lai, X., Jiang, H. and Cope, H., 2009. Volcanism, mass extinction, and carbon isotope fluctuations in the Middle Permian of China. *science*, 324(5931), pp.1179-1182.

Zhang, Y. and Kling, G.W., 2006. Dynamics of lake eruptions and possible ocean eruptions *Annual Review of Earth and Planetary Sciences*, 34, pp.293-324.

CHAPTER 2

Iranian Permian geological setting: overview and selected sections

2.1. INTRODUCTION.....	16
2.2. PERMIAN OF IRAN.....	19
2.3. GLB THEORY IN IRAN.....	24
2.3.1. STRATIGRAPHIC APPROACH AND CANDIDATE SECTIONS FOR	26
2.3.1.1. ALI-BASHI SECTION.....	27
2.3.1.1.1. HISTORICAL BACKGROUND	30
2.3.1.1.2. LITHOSTRATIGRAPHY PERSPECTIVE.....	31
2.3.2.1. BAGH-E-VANG SECTION	39
2.3.2.1.2. HISTORICAL BACKGROUND	41
2.3.2.1.2. LITHOSTRATIGRAPHY PERSPECTIVE.....	42
2.3.3.1. BAGHUK SECTION	49
2.3.3.1.2. HISTORICAL BACKGROUND	49
2.4 REFERENCES	52

2.1. INTRODUCTION

Iran's extended deformed zone is surrounded by the Epi-Versican Turan Platform to the NE, which is part of stable Eurasia, and by the Arabian Plate to the Southwest. The Iranian geology is dominated by the long-standing convergence history between Eurasia and Gondwanan-derived terranes as indicated by numerous ophiolitic belts, fold-and-thrust belts and resistant blocks that remain within the deformation zone (Robert et al. 2014). Two major compressional events, as a consequence of oceanic closures, are described in Iran: (1) the Early Cimmerian orogeny, which is related to the closure of the Paleotethys Ocean, and (2) the Alpine orogeny as a result of the closure of the Neotethys Ocean (Robert et al. 2014). In northeastern Iran, the Paleotethys Ocean separated the Eurasian Plate from the Central Iranian blocks, whereas the Neotethys Ocean opened on the southern margin of the Central Iranian blocks during the Permian (Muttoni et al., 2009a). The Iran Plate and Afghan Block were adjoining parts of the narrow, North-drifting Cimmerian continent collage (Sengor et al., 1988) that closed the Palaeotethys, collided with Eurasia and created the Cimmerian Mountain Chain (Sengor 1984, 1990; Wilmsen et al. 2009) (fig. 2.1).

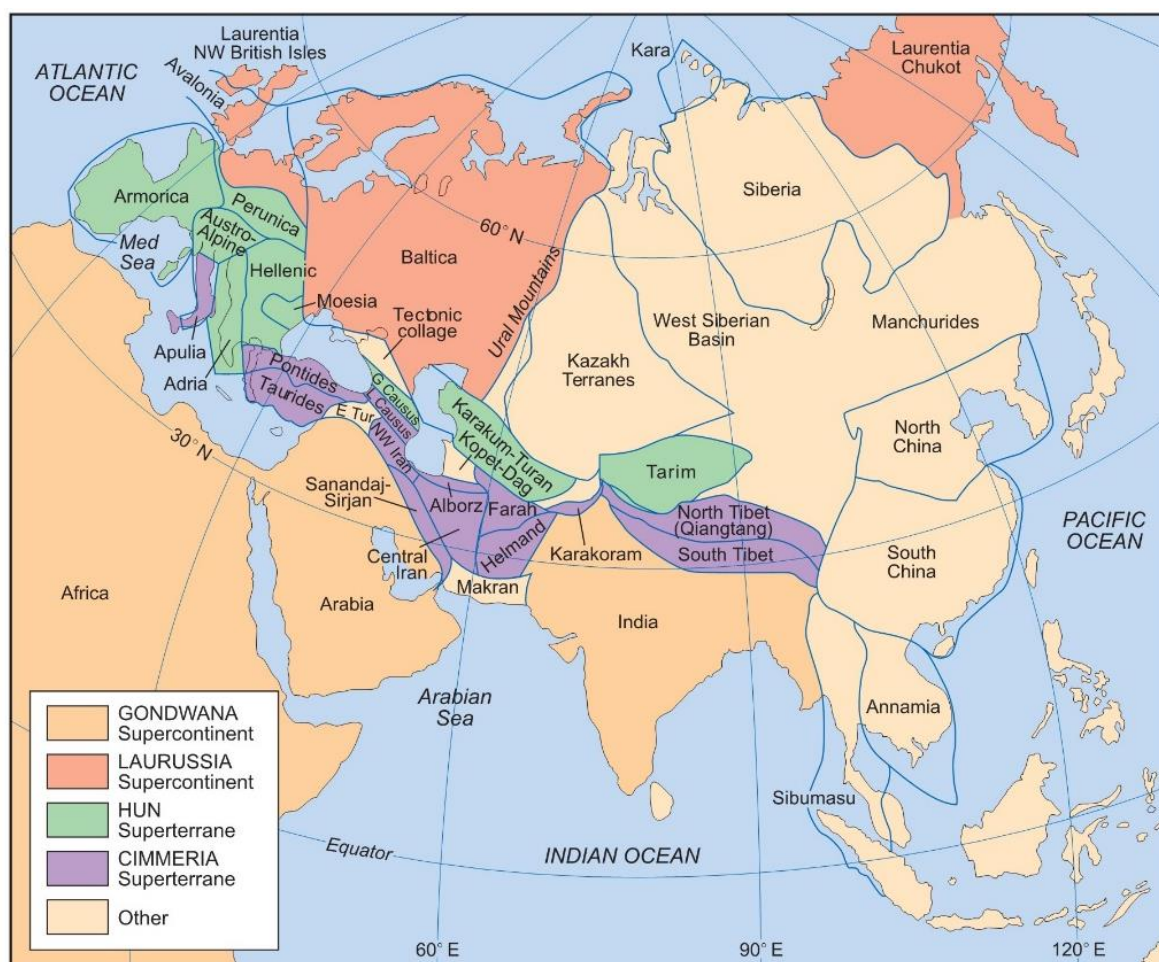


Fig. 2.1.

Fig. 2.1. The majority of the plates and terranes discussed in this review are shown after [Torsvik & Cocks \(2004\)](#). The NW British Isles and the Chukot Peninsula in Russia, the Laurentia Supercontinent included North America and Greenland and Laurentia later collided with Baltica and Avalonia to form the Laurussia Supercontinent. In addition, Arabia, Africa and India, the Gondwana Supercontinent included Antarctica, Australia and Madagascar. Also shown are terranes that may have been part of the Hun and Cimmeria Superterrane. Note that Karakoram in north Pakistan is Cimmerian and different from the Hunic Karakum-Turan terrane ([Ruban et al. 2007](#)).

The timing of the Eo-Cimmerian orogeny, however, has remained controversial, comprising an interval of a few tens of ma, ranging from the late Middle Triassic (e.g., [Saidi et al. 1997](#)), late Carnian–Norian (e.g., [Alavi et al. 1997](#); [Stampfli & Borel 2002](#); [Horton et al. 2008](#)) to the (early) Lias (e.g., [Stocklin 1974](#); [Boulin 1988](#)). The position of the Palaeotethys suture is inferred to lie north of the present-day Alborz Mountains and to continue east–southeastwards between the Koppeh Dagh and the Binalud Mountains into northern Afghanistan ([Stocklin 1974](#); [Berberian & King 1981](#); [Boulin 1988](#); [Alavi 1991, 1996](#); [Alavi et al. 1997](#); [Zanchi et al. 2006, 2009](#); [Wilmsen et al. 2009ab](#)).

In the present-day context of Earth's geological composition, the geographical area recognized as Iran displays a distinctive arrangement where numerous distinct tectonic segments coexist. According to [Stocklin \(1968, 1977\)](#) and [Nabavi \(1976\)](#), Iran can be classified into ten main structural zones: Makran, the Lut Block, Eastern Iran, Kopet Dagh, the Alborz Mountains, the Central Iran Block, the Urumieh-Dokhtar Zone, the Sanandaj-Sirjan zone, the Zagros fold belt, and the Khuzestan plain. Typically, the boundaries of these units are delineated by faults or, in certain instances, tectonic depressions ([Nabavi 1976](#)) (**fig. 2.2**).

The Zagros orogenic belt is formed by the three tectonically linked parallel zones of the Urumieh-Dokhtar magmatic assemblage, the Sanandaj-Sirjan zone, and the Zagros simply folded belt. This orogenic belt stretches from northeast to southwest across Iran and is part of the Alpine-Himalayan orogenic and metallogenic belt. Spanning approximately 2000 km in a northwest-southeast direction, it extends from the East Anatolian Fault in eastern Turkey to the Oman Line in southern Iran ([Alavi 1994](#)). During the extensive stretch of the Paleozoic, the contiguous territories of Northern and Central Iran were engaged in a mutual and interconnected geological narrative ([Angiolini et al. 2007](#)).

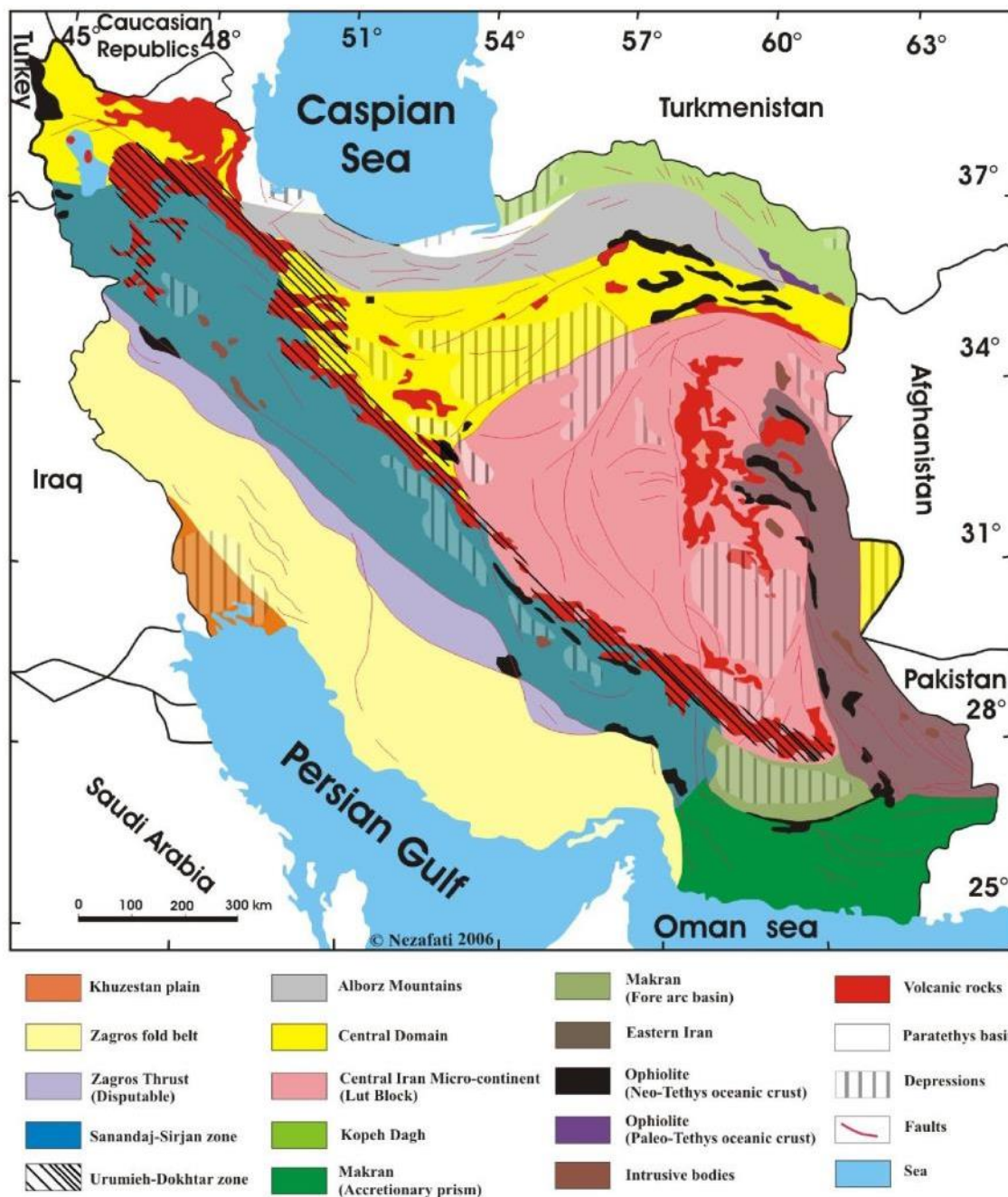


Fig. 2.2. Major geological subdivisions of Iran modified by Nezafati (2006) after Stöcklin (1968, 1977); Nabavi (1976) and publications of the Geological Survey of Iran.

In the Paleozoic Earth's history witnessed a convergence of geological processes that intricately linked these two regions in their developmental trajectories. Angiolini et al. (2007) work, provides valuable insights into this shared evolution, serving as a cornerstone for our understanding of the geological dynamics that unfolded during this epoch. This shared evolution is marked by a notable continuity of Paleozoic sedimentary rock deposits and a consistent distribution of biota (Berberian & King 1981; Leven & Gorgij 2006).

The Sanandaj-Sirjan zone, characterized by its metamorphic nature, exhibits an affinity with Central Iran (Rashidnejad-Omran et al. 2002), while the Zagros belt is geologically linked to the Arabian region (Angiolini et al. 2007). Stöcklin et al. (1974) positioned Northern and Central Iran along the Arabian margin during the Paleozoic era, based on their conclusions on multiple lines of evidence. These include the effects of the Pan-African orogeny on the pre-Paleozoic basement, continuous sedimentary rock sequences from Precambrian to Cambrian between Arabia and Northern/Central Iran, and the absence of Variscan deformation. To reconstruct a broader paleogeographic context, Angiolini et al. (2007) employed selected Late Carboniferous - Early Permian paleomagnetic data to position Iran. These data support a configuration known as Pangea B, as proposed by Irving (1977, 2005); Muttoni et al. (1996, 2003) and Torcq et al. (1997). Muttoni et al. (2003) extend this configuration into the Early Permian, transitioning into a Wegenerian form of Pangea A during the Late Permian - Early Triassic (fig. 2.3). This transformation involves a substantial dextral motion of Laurasia relative to Gondwana, spanning over ≥ 3000 km and occurring primarily along the Variscan suture (Vuolo, 2014).

2.2. PERMIAN OF IRAN

The outcrop of Permian deposits in Iran extended throughout the country and is related to the Hercynian orogeny (Stocklin 1968). The regions encompassing Central Iran, Alborz, Sanandaj-Sirjan, and Lut provinces were unified with Africa as a contiguous and extensive landmass known as the Iran Platform. This connection in the Permian is substantiated by their comparable lithological and sedimentological characteristics to the Zagros Province (Stocklin 1968; Berberian & King 1981; Davoudzadeh & Schmidt, 1984; Heydari et al., 2003). Through the Late Palaeozoic, several Gondwanan terrains, including Sanandaj-Sirjan terrain, Alborz, and Central Iran, broke off the eastern Gondwanan margin due to the Permian Neo-Tethyan opening (Stampfli & Borel 2002, 2004; Angiolini & Carabelli 2010) and moved together with other Cimmerian blocks northward to the equator (Sengör 1979; Stampfli et al. 1991, Stampfli & Borel 2002). Collision with the Eurasian active margin was the result of this movement in the Late Triassic (Stampfli & Borel 2002) which led to their suturing and the formation of mid-ocean ridge basalt (MORB) (Stampfli et al. 1991, Stampfli & Borel 2002) and the closure of an

oceanic basin in the south-western part of Iran (e.g., Stampfli et al. 1991; Angiolini et al. 2000) (figs. 2.1, 2.3).

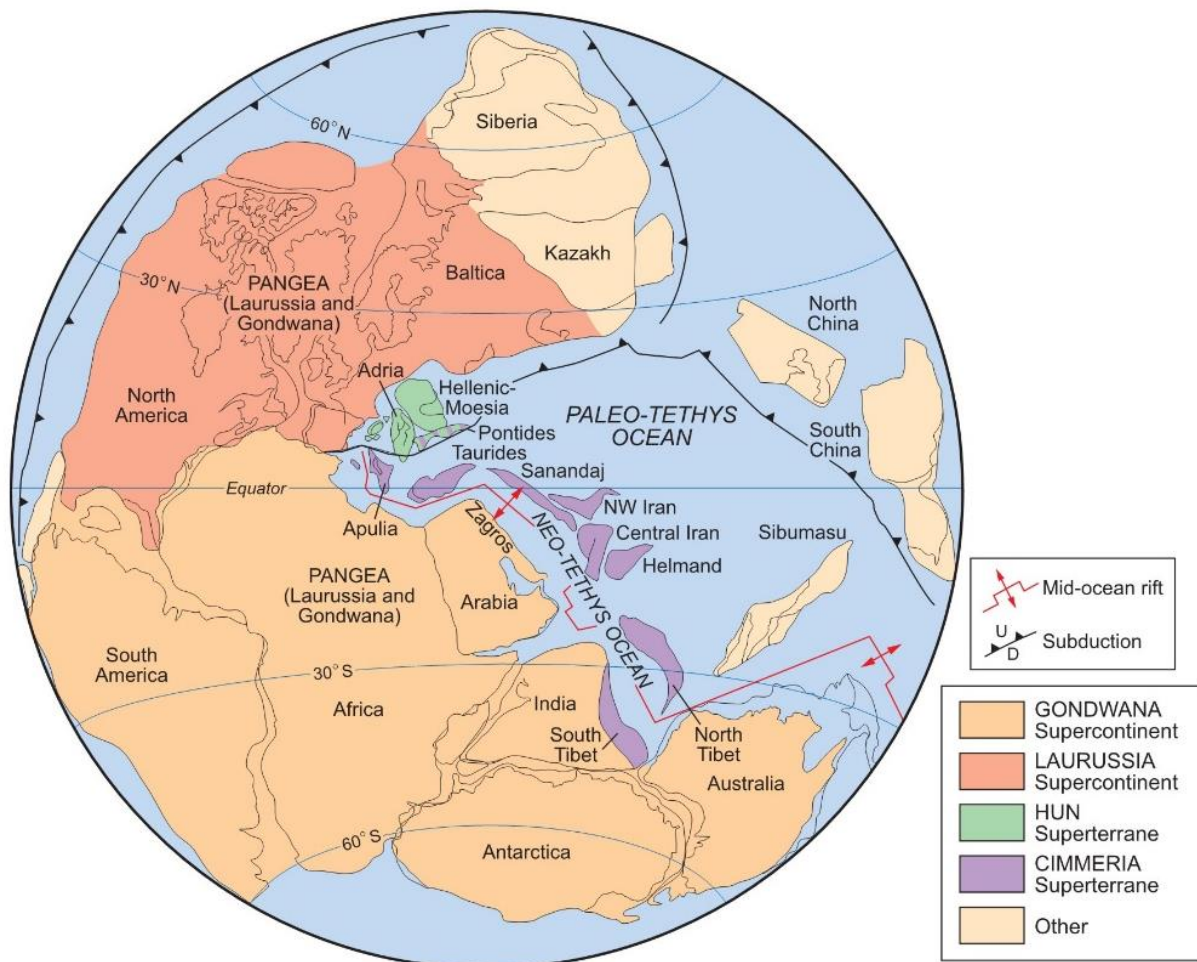


Fig. 2.3. Plate-tectonic reconstruction of the late Permian (Lopingian). In the middle Permian - Triassic the Cimmerian Super-terrane broke away from Gondwana, now part of the Pangea Supercontinent (Gondwana and Laurussia supercontinents, as well as Kazakh, Siberia and other terranes (Ruban et al., 2007).

Kalvoda (2002) proposed that the Alborz terrane was a part of the Late Palaeozoic Laurussia Supercontinent. Angiolini & Stephenson (cited in Ruban et al. 2007), based on a reexamination of Early Permian (Asselian - Early Sakmarian) brachiopods of the Lower Permian Dorud Formation in the Alborz Mountains and a new study of palynomorphs from the same formation, similarly concluded that there is little affinity with Gondwana and the peri-Gondwanan region. Brachiopod fauna data shows affinities with those of Baltica (Urals and of the Russian Platform), and to a lesser extent to the Trogkofel Limestone (Carnic Alps) in the west. In contrast, the palynomorph assemblage is entirely dissimilar from those

recorded from the Asselian - Sakmarian *Granulatisporites confluens* Biozone, which is ubiquitous in the Gondwana region. Also, [Angiolini cited in Ruban et al. \(2007\)](#) concluded that the Alborz, Northwest and Central Iran remained adjacent to one another throughout most of the Palaeozoic. This is reflected by the continuity and common evolution of their Palaeozoic sedimentary rocks and uniform distribution of biota.

Before the Late Permian, the Sanandaj-Sirjan terrane (SST) was linked to the Zagros Mountains and the Arabian Plate ([fig. 2.3](#)). This position stayed stable until its break off as part of the Cimmeria in the Mid-Permian-Triassic ([Berberian & King 1981](#); [Sengör 1990](#); [Grabowski & Norton 1995](#); [Stampfli et al. 2001](#); [Sharland et al. 2004](#); [Scotese 2004](#) and [Ruban et al. 2007](#)). SST occupied approximately the same position since more than 250 My up today ([fig. 2.4](#)) and was adjacent to the Zagros suture in the Palaeozoic era ([Ruban et al. 2007](#)). Additionally, [Stampfli & Borel \(2002\)](#) showed that in the Late Permian, SST as part of the Cimmerian microcontinent and Northwest of Iran, was positioned at the northern margin of SST. Besides, in this period, as a result of the opening of the Neo-Tethys Ocean the Cimmerian microcontinent drifted from Gondwana towards the north and consequently was set near the Equator between the Neo-Tethys and Paleo-Tethys Oceans ([Stampfli & Borel, 2002, 2004](#); [Muttoni et al. 2009ab](#)) ([figs. 2.1-2.5](#)).

Central Iran by [Sengör \(1990\)](#) divided into the Lut, Tabas and Yazd blocks. However, according to [Stampfli & Borel \(2002\)](#), [Von Raumer et al. \(2003\)](#), [Torsvik & Cocks \(2004\)](#), [Scotese \(2004\)](#) and [Golonka \(2004\)](#) Central Iran and Lut are synonyms. [Stampfli et al. \(2001\)](#) mentioned that there were two neighboring terranes: Central Iran and Lut, or Yazd and Lut.

The Zagros Mountains region in southwest Iran forms a part of the Miocene-Pliocene collision zone between the Arabian and Eurasian plates and this region was a part of the Arabian Plate from the late Neoproterozoic to the present-day ([Berberian & King 1981](#); [Sepehr & Cosgrove 2004](#) and [Ruban et al. 2007](#)).

During the Permian-Triassic, the opening of the Neo-Tethys Ocean along the Zagros Suture Zone was accompanied by normal faulting and horsts and graben systems ([Sepehr & Cosgrove 2004](#)) ([figs. 2.3, 2.5](#)). Also, South of the Zagros Mountains, the Makran region in Iran and Pakistan contains the Inner Makran ophiolites and the Cenozoic Makran and Saravan accretionary prisms ([McCall 2002](#); [2003](#)).

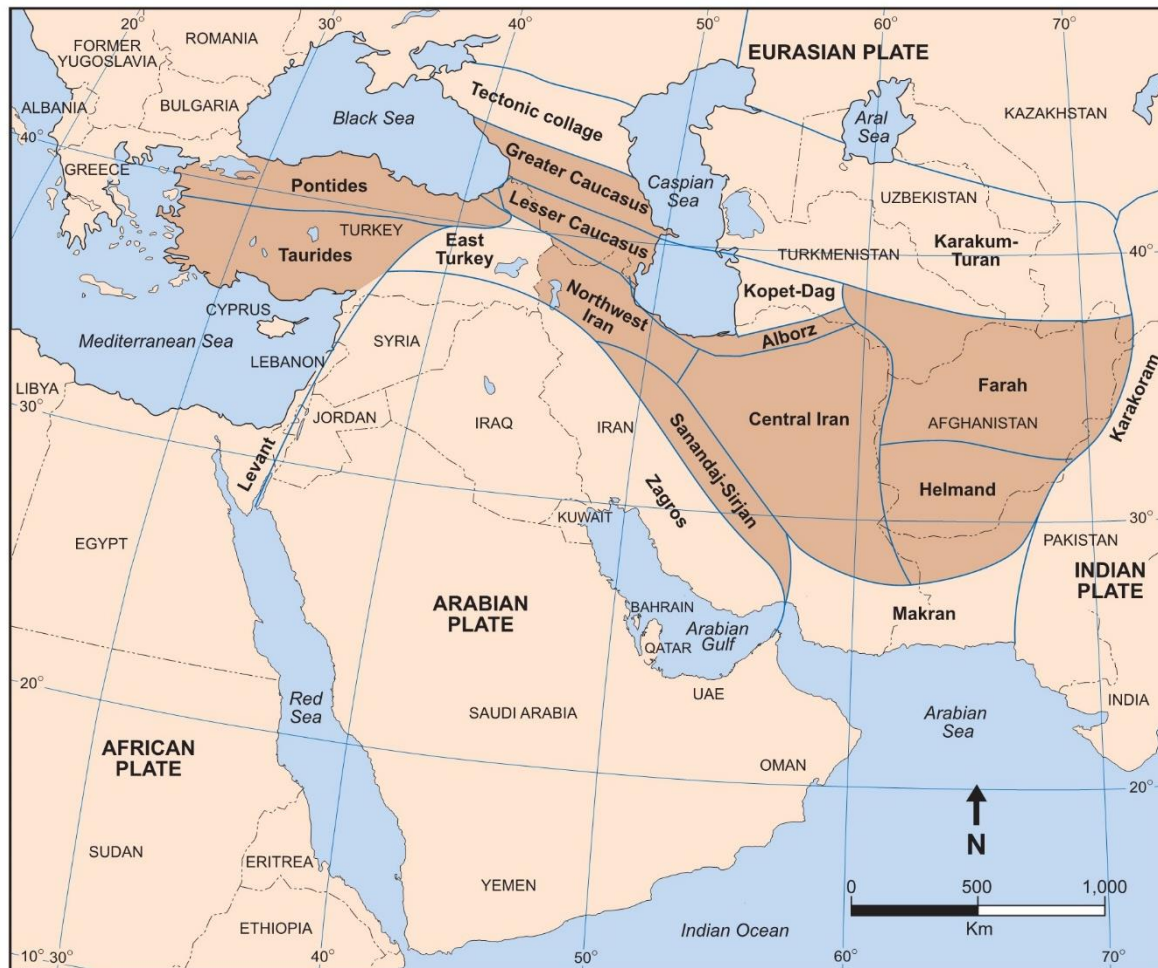


Fig. 2.4. The Middle East region consists of the present-day Arabian and Levant plates and numerous terranes (individual boundaries are shown in blue). During the Paleozoic ten large terranes are variably interpreted to have been adjacent to the Arabian and Levant plates (then attached to Gondwana and later Pangea). The Paleozoic Middle East terranes (colored brown) include Helmand and Farah (Afghanistan, southwest Pakistan and southeast Turkmenistan); Iran's Alborz, Northwest Iran, Sanandaj-Sirjan and Central Iran; Turkey's Pontides and Taurides; and the Greater and Lesser Caucasus between the Caspian and Black seas (Armenia, Azerbaijan, Georgia and southwest Russia). The Makran and East Turkey regions may have a Paleozoic core or could have formed as Mesozoic accretionary terranes (Ruban et al. 2007).

This region is associated with the NE-directed subduction of the Gulf of Oman oceanic crust (a remnant of the Neo-Tethys Ocean) beneath Iran. The Makran core may have amalgamated with Central Iran and Sanandaj-Sirjan during the Triassic (McCall 2003). Therefore, Makran may have formed a part of Mesozoic Cimmeria (Ruban et al. 2007).

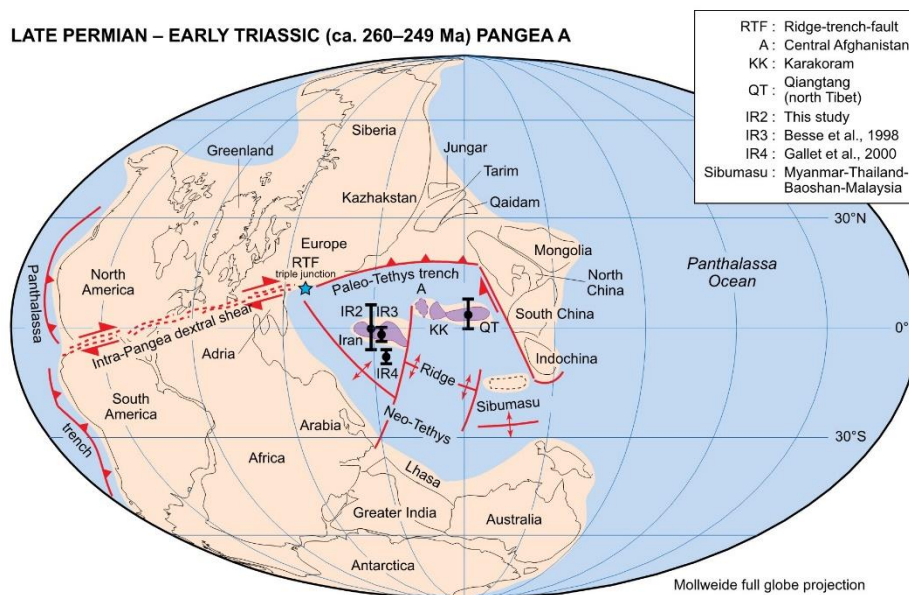


Fig. 2.5. Paleogeographic reconstruction of Pangea undergoing transformation from Pangea B to Pangea A during the Early Permian; reconstruction based on paleomagnetic poles from Table 3. The star to the northeast of Adria indicates the hypothetical location of a ridge-trench-fault (RTF) triple junction adjoining the Gondwana, Laurasia, and Paleo-Tethys plates (Muttoni et al. 2009).

Some of the most important studies on the Permian of Iran could be noted as works by Stepanov et al. (1969); Teichert et al. (1973); Partoazar (2002); Korte et al. (2004); Korte & Kozur (2005); Kozur (2004, 2005); Shabanian & Bagheri (2008); Ghaderi et al. (2013, 2014a, b, 2016); Leda et al. (2014); Korn et al. (2016, 2019, 2021); Schobben et al. (2016, 2017); Arefifars (2017; 2020); Kiessling et al. (2018); Gliwa et al. (2020, 2021); Ghanizadeh-Tabrizi et al. (2021); Arefifard (2020); Heuer et al. (2021); Arefifard & Baud (2022); and Mohammadi et al. (2023). Despite remarkable insights given in these publications, a crucial juncture remains uncharted: the status of the Guadalupian-Lopingian Boundary (GLB) in the Iranian context. The **fig. 2.6** presents the different formations of the Permian in Iran. While these scholarly contributions have propelled our understanding of Iran's Permian period to new heights, a compelling avenue for future research emerges. The quest to discern the GLB's status within Iran's Permian successions beckons as a tantalizing challenge, inviting geologists to embark on detailed sampling and analysis. By bridging this empirical gap, a more comprehensive and nuanced understanding of Iran's Permian geological narrative and its intricate connections to global geological events promises to emerge.

System	Subsystem	Series	Stage	Alborz	Yazd Block (Anarak, study area)	Tabas (Zaladou, Bage-Vang)	Kalmard Block	Sanandaj- Sirjan Zone	Zagros
				Permian	Lopingian	Changansingian			
Wuchiapingian	Nesen Fm.						Hambast Fm.		
Guadalupian	Capitanian	Ruteh Fm.	Jamal Fm.		Jamal Fm.	Hermes Fm.	Abadeh Fm.		Dalan Fm.
	Wordian								
	Rodain						Surmag Fm.		
Cisuralian	Kungurian				Bage-Vang Fm.		Sartakht Fm.		Faraghan Fm.
	Artinskian	Unnamed Fm.							
	Sakmarian	Shah Zied	Tighe- Maadanou Fm.		Tighe- Maadanou Fm.	Chili Fm.			
		Emarat Fm.					Vazhnan Fm.		
	Asselian								

Fig. 2.6. Permian strata in different regions of Iran following Leven & Gorgij (2011) and Wang et al. (2018).

2.3. GLB THEORY IN IRAN

The location of the GLB has always been subject to disagreement. According to Stepanov et al. (1969), the GLB in northwestern Iran lies between the B and C units (fig. 2.7) or for Partoazar, (2002) this boundary is drawn between the Surmagh formation and the formation of Julfa. In addition, as reported by Taraz et al. (1981) the transition from Guadalupian to Lopingian in Hambast Mountain north of Abadeh region (Central Iran) occurred between 3 units and 4 units. Partoazar (2002) considers this point to be between units 6 and 7 (fig. 2.7). It is clear that these two ideas are established by the concepts of lithological and less related biostratigraphic divisions and central Iran suffered so much with the same story and with a different formation. It should be emphasized that forming stratigraphic types, these strata change position over time by Iranian geologists. For example, Partoazar (2002) B and C unit upgrade mentioned by Stepanov et al. (1969) in northwestern Iran from the unit to the Surmag and Julfa Formations or in central Iran C units, considered the Abadeh Formation by Partoazar (2002) (fig. 2.7).

NORTHWEST OF IRAN										CENTRAL IRAN																			
Stepanov et al. 1969			Teichert et al. 1973			Partoazar 2002			Ghaderi 2014 Ghaderi et al. 2014 Ghaderi et al. 2016			Partoazar 2002 Taraz et al. 1981																	
Induan (Early Triassic)	Unit G	Lower Elikah Formation	Claraia Beds	Claraia Beds	Elikah Formation	Induan	Elikah Formation	Unit E	Claraia Beds	Early Induan	Elikah Formation	Claraia Beds	Induan	Lower Triassic	Unit a	Claraia Beds	Early Induan												
	Unit F	Paratirolites Limestone	Paratirolites															Paratirolites	Ali-Bashi Formation	Unit D	Ammonite Zone	Changhsingian	Ali-Bashi Formation	Zai member	Changhsingian	Hambast Formation	Unit 7	Unit 10	Changhsingian
	Unit E	P-T Transitional Beds	Bernhardtites Dzhulfites Tomophoceras Phisonites-Comelicania															Shevrevites Dzhulfites Iranites Phisonites											
Lop. Wuchiapingian	Unit D	Upper Julfa Beds	Haydenella-Pseudowellerella	Julfa Beds	Julfa Formation	Lop. Wuchiapingian	Unit C	Brachiopod Zone	Late Lop. Wuchiapingian	Julfa Formation	Upper Julfa Beds	Loplingian	Abadeh Formation	Unit 6	Unit 9	Late Lop. Wuchiapingian													
	Unit C	Lower Julfa Beds	Pseudogastriceras-Permophricodothyris Araxilevis-Orthotetina Codonofusiella														Shammar Mem.(B) Selgord Mem. (A)	Early Lop. Wuchiapingian	Lower Julfa Beds	Unit 5	Unit 8	Early Lop. Wuchiapingian							
Guadalupian	Unit B	Khachik Beds	Khachik Beds	Khachik Beds	Guadalupian	Guadalupian	Surmaq Formation	Guadalupian	Guadalupian	Khachik Formation	Codonofusiella Limestone	Lopingian	Surmaq Formation	Unit 3	Unit 6	Guadalupian													
	Unit A	Gnishik Beds															Gnishik Beds	Unit 2	Unit 5										
														Upper part of Unit 1	Unit 4														

Fig. 2.7. Historical background of the Guadalupian – Lopingian successions in the northwest of Iran; from Stepanov et al. (1969), Teichert et al. (1973), Partoazar (2002), Ghaderi (2014) and Ghaderi et al. (2014 ab, 2016).

Taraz (1969, 1974), separated the Permian sedimentary sequence in the Abadeh area (Hambast mountain) into seven units (named units 1 to 7) and the Permian units were later assigned to three formations (Taraz et al. 1981), the Surmaq, Abadeh and Hambast formations in ascending order. Also, the strata in the Hambast mountain can serve as a standard for the Central Iranian sections of the Permian–Triassic transition (Heuer et al. 2022) and the Late Permian Hambast Formation has a thickness of approximately 35 m at the type locality (Kuh-e-Hambast) and consists almost entirely of platy and nodular limestone beds (Taraz et al. 1981).

Based on Arefifard (2017), the GLB is located in the middle part of the Jamal Formation in the Bagh-e-Vang section. Accordingly, rare fusulinids in this section, suggest the age of Roadian to lower Capitanian for the Jamal Formation lower part, without demonstrations of the stage boundaries. Jamal Formation upper part of this report lithostratigraphically consists of cream to brown thick-bedded to massive dolomitic limestone. Moreover, its uppermost part is non-

fossiliferous medium-bedded brownish dolomite with the age of Late Permian, probably Wuchiapingian, based on its foraminiferal contents.

Despite the many efforts made in this study to determine the exact age of the Jamal Formation, there are still uncertainties. For example, the presence of index foraminifera in this section is rare, while the basis of Permian biostratigraphy and the index cosmopolitan fossil in this period are conodonts and ammonoids (e.g., [Li et al. 2022](#)), while no trace of them is not mentioned in this report. Also, the location of the GLB is unknown in this section and many other stratigraphic sections in Iran.

[Ghobadipour & Jafarian \(2006\)](#), with a focus on Permian strata of Central Iran in the Chah-e-Riseh section and according to the Foraminiferal content, didn't show the GLB and just reported the age of Late Wordian–Early Wuchiapingian (Late Murghabian–Early Djulfian) for the section. In Zagros Mountain, the Dalan Formation is known as one of the candidates for investigation of the Permian rocks, however, the stage boundaries are also not clear and determined precisely, there.

In the geographically enclosed regions of western and northwestern Iran, specifically located at the northwestern extremity of the Alborz Range, the conodonts that serve as markers for the GLB zone remain unidentified. Presently, these markers are absent, but there is a positive outlook that they will be discovered in the ongoing research.

This faunal absence is due to the shallow paleoenvironment and inappropriate conditions for living the conodonts ([Clark & Hatleberg 1983](#); [Ghaderi 2014](#); [Leonhard et al. 2021](#)). On the other hand, the Permian successions hold a notably rich foraminiferal content, prompting us to seek the boundary based on these collections. The primary locations identified for tracking the GLB are the Julfa Region (Western Alborz-NW Iran Terrane), Tabas Region (Tabas Block, Central Iran); Abadeh Region (Northern Margin of Sanandaj-Sirjan Zone) and Alborz Range (Elikah Valley and Southern Amol).

2.3.1. STRATIGRAPHIC APPROACH AND SECTIONS FOR GLB IRAN

As mentioned, the Permian strata of Iran offer sections that could potentially elucidate the GLB's location. Among the numerous sections investigated, three specific regions Julfa, Tabas, and Abadeh have been chosen for focused study within this project.

These regions were selected after careful consideration and evaluation, as they present promising opportunities to shed light on the dynamics of the GLB in Iran's geological context, The **Ali-Bashi section** located in the Julfa area, the **Bagh-e-Vang section** situated in the northern part of the Tabas area, and the **Baghuk section** in the north of Abadeh (fig. 2.8).

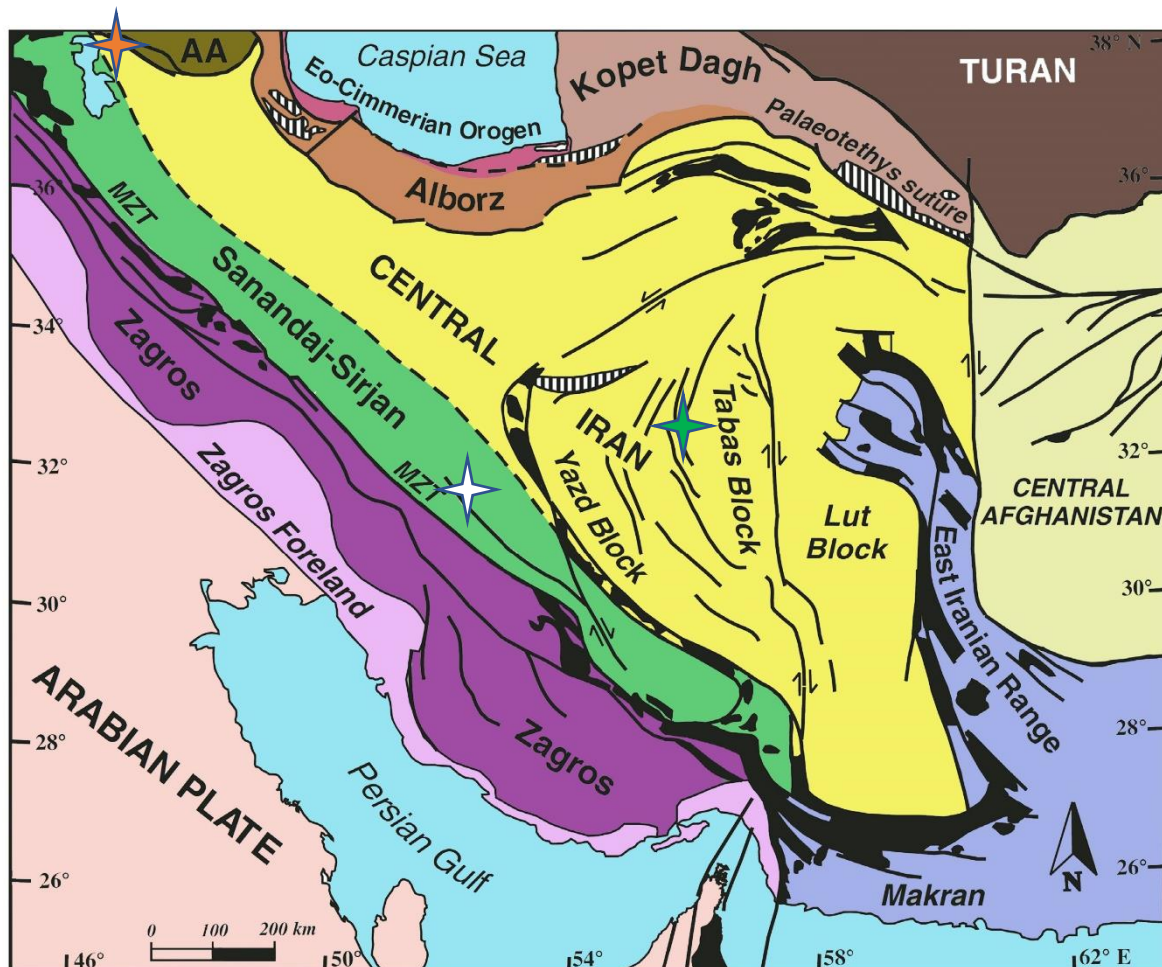


Fig. 2.8. Iran's tectonic illustration (adapted from Angiolini et al. 2007 and Vuolo 2014). Solid black lines represent Mesozoic ophiolites along the Main Zagros Thrust (MZT) and surrounding Central Iran. Shaded areas indicate ophiolites and metamorphic rocks associated with the Cimmerian orogeny. The Astar-Adzerbaijan (AA) block is also denoted. Distinctive colored polygons indicating the position of each section are designated: orange for Ali-Bashi, green for Bagh-e-Vang, and white for Baghuk section.

2.3.1.1. ALI-BASHI SECTION

The Ali-Bashi section (38.945°N , 45.510°E) is located in the Kuh-e-Ali Bashi region, approximately 9 km west of Julfa (as shown in fig. 2.9). This section finds its location in East Azerbaijan, and its geological positioning is indicated in the Iran geological catalog map

(Stocklin et al. 1965 and Alavi 1991), placing it within the northwest region of Iran and is in proximity to the Main Valley section mentioned by Ghaderi et al. (2014). Nestled within the Ali Bashi Mountains, this area offers a vantage point to observe sequences from the Permian to the Early Triassic. These sequences are observable on both the northern and southern banks of the Aras (Araxes) River, near the areas of Julfa in Nakhichevan (Azerbaijan) and Julfa in East Azerbaijan, Iran (figs. 2.8) and the detailed geographical coordinates of this section have been previously outlined in works by Stepanov et al. (1969), Teichert et al. (1973), Ghaderi et al. (2014b), Leda et al. (2014) and Ghaderi et al. 2016.

Julfa (= Julfa , Dzhulfi, or Culfa) is a small town in the south of the Aras River (also known as the Araks, Arax, Araxes, or Araz) and in the vicinity of Iran's border with the Nakhichevan Autonomous Republic. This region is located in the southern limit of the mountains which is called the Southern Caucasus (= Trans Caucasus, Transcaucasia, or Lesser Caucasus). Although the name Caucasus is not usually used for the southern mountains of Aras, there is no doubt that the major structural units of the Transcaucasia region continued in the south-southeast direction and spread from Aras Valley to East Azerbaijan province of Iran (Ghaderi 2014).

The Julfa-Mishudagh-Sahand-Takab region in Azerbaijan province displays distinctive geological characteristics. It features horsts containing small outcrops of Precambrian rocks, while Proterozoic-Early Palaeozoic sedimentary rocks are either scarce or incomplete (Ghaderi et al. 2016). Within the area, a Late Palaeozoic-Triassic platform sequence is well developed, though Jurassic rock occurrences are limited (Stepanov et al. 1969).

Cretaceous deposits exhibit flysch and carbonate facies are present, whereas volcanic-pyroclastic rocks are notably absent. This region demonstrates a rapid transition from volcanic rocks to Palaeogene sedimentary rocks from East to West (Ghaderi 2014). Extensive Neogene molasses rocks are widespread, accompanied by the prominence of shield-shaped volcanic mountains like Sahand, Ararat, and Aragats. The geological formations also exhibit relatively mild tectonic deformations, often manifesting as folded rocks (Mohammadi et al. 2023).

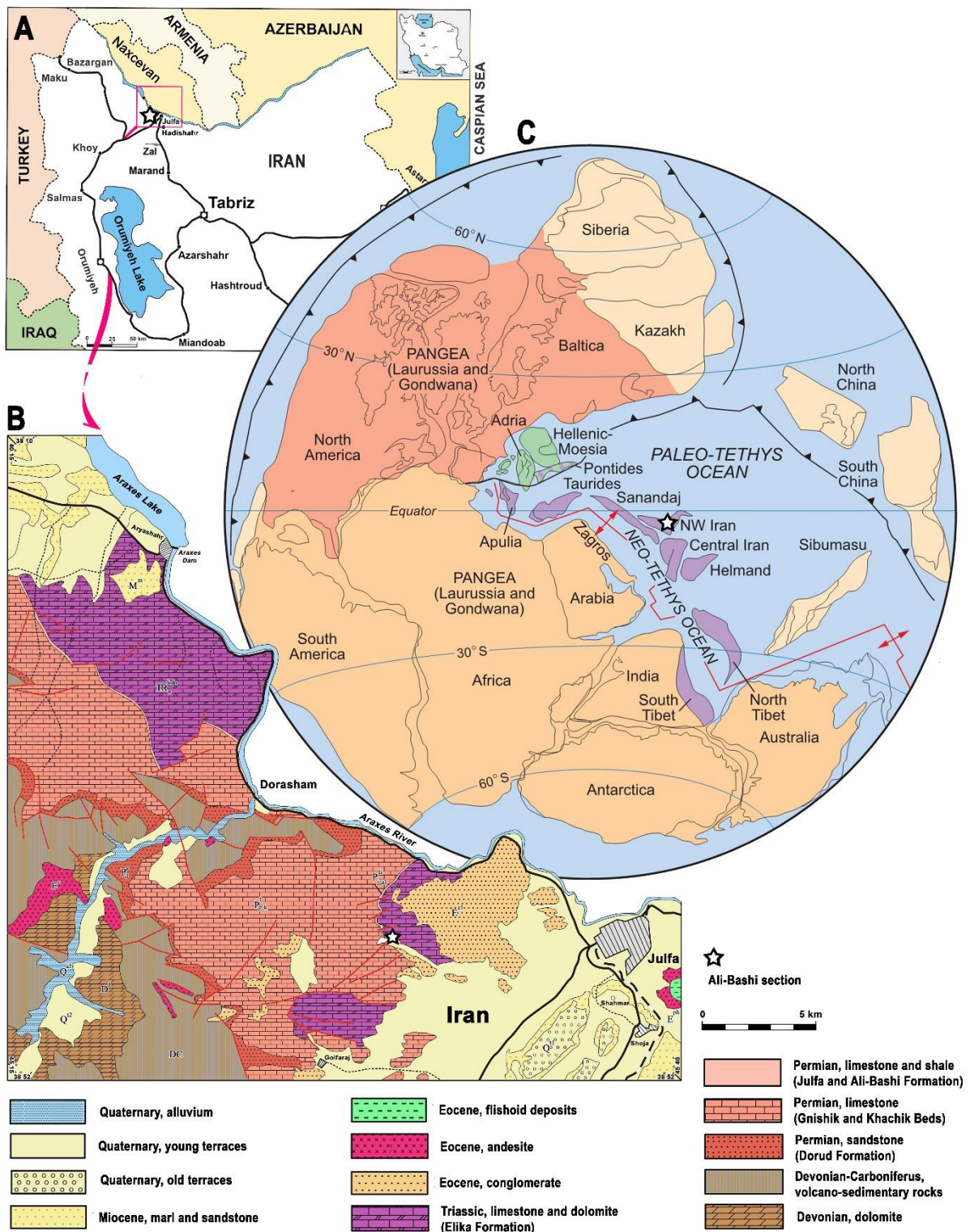


Fig. 2.9. A. location map of the study area in the northwest of Iran (from Ghaderi et al. 2016); B. Geologic map of the study area at the west of Julfa City; the Ali-Bashi section is marked with a white star (from Ghaderi 2014); C. Paleogeographical map of the Lopingian and location of the study area (white star) as a part of a Cimmerian block, close to the equator in the southern hemisphere (from Ruban et al. 2007).

2.3.1.1.1. HISTORICAL BACKGROUND

As far back as 1878, Abich documented various invertebrate fossils in Transcaucasia, from Early Carboniferous. He made these observations near the Araxes Gorge close to Dzhulfa in Armenia (now Nakhichevan, Azerbaijan). Further pioneering investigations were undertaken by Frech and von Arthaber in 1900. They introduced the term 'Djulfa-Schichten' to label these fossil-rich layers. Following this, in 1910, Stoyanov further categorized the Araxes section into 15 distinct lithological units. It was during this time that he also reported the first ammonoids discovered in the latest Permian *Paratirolites* Limestone (see more in Leda et al. 2014).

Stepanov et al. (1969) stand as pioneers in Permian studies in the northwest of Iran, laying the groundwork for all subsequent research endeavors in the region. They identified a total of eight rock units (labeled A–H), spanning a vertical extent of 1010.5 m from the lowermost unit to the uppermost one (depicted in fig. 2.6). Among these, units A and B were attributed to Guadalupian and units C, D, and the lower part of E (transition beds) were credited to Dzhulfian. They denoted unit F as the *Paratirolites* limestone, a grayish-red limestone bed with about 3.6 thickness, contained *Paratirolites* ammonoid and was assigned to Triassic by Stepanov et al. (1969). Units G and H were also compared to the Triassic Elikah Formation, as described by Glaus (1964) in the Alborz Range, North Iran. These units encompassed vermiculate limestone rich in the bivalve *Claraia* (see more Ghaderi et al. 2016).

Unit A (Genishik Beds) with thick-bedded dark-gray bedded limestone covered by Khachik Beds (unit B) with dark-grey thin to thick-bedded cherty limestone and shale. According to Ghaderi et al. (2013), Khachik beds are covered by greenish-gray to cream and red shale, limestone and marl of the Lower and Upper Julfa beds (units C and D). Late Permian Ali-Bashi Formation (units E and F in Stepanov et al. 1969) follows this succession with dark gray to purple shale and red fossiliferous limestone. Teichert et al. (1973) have described four sections at localities 1 to 4, about 500 m apart, and proposed the name Ali Bashi Formation instead of the units E and F of Stepanov et al. (1969).

Partoazar (2002) revisited the sections at Ali Bashi Mountains and resampled them for studying the foraminiferal contents. In his revision, he changed the name of the Genishik and Khachik beds to the newly defined Julfa Formation; however, his compilation was not followed by other geologists. Also, he revised the age of Khachik beds from Guadalupian to Wuchiapingian (Ghaderi et al. 2016).

The designation "Khachik beds" has been alternatively referred to as the "Khachik Formation" within Armenia (as seen in works such as [Kotlyar et al. 1983](#)), and this nomenclature has also been adopted in certain accounts from the Ali Bashi Mountains in Iran (for instance, [Kozur 2005](#); [Ghaderi et al. 2016](#)). In this project, I shall adhere to their practice of utilizing the term "Khachik Formation." Given this substantial contextual background and considering the possible existence of GLB in the Julfa area (Northwest of Iran), the decision was made to focus on the sampling of the Khachik Formation (Khachik beds *sensu* [Stepanov et al. 1969](#)). Further details regarding the methods and materials employed can be found in the upcoming section.

2.3.1.1.2. LITHOSTRATIGRAPHICAL PERSPECTIVE

As mentioned, the Khachik Formation, initially described by [Stepanov et al.](#) in 1969, was first recognized in the Armenia region of the southern Caucasus, named after the Khachik Range ([Arakelian 1964](#)). The Khachik Formation in the southern Caucasus region has subsequently been the subject of various studies and comparisons in different investigations, such as [Pronina \(1988\)](#), [Leven \(1998\)](#), and [Vachard et al. \(2002\)](#). However, in Iran, this sedimentary unit has been a topic of discussion in a few articles following the work of [Stepanov et al. \(1969\)](#) [Partoazar \(2002\)](#), by changing the names of the Genishik Beds (Unit A) to "Selgord Member" and the Khachik Beds (Unit B) to "Shamar Member," and combining these two parts, established a new formation named the "Julfa Formation". However, the Julfa Beds in the northwestern part of Iran collectively correspond to units C and D in [Stepanov et al. \(1969\)](#). This is equivalent to the [Grunt et al. \(1965\)](#) and [Rostovtsev & Azaryan \(1973\)](#) senses for the Julfa Syncline in the southern Caucasus. This new definition, presented by [Partoazar \(2002\)](#), seemingly aimed at revising the stratigraphic framework of this region based on new Iranian names, not only fails to contribute to resolving the issue but also complicates the matching of sequences between the adjacent regions in the northwestern Iran and the southern Caucasus, on an international scale ([Ghaderi 2014](#)). For this reason, in most of recent studies, the basis of the stratigraphy has been considered the same as the original definition by [Stepanov et al. \(1969\)](#) with slight modifications. For instance, due to the significance of the stratigraphy of these sequences on an international scale and the caution against using different names, [Kozur \(2005\)](#) has utilized the term "Khachik Formation" for naming this unit

in the Ali Bashi region, a term also applicable in the Caucasus region. However, [Shabanian & Bagheri \(2008\)](#) have introduced the combined Khachik and Julfa beds under the name "Ruteh Formation for the Khachik beds and Nesen Formation for the Julfa beds Nesen Formation." This difference in perspectives has led to a comprehensive examination in this thesis, focusing on the Khachik beds, which will be referred to as the Khachik Formation following [Sweet \(2003\)](#), [Kozur \(2005\)](#) and [Ghaderi \(2014\)](#) from now on.

Moreover, [Stepanov et al. \(1969\)](#) considered Unit A, with a thickness of 308 meters, equivalent to the Genishik beds, and Unit B, with a thickness of 168 meters, equivalent to the Khachik beds. However, [Partoazar \(2002\)](#) changed the names of these units to the Selgord Member with a thickness of 152 meters and the Shamar Member with a thickness of 120 meters, fluctuating the regional stratigraphy. New field surveys conducted by [Ghaderi in 2014](#) and a re-measurement of the sequences attributed to the Khachik layers indicate that what [Partoazar \(2002\)](#) introduced as the Julfa Formation (comprising Shamar and Salgord members) with a total thickness of 272 meters in the northern margin of the Ali Bashi main valley. Its dip is also illustrated in his article, equivalent only to the Khachik layers and has a thickness of 164.6 meters, showing a slight discrepancy compared to the 168-meter thickness presented by [Stepanov et al. \(1969\)](#). In 2016 revision conducted by [Ghaderi et al](#), were demonstrated that the Khachik Formation itself can be divided into 9 rock-unit, listed from bottom to top as follows: Unit I: *Ungdarella* limestone: Capitanian in age; 30-m thickness, medium- to thick-bedded limestone (bioclastic wackestone/packstone); Unit II: Capitanian in age; 27.75-m thickness, dark- to light gray shale with some intercalations of light-gray thin- to medium-bedded limestone (bioclastic wackestone/packstone); Unit III: Capitanian in age; 8.80-m thickness; light-gray medium-bedded limestone (bioclastic packstone); Unit IV: Capitanian in age; 15.2-m thickness, light-gray shale with many intercalations of light-gray thin- to medium-bedded limestone (bioclastic wackestone to compact bioclastic packstone); Unit V: Capitanian in age; 10.8-m thickness, gray thin- to thick-bedded limestone (bioclastic packstone); Unit VI: Capitanian in age; 9.40-m thickness, light to dark gray thin- to thick-bedded limestone (fossiliferous mudstone, bioclastic wackestone to bioclastic packstone); Unit VII: Capitanian in age; 6.90-m thickness, yellowish thin to medium nodular limestone and very fine seams of shale and gypsum at the basal part, thick-bedded limestone at the middle part (fossiliferous mudstone to bioclastic wackestone), and a diabasic sill at the upper part; Unit VIII: Capitanian?–Wuchiapingian in age; 51.05-m thickness, thick-bedded cliff-forming

limestone (mudstone, bioclastic wackestone, packstone, and *Gymnocodium* floatstone); Unit IX: *Codonofusiella* limestone: Wuchiapingian in age; 4.70-m thickness, gray, green to yellow medium to thick-bedded limestone (mudstone, bioclastic wackestone, packstone, and *Gymnocodium* floatstone) (fig. 2.10).

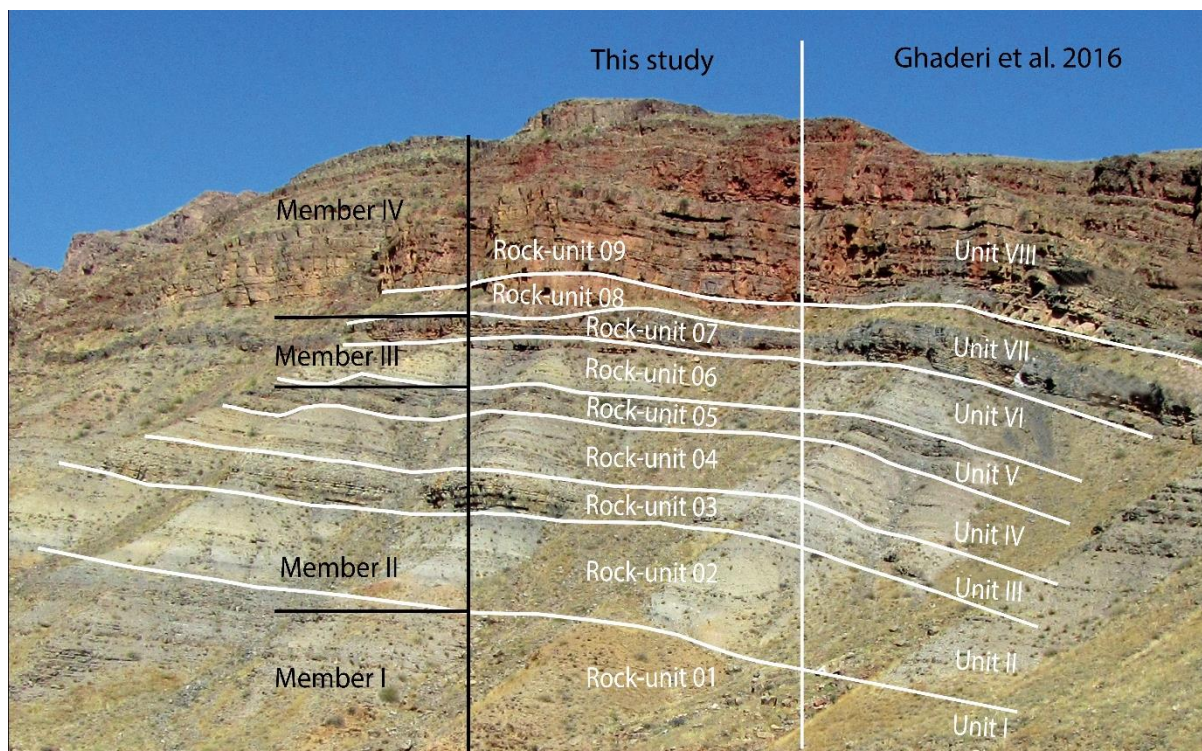


Fig. 2.10. Illustrated comparison of the rock units found in the Khachik Formation within the Ali-Bashi section in this study, juxtaposed with the rock units documented by Ghaderi et al. (2016). Photographs from the Ali-Bashi Section indicate the northeast direction.

In the current project, this formation has also undergone lithological evaluation, resulting in the identification of 15 rock units grouped into four members with the following stratigraphic arrangement from bottom to top:

R01: Alternation of mostly grey thin-bedded and brownish medium-bedded limestone (fossiliferous mudstone, bioclastic wackestone, packstone, algal packstone and floatstone) in the lower part of the rock-unit. This particular part has a thickness of 29.2 meters;

R02: Dark grey shale and grey thin-bedded marly limestone, while marly limestones (bioturbated mudstone, bioclastic wackestone and bioclastic to miliolid packstone) are dominant in the lower part and shales in the middle part. thickness: 23 meters;

R03: Grey thick-bedded limestone (fusulind/miliolid to algal packstone), thickness: 6 meters;

R04: Alternation of dark grey shale and grey thin-bedded limestone (mudstone, bioclastic wackestone/packstone, algal packstone), thickness: 25 meters;

R05: Alternation of light grey thin-bedded limestone (bioclastic to algal packstone) and grey shale, thickness: 7 meters;

R06: Alternation of light grey thin-bedded limestone (bioclastic wackestone, floatstone and algal packstone) and reddish shale, thickness: 9 meters;

R07: Light grey thin-bedded limestone, yellowish nodular limestone (mudstone/fossiliferous mudstone, bioclastic wackestone/packstone and crinoid packstone) and cherty limestone in the upper part of the unit, thickness: 19 meters;

R08: A diabase sill with a thickness of 5 meters;

R09: Alternation of dark-colored cherty limestone with cream thin-bedded limestone, cream calcareous limestone and dark gray thin-bedded limestone (mudstone, algal wackestone and bioclastic packstone to miliolid packstone) in the upper part. Thickness: 23 meters;

R10: Light grey shale with grey thin-bedded limestone in the middle part (algal packstone), thickness: 7.5 meters;

R11: Mostly cream thin-bedded limestone (algal packstone with peloids in the upper part) with 10.5 meters thickness;

R12: Dibasic sill, thickness: 3 meters;

R13: Reddish medium-bedded limestone (mudstone, bioclastic to algal packstone) with cherty limestone in some parts, thickness: 13.5 meters;

R14: Mostly brownish thin-bedded limestone (algal packstone), cherty limestone in some parts, thickness: 5 meters;

R15: Alternation of cream thin-bedded to dark gray medium-bedded limestone (mudstone, bioclastic to algal packstone with peloids) with 6.5 meters thickness (figs. 2.11-2.12).

Moreover, to improve the comprehension of the rock-unit's sequences in the Khachik Formation in the current study, a correlation of lithologies was performed by referring to the report provided by Ghaderi et al. (2016), as meticulously outlined in the accompanying (figs. 2.10, 2.13).

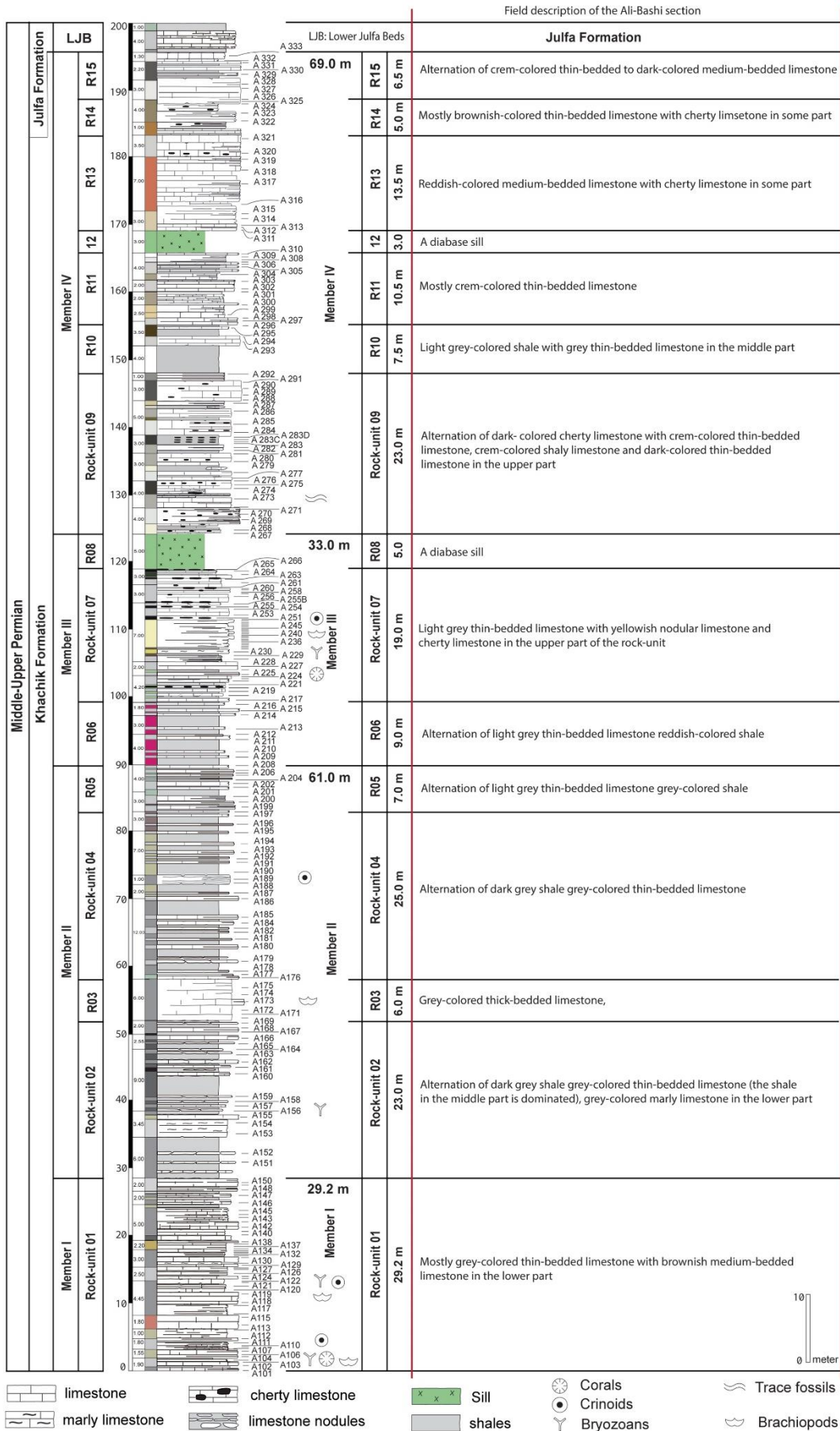


Fig. 2.11. Illustrated representation of the lithostratigraphic column of the Khachik Formation in the Ali-Bashi section, emphasizing its individual rock-units and members, accompanied by field descriptions. The abbreviation "LJB" stands for Lower Julfa Beds.

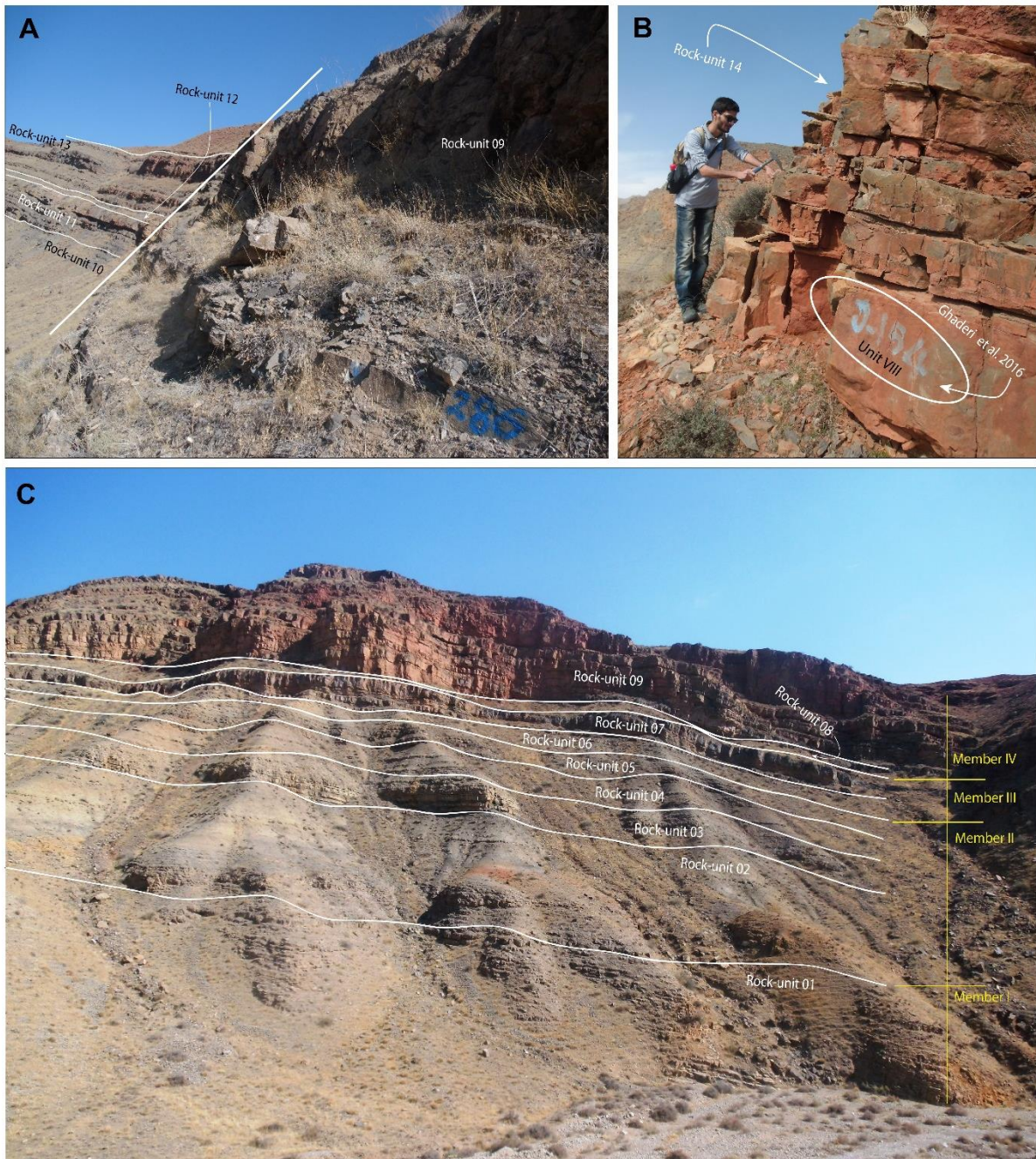


Fig. 2.12. In view A-C, a field landscape photograph captures the Khachik Formation sequences in the Ali-Bashi section, emphasizing its constituent members (oriented towards the northeast for observation).

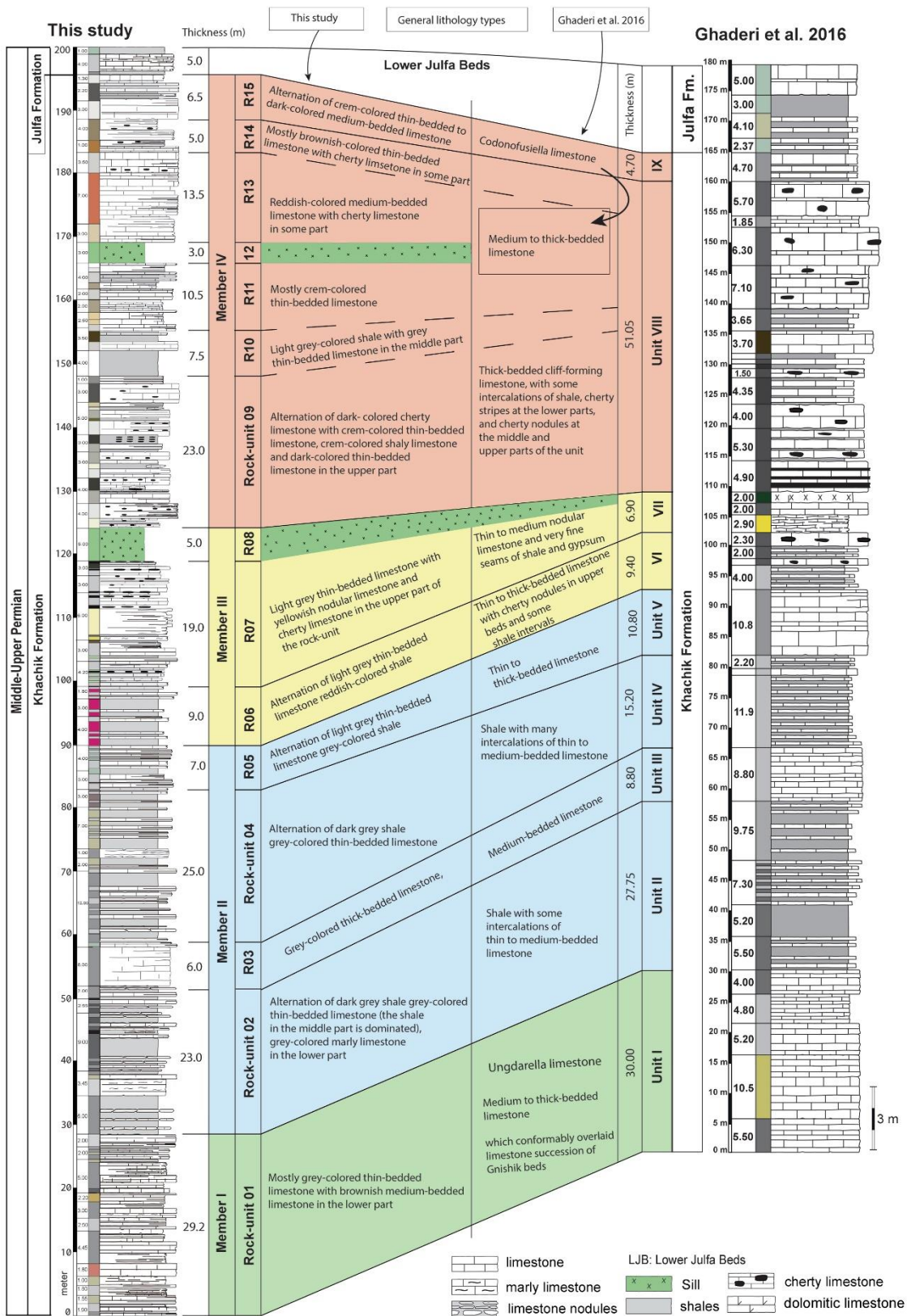


Fig. 2.13. The lithostratigraphic correlation and comparison of lithological characteristics of the rock units outlined in the Khachik Formation in the present study with those documented by Ghaderi et al. (2016).

2.3.1.2. BAGH-E-VANG SECTION

This section, 56.473°N and 33.583°E, is positioned within the Bagh-e-Vang Mountain and is located approximately 45 km from Tabas City (fig. 2.14). Bagh-e-Vang section is situated in the northern mountainous part of the Tabas block, with the high peaks, V-shaped valleys and frequent profound channels (fig. 2.8). The Permian strata in this section called Jamal Formation, following the research conducted by Stocklin et al. (1965), which they extensively studied the Permian deposits in the Jamal Mountains and assumed the name Jamal Formation for these strata. This section crops out on the western flank of the Kuh-e Bagh-e Vang (Mount Bagh-e-Vang).

The Jamal Formation, as observed in Bagh-e-Vang area, reported with various thicknesses from 293 meters (Ruttner et al. 1968) to 300 meters (Leven & Vaziri-Mohaddam 2004). The lower part of the Bagh-e-Vang section is predominantly characterized by siliciclastic deposits, primarily shale and sandstone, constituting the Carboniferous Sardar Formation. The Jamal Formation overlaid the Sardar Formation with a distinct boundary.

Lithostratigraphy of this formation in the Bagh-e-Vang section, particularly in the lower part, is characterized by a horizon of cream-colored calcarenite sandstone and a conglomerate unit. This basal part is followed up by red to gray shale, marl and gray limestone, containing many fossils of free fusulinids, crinoids, corals, sponges, cephalopods and brachiopods (Partoazar 1995). This member is overlain by cherty limestones and dolomite till the middle part of the section which was sampled, too.

Ruttner et al. (1968) originally reported the Bagh-e-Vang Section by identifying both the Sardar and Jamal formations. After about three decades, Partoazar (1995) established the newly defined Jamal group instead of the Jamal Formation and subdivided this group into three informal formations. The lower part of the Jamal Group in Partoazar's concept cropped out very well in the Bagh-e-Vang section. So, he designated the new unit as the Bagh-e-Vang Formation.

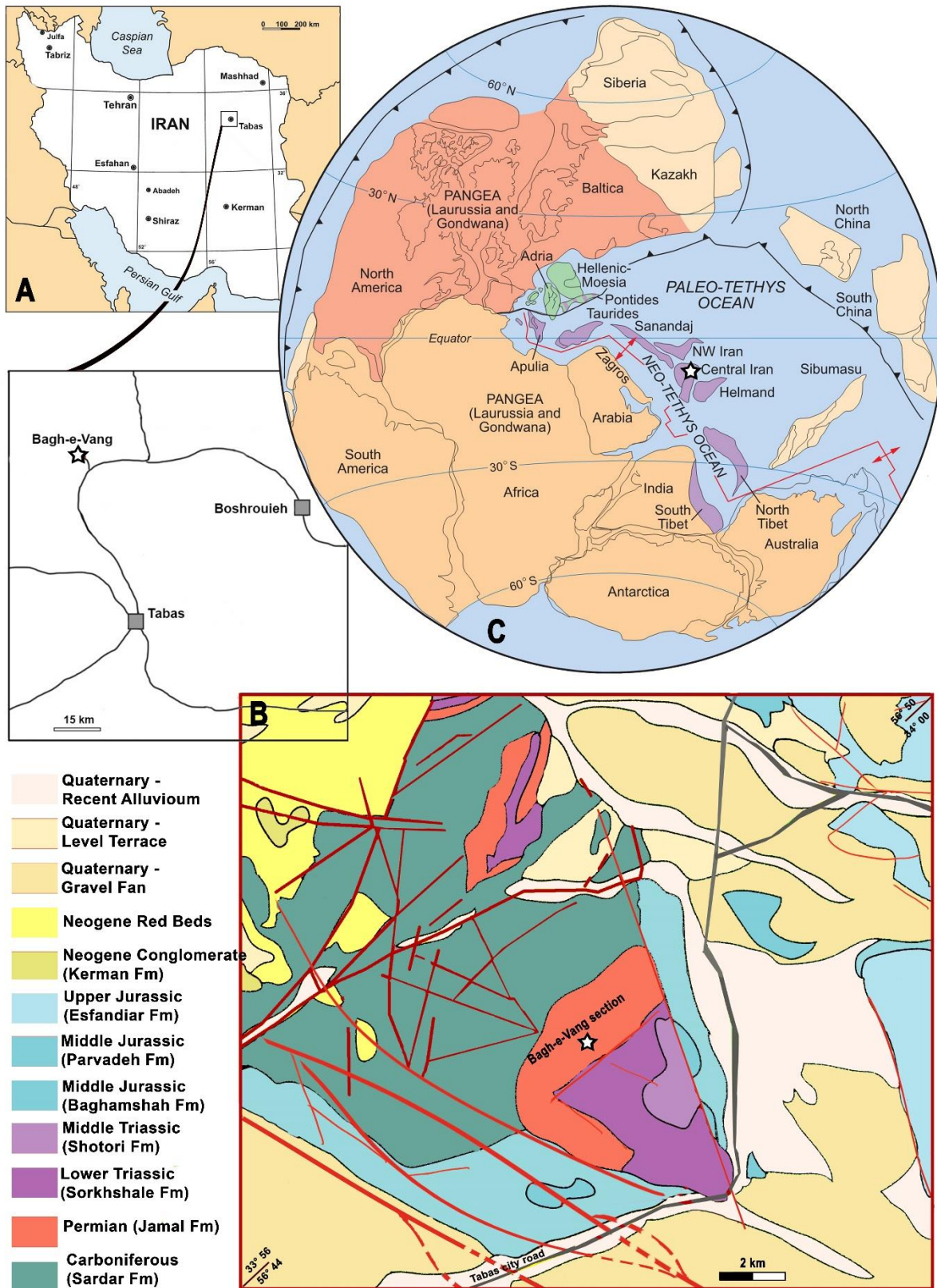


Fig. 2.14. A. location map of the study area in Central Iran (from Leda et al. 2014); B. Geologic map of the study area at the Tabas City; the Bagh-e-Vang section is marked with a white star (from Ataei 2019); C. palaeogeographical map of the Lopingian and location of the study area (white star) as a part of a Cimmerian block, close to the equator in the southern hemisphere (from Ruban et al. 2007).

Recognition of either two or three formations lacks consensus among other researchers. While the term "Bagh-e-Vang" has found its place in the literature, it is occasionally acknowledged solely as a member of the Jamal Formation, as seen in works like [Leven & Vaziri-Mohaddam \(2004\)](#). However, in this thesis, I align with the categorization proposed by [Balini et al. \(2010, 2011, 2012\)](#) and [Vuolu \(2014\)](#), which designates the Bagh-e-Vang unit as a member of the Jamal Formation.

2.3.1.2.1. HISTORICAL BACKGROUND

As a historical appendix, the initial examination and analysis of Permian successions within the Tabas region, specifically within the Shotori Mountains, were conducted by [Clapp \(1940\)](#). Subsequently, [Furon \(1941\)](#) directed his investigations toward the study of "black rocks abundant in fusulinids." However, the inaugural comprehensive geological surveys in the East-Central Iran territory transpired during the 1950s and 1960s, overseen by [Ruttner \(Stöcklin 1968; Rüttner 1968\)](#). [Partoazer \(1995\)](#) followed the Permian sequences in different locations of Iran, upgraded the base of the Jamal Formation into his Bagh-e-Vang formation and proposed Asselian to Sakmarian (Early Permian) ages for this new interval.

[Taheri \(2002\)](#), with a focus on identifying the foraminifers of the Bagh-e-Vang section, has proposed four biozones and presented a Kungurian–Changxiangian (Bolorian – Dorashamian) age for the Jamal Formation in this section. [Leven & Vaziri-Moghaddam \(2004\)](#), by biostratigraphic observation in the 300 m thickness of the Jamal Formation in the Bagh-e-Vang section, suggested the age of the Artinskian – Roadian (Yakhtashin – Kubragandian) for the first 60 meters of the section, distinguished as the Bagh-e-Vang Member. They considered the age of the upper part of the section as the Kubragandian–Dorashamian (= Roadian–Changxiangian).

This section was observed by [Arefifard \(2006\)](#) who presented fusulinid faunas of Kubergandian (Roadian) to the Early Dzhulfian (Wuchiapingian). [Leven et al. \(2007\)](#) documented a few numbers of conodonts from the Bagh-e-Vang Member and assigned it a Guadalupian age. Furthermore, based on the fusulinid assemblages, [Leven & Gorgij \(2011\)](#) proposed the ages of Bolorian to Early Kubergandian (equivalent to Kungurian to the Early Roadian) for the Bagh-e-Vang section.

Vuolo (2014), with conodont stratigraphy, proposed the age of the Early Sakmarian-Kungurian for Jamal Formation in this section. Later, Balini et al. (2015), extracted rare conodont species and reported the ages of Pennsylvanian up to Early-Permian for the Bagh-e-Vang section. Ghalenoee (2019), in a high-resolution sampling of the Bagh-e-Vang member for focus on the zonal marker conodont, determined six-conodont zones and proposed Middle Asselian to Artinskian (Cisuralian series – Early Permian) ages to this member. On the base of this work, the Bagh-e-Vang section has been selected for this PhD thesis project.

2.3.1.2.2. LITHOSTRATIGRAPHICAL PERSPECTIVE

The Jamal Formation, the first unit of the Tabas Group, encompasses the Jamal, Sorkh Shale, and Shotori Formations, originally investigated and established by Stocklin et al. (1965) during geological surveys in the Shotori Mountains. This formation highlights the Permian carbonate rocks in the Tabas block. Situated about 52 kilometers southeast of Tabas along the Tabas-Deyhuk road, it was named the "Jamal Formation" in respect to the Jamal Mountain. In their geological map at a 1:250,000 scale for Boshrouyeh (Stocklin & Nabavi 1969), Stocklin et al. (1965) included a representative cross-section pattern for the Jamal Formation. The distinctive cross-section of this formation, reminiscent of many recognized sedimentological profiles, reveals a unique rock facies and steep incline. Within the designated cross-section area, the Jamal Formation is positioned above the sedimentary beds of the Sardar Formation and is itself overlain by the strata of the Sorkh-Shale Formation.

The type section of the Jamal Formation, as drew by Stocklin et al. (1965), exhibits a total thickness of 473 meters. Subsequently, the National Committee for Stratigraphy of Iran made adjustments by removing the upper 74 meters of the Sardar Formation, characterized by pre-Permian clastic deposits, from its original position and incorporating it into the lower part of the Jamal Formation. As a result, the revised type section of the Jamal Formation now has a thickness of 547 meters. The sedimentological composition, from the base to the top, is detailed as follows:

1. Quartzitic sandstone ranging from white to purple with limonitic facies, measuring 34 meters in thickness;
2. Grey shale with a thickness of 2 meters;
3. White quartzitic sandstone, spanning 16 meters in thickness;

4. Silty shale displaying a dark green color and measuring 1 meter in thickness;
5. White quartzarenite and white quartzitic sandstone, with a combined thickness of 19 meters;
6. Sandy shale exhibiting a light green to grey color, featuring a 40-centimeter coal seam at the base, and measuring 2 meters in thickness;
7. Sandstone is characterized by sandy limestone facies, brown in color, with a thickness of 1 meter;
8. Sandy limestone in brown and grey hues, spanning 3 meters in thickness;
9. Thick-bedded and massive limestone in a dark grey to blue color, measuring 88 meters in thickness;
10. Limestones containing corals, slightly dolomitic, with a thickness of 57 meters;
11. Limestones with corals and a primary limestone layer, having a thickness of 87 meters;
12. Dark grey, thick to massive limestone, accompanied by interbedded dolomitic layers, measuring 33 meters in thickness;
13. Massive limestone with a thickness of 90 meters;
14. Yellow dolomite, accompanied by interbedded layers of brown limestone, with a thickness of 12 meters;
15. Bedded dolomite in yellow, spanning 61 meters in thickness;
16. Thin-bedded dark grey limestone with a thickness of 8 meters;
17. White limestone with a thickness of 1 meter;
18. Bedded dark brown limestone, measuring 6 meters in thickness;
19. Well-bedded dark grey limestone, having a thickness of 6 meters;
20. Dolomitic limestone with distinct layering, accompanied by interbedded layers of yellow and red limestone, with a thickness of 20 meters.

According to [Ruttner et al. \(1968\)](#), the Jamal Formation in the Bagh-e-Vang section comprises approximately 293 meters of siliciclastic and carbonate rocks. It rests upon the green clastic sedimentary sequence of the Sardar Formation and is covered by red to yellowish calcareous shales belonging to the Sorkh-Shale Formation. In this section, the lower part of the Jamal Formation commences with a horizon featuring cream-colored calcareous sandstone and a conglomeratic unit forming the base of the Bagh-e-Vang member. Above this conglomeratic unit, which signifies the onset of the Permian marine transgression ([Partoazar 1995](#)), there are alternating beds of red and gray shale. These shale beds are interbedded with marl and

gray limestone that house a rich abundance of fossils, including foraminifera, crinoids, corals, sponges, cephalopods, brachiopods, and bryozoans.

Besides, the Jamal formations, as observed by [Balini et al. \(2010, 2011, 2012\)](#), exhibit a diverse array of facies across different temporal and spatial contexts, indicating the necessity for a reevaluation of the lithostratigraphic classification of both units ([fig. 2.15](#)).

Furthermore, it appears that these two units share greater similarities with lithostratigraphic groups than with conventional formations. Although certain authors have recently attempted to delineate specific subunits (e.g., the Bagh-e-Vang Member by [Leven & Vaziri Mohaddam in 2004](#)), substantial additional research is still required to comprehensively understand and define these geological components ([Vuolo 2014](#)). Additionally, the highest level of the Sardar Formation (Sardar Group in [Vuolo 2014](#)) consists of finely grained greenish siltstones, interbedded with exceptionally rare, very thinly bedded, fine-grained sandstones. The paleoenvironmental interpretation of this facies remains somewhat uncertain; however, it is currently ascribed to a transitional to a marine environment characterized by a supply of fine-grained siliciclastic. Within the "Bagh-e-Vang Member," there is evidence of a transgression marked by medium to coarse-grained bioclastic grainstone. Particularly at the base, these grainstone indicate a subtidal environment due to the presence of herringbone lamination, as recognized by [Balini et al. \(2010, 2011, 2012\)](#) and [Vuolo \(2014\)](#).

In the ongoing project, an assessment of the geological composition of this formation has been conducted, leading to the recognition of 10 rock units organized into three members. These units are stratigraphically arranged from the bottom to the top as follows:

R01: Cream to grey calcarenite sandstone and grey shale. Additionally, there is grey shale featuring calcareous nodules, along with light grey-colored thick-bedded conglomerate interbedded with thin-bedded limestone. The thickness of this unit is 25 meters;

R02: Thick-bedded grey limestone, interspersed with shale and a conglomerate ranging from grey to brown in the upper part, measuring 34 meters in thickness;

R03. Alternation of thin-bedded brownish limestone and medium-bedded cherty limestone, full of black cherty strips. The total thickness is 53 meters;

R04: Alternation of thin-bedded black limestone and medium-bedded cherty limestone with a brownish color, measuring a total thickness of 37.25 meters;

R05: Cream medium-bedded dolomite featuring fully black chert stripes and nodules, with a thickness of 26 meters;

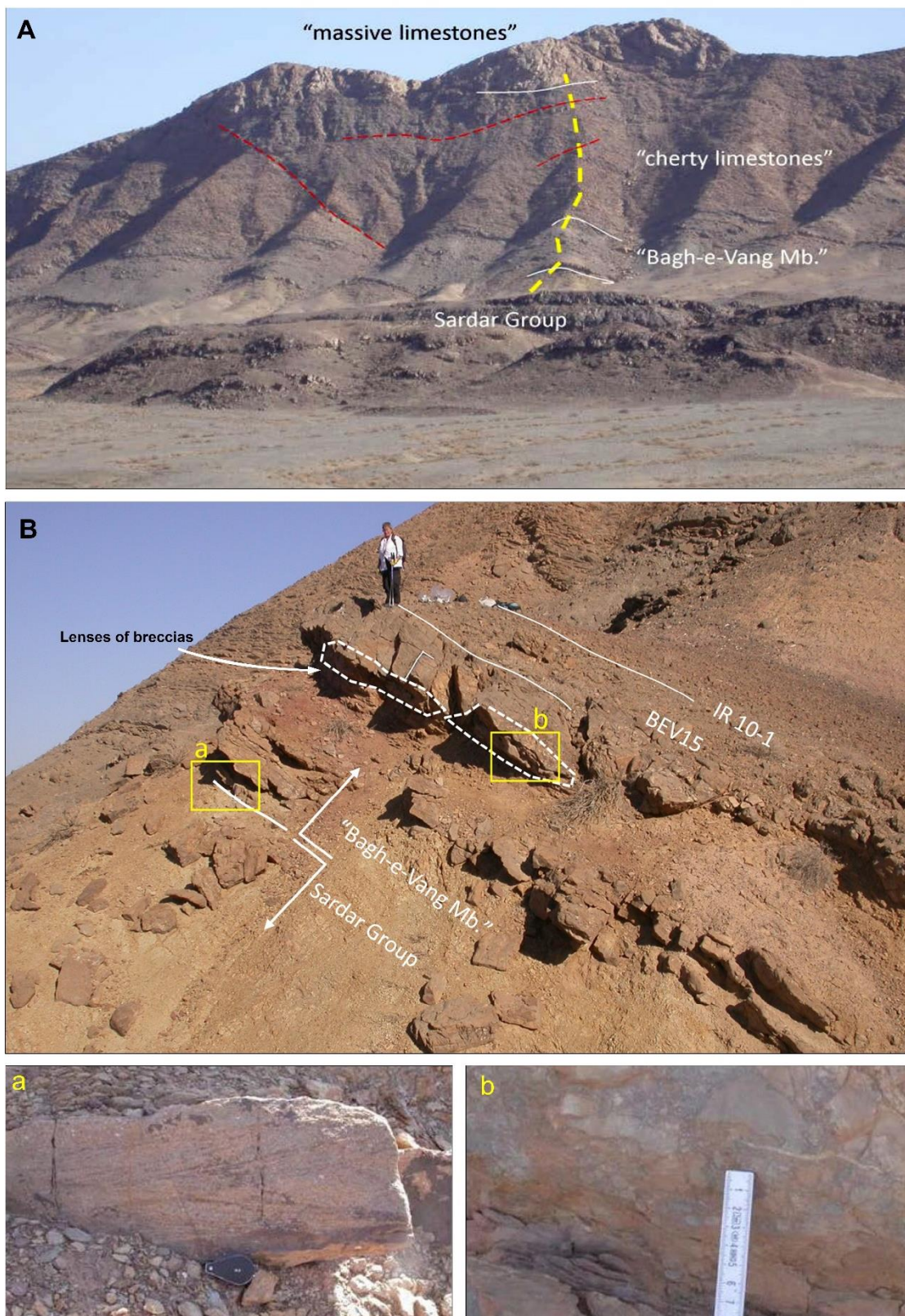


Fig. 2.15. A. The northwestern terminus of Kuh-e-Bagh-e-Vang (adapted from Balini et al. 2010; Vuolu 2014). The yellow dashed line indicates the location of the examined section, while the red dashed line represents major faults. B. The boundary between Sardar and Jamal Groups (adapted from Balini et al. 2010; Vuolu 2014). The yellow line denotes the position of the close-up images depicting various facies of the lower part of the "Bagh-e-Vang Member" (adapted from Balini et al. 2010; Vuolu 2014); a) Herringbone cross-lamination in the initial sandy limestone. b) Detailed view of the calcareous breccias.

R06: Alternation of grey to brownish thin to medium-bedded limestone, characterized by fully black chert stripes and nodules. The thickness measures 35.5 meters;

R07: Light grey thin-bedded dolomitic limestone, with a thickness of 11 meters;

R08: Alternation of dark brown medium-bedded limestone and thin-bedded dolomitic limestone, with a thickness of 8.25 meters;

R09: Brownish thin-bedded limestone, accompanied by a thin-bedded conglomerate in the upper part, has a thickness of 8.15 meters;

R10: Grey to green/brownish-colored medium-bedded limestone with a thickness of 14.5 meters (figs. 2.16-2.17).

Besides, [Partoazar \(1995\)](#) conducted a comparative analysis between the Jamal Formation strata in the type section and the Bagh-e-Vang section, revealing significant variations in lithofacies and, notably, the thickness of sedimentary units. Key findings are as follows:

According to the [Partoazar \(1995\)](#), in the Bagh-e-Vang section, the marine progression initiates with a brief conglomerate bed, measuring 46 meters in thickness and characterized by red shale. Conversely, in the Jamal Formation's type section, a layer of dark gray shale with coal seams is observed on the quartzite base. The Bagh-e-Vang section exhibits a substantial increase in shale content, leading to a distinctive contrast in the visual appearance of the Bagh-e-Vang member. Furthermore, within the Bagh-e-Vang section, limestone beds with a thickness of 130 meters overlay the Bagh-e-Vang member. In contrast, the Jamal Formation type section displays an increase in limestone beds thickness to 306 meters. These findings underscore significant lithostratigraphic differences between the two sections.

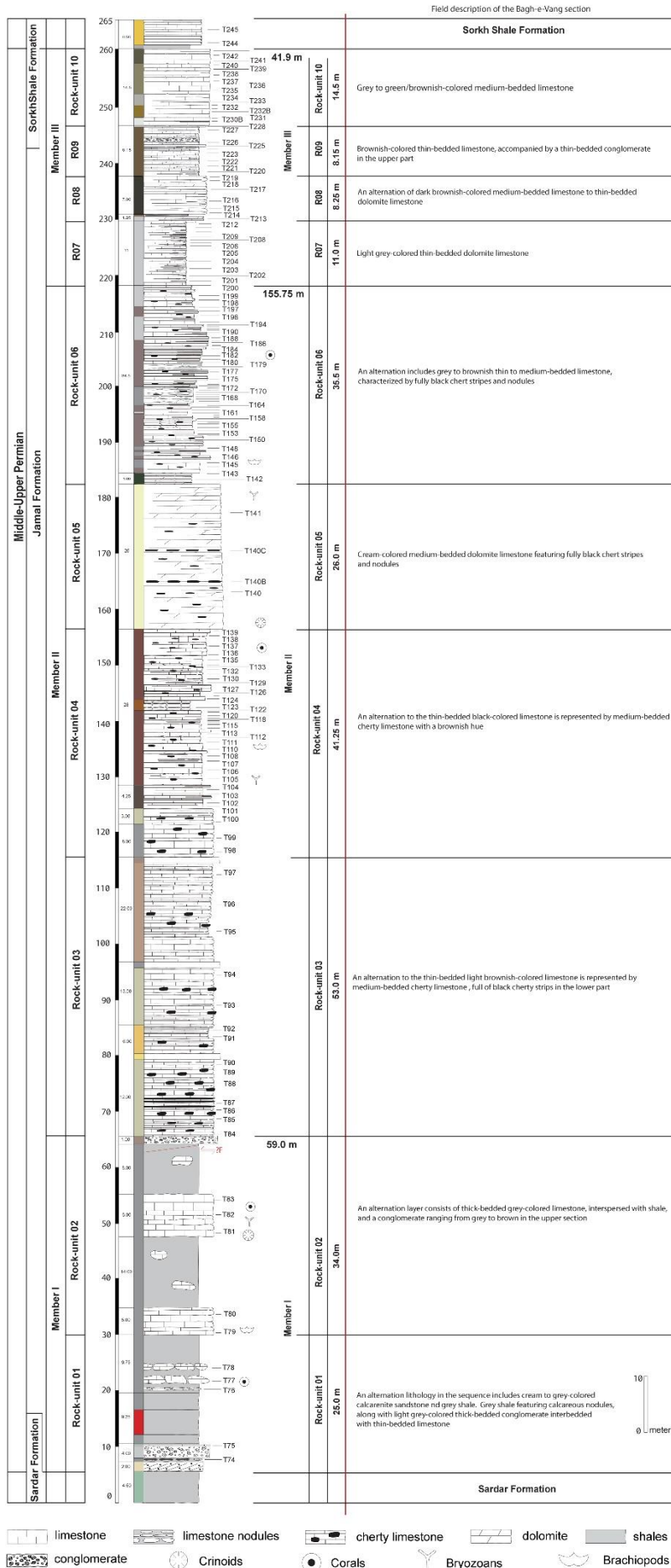


Fig. 2.16. An illustrated depiction of the lithostratigraphic column of the Jamal Formation in the Bagh-e-Vang section, highlighting its specific rock units and members, complemented by field descriptions.

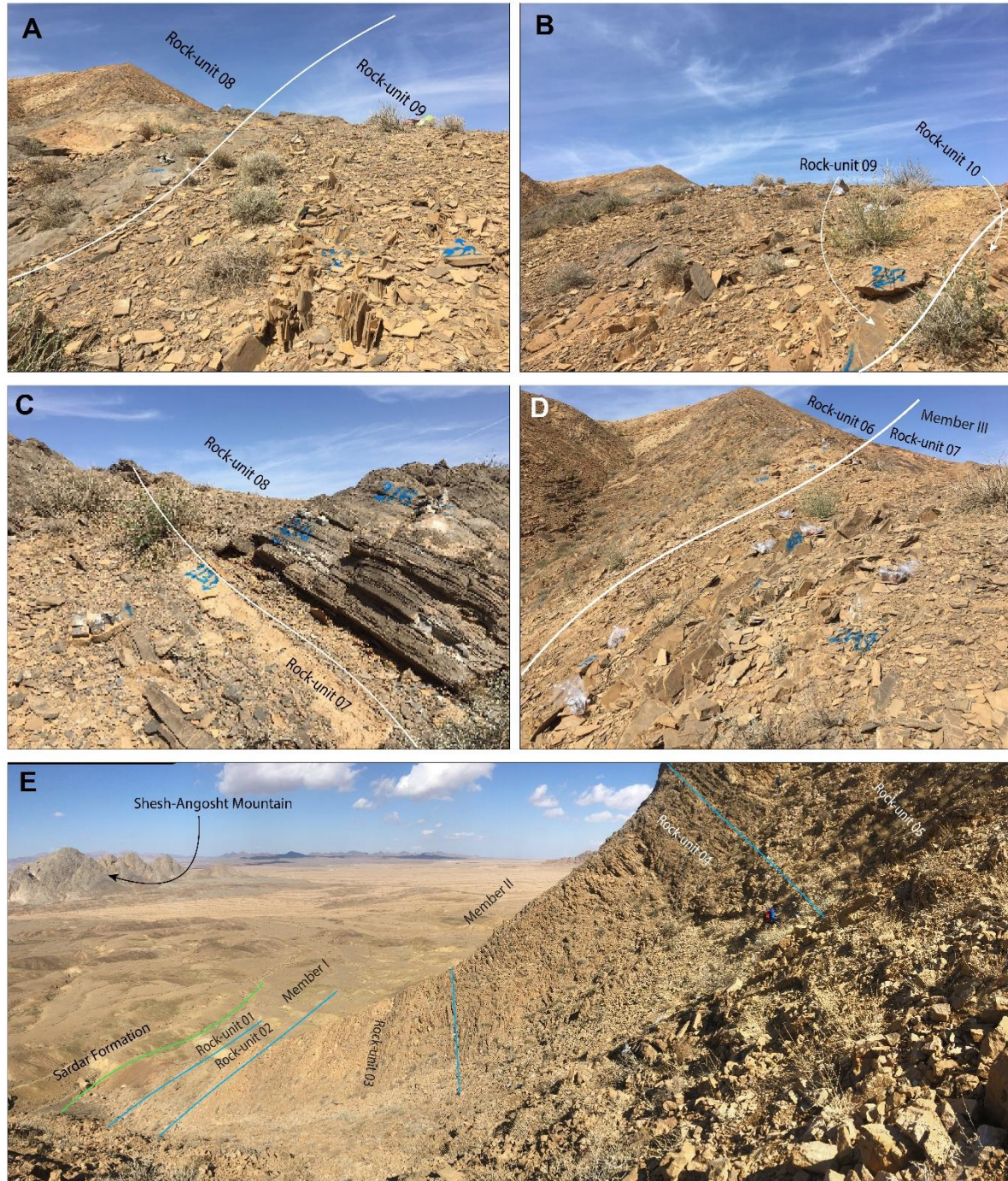


Fig. 2.17. In perspectives A-E, a field landscape image captures the sequences of the Jamal Formation in the Bag-e-Vang section, emphasizing its individual members (oriented towards the northeast for observation).

2.3.1.3. BAGHUK SECTION

The Baghuk section, 31.5675°N and 52.4436°E (Leda et al. 2014) is located in the Baghuk Mountain, positioned in Central Iran, approximately 140 km southeast of Esfahan city and about 45 kilometers northwest of Abadeh Town (fig. 2.18). Paleo-geographically, the outcrop area as part of the Sanandaj-Sirjan Zone on the Cimmerian Microcontinent, near the equator on the Neo-Tethyan shelf (Stöcklin 1968; Nabavi 1976; Stampfli & Borel 2002, 2004; Torsvik & Cocks 2004; Leda et al., 2014) is situated in the western margin of the Paleo-Tethys with a northward drifting history from the northern Peri-Gondwanan region to the paleotropical area during the Permian (Liu et al. 2013) (fig. 2.8).

Additionally, it has been extensively documented that the strata from Upper Permian to Lower Triassic are continuously deposited and contain very abundant fossils including conodonts, ammonoids, brachiopods, and fusulinids (IJRG 1981; Kozur, 2004, 2005; Shen & Mei 2010 and Liu et al., 2013).

2.3.1.3.1. HISTORICAL BACKGROUND

Permian strata in the Baghuk Mountain consist of the Guadalupian Abadeh Formation, the Lopingian Hambast Formation, and the Early Triassic Elikah Formation in ascending order (IJRG 1981). The stratigraphy spanning from the Late Permian to the Early Triassic in this area was initially characterized by Taraz (1969, 1974). He partitioned the Permian sedimentary sequence into seven distinct units (referred to as units 1 to 7 in ascending order) and the Early Triassic sequence into five units (units a to e). Later, the Permian units were categorized into three formations (Taraz et al. 1981): the Surmaq, Abadeh, and Hambast Formations (fig. 2.6). At the type locality (Kuh-e-Hambast), the Late Permian Hambast Formation boasts an approximate thickness of 35 m, primarily comprising platy and nodular limestone beds (Taraz et al. 1981).

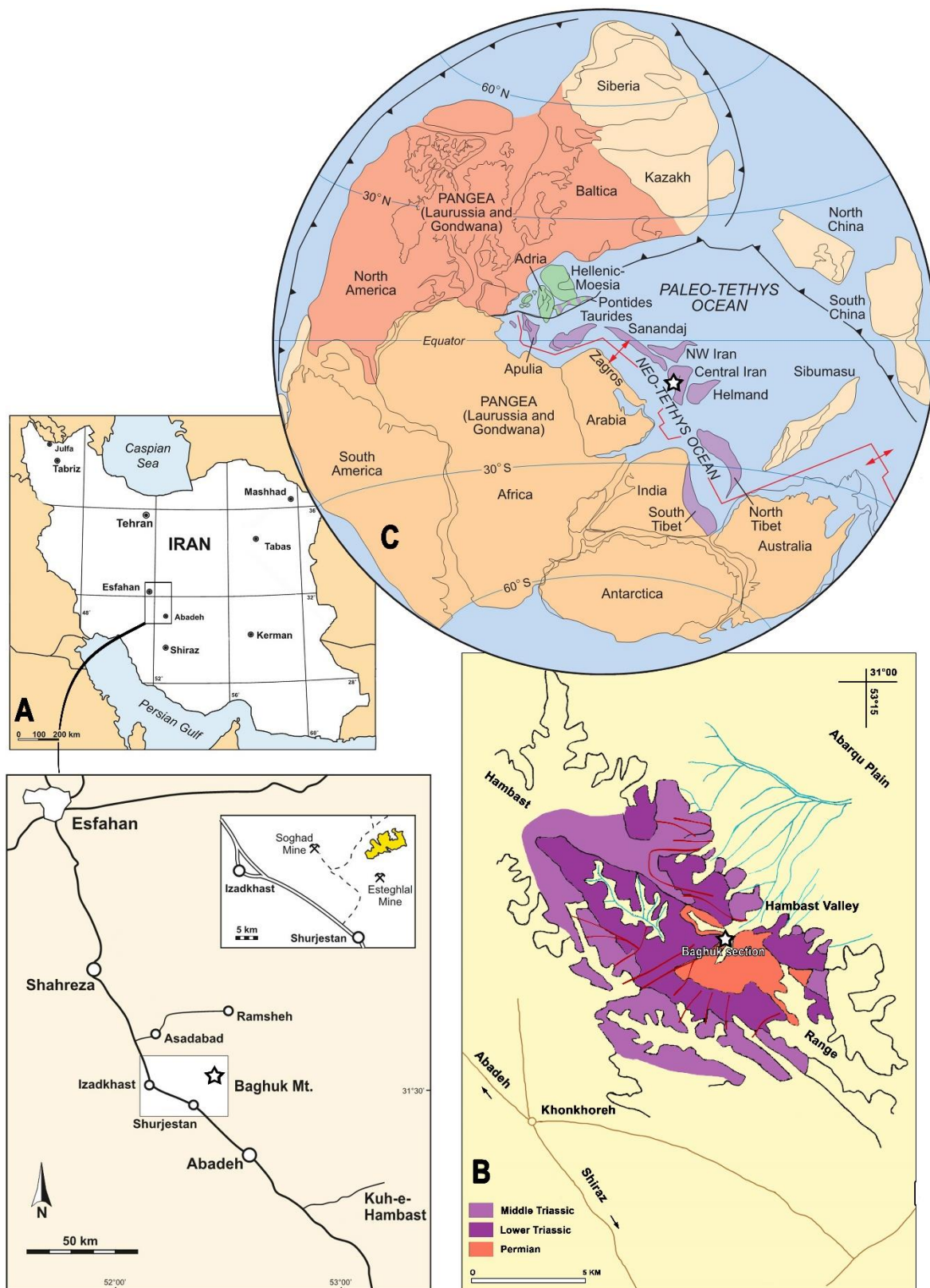


Fig. 2.18. A. location map of the study area in Sanandaj-Sirjan Zone (from Heuer et al. 2021); B. Geologic map of the study area at the North of the Abadeh city; the Bagh-e-Vang section is marked with a white star (from Taraz et al. 1981); C. palaeogeographical map of the Lopingian and location of the study area (white star) as a part of a Cimmerian block, close to the equator in the southern hemisphere (from Ruban et al. 2007).

According to [Taraz et al. \(1981\)](#), the Late Permian stages of Wuchiapingian (Dzhulfian) and Changhsingian (Dorashamian) are represented nearly equally in the strata (see more in [Heuer et al. 2021](#)). The lithological sequence and environmental characteristics of sections within the Hambast Range underwent comprehensive examination, interpretation, and analysis by the research team led by Heydari ([Heydari et al. 2000, 2003](#); [Heydari & Hassanzadeh 2003 in Heuer et al. 2021](#)). They detailed the features of unit 6, which comprises argillaceous, light gray, and bioturbated mudstone from the Late Permian, as well as unit 7, composed of argillaceous, nodular mudstone and wackestone.

Their findings suggested a deposition in a water depth ranging between 100 and 200 m. Meanwhile, the PTB is marked by a bed with microbialite and defined by the first occurrence of the conodont *Hindeodus parvus* ([Heydari et al. 2000](#); [Korte et al. 2004](#); [Shen & Mei 2010](#)). Furthermore, the Abadeh Formation (Units 4–5 in [Taraz et al. 1981](#)) is overlain by the Hambast Formation (Units 6–7 in [Taraz et al. 1981](#)) and then Unit A of the Elikah Formation. The strata in the investigated interval are dominated by limestone that is suitable for geochemical analyses.

The upper part of Unit 4 (upward to -77.6 m to the base of Unit 5) is mainly composed of thin-bedded limestone interbedded with thick black shale containing abundant foraminifers, brachiopods, bryozoans, calcareous algae, gastropods, some conodonts, fusulinids and ammonites. Unit 5 (-77.6 m to -36.7 m) consists of shallow marine thick-bedded carbonate. Unit 6 (-36.7 m to 15.5 m) conformably overlies Unit 5 and is mainly composed of thin-bedded limestone alternated with mudstone containing some ammonoids and fusulinids.

Unit 7 (-15.5 m to -0.9 m) consists of reddish pure limestone containing abundant conodonts ([Kozur 2004](#)) and ammonoids in the topmost part, which is called the *Paratirolites* Bed ([IJRG, 1981](#)). Biostratigraphic models of the Baghuk section have been widely studied (more information in [Leda et al. 2014](#); [Chen et al. 2020](#); [Heuer et al. 2021](#)).

Nevertheless, the majority of these studies have concentrated solely on the Permian-Triassic Boundary (PTB), while the GLB remains a subject of disputation within the context of biostratigraphic interpretations. Drawing upon these explanations, the Baghuk section has been selected as the third section for the investigation of the GLB in this PhD thesis project. Further details regarding the sampling process for this section will be provided in the upcoming chapter.

2.4. REFERENCES

- Alavi, M., Vaziri, H., Seyed-Emami, K. and Lasemi, Y., 1997. The Triassic and associated rocks of the Naxhlak and Aghdarband areas in central and northeastern Iran as remnants of the southern Turanian active continental margin. *Geological Society of America Bulletin*, 109(12), pp.1563-1575.
- Angiolini, L., Caretti, D. and Salatelli, E., 2000. Synthesis and photoinitiation activity of radical polymeric photoinitiators bearing side-chain camphorquinone moieties. *Macromolecular Chemistry and Physics*, 201(18), pp.2646-2653.
- Angiolini, L., Gaetani, M., Muttoni, G., Stephenson, M.H. and Zanchi, A., 2007. Tethyan oceanic currents and climate gradients 300 my ago. *Geology*, 35(12), pp.1071-1074.
- Angiolini, L. and Carabelli, L., 2010. Upper Permian brachiopods from the Nesen Formation, North Iran. *Special Papers in Palaeontology*, 84, pp.41-90.
- Arakelian, R.A., Rauzer-Chernoucouva, D.M. and Reitlinger, E.A., 1964. Significance of Permian Foraminifera of the Transcaucasus for the correlation of Permian deposits within the Tethys. *Stratigraphy of the upper Paleozoic and Mesozoic of the southern biogeographical provinces: 22d Internat. Geol. Cong., Moscow, Soviet Geologists Repts., Problem 16a*, pp.63-75.
- Arefifard, S., 2006. Microbiostratigraphy and microfacies of Permian strata in Shotori, Shirgesht and Kalmard areas. *Unpublished Ph.D. Dissertation, Shahid Beheshti University, Tehran, Iran*.
- Arefifard, S., 2017. Guadalupian cool versus warm water deposits in central Iran: a record of the Capitanian Kamura event. *Geological Magazine*, 156(3), pp.430-446.
- Arefifard, S. and Payne, J.L., 2020. End-Guadalupian extinction of larger fusulinids in central Iran and implications for the global biotic crisis. *Palaeogeography, Palaeoclimatology, Palaeoecology*, 550, p.109743.
- Arefifard, S. and Baud, A., 2022. Depositional environment and sequence stratigraphy architecture of continuous Upper Permian and Lowermost Triassic deep marine deposits in NW and SW Iran. *Palaeogeography, Palaeoclimatology, Palaeoecology*, 603, p.111187.
- Ataei, M.R., 2019. *Study on early Permian corals of the Bagh-e-Vang member of Jamal Formation in the Bagh-e-Vang and Shesh-Angosht stratigraphic sections, north of Tabas, Central Iran*. (MSc. Thesis Ferdowsi University of Mashhad).
- Balini, M., Angiolini, L., Bahramanesh, M., Ghassemi, M.R., Nicora, A., Norouzi, M. and Soleimani, S., 2010. The Carboniferous-Triassic sedimentary record of Central Iran and its correlations with Aghdarband and SanandajSirjan, DARIUS project. *IR09-02*.

- Balini M., Angiolini L., Bahrammanesh M., Nicora A., Sohrabi Z. & Vuolo I. 2011. "The Carboniferous-Permian sedimentary record of Central Iran". DARIUS project IR 09-02 and 2010, annual report 2011, pp. 33.
- Balini M., Nicora A., Sohrabi Z., Angiolini L., Bahrammanesh M., Henderson C., Leven E. J. & Vuolo I. 2012. "Carboniferous and Permian correlations from Central Iran to Sanandaj- Sirjani". DARIUS project 2011 and IR 09-02, 2010, annual report 2012, pp. 44.
- Balini, M., Mandrioli, R., Nicora, A., Angiolini, L., Borlenghi, L.M., Vuolo, I., Shorabi, Z. and Bahramanesh, M., 2015. First report of Upper Pennsylvanian ammonoids and Lower Permian conodonts from Bagh-e-Vang area (Central Iran). *Permophiles*, 62(12), pp.25-27.
- Bayat, M., Baghbani, D., 2007. Study and investigate of small-foraminiferal of the family Biseriammininae in upper Permian strata of Dalan Formation in Oshtorankouh, high-mountain Zagros. *Geology of Iran* 2(5), pp. 3-16, (In Persian).
- Berberian, M. and King, G.C.P., 1981. Towards a paleogeography and tectonic evolution of Iran. *Canadian Journal of Earth Sciences*, 18(2), pp.210-265.
- Boulin, J., 1988. Hercynian and Eocimmerian events in Afghanistan and adjoining regions. *Tectonophysics*, 148(3-4), pp.253-278.
- Chen, J., Shen, S.Z., Zhang, Y.C., Angiolini, L., Gorgij, M.N., Crippa, G., Wang, W., Zhang, H., Yuan, D.X., Li, X.H. and Xu, Y.G., 2020. Abrupt warming in the latest Permian detected using high-resolution in situ oxygen isotopes of conodont apatite from Abadeh, central Iran. *Palaeogeography, Palaeoclimatology, Palaeoecology*, 560, p.109973.
- Clapp, F.G., 1940. Geology of eastern Iran. *Bulletin of the Geological Society of America*, 51(1), pp.1-102.
- Clark, D.L. and Hatleberg, E.W., 1983. Paleoenvironmental factors and the distribution of conodonts in the Lower Triassic of Svalbard and Nepal. *Fossils and Strata*, 15, pp.171-175.
- Davoudzadeh, M. and Schmidt, K., 1984. A review of the Mesozoic paleogeography and paleotectonic evolution of Iran. *Neues Jahrbuch für Geologie und Paläontologie-Abhandlungen*, pp.182-207.
- Ernst, A., Senowbari-Daryan, B. and Rashidi, K., 2006. Lower Permian Bryozoa of the Jamal Formation from Bagh-e Vang (Shotori Mountains, northeast Iran). *Facies*, 52, pp.627-635.
- Furon, R., 1941. Géologie du plateau iranien. *Mémoire du Muséum National d'Histoire Naturelle*, pp.259-263.
- Ghaderi, A., 2014. Stratigraphy and paleoecology of the Upper Permian to Permian–Triassic boundary in the northwest of Iran based on biostratigraphic data of conodonts and brachiopods. PhD thesis, Ferdowsi University of Mashhad, p 488.

- Ghaderi, A., Ashouri, A.R., Korn, D., Mahmoudi Gharaie, M.H. and Leda, L., 2013. New insight on stratigraphic correlation of the Permian-Triassic transitional beds in the Transcaucasus and northwest of Iran: Problems and guidelines. *Sedimentary Facies*, 5(2), pp.221-224.
- Ghaderi, A., Garbelli, C., Angiolini, L., Ashouri, A.R., Korn, D., Rettori, R. and Gharaie, M.H.M., 2014. Faunal change near the end-Permian extinction: the brachiopods of the Ali Bashi Mountains, NW Iran. *Rivista Italiana di Paleontologia e Stratigrafia*, 120(1). DOI: [10.13130/2039-4942/6048](https://doi.org/10.13130/2039-4942/6048)
- Ghaderi, A., Leda, L., Schobben, M., Korn, D. and Ashouri, A.R., 2014. High-resolution stratigraphy of the Changhsingian (Late Permian) successions of NW Iran and the Transcaucasus based on lithological features, conodonts and ammonoids. *Fossil record*, 17(1), pp.41-57. DOI: [10.5194/fr-17-41-2014](https://doi.org/10.5194/fr-17-41-2014), 2014
- Ghaderi, A., Taherpour Khalil Abad, M., Ashouri, A.R. and Korn, D., 2016. Permian calcareous algae from the Khachik Formation at the Ali Bashi Mountains, NW of Iran. *Arabian Journal of Geosciences*, 9, pp.1-11.
- Ghalenoe, F., 2019. *Biostratigraphy of the Jamal Formation Bagh-e-Vang member in the North of Tabas (Central Iran) based on Conodonts* (MSc. Thesis Ferdowsi University of Mashhad).
- Ghobadipour, M., and Jafarian, M., 2006. Biostratigraphy of Late Permian depositional sequence in Northeastern Isfahan (Chahrisheh Area) in Persian.
- Gliwa, J., Forel, M.B., Crasquin, S., Ghaderi, A. and Korn, D., 2021. Ostracods from the end-Permian mass extinction in the Aras Valley section (north-west Iran). *Papers in Palaeontology*, 7(2), pp.1003-1042. DOI: [10.1002/spp2.1330](https://doi.org/10.1002/spp2.1330)
- Gliwa, J., Ghaderi, A., Leda, L., Schobben, M., Tomás, S., Foster, W.J., Forel, M.B., Ghanizadeh Tabrizi, N., Grasby, S.E., Struck, U. and Ashouri, A.R., 2020. Aras Valley (northwest Iran): high-resolution stratigraphy of a continuous central Tethyan Permian–Triassic boundary section. *Fossil Record*, 23(1), pp.33-69. DOI: [10.5194/fr-23-33-2020](https://doi.org/10.5194/fr-23-33-2020)
- Golonka, J., 2002. "Plate-tectonic maps of the Phanerozoic." DOI [10.2110/pec.02.72.0021](https://doi.org/10.2110/pec.02.72.0021)
- Golonka, J., 2004. Plate tectonic evolution of the southern margin of Eurasia in the Mesozoic and Cenozoic. *Tectonophysics*, 381(1-4), pp.235-273.
- Grabowski Jr, G.J. and Norton, I.O., 1995. *Tectonic controls on the stratigraphic architecture and hydrocarbon systems of the Arabian Plate* (No. CONF-951013-). Society of Exploration Geophysicists, Tulsa, OK (United States).
- Grunt, T.A., Ruzhencev, V.E. and Sarycheva, T.G., 1965. Superfamily Athyridacea. *Evolution and Change of Marine Organisms at the Paleozoic-Mesozoic Boundary. Akademiia Nauk SSSR, Trudy Paleontologicheskogo Instituta*, 108, pp.237-253.

- Heuer, F., Leda, L., Moradi-Salimi, H., Gliwa, J., Hairapetian, V. and Korn, D., 2021. The Permian–Triassic boundary section at Baghuk Mountain, Central Iran: carbonate microfacies and depositional environment. *Palaeobiodiversity and Palaeoenvironments*, pp.1-20.
- Heydari, E., Hassanzadeh, J. and Wade, W.J., 2000. Geochemistry of central Tethyan upper Permian and lower Triassic strata, Abadeh region, Iran. *Sedimentary Geology*, 137(1-2), pp.85-99.
- Heydari, E., Hassanzadeh, J., Wade, W.J. and Ghazi, A.M., 2003. Permian–Triassic boundary interval in the Abadeh section of Iran with implications for mass extinction: Part 1 Sedimentology. *Palaeogeography, Palaeoclimatology, Palaeoecology*, 193(3-4), pp.405-423.
- Horton, B.K., Hassanzadeh, J., Stockli, D.F., Axen, G.J., Gillis, R.J., Guest, B., Amini, A., Fakhari, M.D., Zamanzadeh, S.M. and Grove, M., 2008. Detrital zircon provenance of Neoproterozoic to Cenozoic deposits in Iran: Implications for chronostratigraphy and collisional tectonics. *Tectonophysics*, 451(1-4), pp.97-122.
- Iranian-Japanese Research Group, 1981. The Permian and the Lower Triassic Systems in Abadeh region, central Iran. *Mem. Fac. Sci., Kyoto Univ., Ser. Geol. Mineral.*, 47, pp.61-133.
- Irving, E., 1977. Drift of the major continental blocks since the Devonian. *Nature*, 270(5635), pp.304-309. DOI: 10.1038/270304a0
- Irving, E., 2005. The role of latitude in mobilism debates. *Proceedings of the National Academy of Sciences*, 102(6), pp.1821-1828. DOI: 10.1073/pnas.0408162101.
- Kalvoda, J., 2002. *Late Devonian–Early Carboniferous foraminiferal fauna: zonations, evolutionary events, paleobiogeography and tectonic implications* (Vol. 39). Brno, Czech Republic: Masaryk University.
- Kiessling, W., Schobben, M., Ghaderi, A., Hairapetian, V., Leda, L. and Korn, D., 2018. Pre–mass extinction decline of latest Permian ammonoids. *Geology*, 46(3), pp.283-286.
- Korn, D., Ghaderi, A. and Tabrizi, N.G., 2019. Early Changhsingian (Late Permian) ammonoids from NW Iran. *Neues Jahrbuch für Geologie und Paläontologie – Abhandlungen* 293(1): 37-56. DOI: [10.1127/njgpa/2019/0829](https://doi.org/10.1127/njgpa/2019/0829)
- Korn, D., Ghaderi, A., Leda, L., Schobben, M. and Ashouri, A.R., 2016. The ammonoids from the Late Permian Paratirolites Limestone of Julfa (East Azerbaijan, Iran). *Journal of Systematic Palaeontology*, 14(10), pp.841-890.
- Korte, C., Kozur, H.W. and Veizer, J., 2005. $\delta^{13}\text{C}$ and $\delta^{18}\text{O}$ values of Triassic brachiopods and carbonate rocks as proxies for coeval seawater and palaeotemperature. *Palaeogeography, Palaeoclimatology, Palaeoecology*, 226(3-4), pp.287-306.
- Korte, C., Kozur, H.W., Joachimski, M.M., Strauss, H., Veizer, J. and Schwark, L., 2004. Carbon, sulfur, oxygen and strontium isotope records, organic geochemistry and biostratigraphy across the Permian/Triassic boundary in Abadeh, Iran. *International Journal of Earth Sciences*, 93, pp.565-581.

- Kozur, H.W. and Bachmann, G.H., 2005. Correlation of the Germanic Triassic with the international scale. *Albertiana*, 32, pp.21-35.
- Kozur, H.W., 2004. *Pelagic uppermost Permian and the Permian-Triassic boundary conodonts of Iran: Part I: Hallesches Jahrbuch für Geowissenschaften* 18: pp. 39-68.
- Kozur, H.W., 2005. Pelagic uppermost Permian and the Permian–Triassic boundary conodonts of Iran. Part II: investigated sections and evaluation of the conodont faunas. *Hallesches Jahrbuch für Geowissenschaften B, Beiheft* 19:49–86
- Leda, L., Korn, D., Ghaderi, A., Hairapetian, V., Struck, U. and Reimold, W.U., 2014. Lithostratigraphy and carbonate microfacies across the Permian–Triassic boundary near Julfa (NW Iran) and in the Baghuk Mountains (Central Iran). *Facies*, 60, pp.295-325.
- Leonhard, I., Shirley, B., Murdock, D.J., Repetski, J. and Jarochovska, E., 2021. Growth and feeding ecology of coniform conodonts. *PeerJ*, 9, p.e12505.
- Leven, E.J., 1998. Permian fusulinid assemblages and stratigraphy of the Transcaucasia. *Rivista Italiana di Paleontologia e Stratigrafia*, 104(3).
- Leven, E.J., Reimers, A.N. and Kozur, H.W., 2007. First finds of Permian conodonts in eastern Iran and once again on the Guadalupian series base in Permian sections of the Tethyan realm. *Stratigraphy and Geological Correlation*, 15, pp.57-66.
- Leven, E.J. and Mohaddam, H.V., 2004. Carboniferous-Permian stratigraphy and fusulinids of eastern Iran. The Permian in the Bag-e-Vang section (Shirgesht area). *Rivista Italiana di Paleontologia e Stratigrafia*, 110(2).
- Leven, E.J. and Gorgij, M.N., 2011. Fusulinids and stratigraphy of the Carboniferous and Permian in Iran. *Stratigraphy and Geological Correlation*, 19, pp.687-776.
- Li, H., Dong, H., Jiang, H., Wignall, P.B., Chen, Y., Zhang, M., Ouyang, Z., Wu, X., Wu, B., Zhang, Z. and Lai, X., 2022. Integrated conodont biostratigraphy and $\delta^{13}\text{C}_{\text{carb}}$ records from end Permian to Early Triassic at Yiwagou Section, Gansu Province, northwestern China and their implications. *Palaeogeography, Palaeoclimatology, Palaeoecology*, 601, p.111079.
- Liu, X.C., Wang, W., Shen, S.Z., Gorgij, M.N., Ye, F.C., Zhang, Y.C., Furuyama, S., Kano, A. and Chen, X.Z., 2013. Late Guadalupian to Lopingian (Permian) carbon and strontium isotopic chemostratigraphy in the Abadeh section, central Iran. *Gondwana Research*, 24(1), pp.222-232.
- McCall, G.J., 2002. A summary of the geology of the Iranian Makran. *Geological Society, London, Special Publications*, 195(1), pp.147-204.
- McCall, G.J.H., 2003. A critique of the analogy between Archaean and Phanerozoic tectonics based on regional mapping of the Mesozoic-Cenozoic plate convergent zone in the Makran, Iran. *Precambrian Research*, 127(1-3), pp.5-17.

- Mohammadi, P., Ghaderi, A. and Ashouri, A.R., 2023. Lithostratigraphy and biostratigraphy of Wuchiapingian succession in the Qareh-Goz section (south of Julfa, northwest of Iran) based on brachiopods. *Scientific Quarterly Journal, Geosciences*, 33(2), p.128.
- Muttoni, G., Kent, D.V. and Channell, J.E., 1996. Evolution of Pangea: paleomagnetic constraints from the Southern Alps, Italy. *Earth and Planetary Science Letters*, 140(1-4), pp.97-112.
- Muttoni, G., Kent, D.V., Garzanti, E., Brack, P., Abrahamsen, N. and Gaetani, M., 2003. Early Permian Pangea 'B' to Late Permian Pangea 'A'. *Earth and Planetary Science Letters*, 215(3-4), pp.379-394.
- Muttoni, G., Gaetani, M., Kent, D.V., Sciunnach, D., Angiolini, L., Berra, F., Garzanti, E., Mattei, M. and Zanchi, A., 2009a. Opening of the Neo-Tethys Ocean and the Pangea B to Pangea A transformation during the Permian. *GeoArabia*, 14(4), pp.17-48.
- Muttoni, G., Mattei, M., Balini, M., Zanchi, A., Gaetani, M. and Berra, F., 2009b. The drift history of Iran from the Ordovician to the Triassic. *Geological Society, London, Special Publications*, 312(1), pp.7-29.
- Nabavi, M.H., 1976. An introduction to the geology of Iran. *Geological Survey of Iran*, 109.
- Nezafati, N., 2006. Au-Sn-W-Cu Mineralization in the Astaneh-Sarband area, West Central Iran. *Dissertation, Geowissenschaftlichen Fakultät, Universität Tübingen, Tübingen*.
- Partoazar, H., 1995. Permian deposits in Iran. *Treatise on the Geology of Iran*, 22(1-7), p.340.
- Partoazar, H., 2002. Permian-Triassic boundary conodonts from Julfa-Abadeh Belt along Northwest and Central Iran. *Permophiles*, 41, pp.34-40.
- Pronina, G.P., 1988. The late Permian smaller foraminifers of Transcaucasus. *Revue de paléobiologie*, pp.89-96.
- Rachidnejad-Omran, N., Emami, M.H., Sabzehei, M., Rastad, E., Bellon, H. and Piqué, A., 2002. Lithostratigraphie et histoire paléozoïque à paléocène des complexes métamorphiques de la région de Muteh, zone de Sanandaj-Sirjan (Iran méridional). *Comptes Rendus Geoscience*, 334(16), pp.1185-1191.
- Robert, A.M., Letouzey, J., Kavooosi, M.A., Sherkati, S., Müller, C., Vergés, J. and Aghababaei, A., 2014. Structural evolution of the Kopeh Dagh fold-and-thrust belt (NE Iran) and interactions with the South Caspian Sea Basin and Amu Darya Basin. *Marine and Petroleum Geology*, 57, pp.68-87.
- Rostovtsev, K.O. and Azaryan, N.R., 1973. The Permian-Triassic boundary in Transcaucasia.
- Ruban, D.A., Al-Husseini, M.I. and Iwasaki, Y., 2007. Review of Middle East Paleozoic plate tectonics. *GeoArabia*, 12(3), pp.35-56.
- Rüttner, J.R., Spycher, M.A. and Engeler, M.L., 1968. Pulmonary fibrosis induced by cotton fiber inhalation. *Pathologia et Microbiologia*, 32(1), pp.1-14.
- Saidi, A., Brunet, M.F. and Ricou, L.E., 1997. Continental accretion of the Iran Block to Eurasia as seen from Late Paleozoic to Early Cretaceous subsidence curves. *Geodynamica Acta*, 10(5), pp.189-208.

- Schobben, M., Ullmann, C.V., Leda, L., Korn, D., Struck, U., Reimold, W.U., Ghaderi, A., Algeo, T.J. and Korte, C., 2016. Discerning primary versus diagenetic signals in carbonate carbon and oxygen isotope records: An example from the Permian–Triassic boundary of Iran. *Chemical Geology*, 422, pp.94-107.
- Schobben, M., Van De Velde, S., Gliwa, J., Leda, L., Korn, D., Struck, U., Ullmann, C.V., Hairapetian, V., Ghaderi, A., Korte, C. and Newton, R.J., 2017. Latest Permian carbonate carbon isotope variability traces heterogeneous organic carbon accumulation and authigenic carbonate formation. *Climate of the Past*, 13(11), pp.1635-1659.
- Scotese, C.R., 2004. A continental drift flipbook. *The Journal of Geology*, 112(6), pp.729-741.
- Şengor, A.C., 1984. The Cimmeride orogenic system and the tectonics of Eurasia.
- Şengor, A.M.C., 1979. The North Anatolian transform fault: its age, offset and tectonic significance. *Journal of the Geological Society*, 136(3), pp.269-282.
- Şengor, A.M.C., 1990. A new model for the late Palaeozoic—Mesozoic tectonic evolution of Iran and implications for Oman. *Geological Society, London, Special Publications*, 49(1), pp.797-831.
- Şengor, A.M.C., Altiner, D., Cin, A., Ustaömer, T. and Hsü, K.J., 1988. Origin and assembly of the Tethyside orogenic collage at the expense of Gondwana Land. *Geological Society, London, Special Publications*, 37(1), pp.119-181.
- Sepehr, M. and Cosgrove, J.W., 2004. Structural framework of the Zagros fold–thrust belt, Iran. *Marine and Petroleum Geology*, 21(7), pp.829-843.
- Shabanian, R. and Bagheri, M., 2008. Permian in Northwest of Iran. *Permophiles*, 51, pp.28-31.
- Sharland, P.R., Casey, D.M., Davies, R.B., Simmons, M.D. and Sutcliffe, O.E., 2004. Arabian plate sequence stratigraphy—revisions to SP2. *GeoArabia*, 9(1), pp.199-214.
- Shen, S.Z. and Mei, S.L., 2010. Lopingian (Late Permian) high-resolution conodont biostratigraphy in Iran with comparison to South China zonation. *Geological Journal*, 45(2-3), pp.135-161.
- Stampfli, G., Marcoux, J. and Baud, A., 1991. Tethyan margins in space and time. *Palaeogeography, Palaeoclimatology, Palaeoecology*, 87(1-4), pp.373-409.
- Stampfli, G.M., Borel, G.D., Cavazza, W., Mosar, J. and Ziegler, P.A., 2001. Palaeotectonic and palaeogeographic evolution of the western Tethys and Peri-Tethyan domain (IGCP Project 369).
- Stampfli, G.M. and Borel, G.D., 2002. A plate tectonic model for the Paleozoic and Mesozoic constrained by dynamic plate boundaries and restored synthetic oceanic isochrons. *Earth and Planetary Science Letters*, 196(1-2), pp.17-33.
- Stampfli, G.M. and Borel, G.D., 2004. "The TRANSMED transects in space and time: constraints on the paleotectonic evolution of the Mediterranean domain." In *The TRANSMED Atlas. The Mediterranean region from crust to mantle: Geological and geophysical framework of the Mediterranean and the surrounding areas*, pp. 53-80. Berlin, Heidelberg: Springer Berlin Heidelberg.

- Stepanov, D.L., Golshani, F. and Stöcklin, J., 1969. *Upper Permian and Permian-Triassic boundary in North Iran* (No. 12). Geological Survey of Iran.
- Stöcklin, J., 1968. Structural history and tectonics of Iran: a review. *AAPG Bulletin*, 52(7), pp.1229-1258.
- Stöcklin, J., 1974. Possible ancient continental margins in Iran. In *The geology of continental margins* (pp. 873-887). Berlin, Heidelberg: Springer Berlin Heidelberg.
- Stöcklin, J., 1977. Structural correlation of the Alpine ranges between Iran and Central Asia.
- Tabrizi, N.G., Ghaderi, A., Ashouri, A.R. and Korn, D., 2021. A new record of the Permian ammonoid family Cyclolobidae from Julfa (NW Iran). *Neues Jahrbuch für Geologie und Paläontologie-Abhandlungen*, pp.221-230.
- Taheri, A., 2002. *Stratigraphy of Permian deposits (Jamal formation) in Tabas basin* (Doctoral dissertation, PhD Thesis, Isfahan University, Iran).
- Taraz, H., 1969. Permo-Triassic section in central Iran. *AAPG Bulletin*, 53(3), pp.688-693.
- Taraz, H., 1974. Geology of the Surmaq–Deh Bid area, Abadeh Region, central Iran: *Geol. Surv. Iran. Rep.*, (37), p.147.
- Taraz, H., Golshani, F., Nakazawa, K., Shimizu, D., Bando, Y., Ishii, K.I., Murata, M., Okimura, Y., Sakagami, S., Nakamura, K. and Tokuoka, T., 1981. The Permian and the Lower Triassic systems in Abadeh region, central Iran. *Memoirs of the Faculty of Science, Kyoto University. Series of geology and mineralogy*, 47(2), pp.61-133.
- Teichert, C., Kummel, B. and Sweet, W.C., 1973. Permian-Triassic strata, Kuh-e-Ali Bashi, northwestern Iran, pp 359-472.
- Torq, F., Besse, J., Vaslet, D., Marcoux, J., Ricou, L.E., Halawani, M. and Basahel, M., 1997. Paleomagnetic results from Saudi Arabia and the Permo-Triassic Pangea configuration. *Earth and Planetary Science Letters*, 148(3-4), pp.553-567.
- Torsvik, T.H. and Cocks, L.R.M., 2004. Earth geography from 400 to 250 Ma: a palaeomagnetic, faunal and facies review. *Journal of the Geological Society*, 161(4), pp.555-572.
- Vachard, D., Hauser, M., Martini, R., Zaninetti, L., Matter, A. and Peters, T., 2002. Middle Permian (Midian) foraminiferal assemblages from the Batain Plain (Eastern Oman): their significance to Neotethyan paleogeography. *The Journal of Foraminiferal Research*, 32(2), pp.155-172.
- Von Raumer, J.F., Stampfli, G.M. and Bussy, F., 2003. Gondwana-derived microcontinents—the constituents of the Variscan and Alpine collisional orogens. *Tectonophysics*, 365(1-4), pp.7-22.
- Vuolo, I., 2014. *Conodont biostratigraphy from Carboniferous and Permian successions of Pamir, Central Iran and Tunisia* (Doctoral dissertation, PhD Thesis. Università Degli Studi Di Milano, 308p).
- Wang, X., Gorgij, M.N. and Yao, L., 2018. A Cathaysian rugose coral fauna from the upper Carboniferous of central Iran. *Journal of Paleontology*, 93(3), pp.399-415.

- Wilmsen, M., Fürsich, F.T., Seyed-Emami, K. and Majidifard, M.R., 2009b. An overview of the stratigraphy and facies development of the Jurassic System on the Tabas Block, east-central Iran. *Geological Society, London, Special Publications*, 312(1), pp.323-343.
- Wilmsen, M., Fürsich, F.T., Seyed-Emami, K., Majidifard, M.R. and Taheri, J., 2009a. The Cimmerian Orogeny in Northern Iran: Tectono-stratigraphic evidence from the foreland. *Terra Nova*, 21(3), pp.211-218.
- Zanchi, A., Berra, F., Mattei, M., Ghassemi, M.R. and Sabouri, J., 2006. Inversion tectonics in central Alborz, Iran. *Journal of Structural Geology*, 28(11), pp.2023-2037.
- Zanchi, A., Zanchetta, S., Garzanti, E., Balini, M., Berra, F., Mattei, M. and Muttoni, G., 2009. The Cimmerian evolution of the Nakhlak–Anarak area, Central Iran, and its bearing for the reconstruction of the history of the Eurasian margin. *Geological Society, London, Special Publications*, 312(1), pp.261-286.

CHAPTER 3

Material and methods

3.1. INTRODUCTION	62
3.2. EXTRACTION PROCESSING METHODS	62
3.2.1. CONODONT EXTRACTION PROCESSING METHODS	<u>71</u>
3.2.1.1. CH ₂ O ₂ PROTOCOL.....	<u>72</u>
3.2.1.2. CH ₃ COOH PROTOCOL.....	<u>72</u>
3.2.1.3. OUTCOMES FROM THE PROTOCOLS	73
3.2.2. OSTRACOD EXTRACTION PROCESSING METHODS	<u>76</u>
3.2.2.1. HOT ACETOLYSIS	<u>77</u>
3.2.2.2. OUTCOMES FROM THE PROTOCOLS	<u>81</u>
3.2.3. RADIOLARIA EXTRACTION PROCESSING METHODS	<u>83</u>
3.2.3.1. OUTCOMES FROM THE PROTOCOLS	<u>84</u>
3.2.4. THIN SECTION PROCESSING METHODS	<u>85</u>
3.3. CONCLUSION	86
3.4. REFERENCES	<u>87</u>

3.1. INTRODUCTION

The studies of fossils request a preparation of the rocks depending on their composition and the nature of the fossil. Different approaches have to be used. These various techniques underscore the multifaceted nature of sample dissolution and preparation within analytical chemistry and paleontology. Dissolving samples in hard rock is a primary stage in analytical chemistry, and the literature is replete with references detailing various methodologies for sample dissolution (Sulcek & Povondra 1989).

This process isn't confined to chemistry alone; its historical significance in paleontology extends over a century. In the pursuit of fossils, the application of hydrochloric acid as a dissolving agent date as far back as the late 19th century (Jepsson et al. 1999). Microfossils are essential components of sedimentary rocks used for palaeontological, biostratigraphic, palaeoenvironmental and palaeoclimatic investigations. They are usually extracted from rocks using an acid solution, which might vary depending on the embedding rock lithology (Rigo et al. 2023). Simulating nature's gradual erosion process becomes a fundamental technique involving controlled freezing and thawing cycles within laboratory conditions (Remin et al. 2012). Alternate methods are employed for samples that require preservation beyond mere dissolution, such as sand samples housing delicate organisms (Szlauder-Łukaszewska & Radziejewska, 2013).

3.2. EXTRACTION PROCESSING METHODS

Following the initial clarification of prospective sections on geological maps, satellite images, and Google Earth software to ensure their accessibility, the field trip and sampling preparations were subsequently concluded. The first geological field trip was to the Ali-Bashi section in the Julfa region (Northwest of Iran), where sampling took place during the autumn of 2018. At this location, an extensive collection of over 240 rock samples (with an average weight of 3 to 5 kg per sample) was meticulously gathered from a measured thickness of 189 m in the Khachik Formation (Khachik Beds *sensu* Stepanov et al. 1969) (fig. 3.1).

The primary aim of procuring these samples is to facilitate an exhaustive lithostratigraphic and micropaleontological assessment. The extensive array of analyses encompassed a

detailed examination of conodonts, ostracods, foraminifers, radiolarian, and calcareous algae. The diverse nature of these microfossils promised to unlock valuable insights into the geological history encapsulated within this stratigraphic section. Beyond their biological significance, these collected samples held a dual purpose. In addition to the intricate paleontological inquiries, materials were deliberately reserved for future geochemical investigations (figs. 3.2-3.3).

During winter 2020, the second field trip was made in the Bagh-e-Vang section in the Tabas region (Central Iran). A meticulous effort resulted in collecting more than 150 rock samples from an outcrop measuring 260 m thick in the Jamal Formation (figs. 3.4-3.6).

Notably, significant emphasis was placed on delineating both designated sections' outer and inner boundaries during these field excursions. Furthermore, an extensive array of photographs, captured from diverse vantage points, was meticulously documented to elucidate the geological phenomena intrinsic to these sections vividly.

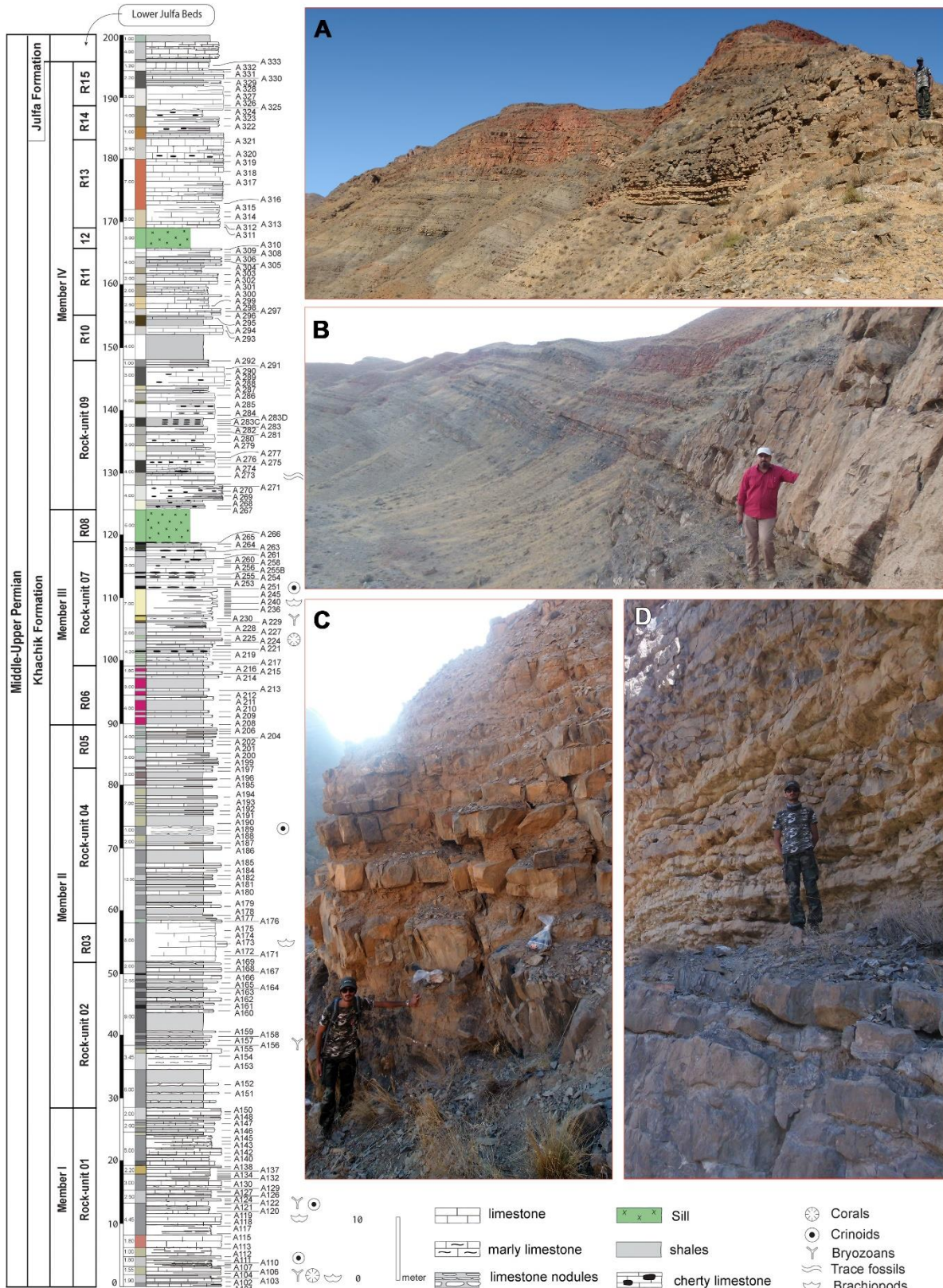


Fig. 3.1. Stratigraphic recording, field visuals, and sampling of the Khachik Formation at the Ali-Bashi Section. A. Field photographs of the lower part of the Khachik Beds, providing a northward perspective; B. A panoramic view of the upper parts of the Khachik Beds, featuring prominently bedded to massive cherty limestones, with a northwest-facing perspective; C. Close-up picture of the grey-colored limestone from the Khachik Beds, as viewed from the north; D. Picture of medium-bedded, cream-colored nodular formations, offering a north-westward perspective.



Fig. 3.2. Ali-Bashi section in the Julfa region: A. Dark grey-color thick-bedded limestone of of rock-unit 14 of Khachik Formation (the red color is the result of altering layers of Neogene red-beds that cover Khachik beds), north-western view; B. Grey-color limestone of rock-unit 05 from Khachik Formation, view from north; C. Crem-color nodular medium-bedded limestone of rock-unit 07 of Khachik Formation in the Ali-Bashi Mountain view to the north-west.

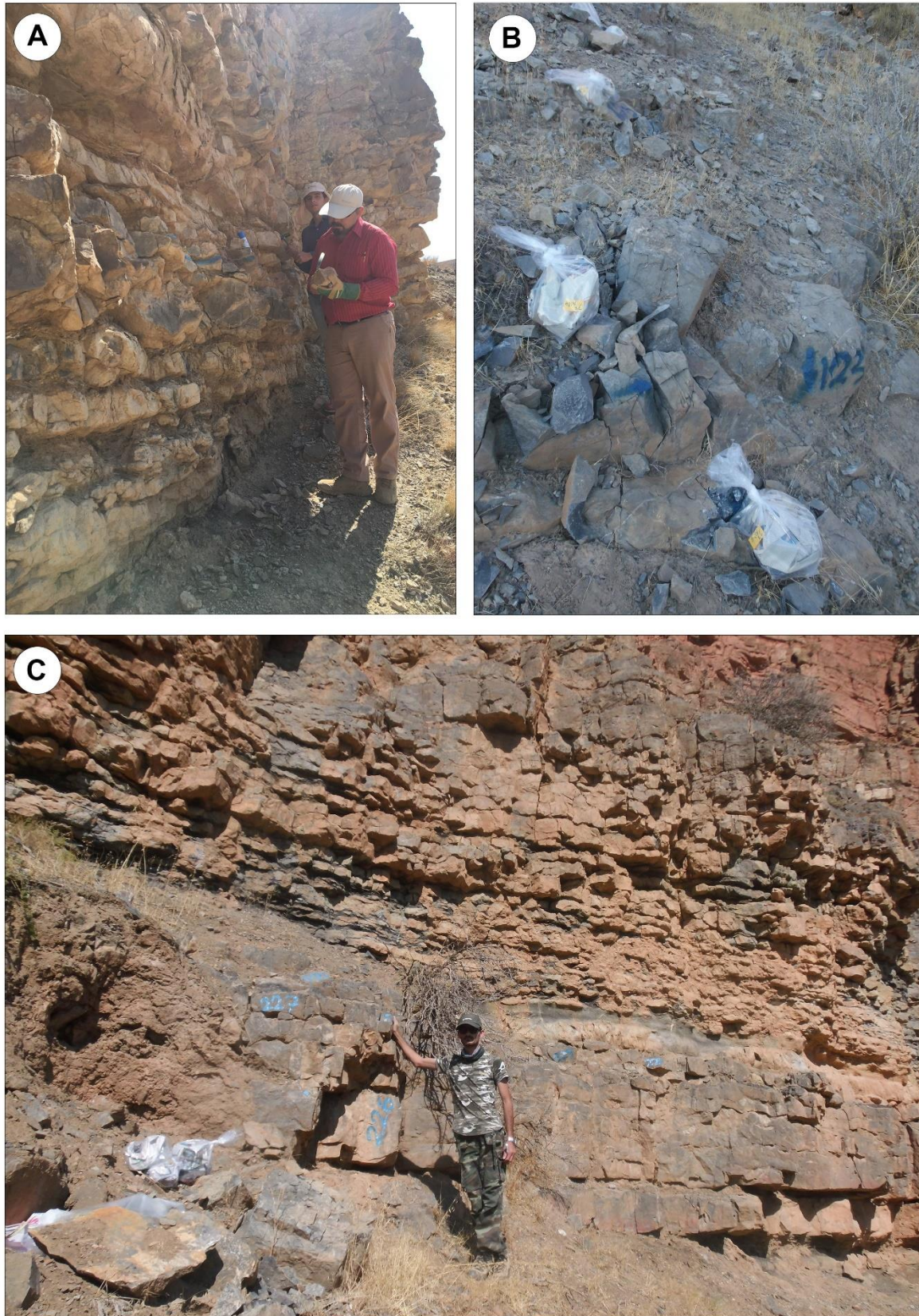


Fig. 3.3. Ali-Bashi section in the Julfa region: A. Crem-color medium to thick-bedded nodular limestone in some part of Khachik beds eyes view to the north-east; B. Grey-color limestone of rock-unit 09 in the lower part of section (rock-unit 01) of Khachik strata, eyes view to the north; C. Light grey-color thick-bedded limestone in the lower part (rock-unit 07) with thin-bedded in the upper part of Khachik Formation in the Ali-Bashi Mountain eyes view to the north.

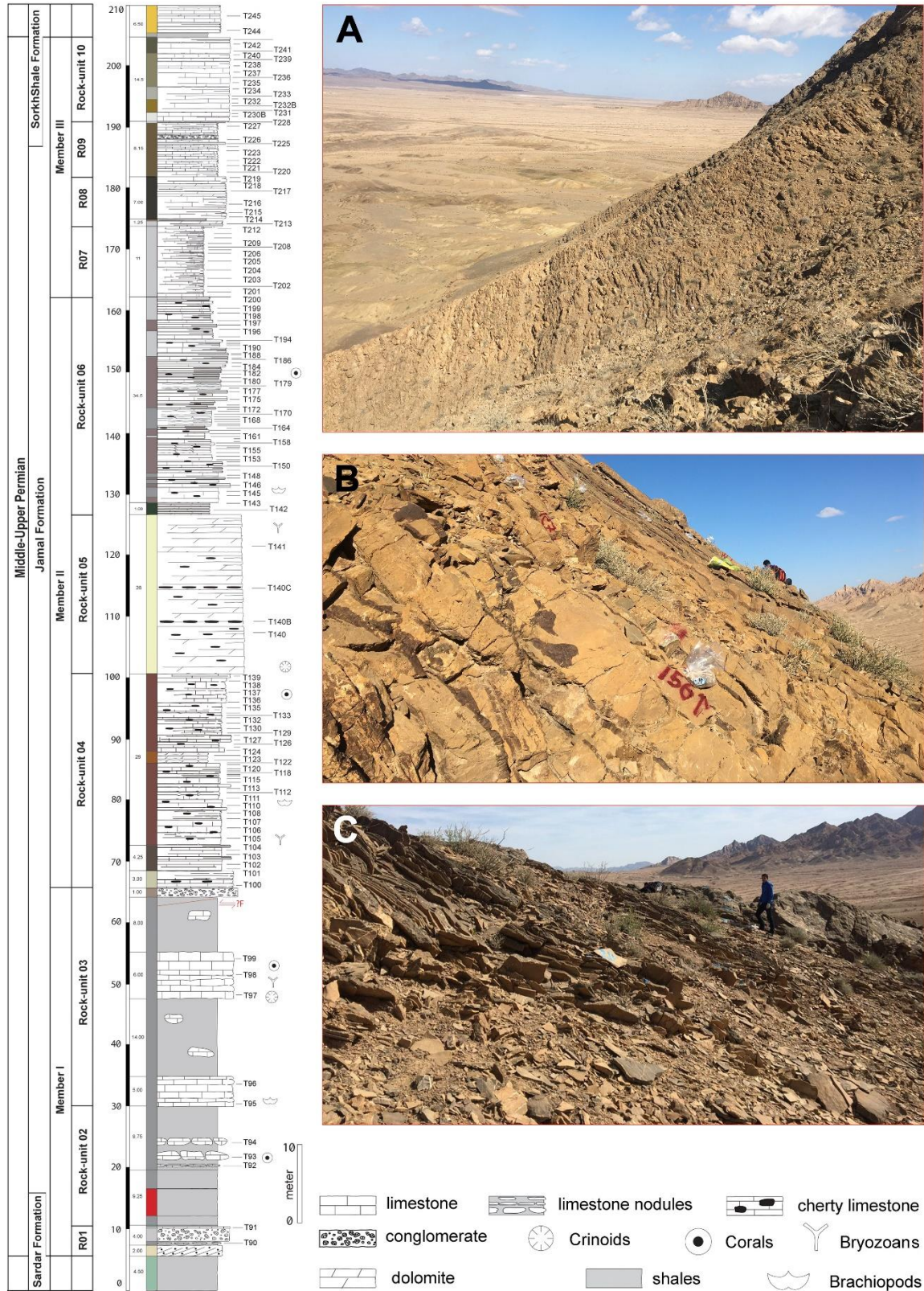


Fig. 3.4. Stratigraphic recording, field visuals, and sampling of the Jamal Formation at Bagh-e-Vang Section. A. A panoramic view, with a north-west-facing perspective; C. Close-up picture of the cream-colored limestone derived from the middle part of the section, as viewed from the north; D. A visual representation of thin-bedded, cream-colored to yellowish strata of the lower part, north-westward perspective.



Fig. 3.5. Field pictures showing of Bagh-e-Vang strata in Tabas region: A. Shown samples from crem-color medium to thick-bedded limestone of rock-unit 03 with cherts in some part; B. Cream to yellowish-color thick to tiny-bedded limestone of rock-unit 06; C) North-westly view of Permian strata of Bagh-e-Vang section (member II identified in this study).

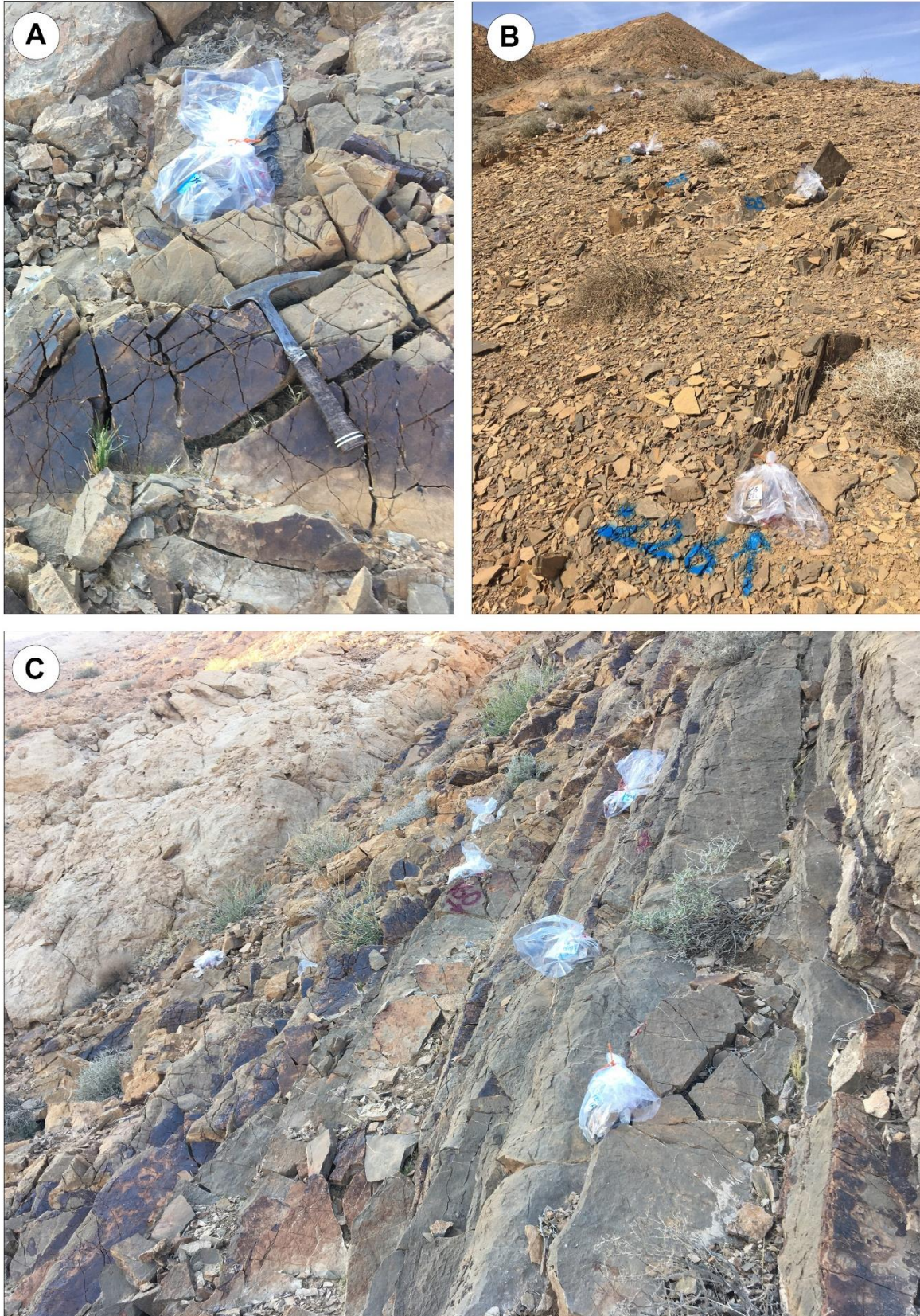


Fig. 3.6. Field pictures showing of Bagh-e-Vang strata in Tabas region: A. A cherty sample; B. Yellowish-color tiny-bedded limestone of upper part (rock-unit 09), view to north; C. Alternation of grey-color thick-bedded limestone with cherty layer of rock-unit 06, westly view.

Furthermore, detailed stratigraphic logs of the chosen sections were precisely transcribed bed by bed onto cross-section paper during sampling. This comprehensive record accounted for the stratigraphic sequence and meticulously documented fossil contents, variations in facies, and lithostratigraphic characteristics such as color transitions, thickness, and rock origins.

Sampling the Baghuk section, situated close to the Sanandaj-Sirjan Zone, we encountered specific obstacles that impeded our progress, including COVID-19 pandemic, climatic conditions and protests crisis across in Iran. The climatic conditions in Iran, especially, can present formidable barriers for field geologists and the intricate task of geological sampling. Within the confines of the Sanandaj-Sirjan Zone, the Abadeh region, much like the Tabash area, contends with adverse climate conditions spanning from spring to summer. This particular timeframe poses significant challenges for those engaged in field-oriented geological pursuits. Regrettably, the economic crisis in Iran set off a wave of extensive protests, ushering in a prolonged period of unrest throughout the nation this year. This pervasive turmoil took a direct toll on our meticulously planned Abadeh field trip, causing interruptions that culminated in the trip being canceled on three separate instances.

The persistent challenges posed by the prevailing circumstances necessitated these regrettable decisions. This third noteworthy factor significantly disrupted GBL activities in Iran, stemming from the emergence of the COVID-19 pandemic. Consequently, the sampling efforts directed toward the Baghuk section experienced a series of recurring delays. Considering the explanations above, it is regrettable that we must confirm the complete cancellation of the sampling for the Baghuk section. Nevertheless, I should actively consider integrating this undertaking into forthcoming projects.

From this standpoint, in pursuit of achieving the research objectives and identifying microfossils such as conodonts, ostracods, and radiolarians in the sedimentary sequences of the Ali-Bashi and Bagh-E-Vang sections, as well as precisely determining the location of the Guadalupian-Lopingian boundary (GLB) within these stratigraphical segments, extraction techniques have been employed. A more comprehensive elucidation will be presented in the subsequent sections.

3.2.1. CONODONT EXTRACTION METHODS

Conodonts are small elements of the feeding apparatus of a marine eel-like organism that lived in the Paleozoic to Triassic oceans; however, recently, some occurrences were reported by [Du et al. \(2020\)](#) in the early Hettangian of North America and Hungary. Conodonts were almost ubiquitously diffused from lower to higher latitudes and their biostratigraphic power is well known. These marine organisms, characterized by their elongated, armless, unarmored and eel-like form, also featured large eyes ([Purnell 1995](#)). Conodont elements are tooth-like structures composed of phosphate, and their current understanding suggests they were integral to the feeding apparatus of an extinct early vertebrate (conodont animal). Their abundance and distribution make them an irreplaceable tool for constructing bio-chronostratigraphic scales for the Conodontozoic ([Ferreti et al. 2020](#)).

They are ideal biomarkers for global scale correlations and GSSPs definitions ([Briggs et al. 1983](#); [Purnell 1995](#); [Voulo 2014](#)). 19 of the 48 Palaeozoic Stages were defined based on conodont bioevents and three are in a phase of definition while, in the Triassic, 3 of the 7 Stages are based on conodonts ([Shen et al. 2012](#)).

Conodonts generally are recovered from shales, marls, and, in particular, limestones. Carbonate rocks are dissolved using dilute organic acetic and formic acids ([Rigo et al. 2023](#)). They are occasionally observed on bedding planes, although they are primarily extracted through processes involving the dissolution of carbonate rock using a 10% solution of acetic acid ([Jeppsson et al. 1999](#)), or acetic (CH_3COOH), formic (CH_2O_2), or monochloric acid ($\text{ClCH}_2\text{CO}_2\text{H}$).

Alternatively, they can be separated from shale by boiling with Quaternary-O detergent. Often, a combination of these methods is employed. Subsequent steps involve sieving to retain particles larger than 75 μm , categorized as sand-size, which are then subjected to drying. Density separation is then carried out using heavy liquids with a specific gravity of 2.85, such as tetrabromoethane or sodium polytungstate; it's important to note that certain elements possess a particular gravity of 2.93.0 ([Gradeatin et al. 2020](#)). For the investigation of conodont content within the geological strata of the Khachik and Jamal Formations in the

Ali-Bashi and Bagh-E-Vang sections, a systematic process involving the iterative use of CH_2O_2 and CH_3COOH preparation methods was employed, performed.

3. 2. 1.1. CH_2O_2 PROTOCOL

Formic acid (CH_2O_2) is usually used to prepare micro-vertebrate fossils. In this preparation protocol, dust and other pollution were washed out by water after breaking rock samples into approximately 5 cm pieces with a hammer. Then, samples were immersed in 10% CH_2O_2 and after 24 hours, they were washed with water to neutralize the acid. Due to the heightened solubility of formic acid and its potential to affect the surface integrity of conodonts specimens, the subsequent neutralization step with water holds significant importance. It is advisable to conclude this process with a more generous amount of water. Additionally, to preserve specimens, it is recommended to conduct a gradual and thorough sample washing. Sieving is the next step to wipe the argillaceous sediments. Due to the microfossil sizes, two sieves, 1 mm and 63 μm , should be used. Then, the remaining deposits are transferred to a plastic bowl for drying. Repeating and continuing this CH_2O_2 preparation process is necessary until the rock is entirely dissolvable. In brief, this protocol could be investigated in two parameters: advantages and disadvantages (figs 3.7-3.8).

The benefits of the CH_2O_2 preparation method included: a) the protocol is easy to set up and does not require any hi-tech laboratory equipment; b) the use of 10% CH_2O_2 is economically affordable; c) the protocol requires less water for neutralization part than the other washing methods; d) repeating the protocol does not require a drying step and it is possible to sink again the sample in the acid immediately after the previous washing process; e) environmental pollution less effected by using this protocol by using 10% of CH_2O_2 , less acidity is used in this method less acid enters the recycling cycle. In contrast, this method has some weaknesses: a) CH_2O_2 , a relatively strong acid, makes an impression on soft-rock sediments and microfossils with fragile textures; b) CH_2O_2 is combustible and can be ignited.

3. 3. 2. CH_3COOH PROTOCOL

Acetic acid (CH_3COOH) is one of the simplest carboxylic acids. In the CH_3COOH technique, depending on the acid concentration, the immersion duration differs. For instance, when 10%

CH₃COOH is used for extraction, the immersion time is four days, and for 15% CH₃COOH, the duration is only three days. According to the rock resistance, 10% CH₃COOH for soft and 15% CH₃COOH for hard rocks are used in this method (figs 3.7-3.8). Like the previous protocol, the advantages of this method are: a) setting up the protocol is a breeze, as it does not demand advanced laboratory equipment. b) the use of 15% CH₃COOH makes it inexpensive; c) water washing part for neutralization requires less water; d) repeating the protocol does not require the drying part of rock samples; e) the environment is less polluted by using this protocol; f) CH₃COOH as a weak acid has a less destructive effect on soft rocks and microfossils with fragile textures.

3. 3. 4. OUTCOMES FROM THE PROTOCOLS

Following extensive and meticulous preparation efforts and adhering to a meticulously designed protocol aimed at identifying conodont elements, a comprehensive analysis was conducted on more than 240 samples sourced from the Khachik Formation (referred to as Khachik Beds by [Stepanov et al. 1969](#)) in the Ali-Bashi section. The CH₂O₂ technique was employed during the sample preparation process, repeated at least three times for each sample, spanning over seven months (from spring to autumn of 2019).

Despite the rigorously executed procedures, the endeavor to trace these zonal markers of microfossils through high-performance microscopic sediment examination, unfortunately, did not yield the desired outcomes. The absence of conodonts in this particular section considered a promising candidate for conodont biostratigraphy, sent shockwaves through this project's scope. In a last attempt, even the final 30 samples from the concluding segment of the section underwent additional preparation using the acetic acid technique. Regrettably, this effort yielded the same results, maintaining the field's disappointment.



Fig. 3.7. Laboratory images showcasing the preparation of samples from the Ali-Bashi and Baghe-Vangh sections in Iran for conodont extraction, employing two distinct techniques (10% CH_2O_2 and 15% CH_3COOH).



Fig. 3.8. A-B. Depicts a series of laboratory images highlighting the preparation of samples from the Ali-Bashi and Bagh-e-Vangh sections for conodont extraction, utilizing two distinct techniques (10% CH₂O₂ and 15% CH₃COOH). Additionally: C. Illustrates the selection of cube-rock samples from both sections intended for thin section preparation and chemo-stratigraphy analysis. D. Depicts cherty samples chosen from both sections for chemo-stratigraphy analysis.

In the Bagh-e-Vang section, before the lockdown in 2020, most collected samples (more than 150 rock samples) were sourced from relatively less hard limestones. In this scenario, the approach of employing the diluted CH_3COOH technique was adopted to explore conodonts. Furthermore, after several months of dedicated effort and the meticulous examination of over 150 samples under the microscope, the second section conclusively showed the absence of conodonts.

3.2.2. OSTRACOD EXTRACTION PROCESSING METHODS

Ostracods, microcrustaceans that emerged during the Cambrian or Ordovician period, continue to evolve. They have successfully inhabited diverse aquatic environments, ranging from the deep bathyal plains to temporary ponds on land. Most ostracods (approximately 98%) are benthic, and their larval have the same way of life.

This behavior renders ostracods highly valuable as palaeoecological indicators, reflecting changes in water depth, salinity, and oxygen levels (Crasquin & Forel 2014). Due to their exceptional adaptability and ability to endure challenging conditions, ostracods have often been regarded as indicators of brackish environments. An example of their remarkable adaptability is the survival of a species (*Cyprideis torosa*) in the modern Aral Sea among the limited surviving fauna, as noted by Boomer et al. (2000). Despite this adaptability, their primary abundance lies within marine ecosystems.

Ostracods have a carapace in calcium carbonate. Hydrofluoric acid can extract them in the marine strata from siliceous host rocks like cherts, cherty limestones, and siliceous shales (Horne & Siveter 2016). The main problem is to extract calcareous carapace from limestones or carbonated rocks. Also, to obtain ostracods from the riverine sediments (River Odra, western part of Poland), Szlauer-Łukaszewska & Radziejewska (2013) used two different techniques of aeration and deterioration versus hand sorting to save time in the preparation of these sediments.

The most common process is hot acetolysis using pure acetic acid at 60°C (Lethiers & Crasquin-Soleau 1988; Crasquin-Soleau et al. 2005). In light of the time constraints imposed on this project and the substantial sample collection volume of both sections, the Ali-Bashi section was singled out to extract these microfossils and conduct subsequent interpretations.

Our extraction technique of ostracods involves diluted formic acid (CH_2O_2) and acetic acid (CH_3COOH), bypassing hot acetolysis. Recognizing the resemblance of these two protocols (diluted formic acid and acetic acid) to the method utilized for conodont extraction, repetition in their description is sidestepped, and their results are alluded to in the ensuing section. This section will mainly delve into comprehensively elucidating the hot acetolysis protocol.

3.2.2.1. HOT ACETOLYSIS PROTOCOL

The hot acetolysis method (Crasquin et al. 2005) is highly effective in extracting ostracods from hard carbonate sediment. The process consists of four steps: crushing, dehydration, acetolysis, and settling and washing. To begin, rock samples weighing 400-500 g are crushed into small pieces measuring several cm^3 to increase the reaction surface. These crushed rocks are then dehydrated to minimize the impact of humidity on the performance of anhydrous CH_3COOH and prevent any reaction with acid. To achieve this, they are placed in a heatproof glass receptacle and left in a dryer (maximum 70°C) for 48-72 hours to eliminate all residual water. The third step involves acetolysis, where the samples are removed from the dryer and allowed to cool down for approximately 30 minutes. Next, CH_3COOH 99% (anhydrous) is added to the glass container until the sample is completely covered with acid. The pot is then placed on a heating sand-bath set at a temperature of $60\text{-}80^\circ\text{C}$. Finally, the last step involves settling and washing the sample.

The multiple repetitions of this method have led me to make some remakes and updates on the Crasquin et al. (2005) protocol. One significant change is in the crushing step, which is crucial for enhancing the performance of pure CH_3COOH ; the reaction level increases by reducing the size of the samples to less than two centimetres. To conserve laboratory glassware and mitigate sample loss, it is essential to cool the samples for approximately 30 minutes before transferring them to the oven during the dehydration phase (It is recommended to use high lab glasses with narrow widths for optimal results in acetolysis).

Additionally, suppose the sand-bath temperature is set between $60\text{-}80^\circ\text{C}$. In that case, verifying the samples at least once a day is essential to avoid acid boiling or glass fracturing (this verification can be skipped if the sand-bath temperature is lower than 40°C). During the neutralization step, it would be preferable to put the samples under a tap for up to 30 minutes

and drain the water from the sample glass at least five times. The samples are placed in a heatproof glass container to repeat the technique and dried in a drier (maximum 70°C) for 48-72 hours. If there is any acid residue on the sediments, they are rinsed once more.

Furthermore, acid cement may be formed during the dissolution process, especially in soft-rock samples, resulting in the massing of sediments. If this occurs, stopping the operation and submerging the pieces underwater is crucial to prevent damage or loss of ostracods and samples. The immersion of samples in water should be done expertly and completed before any acid reactions occur because any extra acetic acid combined with water can generate an acid reaction that damages ostracod valves (figs 3.9-3.11).



Fig. 3.9. Complete series of laboratory procedures conducted in CR2P, France, encompassing various stages such as sample transportation (A-B) and the subsequent preparation utilizing the hot acetolysis protocol according to [Crasquin et al. \(2005\)](#) (C-F).

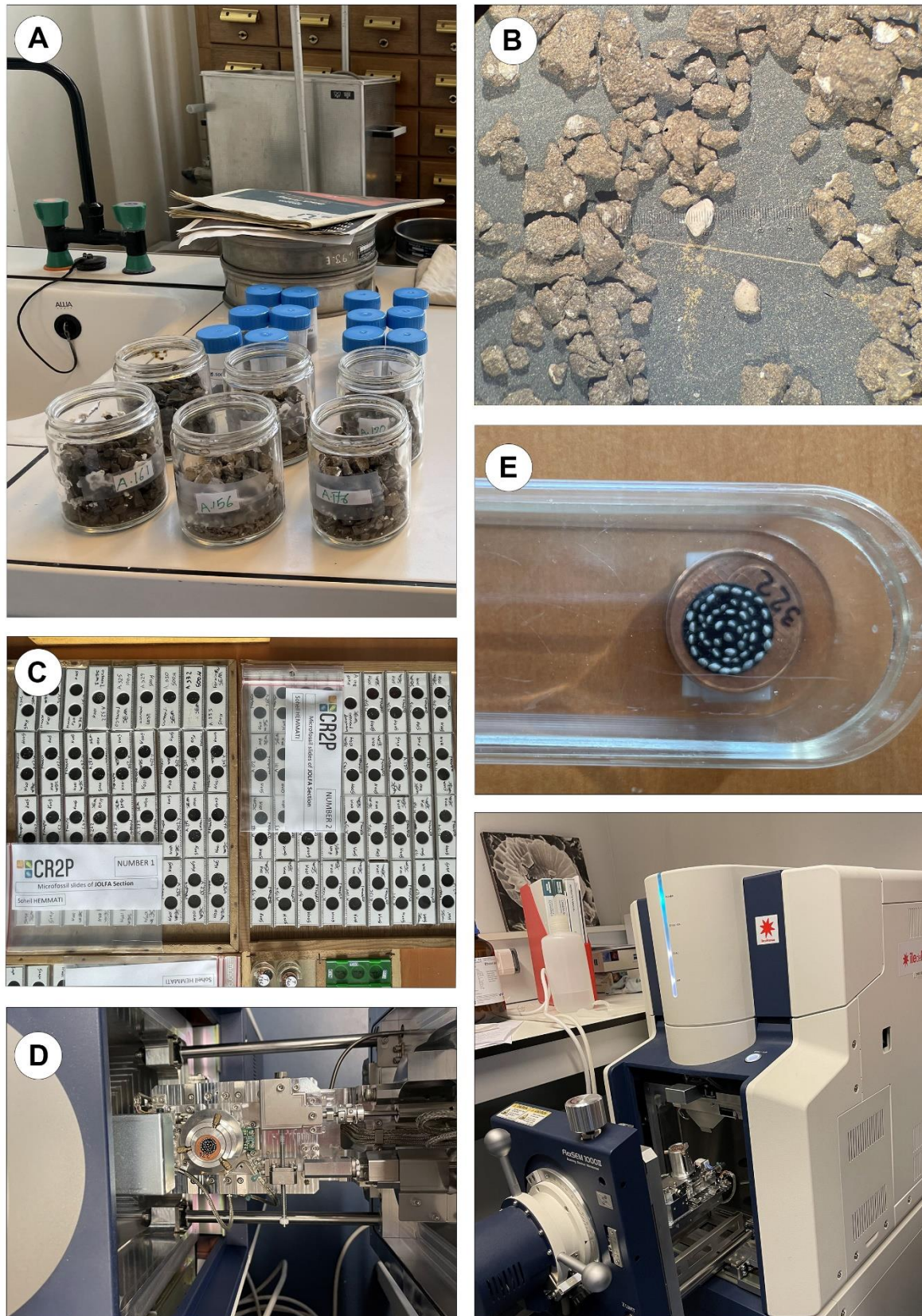


Fig. 3.10. Laboratory procedures carried out on the Ali-Bashi section in France: A. Implementation of the hot acetolysis protocol; B. Ostracod carapaces discovered within the sediment of the Ali-Bashi section; C. Comprehensive collection of ostracods extracted from this particular section; D-E. Scanning electron microscopy (SEM) images depicting ostracods from the Ali-Bashi section.

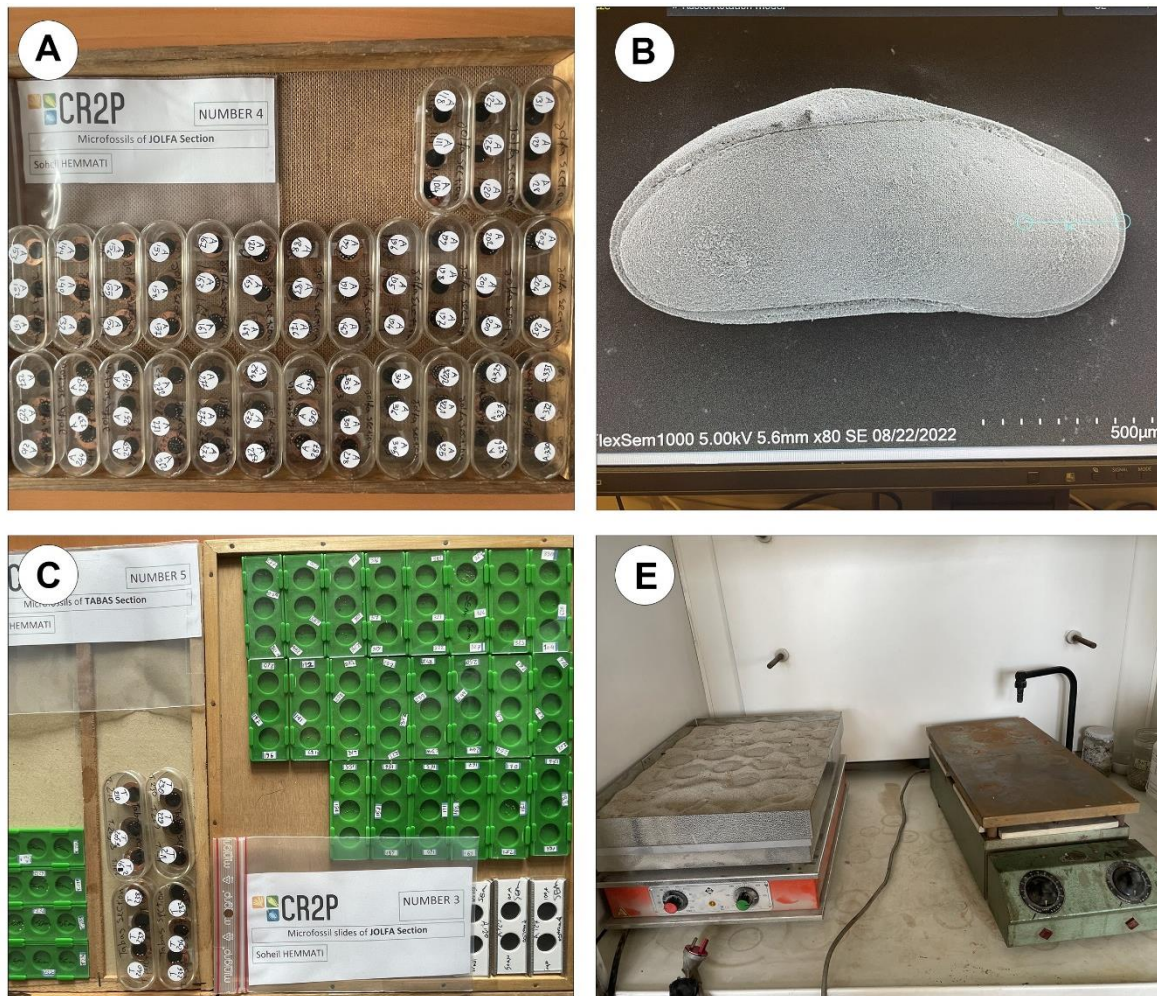


Fig. 3.11. Laboratory procedures conducted on both sections in France: A. Ostracods affixed onto carbon tapes for SEM analysis; B. SEM imagery capturing ostracod valves sourced from the Ali-Bashi section; C. Complete collection of extracted ostracods from the Ali-Bashi section (Stored at CR2P); D. Disruption in the operation of the sand-bath.

3.2.2.2. OUTCOMES FROM THE PROTOCOLS

CH₂O₂ as the first protocol treated on more than 240 samples of the Ali-Bashi section. Repetition of the CH₂O₂ technique successfully achieved the desired outcome and significantly improved the performance of the preparation methods. The obtained ostracods from this protocol have proper preservation and using this preparing method resulted in a determination of 12 species. These species are (plate 4.5 in chapter 4 pages, 137-139): *Bairdia deducta deducta* (Zalanyi, 1974), *Bairdia hungarica* Zalanyi, 1974, *Bairdia* sp., *Fabalitypris parva*, Wang 1978, *Fabalitypris* sp. 1, *Fabalitypris* sp. 2, *Fabalitypris* sp. 3, *Fabalitypris* sp. 4,

Hollinella (Hollinella) herrickana (Girty, 1909), *Hollinella* sp., *Sargentina transitia* (Kozur, 1985) and *Silenites* sp. Amongst these assemblages, *Bairdia* sp., *Hollinella (Hollinella) herrickana* (Girty, 1909), *Fabalitypris* sp. 1, *Fabalitypris* sp. 2, *Fabalitypris* sp. 3, *Fabalitypris* sp. 4, *Sargentina transitia* (Kozur, 1985) and *Silenites* sp., were obtained exclusively through the diluted CH₂O₂ protocol from dolomitized limestones. This is significant because these species were not commonly recovered from the hard dolomitized rocks.

Despite our great efforts and following this protocol step by step, the use of the CH₃COOH technique in the preparation of over 240 samples from the Ali-Bashi section failed. The utilization of varying concentrations of CH₃COOH (10% and 15%) in this research showed that the ostracod valves were damaged. Despite attempting to repeat the CH₃COOH process, it failed to achieve high preservation of the ostracods. This phenomenon can be attributed to the interaction and mixture between water and CH₃COOH.

The combined action of these substances facilitates the degradation of ostracod valves. This condition may result from a chemical interaction between acetic acid and water that causes rapidly producing bubbles that could harm the delicate valves of ostracods. Additionally, it was observed that an elevated acid concentration leads to more severe damage to the valves, as a higher concentration results in more bubbles being released within a shorter timeframe (refer to plate 4.5 M1 – M3 in chapter 4, 137).

I was disappointed by the unexpectedly poor performance of the diluted CH₃COOH technique; the higher solubility of formic acid in water and its superior ability to penetrate sediment particles made it a more effective method for separating ostracod valves from the sediment matrix. The obtained ostracods using the formic acid technique were of higher quality than those obtained using the acetic acid technique, particularly in hard-rock carbonates. Furthermore, the formic acid technique proved to be more successful in preserving the original morphology of the ostracod valves in these rocks.

I also tested the hot acetolysis protocol (Crasquin et al. 2005). I successfully extracted many well-preserved ostracods after applying this method to samples with a high potential for ostracod content in the Ali-Bashi section. This preparation method facilitated the identification of 59 species including (plates 4.1-4.4 in Chapter 4 pages, 130-136): *Acratia changxingensis* (Shi, 1987); *Acratia* sp.; *Bairdia deducta deducta* (Zalanyi, 1974); *Bairdia elcapitanensis* Forel 2021; *Bairdia* cf. *fangnianqiao* Crasquin, 2010; *Bairdia grotei* Chitnarin,

2017 *Bairdia hungarica* Zalanyi, 1974; *Bairdia khaokanaensis* Chitnarin, 2017; *Bairdia radlerae* Kellett, 1934; *Bairdia rhomboidalis* Hamilton, 1942; *Bairdia* cf. *songthami* Chitnarin et al. 2017; *Bairdia* sp.30 sensu Chitnarin, 2009; *Bairdia* sp. 1; *Bairdia* sp. 2; *Bairdia* sp. 3; *Bairdia* sp. 4; *Bairdia* sp. 5; *Bairdia* sp. 6; *Bairdia* sp. 7; *Bairdia* sp. 8; *Bairdia* sp. 9; *Bairdia* ? sp.; *Bairdiacypris longirobusta* Chen, 1958; *Bairdiacypris* sp. 6 sensu Zazzali et al., 2015; *Bairdiacypris* sp. B sensu Tarnac et al., 2021; *Bairdiacypris* sp. 1; *Bairdiacypris* sp. 2; *Bairdiacypris* sp. 3; *Bairdiacypris* sp. 4; *Bairdiacypris* sp. 5; *Bairdiacypris* sp. 6; *Bairdiacypris* sp. 7; *Bairdiacypris* sp. 8; *Bairdiacypris* sp. 9; *Bairdiacypris* sp.; *Ceratobairdia sexagintaduella* Forel, 2021; *Ceratobairdia*? cf. *crenata* Chen, 1982; *Fabalitypris acetata* (Coryell & Billings, 1932); *Fabalitypris glennensis* (Harlton, 1927); *Fabalitypris parva* Wang, 1978; *Fabalitypris reniformis* (Chen, 1958) sensu Wang, 1978; *Fabalitypris* sp. 5; *Fabalitypris* sp. 6; *Fabalitypris* sp. 7; *Hollinella* (*Hollinella*) *martensiformis* Crasquin et al., 2010 ; *Hollinella* sp. ; *Indivisia* sp. 1 sensu Forel et al. 2015; *Kempfina qinglaili* (Crasquin, 2008); *Kempfina* sp. 1 ; *Liuzhinia julfensis* Gliwa, 2021; *Praezabythocypris pulchra* Kozur, 1985; *Praezabythocypris* sp. 1; *Pseudacanthoscapha striatula* (Shi, 1982); *Reviya* sp. A; *Sargentina minuta* Wang, 1978; *Sargentina* sp.; and *Sulcella sulcata* Coryell & Sample, 1932. In the next chapter, these species will be systematically discussed in detail.

3.2.3. RADIOLARIA EXTRACTION METHOD

Radiolarians are single-celled, marine zooplankton floating near the surface or at depths of hundreds of meters. They belong to Phylum Radiozoa. The size of the radiolarian varies from 30 µm to 2 mm, and some form macroscopic colonies that may reach a size of a centimeter or more extensive. Temperature, salinity and nutrient characteristics of the water masses control the distribution of radiolarian assemblages (Sharma & Daneshian, 1998).

According to our field geological observation, in the strata of the Ali-Bashi and Bagh-e-Vang sections, cherty-nodular, and cherty-limestone variations up to cherty layers occur. As a result, delving into the inherent nature of these rock formations holds significant implications for understanding the Guadalupian Lopingian boundary (GLB) and the cherty sequences that marked this particular timeframe. Consequently, a deliberate selection process yielded

twelve cherty samples from the Ali-Bashi section and eight from the Bagh-e-Vang section, explicitly investigating their radiolarian potential.

The method employed draws from the characterization detailed by [Pessagno & Newport \(1972\)](#) for extracting these microfossils from cherts. This technique encompasses a series of steps meticulously applied to facilitate the extraction process:

Initially, a chert sample fragment undergoes an etching process utilizing concentrated hydrofluoric acid (HF 52-55%) for three to five minutes. The sample is carefully removed from the acid solution and given a gentle water rinse. Identifying Radiolaria distinctly protruding from the etched surface suggests the potential for extracting numerous Radiolaria.

Next, the sample is subjected to crushing, accomplished using a rock crusher or a steel mortar and pestle, resulting in the formation of fragments measuring 1 to 5 cm in size. Following this, the crushed chert fragments are placed within a plastic beaker containing dilute HF (10%) and left to interact for 24 hours. In some instances, adjustments in the degree of acid dilution or variations in reaction duration may be necessary based on specific cases.

The solution is discarded upon completion of the acid treatment, and the sample undergoes thorough washing. For the isolation of radiolarian specimens, a two-sieve approach is employed. The mesh with a 2 mm aperture retains undissolved sediment, while the 0.1 mm sieve captures smaller specimens. Subsequently, the residue that passes through the 0.1 mm sieve is transferred to a container and dried.

3.2.3.1. OUTCOMES FROM THE PROTOCOLS

Despite our dedicated efforts and rigorous adherence to the prescribed protocol, my attempt to utilize the HF technique in preparing twenty cherty samples collected from the Ali-Bashi and Bagh-e-Vang sections ([fig. 3.8D](#)). No radiolarian specimens were detected within the sediment of either set of samples. Nevertheless, my efforts were only partially in vain, as I did encounter a substantial quantity of sponge spicules. The presence of these sponge spicules presents an opportunity for future research. A more intricate examination of these spicules may offer valuable insights into the origin and formation of the cherty limestones within the Ali-Bashi and Bagh-e-Vang sections. By redirecting my focus toward this alternative angle, I

remain confident in unlocking a deeper understanding of the geological processes and ecological dynamics that have shaped these formations over time.

3.2.4. THIN SECTION PROCESSING METHOD

Considering the timeline constraints and the overarching objectives guiding this project, the emphasis on microfacies studies has been shifted to a secondary position. This strategic adjustment allows me to allocate my resources and efforts more effectively, ensuring a comprehensive exploration of the primary goals and an insightful examination of the Ali-Bashi section's palaeoenvironmental aspects (fig. 3.8C). Nearly 250 thin sections were realized in the sediments of the Khachik Formation (Khachik Beds *sensu* Stepanov et al. 1969) in the Ali-Bashi section.

A thorough analysis (involving at least five randomly selected fields) of the microfacies in thin sections obtained from the Khachik Formation's carbonate rocks at the Ali-Bashi section has revealed 28 sub-microfacies. These sub-microfacies, derived from the classification system established by Embry & Klovan (1971) and documented in Flugel (2010)'s ramp zones, correlate with 15 distinct microfacies. The assemblage of microfacies groups, ranging from MKL1 to MKL2, indicates a lagoonal environment, while the sedimentary microfacies from MKR2 to MKR3 exhibit features characteristic of a restricted inner ramp setting. The placement of microfacies groups, MKO1 to MKO4, suggests a confined setting after the limited development of microfacies within the inner ramp's final segments under an open marine environment. Microfacies groups MKM1 to MKM3 are inferred to have been deposited after the open marine environment within the mid-ramp zones, whereas MKT1 to MKT3 were identified in the initial segments of the outer ramp, corresponding to the Toe-of-slope position within the carbonate shelf setting. Additionally, adhering to the standard microfacies that Flugel (2010) designated, the study proposes ten microfacies of the RMF type, along with their corresponding 4 SMFs for the studied strata. According to the evaluation of the collected information from the identified microfacies, the depositional environment of the Khachik Formation in the Ali-Bashi section in the ramp carbonate platform ranges from the initial parts of the inner ramp to the outer ramp. Furthermore, there was no evidence of any sedimentary deposits belonging to deltaic, coastal, or continental

environments in the Khachik Formation, indicating that the deposition of the Khachik Formation sequences took place at least in a sedimentary environment away from the shoreline and the marginal basin deposits. Moreover, based on the standard facies zones (FZ) introduced by [Wilson \(1975\)](#), three FZs exhibiting a shallowing-upward trend, namely FZ8, FZ7, and FZ3, have been successfully delineated (see more details in Chapter 5).

Two hundred forty thin sections were prepared in the rocks of the Jamal Formation of the Bagh-e-Vang section; yet, it is imperative to underscore, as previously highlighted, that the constraints of the project's timeline constrained a thorough exploration of this dataset. Nevertheless, a commitment remains to delve more profoundly into this aspect in the imminent timeframe, with the primary goal of sharing and disseminating the acquired insights through a forthcoming publication.

3.3. CONCLUSION

Despite my diligent preparation efforts, no conodonts were found in the two studied sections. In the same way, unfortunately, no radiolarian specimens were discernible.

The ostracods obtained through the CH_2O_2 protocol exhibit excellent preservation, and this preparation method led to the identification of 8 species from dolomitized hard-rocks. Additionally, I used the hot acetolysis protocol proposed by [Crasquin et al. \(2005\)](#) and successfully extracted a significant number (59 specimens) of exceptionally well-preserved ostracods.

Microfacies analysis in the Ali-Bashi section identified 28 sub-microfacies, which were derived from 15 distinct microfacies. The assemblage of microfacies groups ranges from MKL1 to MKL2 (lagoonal) and MKR2 to MKR3 (restricted). The MKO1 to MKO4 (open-marine) is in the inner ramp's final part. Microfacies groups MKM1 to MKM3 are inferred to have been deposited after the open marine environment in the mid-ramp zones, whereas MKT1 to MKT3 were identified in the initial part of the outer ramp, corresponding to the Toe-of-slope position in the carbonate shelf setting. Additionally, adhering to the standard microfacies that [Flügel \(2010\)](#) designated, the study proposes ten microfacies of the RMF type, along with their corresponding 4 SMFs for the studied strata. Besides, based on the standard facies zones (FZ)

introduced by Wilson (1975), three FZs exhibiting a shallowing-upward trend, namely FZ8, FZ7, and FZ3, have been successfully delineated.

3.6. REFERENCES

- Boomer, I., Aladdin., Plotnikov, I. and Whatley, R., 2000. "The palaeolimnology of the Aral Sea: a review. *Quaternary Science Reviews* 19, 13: 1259-1278.
- Briggs, D.E., Clarkson, E.N. and Aldridge, R.J., 1983. The conodont animal. *Lethaia*, 16(1), pp.1-14.
- Crasquin, S. and Forel, M.B., 2014. Ostracods (Crustacea) through Permian–Triassic events. *Earth-Science Reviews*, 137, pp.52-64.
- Crasquin, S. and Kershaw, S., 2005. Ostracod fauna from the Permian–Triassic boundary interval of South China (Huaying Mountains, eastern Sichuan Province): palaeoenvironmental significance. *Palaeogeography, Palaeoclimatology, Palaeoecology*, 217(1-2), pp.131-141.
- Du, Y., Chiari, M., Karádi, V., Nicora, A., Onoue, T., Pálffy, J., Roghi, G., Tomimatsu, Y. and Rigo, M., 2020. The asynchronous disappearance of conodonts: New constraints from Triassic-Jurassic boundary sections in the Tethys and Panthalassa. *Earth-Science Reviews*, 203, p.103176.
- Dunham, R.J., 1962. Classification of carbonate rocks according to depositional textures.
- Embry, A.F. and Klovan, J.E., 1971. A Late Devonian reef tract on northeastern Banks Island, NWT. *Bulletin of Canadian Petroleum Geology*, 19(4), pp.730-781.
- Flügel, E. and Munnecke, A., 2010. *Microfacies of carbonate rocks: analysis, interpretation and application* (Vol. 976, p. 2004). Berlin: Springer.
- Gabbott, S.E., Aldridge, R.J. and Theron, J.N., 1995. A giant conodont with preserved muscle tissue from the Upper Ordovician of South Africa. *Nature*, 374(6525), pp.800-803.
- Gradstein, F.M., Ogg, J.G., Schmitz, M.D. and Ogg, G.M. eds., 2020. *Geologic time scale 2020*. Elsevier.
- Horne, D.J. and Siveter, D.J., 2016. Collecting and processing fossil ostracods. *Journal of Crustacean Biology*, 36(6), pp.841-848.
- Jeppsson, L., Anehus, R. and Fredholm, D., 1999. The optimal acetate buffered acetic acid technique for extracting phosphatic fossils. *Journal of Paleontology*, 73(5), pp.964-972.
- Lethiers, F. and Crasquin-Soleau, S., 1988. Comment extraire les microfossiles à tests calcitiques des roches calcaires dures. *Revue de micropaléontologie*, 31(1), pp.56-61.
- McMenamin, M.A., 2016. Mat farmers. *Dynamic Paleontology: Using Quantification and Other Tools to Decipher the History of Life*, pp.79-96.
- Pessagno Jr, E.A. and Newport, R.L., 1972. A technique for extracting Radiolaria from radiolarian cherts. *Micropaleontology*, pp.231-234.

- Purnell, M.A., 1995. Large eyes and vision in conodonts. *Lethaia*, 28(2), pp.187-188.
- Remin, Z., Dubicka, Z., Kozłowska, A. and Kuchta, B., 2012. A new method of rock disintegration and foraminiferal extraction with the use of liquid nitrogen [LN₂]. Do conventional methods lead to biased paleoecological and paleoenvironmental interpretations? *Marine Micropaleontology*, 86, pp.11-14.
- Rigo, M., Onoue, T., Wu, Q., Tomimatsu, Y., Santello, L., Du, Y., Jin, X. and Bertinelli, A., 2023. A new method for extracting conodonts and radiolarians from chert with NaOH solution. *Palaeontology*, 66(4), p.e12672.
- Sharma, V. and Daneshian, J., 1998. Miocene Radiolaria from Nicholson and John Lawrence Islands, Andaman Sea. *Geological Society of India*, 52(6), pp.695-707.
- Shen, S.Z., Yuan, D.X., Henderson, C.M., Tazawa, J. and Zhang, Y.C., 2012. Implications of Kungurian (Early Permian) conodonts from Hatahoko, Japan, for correlation between the Tethyan and international timescales. *Micropaleontology*, pp.505-522.
- Stepanov, D.L., Golshani, F. and Stöcklin, J., 1969. *Upper Permian and Permian-Triassic boundary in North Iran* (No. 12). Geological Survey of Iran.
- Stucky, R.K., 1996. Paleontology: The window to science education. *The Paleontological Society Papers*, 2, pp.11-14.
- Sulcek, Z. and Povondra, P., 1989. Methods of decomposition in inorganic analysis.
- Szlauer-Łukaszewska, A. and Radziejewska, T., 2013. Two techniques of ostracod (Ostracoda, Crustacea) extraction from organic detritus-rich sediments. *Limnologica*, 43(4), pp.272-276.
- Vuolo, I., 2014. *Conodont biostratigraphy from Carboniferous and Permian successions of Pamir, Central Iran and Tunisia* (Doctoral dissertation, PhD Thesis. Università Degli Studi Di Milano, 308p).
- Wilson, J.L., 1975. *Carbonate facies in geologic history*, pp. 471, Berlin (Springer).

CHAPTER 4

Ostracods: concepts and systematic paleontology

4.1. GENERALITY.....	90
4.2. HISTORICAL BACKGROUNDS.....	90
4.3. ELEMENTS OF DESCRIPTION	93
4.4. SYSTEMATICS.....	95
4.5. CONCLUSION	128
4.6. REFERENCES	141

4.1. GENERALITY

Ostracods are aquatic benthic microcrustaceans characterized by their bivalved calcified carapace and they are accepted to be one of the most efficient paleoecological indices (Crasquin-Soleau et al. 1999). The shell protects the body as all the other crustaceans, ostracods grow by successive moultings until they reach adult stage (Moore 1961; Forel et al. 2014). they have the most complete paleontological record in arthropod group (Rodriguez-Lazaro & Ruiz-Munoz 2012). The size varies from 0.15 to 2.0 mm, although exceptionally large specimens can extend to 80 mm in length.

Ostracods display adaptability to a wide range of aquatic environments, encompassing freshwater and marine habitats (Moore 1961). Additionally, certain extant ostracod species have adapted to moist soil or leaf litter environments. In the field of micropaleontology, ostracods hold significant significance, serving crucial roles in biostratigraphy, assisting in the determination of paleoenvironments and paleoclimates, and playing indispensable roles as indicators of ancient shorelines and plate distributions (Chitnarin 2009).

4.2. HISTORICAL BACKGROUND OF OSTRACODS

Ostracods are significant components of the meiofauna known from the Early Paleozoic (Moore 1961; Salas et al. 2007) and they have the most complete fossil record of the arthropods. More than 65,000 living and fossil taxa have been documented (Horne et al. 2002; Ikeya et al. 2005; Williams et al. 2008), yet only approximately half of the 20,000 extant species have received formal descriptions. The majority of these formally described species are found in marine and transitional aquatic environments, with around 2,000 species identified in fresh waters (Martens et al. 2008).

The earliest unquestionable ostracods, exhibiting preserved soft anatomy, originate from deposits dating back 425 million years in the Silurian period of England (Siveter et al. 2003, 2007). Fossilized ostracod carapaces, using the term 'carapace' in the context defined by Siveter et al. (2003), suggest a more ancient history for this group, potentially extending back to at least the Early Ordovician (Tinn & Meidla 2004; Salas et al. 2007). Two arthropod categories, bradoriids and phosphatocopids, recognized as potential precursors to ostracods (Silvester-Bradley 1961), are prevalent in Cambrian rocks globally (fig. 4.1).

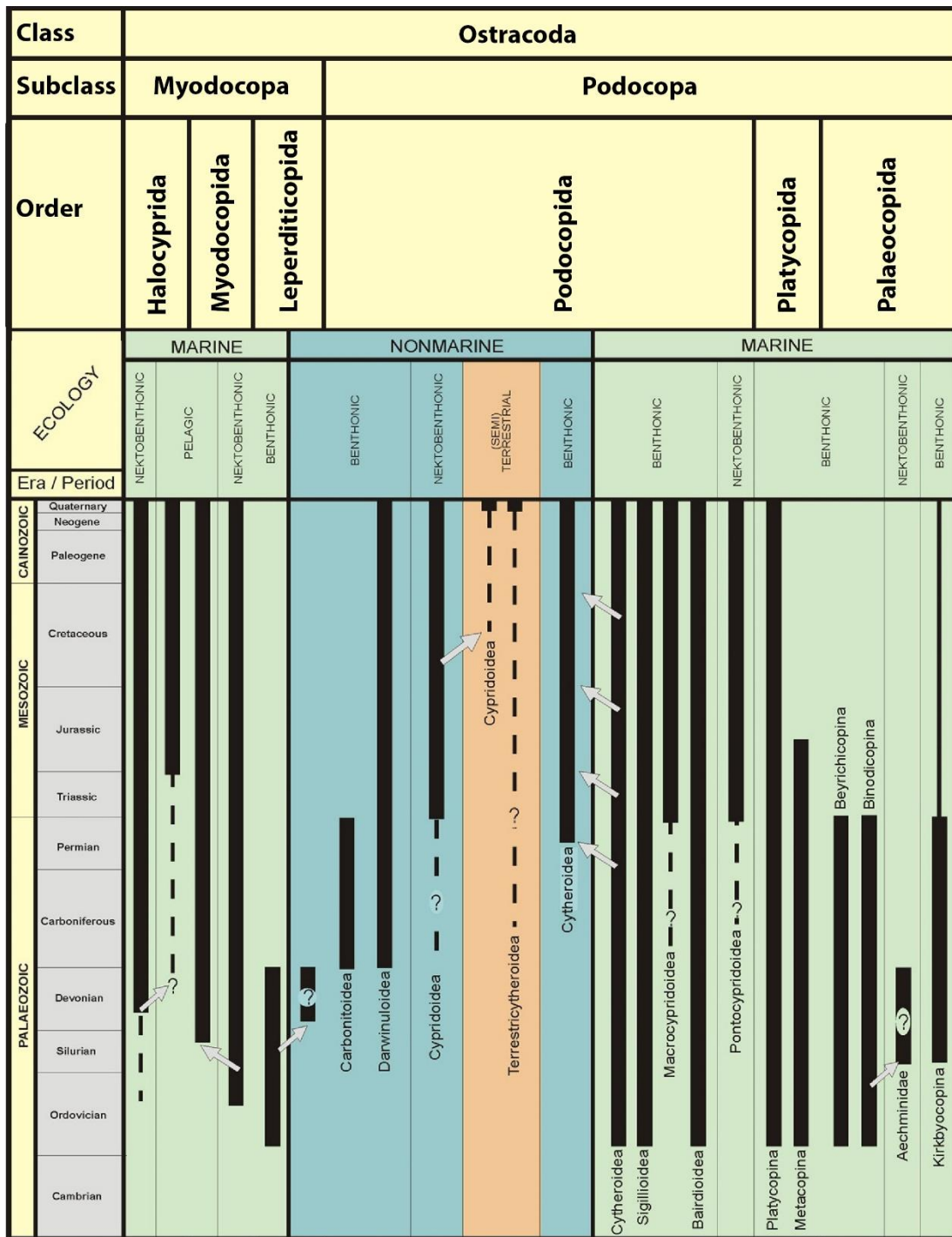


Fig. 4.1. Stratigraphical timelines of the major ecological radiations of the Ostracoda, modified after Horne (2003, 2005 see in Rodriguez-Lazaro & Francisco Ruiz-Munoz 2012). The white polygon symbolizes the change of life-models in these microfossils over the geological time scale (more information see Horne 2003).

Permian marine ostracod communities underwent significant change up until the End-Permian extinction. If the behavior of the group through the Permian – Triassic are quite well known (see synthesis in Crasquin & Forel 2014), their response to the so-called end-

Guadalupian mass extinction remains enigmatic (Tarnac et al. 2021). indeed, they have been abundantly documented from the PTB transition worldwide, displaying extinction rates ranging from 68 to 100% depending on the locality (Crasquin & Forel 2014). Some representatives of Carboniferous – Permian are illustrated on fig. 4.2.

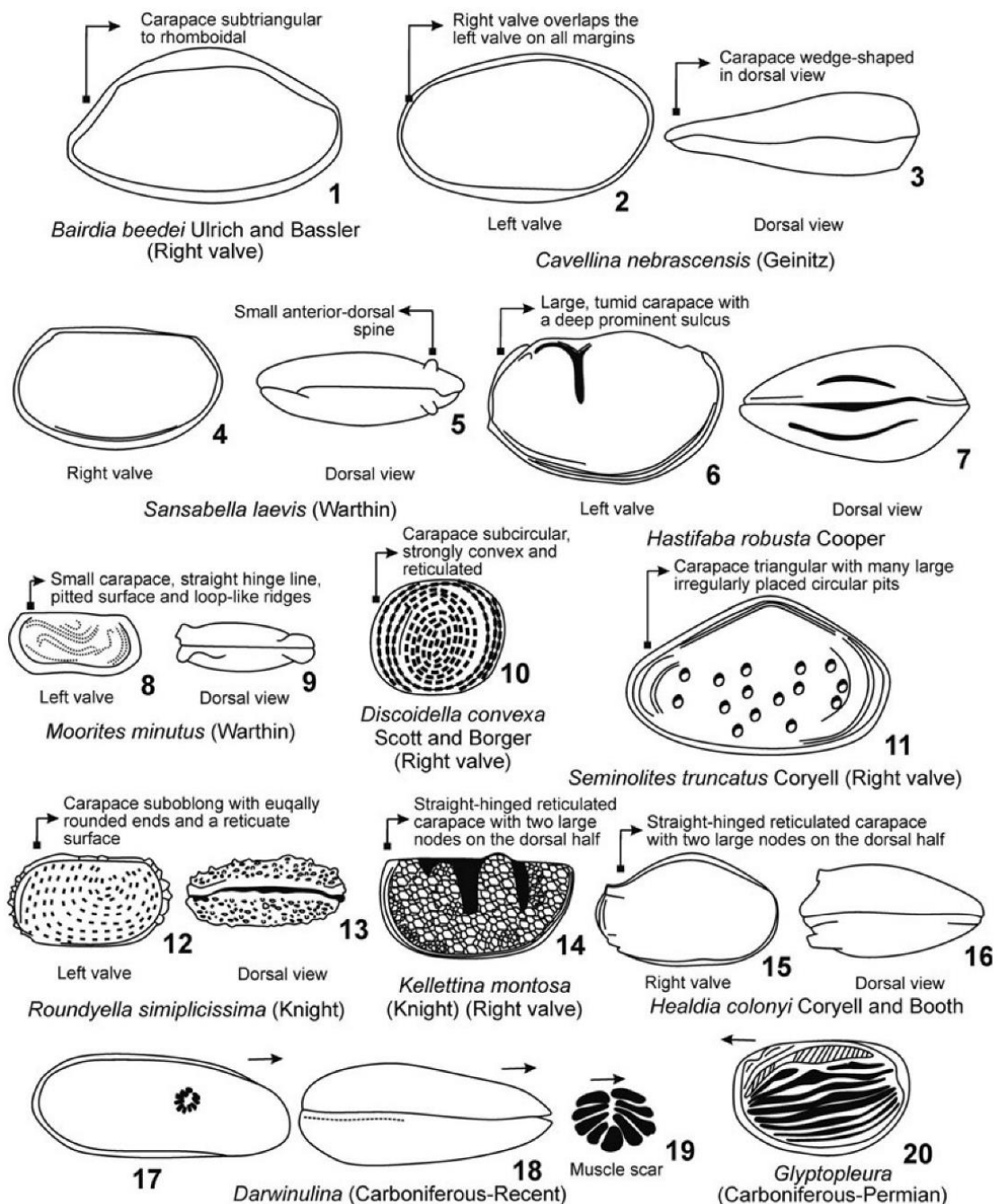


Fig. 4.2. Representative species of some Pennsylvanian (Carboniferous) to Permian ostracods 1: *Bairdia beedei* Ulrich & Bassler (Right valve); 2–3: *Cavellina nebrascensis* (Geinitz); 2: Left valve; 3: Dorsal view; 4–5: *Sansabella laevis* (Warthin); 4: Right valve; 5: Dorsal view; 6–7: *Hastifaba robusta* Cooper; 6: Left valve; 7: Dorsal view; 8–9: *Moorites minutus* (Warthin); 8: Left valve; 9: Dorsal view; 10: *Discoidella convexa* Scott & Borger (Right valve); 11: *Seminolites truncatus* Coryell (Right valve); 12–13: *Roundyella simplicissima* (Knight); 12: Left valve; 13: Dorsal view; 14: *Kellettina montosa* (Knight) (Right valve); 15–16: *Healdia colonyi* Coryell & Booth; 15: Right valve; 16: Dorsal view; 17–19: *Darwinulina*; 19: Muscle scar; 20: *Glyptopleura*, (Jain 2020).

Despite their potential for paleoenvironmental studies, ostracods of Late Paleozoic Iran have not been widely investigated; only few papers were published: one on the Late Middle Permian in Zal section NW of Iran (Mette et al. 2008) and another on Late Permian/Early Triassic of Julfa and Ali-Bashi Formations in Zal section in NW of Iran (Mette 2010). Forel et al. (2014) investigated ostracods of Permian-Triassic of Elika Formation in the Elika River section in the Central Iran and reported 79 species belonging to 38 genera. Gliwa et al. (2020) focused on ostracod of Aras Valley section in the NW Iran. In this paper, 62 species with one genus and ten species newly described.

4.3. ELEMENTS OF DESCRIPTION

Shell morphology is the main tool in ostracod classification for Paleozoic ostracods, where soft bodies are seldom preserved. It necessitates the examination of external characteristics. Internal attributes such as muscle scars and hingement become crucial for younger fossils but are not addressed here. The contour or configuration of an ostracod can be described as ovate, elliptical, quadrate, and so on (see fig. 4.3).

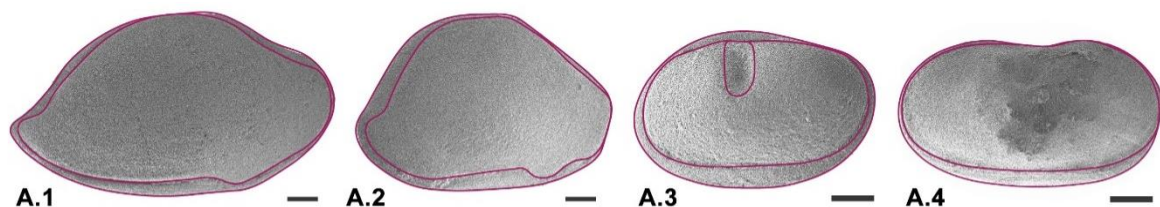


Fig. 4.3. Illustrative instances of selected ostracods from this research include:

A.1. *Bairdia hungarica* Zalanyi, 1974, right lateral view of the complete carapace showing the Bairdian-shape outline. A.2. *Bairdia* sp. 7, right lateral view of the complete carapace, showing subtriangular outline. A.3. *Sargentina chantarameei* Chitnarin et al. 2012, left lateral view of the complete carapace showing subovate outline. A.4. *Sargentina minuta* Wang, 1978, left lateral view of the incomplete carapace, showing elliptic outline.

These distinguishing features valuable for classifying fossil taxa include: 1. carapace shape; 2. Characteristics of overlap, location, and degree; 3. Dimorphism nature; 4. Surface ornamentation; 5. features of the marginal zone. For post-Palaeozoic ostracods, additional features become significant, such as: 1. Position and arrangement of muscle scars; 2. Attributes of normal and marginal pore canals; 3. The form of selvages and flanges (Moore

1961). The ostracod carapace is produced by the epidermis. Similar to other crustaceans, the cuticle starts off soft during its formation and subsequently undergoes a hardening process known as sclerotization. The left and right valves are created through mineralization and are linked by a slender, permanently soft strip of cuticle called the ligament. These valves are connected by an adductor muscle that traverses the body and attaches to the inner surface of the outer lamella (Chitnarin 2009). The descriptive used features are presented on fig. 4.4

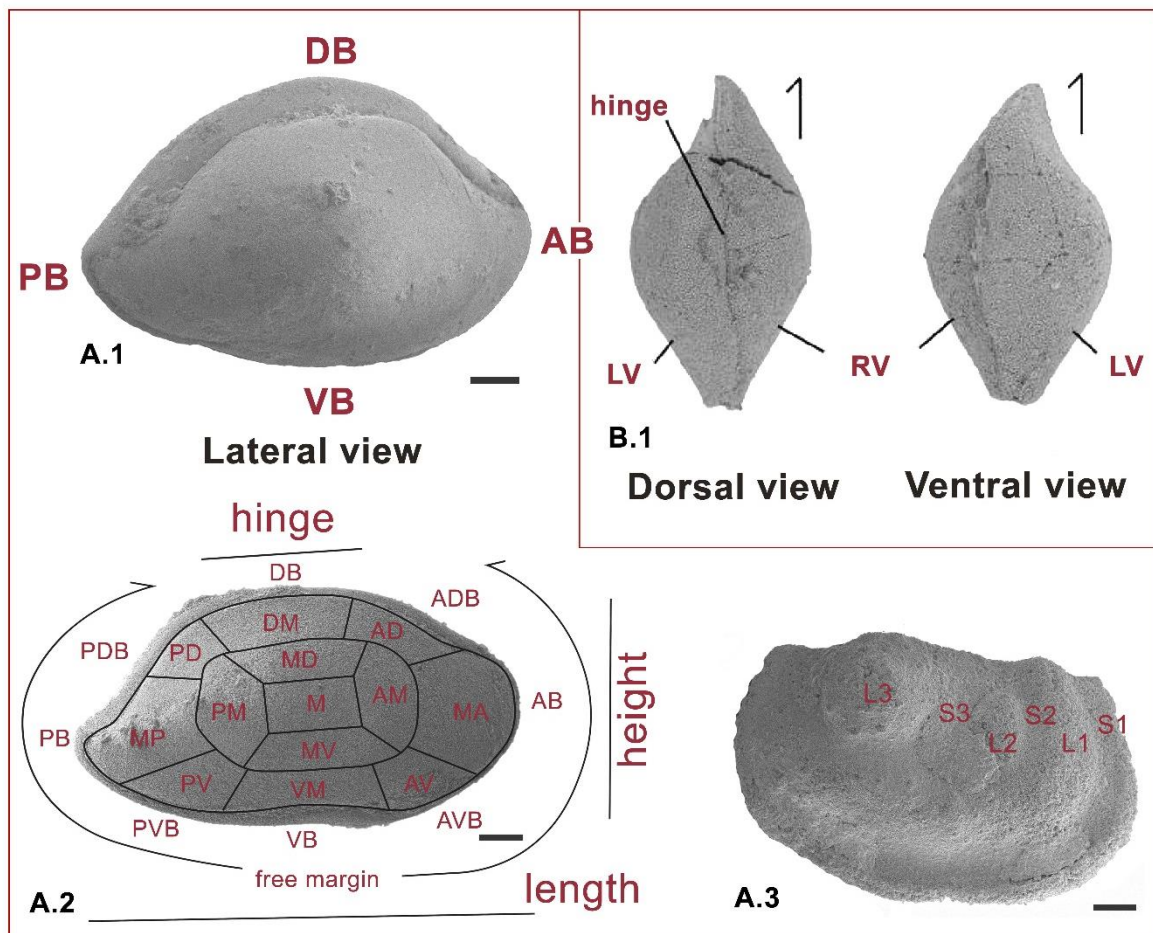


Fig. 4.4. Feature of carapace in lateral, dorsal and ventral views. A.1. *Bairdia deducta deducta* (Zalanyi 1974) with lateral view. Abbreviations: PB: posterior border, DB: dorsal border, AB: anterior border, VB: ventral border. A.2. *Bairdia songthami* Chitnarin et al. 2017 abbreviations, M: median, AM: anteromedian, MA: mid-anterior, PM: posteromedian, MP: mid-posterior, MD: dorsomedian, DM: mid-dorsal, MV: venterodorsal, MV: mid-ventral, AD: anterodorsal, AV: anterodorsal, PD: posterodorsal, PV: posteroventral, DB: dorsal border, ADB: anterodorsal border, AB: anterior border, AVB: anteroventral border, VB: ventral border, PVB: posteroventral border, PB: posterior border, and PDB: posterodorsal. A.3. *Hollinella (Hollinella) herrickana* (Girty 1909), with lobes, sulcus, and frill of ornamentations. B.1. Carapace in dorsal and ventral views, (*Bairdia* sp.5 in Chitnarin 2009).

Most of ostracods have sexual reproduction. Sexual dimorphism could be present in the carapace, particularly on female ones. They are called heteromorph and could exhibit more swollen posterior region, pronounced ventral lobes, rounded bulges such as brood pouches, or broad frills. Males and juvenile forms, are referred to tecomorphs. This sexual dimorphism has been particularly observed in order Palaeocopida, as Kloedenellid dimorphism (Chitnarin 2009). Class Ostracoda is subdivided in two Subclass Myodocopa and Podocopa. Subclass Myodocopa is subdivided in 3 orders Halocyprida, Myodocopida and Leperditicopida. Subclass Podocopa is subdivided in 3 orders Podocopida, Platycopida and Palaeocopida (fig. 4.1)

4.4. SYSTEMATICS

Taxonomy (identification and naming) is the base of systematics that focuses on the classification, of organisms. 67 specimens were extracted from over 240 samples.

A total of 1169 specimens were photographed with scanning electron microscopy (SEM). These ostracod specimens were cross-referenced with existing Permian ostracod publications. I have identified and cataloged 67 species belonging to 15 genera (table 4.1).

Different extraction methods were applied and tested. Hot and cold CH₃COOH; cold CH₂O₂ acid (Hemmati et al., submitted). Applying the CH₂O₂ method yielded outcomes that enabled me to identify the respective species. These species are: *Bairdia deducta deducta* (Zalanyi, 1974); *Bairdia hungarica* Zalanyi, 1974; *Bairdia* sp.; *Fabalitypris parva* Wang, 1978, *Fabalitypris* sp. 1; *Fabalitypris* sp. 2; *Fabalitypris* sp. 3; *Fabalitypris* sp. 4; *Hollinella* (*Hollinella*) *herrickana* (Girty 1909), *Hollinella* sp., *Sargentina transita* (Kozur 1985) and *Silenites* sp. (Plate 4.5; fig. 4.5).

The applied of the hot acetolysis preparation method described by Crasquin et al. (2005) allows to me to identified these species as follows (Plates 4.1-4.4; fig. 4.6):

Acratia changxingensis (Shi, 1987); *Acratia* sp.; *Bairdia deducta deducta* (Zalanyi, 1974); *Bairdia elcapitanensis* Forel 2021; *Bairdia* cf. *fangnianqiao* Crasquin, 2010; *Bairdia grotei* Chitnarin, 2017 *Bairdia hungarica* Zalanyi, 1974; *Bairdia khaokanaensis* Chitnarin, 2017; *Bairdia radlerae* Kellett, 1934; *Bairdia rhomboidalis* Hamilton, 1942; *Bairdia* cf. *songthami* Chitnarin et al. 2017; *Bairdia* sp.30 sensu Chitnarin, 2009; *Bairdia* sp. 1; *Bairdia* sp. 2; *Bairdia* sp. 3; *Bairdia* sp. 4; *Bairdia* sp. 5; *Bairdia* sp. 6; *Bairdia* sp. 7; *Bairdia* sp. 8; *Bairdia* sp. 9; *Bairdia* ? sp.; *Bairdiacypris longirobusta* Chen, 1958; *Bairdiacypris* sp. 6 sensu Zazzali et al., 2015;

Bairdiacypris sp. B *sensu* Tarnac *et al.*, 2021; *Bairdiacypris* sp. 1; *Bairdiacypris* sp. 2; *Bairdiacypris* sp. 3; *Bairdiacypris* sp. 4; *Bairdiacypris* sp. 5; *Bairdiacypris* sp. 6; *Bairdiacypris* sp. 7; *Bairdiacypris* sp. 8; *Bairdiacypris* sp. 9; *Bairdiacypris* sp.; *Ceratobairdia sexagintaduella* Forel, 2021; *Ceratobairdia?* cf. *crenata* Chen, 1982; *Fabalitypris acetalata* (Coryell & Billings, 1932); *Fabalitypris glennensis* (Harlton, 1927); *Fabalitypris parva* Wang, 1978; *Fabalitypris reniformis* (Chen, 1958) *sensu* Wang, 1978; *Fabalitypris* sp. 5; *Fabalitypris* sp. 6; *Fabalitypris* sp. 7; *Hollinella* (*Hollinella*) *martensiformis* Crasquin *et al.*, 2010 ; *Hollinella* sp. ; *Indivisia* sp. 1 *sensu* Forel *et al.* 2015; *Kempfina qinglaili* (Crasquin, 2008); *Kempfina* sp. 1 ; *Liuzhinia julfensis* Gliwa, 2021; *Praezabythocypris pulchra* Kozur, 1985; *Praezabythocypris* sp. 1; *Pseudacanthoscapha striatula* (Shi, 1982); *Reviya* sp. A; *Sargentina minuta* Wang, 1978; *Sargentina* sp.; and *Sulcella sulcata* Coryell & Sample, 1932.

Table 4.1. Taxonomic list of all ostracod species identified from the Ali-bashi section, Julfa region, northwest of Iran, Guadalupian, Late Permian.

<p>Class OSTRACODA Latreille, 1802</p> <p>Order PODOCOPIDA Sars, 1866</p> <p>Suborder PODOCOPINA Sars, 1866</p> <p>Superfamily BAIRDIOIDEA Sars, 1888</p> <p>Family BAIRDIIDAE Sars, 1888</p> <p>Genus <i>Acratia</i> Delo, 1930 <i>Acratia changxingensis</i> (Shi, 1987) <i>Acratia</i> sp.</p> <p>Genus <i>Bairdia</i> McCoy, 1844 <i>Bairdia deducta deducta</i> (Zalanyi, 1974) <i>Bairdia elcapitanensis</i> Forel 2021 <i>Bairdia</i> cf. <i>fangnianqiao</i> Crasquin, 2010 <i>Bairdia grotei</i> Chitnarin, 2017 <i>Bairdia hungarica</i> Zalanyi, 1974 <i>Bairdia khaokanaensis</i> Chitnarin, 2017 <i>Bairdia radlerae</i> Kellett, 1934 <i>Bairdia rhomboidalis</i> Hamilton, 1942 <i>Bairdia</i> cf. <i>songthami</i> Chitnarin <i>et al.</i> 2017 <i>Bairdia</i> sp.30 <i>sensu</i> Chitnarin, 2009 <i>Bairdia</i> sp. 1 <i>Bairdia</i> sp. 2 <i>Bairdia</i> sp. 3 <i>Bairdia</i> sp. 4</p>	<p>Genus <i>Ceratobairdia</i> Sohn, 1954 <i>Ceratobairdia sexagintaduella</i> Forel, 2021 <i>Ceratobairdia?</i> cf. <i>crenata</i> Chen, 1982</p> <p>Genus <i>Fabalitypris</i> Brady, 1880 <i>Fabalitypris acetalata</i> (Coryell & Billings, 1932) <i>Fabalitypris glennensis</i> (Harlton, 1927) <i>Fabalitypris parva</i> Wang, 1978 <i>Fabalitypris reniformis</i> (Chen, 1958) <i>sensu</i> Wang, 1978 <i>Fabalitypris</i> sp. 1 <i>Fabalitypris</i> sp. 2 <i>Fabalitypris</i> sp. 3 <i>Fabalitypris</i> sp. 4 <i>Fabalitypris</i> sp. 5 <i>Fabalitypris</i> sp. 6 <i>Fabalitypris</i> sp. 7</p> <p>Genus <i>Kempfina</i> Crasquin 2010 <i>Kempfina qinglaili</i> (Crasquin, 2008) <i>Kempfina</i> sp. 1</p> <p>Genus <i>Liuzhinia</i> Zheng, 1976</p>
--	--

<p><i>Bairdia</i> sp. 5 <i>Bairdia</i> sp. 6 <i>Bairdia</i> sp. 7 <i>Bairdia</i> sp. 8 <i>Bairdia</i> sp. 9 <i>Bairdia</i> ? sp.</p> <p>Genus <i>Bairdiacypris</i> Badfield, 1935 <i>Bairdiacypris longirobusta</i> Chen, 1958 <i>Bairdiacypris</i> sp. 6 sensu Zazzali et al., 2015 <i>Bairdiacypris</i> sp. B sensu Tarnac et al., 2021 <i>Bairdiacypris</i> sp. 1 <i>Bairdiacypris</i> sp. 2 <i>Bairdiacypris</i> sp. 3 <i>Bairdiacypris</i> sp. 4 <i>Bairdiacypris</i> sp. 5 <i>Bairdiacypris</i> sp. 6 <i>Bairdiacypris</i> sp. 7 <i>Bairdiacypris</i> sp. 8 <i>Bairdiacypris</i> sp. 9 <i>Bairdiacypris</i> sp.</p>	<p><i>Liuzhinia julfensis</i> Gliwa, 2021</p> <p>Suborder KLOEDENELLOCOPINA Scott, 1961 Superfamily KLOEDENELLOIDEA Ulrich & Bassler, 1908 Family BAIRDIOCYPRIDIDAE Shaver, 1961 Genus <i>Silenites</i> Coryell and Booth, 1933 <i>Silenites</i> sp.</p> <p>Family BYTHOCYPRIDIDAE Maddocks, 1969 Genes <i>Praezabythocypris</i> Kozur, 1985 <i>Praezabythocypris pulchra</i> Kozur, 1985 <i>Praezabythocypris</i> sp. 1</p> <p>Family GEROIIDAE Gründel, 1962 Genus <i>Pseudacanthoscapha</i> Kozur, 1985 <i>Pseudacanthoscapha striatula</i> (Shi, 1982)</p> <p>Family KNOXITIDAE Egorov, 1950 Genus <i>Sargentina</i> Coryell & Johnson, 1939 <i>Sargentina minuta</i> Wang, 1978 <i>Sargentina transita</i> (Kozur, 1985) <i>Sargentina</i> sp.</p>
<p>Order PALAEOCOPIIDA Henningsmoen, 1953? Superfamily PARAPARCHITIDEA Scott, 1959 emend. Sohn, 1971 Family INDIVISIIDAE Egorov, 1954 Genus <i>Indivisia</i> Zaspelova, 1954 <i>Indivisia</i> sp. 1 sensu Forel et al., 2015</p> <p>Order RETICULOCOPIIDA Kozur, 1993 Suborder PUNCIOCOPINA Schallreuter, 1968 Superfamily KIRKBYACEA Ulrich & Bassler, 1906 Family Kirkbyidae Ulrich & Bassler, 1906 Genus <i>Reviya</i> Sohn, 1961 <i>Reviya</i> sp.</p>	<p>Suborder BERICHICOPINA Scott, 1961 Superfamily HOLLINOIDEA Swartz, 1936 Family HOLLINELLIDAE Bless & Jordan, 1971 Genus <i>Hollinella</i> Coryell, 1928 emend. Kellett, 1929 <i>Hollinella</i> (<i>Hollinella</i>) <i>herrickana</i> (Girty, 1909) <i>Hollinella</i> (<i>Hollinella</i>) <i>martensiformis</i> Crasquin et al., 2010 <i>Hollinella</i> sp.</p>
<p>Order PLATYCOPIIDA Sars, 1866 Suborder PLATYCOPINA Sars, 1866</p>	

Superfamily CAVELLINOIDEA Egorov, 1950**Family CAVELLINIDAE Egorov, 1950**Genus *Sulcella* Coryell & Sample, 1932*Sulcella sulcata* Coryell & Sample, 1932

Following abbreviations are used in the systematic descriptions: AB, anterior border; ADB, anterodorsal border; AVB, anteroventral border; DB, dorsal border; H, height; Hmax, maximum height; L, length; Lmax, maximum length; LV, left valve; PB, posterior border; PDB, posterodorsal border; PVB, posteroventral border; RV, right valve; VB, ventral border; W, width; Wmax, maximum width.: AB, anterior border; ADB, anterodorsal border; AVB, anteroventral border; DB, dorsal border; H, height; Hmax, maximum height; L, length; Lmax, maximum length; LV, left valve; PB, posterior border; PDB, posterodorsal border; PVB, posteroventral border; RV, right valve; VB, ventral border; W, width; Wmax, maximum width. I use here the classification of [Moore \(1961\)](#), [Lethiers \(1981\)](#) and [Horne et al. \(2002\)](#).

All the specimens are deposited in the collections of National natural History Museum (MNHN) in Paris, France and will received numbers MNHN.F.F ([table 4.1](#); plates. 4.1-4.6).

Class OSTRACODA Latreille, 1802

Order PODOCOPIIDA Sars, 1866

Suborder PODOCOPINA Sars, 1866

Superfamily BAIRDIOIDEA Sars, 1888

Family BAIRDIIDAE Sars, 1888

Genus *Acratia* Delo, 1930*Acratia changxingensis* (Shi, 1987)

(Plate 4.1 A)

Acratia changxingensis (Shi, 1987): Crasquin et al. 2004 pl.3 fig 21-24.

MATERIAL. – 2 complete carapaces.

OCCURRENCES. – Permian - Triassic boundary, Çürük dag section, Western Taurus, Antalya Nappes, Turkey (Crasquin et al. 2004). Khachik Formation (A. 191 and A. 204) Guadalupian, Ali-Bashi section, Iran (this study).

DIMENSIONS. – L= 41–65µm; H= 24–32µm; H/L= 0.49 – 0.58.

DISCUSSION. – The genus *Acratia* is recognized by presence of special feature called Acratian beak. The carapace is small to medium-sized, elongated and this species has a cute AB and the acratian neck is distinct as a hooklike shape. The AB exhibits a generous radius of curvature, with its maximum convexity situated at the midpoint and the dorsal outline is broadly arched, DB is straight, ADB and PDB are convex.

Acratia sp.

(Plate 4.1 B)

MATERIAL. – 1 complete carapace.

OCCURRENCES. – Khachik Formation (samples A. 188), Guadalupian, Ali-Bashi section, Iran (this study).

DIMENSIONS. – L= 51µm; H= 24µm; H/L= 0.47.

REMARKS. – *Acratia* sp. possesses a sub-trapezoidal carapace, with both the ADB and PDB appearing long and maintaining a straight profile. The AB is laterally flattened and exhibits a rounded shape with a medium radius of curvature, with its maximum convexity situated below the midpoint. The PB is acuminate and positioned at the same level as the VB.

Genus *Bairdia* McCoy, 1844

Bairdia deducta deducta Zánályi, 1974

(Plate 4.1 C1-C4; Plate 4.5 A1-A6)

Bairdia deducta sp.nov. Zánályi, 1974: 196, 197, pl. 12, fig. 1a-c.

Bairdia deducta deducta Zánályi, 1974 - Crasquin-Soleau & Baud 1998: pl. 8, figs. 10-13, 16.

- Chitnarin *et al.* 2017: 666-667, figs. 11, J-L.

Cryptobairdia deducta deducta (Zánályi): Kozur:1985a pl. 6, fig. 2.

MATERIAL. – 20 complete carapaces.

OCCURRENCES. – Lopingian, Nagyvisnyó Formation, Bükk Mountains, Hungary, (Kozur 1985a); Late Guadalupian-Early Lopingian Episkopi Formation, Hydra Island, Greece (Crasquin-Soleau & Baud 1998); Cisuralian, Tham Nam Maholan section, Nam Maholan

Formation, Loei Province, northeast Thailand; Guadalupian, Ban Naen Sawan I section, Pha Nok Khao Formation, Phetchabun Province, central Thailand, Late Guadalupian Khao Som Phot section, Tak Fa Formation, Lopburi Province, central Thailand, (Chitnarin *et al.* 2017). Khachik Formation (samples A. 152, A. 156, A. 168, A. 176, A. 188, A. 197, A. 202, A. 203 A. 204, A. 210, A. 244 and A. 278), Guadalupian, Ali-Bashi section, Iran (this study).

DIMENSIONS. – L= 99–108 μ m; H= 56– 65 μ m; H/L= 1.64 – 1.77.

DISCUSSION. – Carapace compact and subtriangular; dorsal and ventral margins arche. LV strongly overlaps RV with maximum in dorsal part; flattening of AB and dorso-median part of the carapace; thickening of the carapace in ventral part (fig. 4.4 A.1).

Bairdia elcapitanensis Forel, 2021

(Plate 4.1 D)

Bairdia elcapitanensis Forel sp. nov. - Tarnac et al. 2021: 29-30, figs 7P–R, 8A–B.

MATERIAL. – 1 broken carapace.

OCCURRENCES. – Roadian (Middle Permian), Quarry section, Williams Ranch Member, Cutoff Formation, Guadalupe Mountains, West Texas, USA (Tarnac et al. 2021). Khachik Formation (sample A. 170), Guadalupian, Ali-Bashi section, Iran (this study).

DIMENSIONS. – L= 91 μ m; H= 45 μ m; H/L= 0.49.

DISCUSSION. – The carapace is a sub-triangular shape with irregular valves that asymmetrically overlap. The dorsal margin is uniformly convex, and PDB and ADB are nearly straight. The AB has a small radius of curvature and is positioned above the (mid-H. The VB is mostly straight, with only a slight concavity. The PB is narrow, with its maximum convexity located very ventrally.

Bairdia cf. fangnianqiao Crasquin, 2010

(Plate 4.1 E)

cf. *Bairdia fangnianqiao* Crasquin 2010: Crasquin et al. 2010: 342-344, fig. 9K-N.

MATERIAL. – 2 complete carapaces.

OCCURRENCES. – Khachik Formation (samples A. 132 and A. 140), Guadalupian, Ali-Bashi section, Iran (this study).

DIMENSIONS. – L= 93 μ m; H= 43 μ m; H/L= 0.46.

DISCUSSION. – The specimens are closed to *Bairdia fangnianqiao* Crasquin, 2010 from the latest Permian of the Meishan section (Crasquin et al. 2010a). However, they can be distinguished by a smaller H/L ratio and a consistently arched dorsal outline of LV.

Bairdia cf. grotei Chitnarin, 2017

(Plate 4.1 F)

cf. *Bairdia grotei* Chitnarin, 2017 n.sp. - Chitnarin et al. 2017: 660-662, fig. 7, A-F.

MATERIAL. – 1 complete carapace.

OCCURRENCES. – Asselian-Sakmarian, Early Permian, Nong Phai section, Pha Nok Khao Formation, Indochina block, Central Thailand (Chitnarin et al. 2017). Khachik Formation (sample A. 294), Guadalupian, Ali-Bashi section, Iran (this study).

DIMENSIONS. – L= 91 μ m; H= 51 μ m; H/L= 0.56.

DISCUSSION. – The specimens could be compared to cf. *Bairdia grotei* Chitnarin, 2017 from Indochina block from Central Thailand. Here the DB is longer and less inclined. Nong Phai section, Pha Nok Khao Formation, Asselian-Sakmarian, Early Permian of the Indochina block from Central Thailand.

Bairdia hungarica Zálányi, 1974

(Plate 4.1 G1-G9; Plate 4.5 B1-B4)

Bairdia hungarica sp.nov. - Zálányi, 1974: 192- 193, pl. 9, fig. 3a-d.

Fabalitypris hungarica (Zálányi): Kozur: 1985a pl. 3, fig. 3.

MATERIAL. - 17 complete carapaces.

OCCURRENCES. - Lopingian, Nagyvisnyó Formation, Bükk Mountains, Hungary, (Kozur 1985a). Khachik Formation (samples A.144, A. 171, A. 176, A. 188, A. 192, A. 207, A. 204, and A. 210, A. 251, A. 279, A. 301 and A. 322) Guadalupian, Ali-Bashi section, Iran (this study).

DIMENSIONS. - L=85 – 94 μ m; H= 52 – 62 μ m; H/L= 0.61 – 0.65.

DISCUSSION. – Carapace subtriangular to rhomboidal, Dorsal margin arched at LV; ADB, DB, PDB straight at RV. VB concave at RV; slight overlap all around the carapace.

Bairdia khaokanaensis Chitnarin, 2017

(Plate 4.1 H)

Bairdia khaokanaensis Chitnarin n.sp.: Chitnarin et al. 2017: 653-658, fig. 3 A-D.

MATERIAL. – 1 complete carapace.

OCCURRENCES. – Early-Middle Permian (Cisarulian-Guadalupian), Central Thailand, Indochina Block (Chitnarin et al. 2017). Khachik Formation (sample A. 294), Guadalupian, Ali-Bashi section, Iran (this study).

DIMENSIONS. – L= 84µm; H= 43µm; H/L= 0.52.

DISCUSSION. – Carapace elongated (H/L=0.52); AB with quite large radius of curvature; PVB flattened; PB with very small radius of curvature; very small overlap all around the carapace.

Bairdia radlerae Kellett, 1934

(Plate 4.1 I1-I2)

Bairdia radlerae Kellett 1934: 125, pl. 14 figs 3a–c. – Sohn 1960: 31. - Tarnac et al. 2021: fig. 7 L-M.

MATERIAL. – 2 complete carapaces.

OCCURRENCES. – Asselian, Sakmarian, Early Permian, Kansas, USA, (Kellett 1934). Roadian (Middle Permian), Quarry section, Williams Ranch Member, Cutoff Formation, Guadalupe Mountains, West Texas, USA (Tarnac et al. 2021). Khachik Formation (sample A. 203), Guadalupian, Ali-Bashi section, Iran (this study).

DIMENSIONS. – L= 85µm; H= 53µm; H/L= 0.62.

DISCUSSION. – Carapace with rhomboidal shape; PB with small radius of convexity with maximum of curvature located high; AB with large radius of curvature, quite vertical in its upper part.

Bairdia rhomboidalis Hamilton, 1942

(Plate 4.1 J)

Bairdia rhomboidalis Hamilton 1942: 715, pl. 110 figs 11a–b.– Sohn 1960: 31, pl. 1 figs 26–27. - Tarnac et al. 2021: fig. 7 N.

MATERIAL. – 1 complete carapace.

OCCURRENCES. – Roadian, Middle Permian, Texas, USA (Hamilton 1942). Capitanian, Middle Permian, Bell Canyon Formation, Guadalupe Mountains, West Texas, USA (Tarnac et al. 2021). Khachik Formation (samples A. 204 and A. 279), Guadalupian, Ali-Bashi section, Iran (this study).

DIMENSIONS. – L= 89µm; H= 47µm; H/L= 0.52.

DISCUSSION. – Carapace rhomboidal; LV overlaps RV all around the carapace except at AB; PDB, DB and ADB straight at RV, convex at LV; VB nearly straight at both valves.

Bairdia cf. songthami Chitnarin, 2017

(Plate 4.1 K1-K3)

cf. *Bairdia songthami* Chitnarin n. sp. – Chitnarin et al. 2017: 660, Figs 3M-P, 6.

MATERIAL. – 4 complete carapaces.

OCCURRENCES. – Khachik Formation (sample A. 111, A. 157, A. 192 and A. 204), Guadalupian, Ali-Bashi section, Iran (this study).

DIMENSIONS. – L= 65–110µm; H= 32 –56µm; H/L= 0.49 – 0.50.

DISCUSSION. – Carapace flat, elongated close to *Bairdia songthami* Chitnarin, 2017 from Early-Middle Permian of Thailand (Chitnarin et al. 2017). The present specimens do not exhibit the ventral ridge of Thailand specimens (fig. 4.4 A.2).

Bairdia sp.30 *sensu* Chitnarin, 2009

(Plate 4.1 L1-L2)

Bairdia sp.30 *sensu* Chitnarin, 2009: 114, Plate 7 figs. 4-5.

MATERIAL. – 2 complete carapaces.

OCCURRENCES. – Early-Late Permian, Central Thailand, Indochina Block (Chitnarin 2009). Khachik Formation (samples A. 327 and A. 330) Guadalupian, Ali-Bashi section, Iran (this study).

DIMENSIONS. – L= 71– 89 μ m; H= 43– 53 μ m; H/L= 0.50 – 0.60.

DISCUSSION. – *Bairdia* sp.30, as described by Chitnarin (2009), has a subelliptical carapace. AB with large radius of curvature with maximum located high; LV strongly overlaps the RV in the DB.

Bairdia sp.1

(Plate 4.1 M1-M3)

MATERIAL. – 3 complete carapaces.

OCCURRENCES. –Khachik Formation Unit VI (samples A. 202, A. 204 and A. 207), Guadalupian, Ali-Bashi section, Iran (this study).

DIMENSIONS. – L= 55–87 μ m; H= 31–51 μ m; H/L= 0.57 – 0.58.

REMARKS. – The carapace is short and laterally flattened. In the RV, the DB is straight, while in the LV, it exhibits a slight convexity. The ADB is nearly straight in both valves. The VB is concave, whereas on the LV, it is almost straight. The PVB is nearly straight, and the posterior end aligns with it. The PB has a small radius of curvature, with its highest convexity positioned relatively low.

Bairdia sp. 2

(Plate 4.1 N)

MATERIAL. – 1 broken carapace.

OCCURRENCES. – Khachik Formation (sample A. 301) Guadalupian, Ali-Bashi section, Iran (this study).

DIMENSIONS. – L= 96 μ m; H= 46 μ m; H/L= 0.48.

REMARKS. – The carapace takes on a semi-bean to sub-elliptical shape. The PB exhibits a pronounced curve, with its peak convexity situated prominently. The AB, it is rounded with a medium-sized radius of curvature.

Bairdia sp. 3

(Plate 4.1 O1-O4)

MATERIAL. – 7 complete carapaces.

OCCURRENCES. – Lopingian (Late Permian), Elikah River section, Central Alborz Mountains, North of the Iran (Forel et al. 2015). Khachik Formation (samples A. 156, A. 167, A. 192, A. 203, A. 259 and A. 262) Guadalupian, Ali-Bashi section, Iran (this study).

DIMENSIONS. – L= 79– 82 μ m; H= 41–43 μ m; H/L= 0.52–0.53.

DISCUSSION. – The carapace has a sub-elliptical shape, featuring a straight DB. However, the ADB shows a subtle convexity. The PB has a small radius of curvature, while the AVB takes on a convex form.

Bairdia sp. 4

(Plate 4.1 P)

MATERIAL. – 2 complete carapaces.

OCCURRENCES. – Khachik Formation (sample A. 301 and A. 332), Guadalupian, Ali-Bashi section, Iran (this study).

DIMENSIONS. – L= 50– 61 μ m; H= 19– 21 μ m; H/L= 0.35 – 0.39.

REMARKS. – *Bairdia* sp. 4 is distinguished by its carapace shape, which closely resembles that of a bean. There is a wide and robust overlap of the LV over the RV. Both the ADB and PDB are broadly convex curvature. The VB exhibits a pronounced concavity.

Bairdia sp. 5

(Plate 4.2 A)

MATERIAL. – 1 complete carapace.

OCCURRENCES. – Khachik Formation (sample A. 204), Guadalupian, Ali-Bashi section, Iran (this study).

DIMENSIONS. – L= 132 μ m; H= 91 μ m; H/L= 0.68.

REMARKS. – Very short carapace; AB with very small short and thick carapace; AB and PB with small radius of curvature and maximum located high; VB very convex; LV overlaps RV strongly on dorsal margin.

Bairdia sp. 6

(Plate 4.2 B)

MATERIAL. – 1 incomplete carapace.

OCCURRENCES. – Khachik Formation (sample A. 327), Guadalupian, Ali-Bashi section, Iran (this study).

DIMENSIONS. – L= 93 μ m; H= 46 μ m; H/L= 0.49.

REMARKS. – This specie characterized by subelliptical carapace, dorsal and ventral outlines are broadly convex. AB is round with medium radius of curvature and PB is round with large radius of curvature, the maximum convexities are located at mid-height.

Bairdia sp.7

(Plate 4.2 C1-C3)

MATERIAL. – 4 complete carapaces.

OCCURRENCES. – Khachik Formation (samples A. 118, A. 161, A. 163 and A. 192), Guadalupian, Ali-Bashi section, Iran (this study).

DIMENSIONS. – L= 62–92 μ m; H= 41–57 μ m; H/L= 0.62 – 0.67.

REMARKS. – *Bairdia* sp. 7 Characterized by short straight DB, straight VB; flattening of AVB; strong overlap of LV on RV; perhaps it is a new species.

Barida sp. 8

(Plate 4.2 D)

MATERIAL. – 1 complete carapace.

OCCURRENCES. – Khachik Formation (sample A. 161), Guadalupian, Ali-Bashi section, Iran (this study).

DIMENSIONS. – L= 50 μ m, H=31 μ m, H/L= 0.62.

REMARKS. – *Barida* sp. 8 is characterized by a subelliptical carapace with a broadly arched dorsal outline. It features a long ADB, a convex PDB and a convex ventral outline. Both the AB and PB are rounded, with the AB being narrower than the PB. The highest curvature point of the AB is positioned above the midpoint in terms of height. Notably, the LV significantly overlaps the RV at both the DB and VB.

Barida sp. 9

(Plate 4.2 E1-E2)

MATERIAL. – 1 complete and 1 incomplete carapaces.

OCCURRENCES. – Khachik Formation U (samples A. 192 and A. 200), Guadalupian, Ali-Bashi section, Iran (this study).

DIMENSIONS. – L= 87-92 μ m, H= 50-53 μ m, H/L= 0.55-.057.

REMARKS. – The carapace exhibits a shape ranging from subelliptical to rectangular. The RV is larger than the LV and extends along the entire free edge. At the dorsal edge, both valves share equal height. The anterior margin is straight, with a slight convergence towards the dorsal margin as we move towards the posterior. The hind edge is rounded, forming a point in the upper third and displaying a pronounced bevel at its lower part.

Bairdia? sp.

(Plate 4.2 F)

MATERIAL. – 1 complete carapace.

OCCURRENCES. – Khachik Formation (sample A. 330), Guadalupian, Ali-Bashi section, Iran (this study).

DIMENSIONS. – L= 101µm; H= 59µm; H/L= 0.58.

REMARKS. – The morphological shape of this specimen resembles the typical form found in the *Barida* genus. AB Slightly convex to straight and PB strongly convex. Nevertheless, lacking characteristics are available to assign it to a specific species.

Bairdia sp.

(Fig.4.6 C1-C4)

MATERIAL. – 7 incomplete carapaces.

OCCURRENCES. – Khachik Formation Unit VI (samples A. 158, A. 171, A. 176, A. 188, A. 204 and A. 210) Guadalupian, Ali-Bashi section, Iran (this study).

DIMENSIONS. – L=87.9 – 93.7 µm; H= 53.9 – 61.5 µm; H /L= 0.61 – 65

REMARKS. – Carapace subtriangular to rhomboidal, with strong dorsal overlap of left valve on right one; straight DB, ADB and PVB at right valve. However, there is no enough characteristics to give a species attribution.

Genus *Bairdiacypris* Badfield, 1935

Bairdiacypris longirobusta Chen, 1958

(Plate 4.2 G1-G13)

Bairdiacypris longirobusta: Chen, 1958: 255. pl.7, figs.1-3. - Shi & Chen, 1982: 136, pl.10, figs.12-18. - Shi & Chen, 1987: pl.12, figs.21-22. - Shi & Chen, 2002: pl.21, figs.4-7. - Chitnarin et al., 2017: 670-671, Fig. 15M.

MATERIAL. – 7 complete and 6 incomplete carapaces.

OCCURRENCES. – Early Permian, Kwanshan and Lungtan sections, Chihhsia Limestone, Nanking Province (Chen, 1958). Latest Permian, Nantong section, Jiangsu Province (Chen & Shi, 1982). Latest Permian, Meishan section, Zhejiang Province, (Shi & Chen, 1987). Latest Permian, Matan and Pingding sections, Guangxi. South China (Shi & Chen, 2002). Early-Middle Permian (Cisarulian-Guadalupian), Central Thailand, Indochina Block (Chitnarin et al. 2017). Khachik Formation (sample A. 156, A. 159, A. 167, A. 287, A. 290 and A. 332), Guadalupian, Ali-Bashi section, Iran (this study).

DIMENSIONS. – L= 110 – 120 μ m; H= 57 – 59 μ m; H/L=0.49 – 0.51.

DISCUSSION. – Carapace bean-shaped; ADB, DB and PDB straight at RV and convex at LV. This species exhibits very strong variations.

Bairdiacypris sp. 6 *sensu* Zazzali et al., 2015

(Plate 4.2 H)

Bairdiacypris sp. 6 *sensu* Zazzali et al., 2015: Zazzali et al., 2015: 298, fig. 10, J.

MATERIAL. – 1 complete carapace.

OCCURRENCES. – Late Permian (Early Lopingian), Wuchiapingian Formation, Chaotian section, Sichuan Province, South China (Zazzali et al. 2015). Khachik Formation (sample A. 330), Guadalupian, Ali-Bashi section, Iran (this study).

DIMENSIONS. – L= 50 μ m; H= 24 μ m; H/L= 0.47.

REMARKS. – The carapace takes on a sub-elliptical to sub-trapezoidal shape. It features a substantial and sturdy overlap of the LV over the RV. The VB displays a pronounced concavity. Additionally, both the ADB and PDB present a wide and gentle convex curvature, while the DB remains nearly straight.

Bairdiacypris sp. B *sensu* Tarnac et al., 2021

(Plate 4.2 I1-I5)

Bairdiacypris sp. B *sensu* Tarnac et al., 2021: Tarnac et al., 2021: fig. 8 G.

MATERIAL. – 5 complete carapaces.

OCCURRENCES. – Capitanian, Middle Permian, Bell Canyon Formation, Guadalupe Mountains, West Texas, USA (Tarnac et al. 2021). Khachik Formation (sample A. 210, A. 322 and A. 325), Guadalupian, Ali-Bashi section, Iran (this study).

DIMENSIONS. – L= 84 – 87 μ m; H= 45 – 47 μ m; H/L= 0.53 – 0.54.

DISCUSSION. – The carapace is a sub-trapezoidal to sub-ellipsoidal shape. The PB along with the AB displays a broad and gentle convex curve. The DB is somewhat wide and slightly convex, while the VB features a deep concavity.

Bairdiacypris sp. 1

(Plate 4.1 J1-J4)

MATERIAL. – 2 complete and 4 incomplete carapaces.

OCCURRENCES. – Khachik Formation (samples A. 140, A. 152, A. 158, A. 171, A. 176, A. 188, A. 202, A. 204, A. 207, A. 210 and A. 239) Guadalupian, Ali-Bashi section, Iran (this study).

DIMENSIONS. – L=87 – 93 μ m; H= 53 – 61 μ m; H/L= 0.61 – 0.65.

REMARKS. – Carapace subtriangular to rhomboidal; strong dorsal overlap of LV on RV; straight DB, ADB and PVB at RV. However, there is no enough characteristics to give specific attribution.

Bairdiacypris sp. 2

(Plate 4.2 K1-K3)

MATERIAL. – 6 carapaces.

OCCURRENCES. – Khachik Formation (sample A. 191, A. 202, A. 203, A. 279, A. 294 and A. 301), Guadalupian, Ali-Bashi section, Iran (this study).

DIMENSIONS. – L= 96 – 98 μ m; H= 45 – 51 μ m; H/L=0.46 – 0.52.

REMARKS. – *Bairdiacypris* sp. 1 with semi-bean to sub-elliptical shape; small and rounded PB, with maximum of curvature located below the mid height; narrow overlap of LV on RV around the entire carapace; maximum of H located in pposterior part of the carapace. This species lacks sufficient similarities to be compared to any known species.

Bairdiacypris sp. 3

(Plate 4.2 L)

MATERIAL. – 1 complete carapace.

OCCURRENCES. – Khachik Formation (sample A. 332), Guadalupian, Ali-Bashi section, Iran (this study).

DIMENSIONS. – L= 67 μ m; H= 35 μ m; H/L= 0.52.

REMARKS. – The carapace is laterally flattened towards both the front and back. The LV, the dorsal outline shows a consistently convex shape, while in the RV ADB, and PDB are all straight. On the LV, the VB is straight, whereas on the RV, it curves inwards, forming a concavity.

Bairdiacypris sp. 4

(Plate 4.3 A)

MATERIAL. – 1 complete carapace.

OCCURRENCES. – Khachik Formation (sample A. 207), Guadalupian, Ali-Bashi section, Iran (this study).

DIMENSIONS. – L= 69 μ m; H= 41 μ m; H/L= 0.59.

REMARKS. – The carapace is Intense semi-bean shape. The LV, overlapped of the RV in the all of carapace eception in the PB part; DB is slighty convex; AB and PB are gently convex; VB is gently convcave.

Bairdiacypris sp. 5

(Plate 4.3 B)

MATERIAL. – 1 incomplete carapace.

OCCURRENCES. – Khachik Formation (sample A. 207), Guadalupian, Ali-Bashi section, Iran (this study).

DIMENSIONS. – L= 76 μ m; H= 34 μ m; H/L= 0.44.

REMARKS. – The carapace is semi-elliptical shape; The LV overlape RV that this state is very clear and thick in the DB; PB and Ab are convex.

Bairdiacypris sp. 6

(Plate 4.3 C)

MATERIAL. – 1 complete carapace.

OCCURRENCES. – Khachik Formation (sample A. 207), Guadalupian, Ali-Bashi section, Iran (this study).

DIMENSIONS. – L= 69 μ m; H= 37 μ m; H/L= 0.53.

REMARKS. – The carapace is semi-elliptical to semi-trapezoidal; PB is semi-spindle-shape; AB is convex; DB slightly convex; VB slightly concave.

Bairdiacypris sp. 7

(Plate 4.3 D)

MATERIAL. – 1 complete carapace.

OCCURRENCES. – Khachik Formation (sample A. 191), Guadalupian, Ali-Bashi section, Iran (this study).

DIMENSIONS. – L= 77 μm ; H= 33 μm ; H/L= 0.42.

REMARKS. – The carapace is semi-trapezoidal. The LV overlaps of the RV in the all the cap carapace and in the DB is spindle-shaped; PB and AB convex; VB is VB slightly concave; ADB is straight; PDB is slightly convex. It might represent a novel species; however, insufficient material is available to put forth a formal description.

Bairdiacypris sp. 8

(Plate 4.3 E)

MATERIAL. – 1 complete carapace.

OCCURRENCES. – Khachik Formation (sample A. 191), Guadalupian, Ali-Bashi section, Iran (this study).

DIMENSIONS. – L= 127 μm ; H= 64 μm ; H/L= 0.50.

REMARKS. – *Bairdiacypris* sp. 8 features a triangular overlap area along the DB. Both AB and PB are rounded with significant radii of curvature, with their highest points of convexity situated at and below the midpoint of the height, respectively.

Bairdiacypris sp. 9

(Plate 4.3 F)

MATERIAL. – 1 complete carapace.

OCCURRENCES. Khachik Formation (sample A. 207), Guadalupian, Ali-Bashi section, Iran (this study).

DIMENSIONS. – L= 121µm; H= 57µm; H/L= 0.47.

REMARKS. – *Bairdiacypris* sp. 9 characterized by straight DB, concave VB. AB is broadly rounded and PB is round with medium radius of curvature.

Bairdiacypris sp.

(Plate 4.5 C1-C4)

MATERIAL. - 7 complete and 4 incomplete carapaces.

OCCURRENCES. – Khachik Formation (samples A. 140, A. 152, A. 158, A. 171, A. 176, A. 188, A. 202, A. 204, A. 207, A. 210 and A. 239) Guadalupian, Ali-Bashi section, Iran (this study).

DIMENSIONS. – L=89 – 96µm; H= 54 – 62µm; H/L= 0.60 – 0.64.

REMARKS. – Carapace with sub-trapezoidal shape; BP with small radius of curvature and AB with very large radius of curvature; DB almost straight at booth valves. The PB exhibits a spindle-like form, while the AB showcases a broad and gentle convex curve. The DB remains almost straight, and there is a slight concavity in the VB

Genus *Ceratobairdia* Sohn, 1954

Ceratobairdia sexagintaduella Forel, 2021

(Plate 4.3 G)

Ceratobairdia sexagintaduella Forel Forel sp. nov. - Tarnac et al 2021: 36-38, fig. 9 D-J

MATERIAL. – 2 complete carapaces.

OCCURRENCES. – Roadian, Middle Permian, Guadalupe Mountains, West Texas (Tarnac et al 2021). Khachik Formation (samples A. 183, A. 191) Guadalupian, Ali-Bashi section, Iran (this study).

DIMENSIONS. – L= 72–76µm; H= 35–41µm; H/L= 0.48 – 0.53.

DISCUSSION. – This species of *Ceratobairdia* with a lamellar overlap of LV over RV and a curved latero-ventral ridge delimiting a flat venter lacking a posterior spine (Tarnac et al 2021).

Ceratobairdia? cf. *crenata* Chen, 1982

(Plate 4.3 H)

cf. *Ceratobairdia rnata* Chen n.sp.- Chen & Shi, 1982: 127-128, pl.5, figs 4-7.

MATERIAL. – 1 complete carapace.

OCCURRENCES. – Khachik Formation (sample A. 294), Guadalupian, Ali-Bashi section, Iran (this study).

DIMENSIONS. – L= 83µm; H= 51µm; H/L= 0.61.

DISCUSSION. – Carapace with subtriangular shape. DB broad and almost straight; LV overlaps RV along the entire carapace, except at ADB and AVB. Presence of a strong ridge on the median part of the carapace. I specimen is close from *Ceratobairdia rnata* Chen, 1982 from latest Permian of Hubei (China) but here there is only one ridge instead of two. This is also the reason of doubt on the genus.

Genus *Fabalitypris* Cooper, 1946

Fabalitypris acetalata (Coryell & Billings, 1932)

(Plate 4.3 I1-I3)

Bairdia acetalata Coryell & Billings, 1932: 173, pl. 17 fig. 5.

Fabalitypris acetalata – Sohn 1960 (with all previous synonymy therein): 62. – Tarnac et al. 2021: Figs 8, I–J.

MATERIAL. – 6 complete carapaces.

OCCURRENCES. – Pennsylvanian, Kansas, Texas, Illinois, USA, (Coryell & Billings 1932; Sohn 1960). Permian, Nebraska, USA (Sohn 1960). Roadian, Middle Permian, Cutoff Formation, Guadalupe Mountains, West Texas, USA, (Tarnac et al. 2021). Khachik Formation (sample A. 202, A. 203, A. 262, A. 329 and A. 332), Guadalupian, Ali-Bashi section, Iran (this study).

DIMENSIONS. – L= 81–85µm; H= 41–43µm; H/L= 0.50 – 0.51.

DISCUSSION. – Carapace with sub-ellipsoidal to sub-trapezoidal shape. Both PB and AB are gently convex. DB broadly curved; VB straight. LV overlaps RV all around the carapace.

Fabalitypris glennensis (Harlton, 1927)

(Plate 4.3 J)

Bairdia glennensis Harlton, 1927: 210, pl. 33 fig. 10.

Bairdia glennensis – Kellett 1935: 133, pl. 18 figs 4a–e.

Fabalitypris glennensis – Sohn 1960: pl. 3 figs 9–10. — Yi 1993: 62, pl. 3 figs 9–10. — Shi & Chen 2002: 86, pl. 23 figs 1–2. — Tarnac et al. 2021: fig. 8K.

MATERIAL. – 1 complete carapace.

OCCURRENCES. – Pennsylvanian, Kansas, Oklahoma, USA, Kasimovian, (Harlton 1927; Kellett 1935; Sohn 1960). Early Permian, Hubei, China, Kungurian, (Yi 1993). Changhsingian, Late Permian, Sichuan, China, (Shi & Chen 2002); sample 4 (GM5), Capitanian, Middle Permian, Bell Canyon Formation, Guadalupe Mountains, West Texas, USA (Tarnac et al. 2021). Khachik Formation (sample A. 276), Guadalupian, Ali-Bashi section, Iran (this study).

DIMENSIONS. – L= 91µm; H= 45µm; H/L= 0.49.

DISCUSSION. – The Carapace is very elongate, large; in lateral view dorsum and venter almost parallel; dorsum long and straight, venter long and almost straight, slightly concave at the center; anterior end evenly rounded; posterior beak low, bluntly rounded in the adult and rather pointed in the young species (Kellett 1935).

Fabalitypris parva Wang, 1978

(Plate 4.3K; Plate 4.5 D1-D4)

Fabalitypris parva: Wang 1978: 293, pl. 2, figs. 12a-b, 13a-b. - Crasquin-Soleau *et al.* 2004: 286, pl. 3, figs. 4-5. - Mette 2008: pl. 2, fig. 8. - Crasquin *et al.* 2010: 353, fig. 9A'-B'. - Forel, 2012: fig 11, l.

Fabalitypris hungarica Wang 1978: Kozur, 1985b, 82, pl. 2, figs. 2, 9, 10.

Bairdiacypris opulenta Wang 1978: Shi & Chen, 1987, 51, pl. 13, fig. 10.

MATERIAL. – 10 complete carapaces.

OCCURRENCES. – Wuchiapingian and Changhsingian (Lopingian) Longtan and Changxing Formations, Guizhou and Yunnan Provinces, South China (Wang 1978). Lopingian, Bükk

Mountains, Hungary, Late Moscovian, Carboniferous, (Kozur 1985b). Lopingian, Changxing formation, Meishan section, Zhejiang Province, South China, Changhsingian, (Shi & Chen 1987; Crasquin *et al.* 2010). Wuchiapingian and Changhsingian (Lopingian), Çürük dağ section, Western Taurus, Turkey, (Crasquin-Soleau *et al.* 2004). Lopingian, Zal section, Iran, Changhsingian, (Mette 2008). Lopingian- Early Triassic, Dajiang section in the southern Guizhou Province, South China, (Forel 2012). Khachik Formation (samples A. 151, A. 154, A. 155, A. 176, A. 191, A. 194, A. 204, A. 210 and A. 278), Guadalupian, Ali-Bashi section, Iran (this study).

DIMENSIONS. – L= 84 – 94µm; H= 32 – 47µm; H/L= 0.38 – 0.50.

DISCUSSION. – The carapace is sub-bean shaped with valve surface smooth; LV slightly overlaps RV all around the carapace; end margins broadly rounded; DB, ADB, PDB straight at RV, arched at LV; overlap moderate; VB slightly concave.

REMARKS. – *Fabalitypris parva* Wang, 1978 exhibits a bean-shaped carapace, and previous records indicate that it is present from the Late Moscovian (Carboniferous; Kozur 1985b) to the Changhsingian (Lopingian; Wang 1978; Shi & Chen 1987; Crasquin-Soleau *et al.* 2004, Mette 2008, Crasquin *et al.* 2010). Despite this extensive stratigraphic range, some Carboniferous occurrences are doubtful, since most are from the Lopingian period. In the context of designating *Fabalitypris hungarica* Kozur, 1985b as a synonym of *Fabalitypris parva* Wang, 1978, Crasquin *et al.* (2010) noted distinctions, such as *Fabalitypris hungarica* Kozur, 1985b displaying a more rounded PB and a higher location of maximum convexity compared to *Fabalitypris parva* (see more in Forel 2012).

Fabalitypris reniformis (Chen, 1958) *sensu* Wang, 1978

(Plate 4.3 L1-L2)

Fabalitypris reniformis (Chen, 1958) *sensu* Wang, 1978: Forel *et al.* 2013: 216, fig. 22 O.

MATERIAL. – 2 complete carapaces.

OCCURRENCES. – Permian–Triassic boundary, Bükk Mountains, Hungary, south Tibet (Forel *et al.* 2013). Khachik Formation (sample A. 332) Guadalupian, Ali-Bashi section, Iran (this study).

DIMENSIONS. – L= 57.40 – 58.60 µm; H= 29.90 – 32.10 µm; H/L= 0.52 – 0.54.

DISCUSSION. – Carapace sub-trapezoidal PB with medium radius of curvature; AB with moderate radius of curvature with maximum at midH; DB, ADB and PDB regularly arched; VB straight at LV, concave at RV; continuous overlap LV on RV all around carapace,

Fabalitypris sp. 1

(Plate 4.5 E)

MATERIAL. – 3 complete carapaces.

OCCURRENCES. – Khachik Formation (samples A. 151, A. 154 and A. 210), Guadalupian, Ali-Bashi section, Iran (this study).

DIMENSIONS. – L= 89–92 μ m; H= 29–35 μ m; H/L= 0.32–0.38.

REMARKS. – The carapace is semi-elliptical shape with DB slightly convex and VB straight. The AB cently convex and the PB convex.

Fabalitypris sp. 2

(Plate 4.5 F)

MATERIAL. – 1 complete carapace.

OCCURRENCES. – Khachik Formation (sample A. 210), Guadalupian, Ali-Bashi section, Iran (this study).

DIMENSIONS. – L= 94 μ m; H= 45 μ m; H/L= 0.47.

REMARKS. – The carapaces sub-triangular with valve surface smooth and the studied specimen has dorsal outline broadly arched.

Fabalitypris sp. 3

(Plate 4.5 G)

MATERIAL. – 1 incomplete carapace.

OCCURRENCES. – Khachik Formation (samples A. 210), Guadalupian, Ali-Bashi section, Iran (this study).

DIMENSIONS. – L= 86 μ m; H= 28 μ m; H/L= 0.32.

REMARKS. – The carapace is bean-shape; DB convex; VB slightly concave; PB and AB convex.

Fabalicypris sp. 4

(Plate 4.5 H)

MATERIAL. – 1 incomplete carapaces.

OCCURRENCES. – Khachik Formation (sample A. 238), Guadalupian, Ali-Bashi section, Iran (this study).

DIMENSIONS. – L= 82 μ m; H= 31 μ m; H/L= 0.38.

REMARKS. – Carapace sub-bean shaped. Our specimens are not complete, particularly in the anterior region. Therefore, it is impossible to give specific attribution.

Fabalicypris sp. 5

(Plate 4.3 M1-M2)

MATERIAL. – 1 complete and 1 incomplete carapaces.

OCCURRENCES. – Khachik Formation (samples A. 204 and A. 210), Guadalupian, Ali-Bashi section, Iran (this study).

DIMENSIONS. – L= 96.90 – 100.20 μ m; H= 40.30 – 42.70 μ m; H/L= 0.41 – 0.42.

DISCUSSION. – The carapace is bean-shaped carapace to sub-elongated with valve surface smooth. both AB and PB exhibits a gentle convexity. The DB is somewhat straight, while the VB is wide and expansively curved.

Fabalicypris sp. 6

(Plate 4.3 N1-N2)

MATERIAL. – 2 complete and 1 incomplete carapaces.

OCCURRENCES. – Khachik Formation (sample A. 151, A. 152 and A. 210), Guadalupian, Ali-Bashi section, Iran (this study).

DIMENSIONS. – L= 103 – 106 μ m; H= 32 – 39 μ m; H/L= 0.25 – 0.36.

REMARKS. – The carapace is elongated, featuring a regularly arched DB on the LV and a straight DB on the RV. The ADB and PDB are straight on the RV and arched on the LV. The AB is rounded, while the PB tapers. This form is very particular with a PB with maximum of

curvature located high and Hmax located in posterior part of carapace; It could be a new species but there is not enough material to propose a formal description.

Fabalicypis sp. 7

(Plate 4.3 O)

MATERIAL. – 4 complete carapaces.

OCCURRENCES. – Khachik Formation (samples A. 204, and A. 210), Guadalupian, Ali-Bashi section, Iran (this study).

DIMENSIONS. – L= 86 – 90 μ m; H= 27 – 33 μ m; H/L= 0.31 – 0.36.

REMARKS. – The carapace is sub-bean shaped with valve surface smooth; LV obviously and very widely overlaps RV all around the carapace; DB, ADB and PDB is slightly convex; VB slightly straight.

Genus *Kempfina* Crasquin, 2010

Kempfina qinglaili (Crasquin, 2008)

(Plate 4.3 P1-P3)

Kempfina qinglaili (Crasquin, 2008) – Crasquin et al. 2008: 244-246; Gliwa et al. 2021: fig. 13 G-L.

MATERIAL. – 4 complete carapaces.

OCCURRENCES. – Latest Permian of the Southern Alps (Italy) and Guizhou, Zhejiang and Hubei provinces (South China) (Crasquin et al. 2008). End of Permian age, Aras Valley section, Julfa region, northwest of Iran (Gliwa et al. 2021). Khachik Formation (samples A. 167, A. 207, A. 244 and A. 284), Guadalupian, Ali-Bashi section, Iran (this study).

DIMENSIONS. – L= 69 – 71 μ m; H= 41 – 42 μ m; H/L= 0.59 – 0.60.

DISCUSSION. – Carapace robust The LV extends over the RV across the entire carapace, with the smallest overlap observed at the front lower border and rear upper border. Both the DB and VB display a slight straightness.

Kempfina sp. 1

(Plate 4.3 Q)

MATERIAL. – 1 incomplete carapace.

OCCURRENCES. – Khachik Formation (sample A. 200), Guadalupian, Ali-Bashi section, Iran (this study).

REMARKS. – There is only 1 incomplete carapace with a dorsal view of this species. Consequently, based on the dorsal perspective, the carapace appears to take on a semi-spindle form, featuring a smooth valve surface and a distinctly arched hinge along the dorsal border outline.

Genus *Liuzhinia* Zheng, 1976

Liuzhinia julfensis Gliwa et al., 2021

(Plate 4.3 R1-R2)

Liuzhinia? sp.1: Mette 2008: p. 215, pl. 2, figs 15–17.

Liuzhinia sp. 1; Mette 2010: p. 31, pl. 4, figs 7–9.

Liuzhinia julfensis Gliwa n.sp.: Gliwa et al. 2021: 19- 20, Fig. 15 AA-AF.

MATERIAL. – 1 complete and 1 incomplete carapaces.

OCCURRENCES. – End of Permian age, Aras Valley section, Julfa region, northwest of Iran (Gliwa et al. 2021). Khachik Formation (samples A. 157 and A. 161), Guadalupian, Ali-Bashi section, Iran (this study).

DIMENSIONS. – L= 53 – 65µm; H= 25 – 33µm; H/L= 0.47 – 0.50.

DISCUSSION. – The carapace is elongated, subtrapezoidal shape when viewed from the side, with the Hmax situated in the anterior third of its Lmax. There is a very thin overlap of the larger LV, especially noticeable along the VB. The dorsal margin is mostly straight but may have a slight rounding, with a gentle angle between the PDB and DB located in the posterior fourth of Lmax. The DB is gently convex and smoothly rounded, extending uniformly towards the AB. (for further details, refer to [Gliwa et al. 2021](#)).

Suborder KLOEDENELLOCOPINA Scott, 1961

Superfamily KLOEDENELLOIDEA Ulrich & Bassler, 1908

Family BAIRDIOCYPRIDIDAE Shaver, 1961

Genus *Silenites* Coryell and Booth, 1933

Silenites sp.

(Plate 4.5 J1-J2)

MATERIAL. - 2 incomplete carapaces.

OCCURRENCES. - Khachik Formation (sample A. 238), Guadalupian, Ali-Bashi section, Iran (this study).

DIMENSIONS. - L= 58 – 98 μ m; H= 31 – 53 μ m; H /L= 0.52–0.54

REMARKS. - This specimen of *Silenites* with sub-oval carapace, however the lack of some features like: arched dorsal outline or DB of RV, AB and PB, it prevented it from being named as a specific species of *Silenites* genus.

Family BITHOCYPRIDIDAE Maddocks, 1969

Genus *Praezabythocypris* Kozur, 1985

Praezabythocypris pulchra Kozur, 1985

(Plate 4.3 S1-S2)

Praezabythocypris pulchra Kozur 1985b: plate 17, fig. 13. - Kozur 1991: Plate 1 fig. 13. - Gliwa et al. 2021: Fig. 13 Y-AB.

MATERIAL. – 1 complete and 1 incomplete carapaces.

OCCURRENCES. – Lopingian, Bükk Mountains, Hungary, Late Moscovian, Carboniferous, (Kozur 1985b). Late Permian, Western Sicily (Kozur 1991). End of Permian age, Aras Valley section, Julfa region, northwest of Iran (Gliwa et al. 2021). Khachik Formation (samples A. 207 and A. 302), Guadalupian, Ali-Bashi section, Iran (this study).

DIMENSIONS. – L= 73.40 – 75.70 μ m; H= 38.30 – 41.20 μ m; H/L= 0.52 – 0.54.

DISCUSSION. – The carapace has a sub-oval to robustly sub-oval shape. the LV is markedly taller than the RV, protruding beyond it along the entire perimeter, with a particularly noticeable extension in the dorsal and central-ventral areas. The front edge is gently rounded,

while the rear edge is slightly more pointed. The dorsal edge of the LV exhibits a subtle to pronounced convex curve. In the RV, the central dorsal section is generally straight, with a slight to noticeable backward fold. The ventral outline is concave, and the surface of the shell is smooth (see more in [Kozur 1985b](#)).

Praezabythocypris sp. 1

(Plate 4.3 T)

MATERIAL. – 1 complete carapace.

OCCURRENCES. – Khachik Formation (sample A. 167), Guadalupian, Ali-Bashi section, Iran (this study).

DIMENSIONS. – L= 103µm; H= 46µm; H/L= 0.45.

REMARKS. – *Praezabythocypris* sp. 1 has a steep PDB; a more inclined DB at the RV; a longer and less rounded AVB, and a posterior maximum curvature that is situated more ventrally.

Family GEROIIDAE Gründel, 1962

Genus *Pseudacanthoscapha* Kozur, 1985

Pseudacanthoscapha striatula (Shi, 1982)

(Plate 4.3 U)

Acratia? *striatula* Shi in Chen & Shi, 1982: 139, pl. 11, figs 9–11.

Pseudacanthoscapha beckeri Kozur, 1985a: 110, pl. 18, fig. 9.

Acratia striatula Shi: Shi & Chen, 1987: 49, pl. 11, figs 13–18, pl. 17, figs 1–4.

Pseudacanthoscapha beckeri Kozur, 1985: Mette, 2008: pl. 2, fig. 1.

Pseudacanthoscapha striatula (Shi, 1982): Crasquin et al. 2010: 362, fig. 20 D.

MATERIAL. – 1 complete carapace.

OCCURRENCES. – Wuchiapingian (Dzulfian), Bukk Mountains, Hungary, (Kozur 1985). Latest Permian Mianyang, Hubei Province, (Chen & Shi 1982 in Crasquin et al. 2010). Changhsingian, Late Permian, Meishan section, Baoqing Member (Shi & Chen 1987). Wuchiapingian, Zal section, Julfa region, northwest of Iran, (Mette 2008). Permian-Triassic boundary, Meishan

stratotype, Zhejiang Province, South China (Crasquin et al. 2010). Khachik Formation (sample A. 274), Guadalupian, Ali-Bashi section, Iran (this study).

DIMENSIONS. – L= 80µm; H= 43µm; H/L= 0.54.

DISCUSSION. – The carapace is sizeable, displaying an ellipsoidal to fusiform shape. It features laterally strongly curved shells, and in the central part, it is adorned with robust, closely spaced longitudinal ribs. The LV is larger than the RV. Both valves have front flaps adorned with elongated, thorn-like flanges. At the rear, the LV has a long extension resembling thorns, which is open at the proximal end. This extension accommodates the shorter, essential extension of the RV, creating a complementary fit (Kozur 1985a).

Family KNOXITIDAE Egorov, 1950

Genus *Sargentina* Coryell & Johnson, 1939

Sargentina minuta Wang, 1978

(Plate 4.3 V1-V5; Plate 4.4 A1-A2)

Sargentina minuta Wang, 1978: Crasquin-Soleau et al., 1999: 176, pl. 3, figs 3–4.

Sargentina minuta Wang, 1978: Angiolini et al., 1999: 177, photo 15, 13.

MATERIAL. – 4 complete and 2 incomplete carapaces.

OCCURRENCES. – Khachik Formation (samples A. 144 and A. 151), Guadalupian, Ali-Bashi section, Iran (this study).

DIMENSIONS. – L= 56 –75µm; H= 31 – 36µm; H/L= 0.48 – 0.55.

DISCUSSION. – The carapace appears elongated and takes on a subrectangular shape when viewed from the side. The DB is straight and The AB is broadly rounded, with the maximum convexity positioned at the midpoint in terms of height. In the RV, the VB is straight, while in the LV, it exhibits a slight concavity. The PB is rounded, with the highest point of convexity located above the midpoint in height.

Sargentina transita (Kozur, 1985)

(Plate 4.5 I)

Italogesina transita: Kozur, 1985b: p.17, Pl.3; Fig. 9-11; Gerry et al. p.206, pl.2, fig.20

Sargentina transitia (Kozur, 1985) Crasquin-Soleau et al. 1999: pl.3, fig.5-8; Honigstein et al. 2005: p. 409, 419, Pl.2; fig. 13; Crasquin-Soleau et al. 2005b: pl. 4, figs. 4.1-4.7

MATERIAL. – 3 complete carapaces.

OCCURRENCES. – Early Lopingian of Bükk Mountains, Hungary (Kozur, 1985b), Lopingian of Israel (Gerry *et al.* 1987, Honigstein & Rosenfeld 2005); Guadalupian of Sultanate of Oman (Crasquin-Soleau *et al.* 1999); Guadalupian of Saudi Arabia (Crasquin-Soleau *et al.* 2005). Khachik Formation (samples A. 176, A. 204 and A. 210), Guadalupian, Ali-Bashi section, Iran (this study).

DIMENSIONS. – L= 79 – 81 μ m; H= 48 – 53 μ m; H/L= 0.61 – 0.65.

DISCUSSION. – The specimens are attributed to *Sargentina transitia* (Kozur 1985) in regards of their sub-rectangular carapace, the overlap of LV on RV slight and the sulcus shallow for the genus. The figured specimen could be a female due to the very rounder and large posterior part of the carapace.

Sargentina sp.

(Plate 4.4 B1-B5)

MATERIAL. – 8 complete and 3 incomplete carapaces.

OCCURRENCES. – Khachik Formation (samples A. 125, A. 128, A. 140, A. 150, A. 156, A. 191 and A. 194), Guadalupian, Ali-Bashi section, Iran (this study).

DIMENSIONS. – L= 67–109 μ m; H= 43– 74 μ m; H/L= 0.64 – 0.67.

REMARKS. – The carapace outline, when viewed from the lateral, appears subelliptical. The DB is straight in the LV and convex in the RV. S2, which is elongated and slender, is situated on the dorsomedian portion and appears round and shallow in shorter specimens. The AB is broadly rounded, with the highest point of convexity just below the midpoint in terms of height. The VB is convex in the RV and slightly concave in the LV. The PB is more narrowly rounded, with the maximum convexity located at or above the midpoint in height.

Suborder BERICHICOPINA Scott, 1961

Superfamily HOLLINOIDEA Swartz, 1936

Family HOLLINELLIDAE Bless & Jordan, 1971

Genus *Hollinella* Coryell, 1928 emend. Kellett, 1929

Hollinella (Hollinella) herrickana (Girty, 1909)

(Plate 4.5 I1-I3)

Hollina herrickana: Girty 1909; 115, pl. 8, figs. 10, 11.

Hollinella herrickiana [sic!] – Kellett 1929:197; 1934: 626. — Delo 1930: 156, pl. 12, fig. 4. — Bassler & Kellett 1934: 333.

Hollinella tuberculata (Girty 1909): Belousova 1965: 254, pl. 46, fig. 2a-c.

Hollinella (Hollinella) herrickana – Bless & Jordan 1972: 38, 39. — Lethiers *et al.* 1989: 230, pl. 1, figs. 2-4. — Crasquin-Soleau *et al.* 1999: pl. 2, fig. 5. - Chitnarin *et al.* 2012: 828 fig. 19E, F.

MATERIAL. – 4 complete and 2 incomplete carapaces.

OCCURRENCES. – Cisuralian, Yeso Formation, New Mexico (USA); Texas (USA), Late Carboniferous (Girty 1909; Kellett 1929; Delo 1930; Bassler & Kellett 1934); Caucasus (Russia), Lopingian (Belousova 1965). Late Guadalupian, Merbah el Oussif unit, Jebel Tebaga, Tunisia, (Lethiers *et al.* 1989). Guadalupian, Khuff Formation, Sultanate of Oman, (Crasquin-Soleau *et al.* 1999). Cisuralian, Khao Kana section, Pha Nok Khao Formation, Phetchabun Province, Central Thailand, (Chitnarin *et al.* 2012). Khachik Formation (samples A. 151, A. 158, A. 188, A. 210 and A. 238), Guadalupian, Ali-Bashi section, Iran (this study).

DIMENSIONS. – L= 82 – 98 μ m; H= 40 – 65 μ m; H/L= 0.49 – 0.66

DISCUSSION. – Straight-hinged reticulated carapace with two large lobes. These specimens are assigned to *Hollinella (Hollinella) herrickana* from the Late Carboniferous-Guadalupian of USA, Russia, Arabia, Tunisia and Central Thailand. L1 connected with ventral lobe, L2 quite well expressed and L3 bulbous by long and connecting L1 and L2, bulbous L3 (overpass DB) and velate structure large; here the reticulation and punctuation of Thai specimens is not observable (Chitnarin *et al.* 2012) (fig. 4.4-A.3).

Hollinella (Hollinella) martensiformis Crasquin et al. 2010

(Plate 4.4 C1-C2)

Hollinella (Hollinella) martensiformis: Crasquin et al. 2010: fig. 4 D-F.

MATERIAL. – 2 complete carapaces.

OCCURRENCES. – Permian-Triassic boundary, Meishan stratotype, Zhejiang Province, South China (Crasquin et al. 2010). Khachik Formation Unit VI (samples A. 153, d A. 154), Guadalupian, Ali-Bashi section, Iran (this study).

DIMENSIONS. – L= 82 – 90 μ m; H= 49 – 58 μ m; H/L= 0.59 – 0.64.

DISCUSSION. – According to [Crasquin et al. \(2010\)](#), the carapace exhibits a long, straight DB, with clearly defined cardinal angles measuring approximately 110° to 120° each. The AB showcases a pronounced radius of curvature, with the highest curvature point situated just slightly above the midpoint in terms of height. The VB displays a consistently arched profile, with its maximum height positioned in front of the midpoint of its length. The PB has a small radius of curvature, and its highest curvature point is located near the DB. The carapace features a frill composed of regularly spaced, individualized tubercles. In larger specimens, L1 and S1 can be observed, but they are not discernible in smaller ones. L2 is located in front of the midpoint of the carapace's length and in the upper quarter of its height. S2 is situated above the midpoint of the carapace's height. L3 is minimally expressed in smaller forms but extends beyond the hinge line in the largest specimens. The maximum thickness of the carapace is found at the midpoint of its length, and the surface may exhibit a reticulated pattern.

Hollinella sp.

(Plate 4.4 D1-D2; Plate 4.5 J)

MATERIAL. – 4 incomplete carapaces.

OCCURRENCES. – Khachik Formation (samples A. 188, A. 194 and A. 238), Guadalupian, Ali-Bashi section, Iran (this study).

DIMENSIONS. – L= 83 – 99 μ m; H= 52 – 64 μ m; H/L= 0.62 – 0.64.

REMARKS. – This specimen is assigned to *Hollinella* based on the presence of bulbous L3 and possible adventral structure, but preservation is too poor for specific assignment.

Order PALAEOCOPIDA Henningsmoen, 1953?

Superfamily PARAPARCHITIDEA Scott, 1959 emend. Sohn, 1971

Family INDIVISIIDAE Egorov, 1954

Genus *Indivisia* Zaspelova, 1954

Indivisia sp. 1 *sensu* Forel et al., 2015

(Plate 4.4 E)

Indivisia sp. 1 *sensu* Forel et al. 2015: Forel et al. 2015: fig. 17 AB-AC.

MATERIAL. – 1 complete carapace.

OCCURRENCES. – Lopingian (Late Permian) to the Griesbachian (Early Triassic), Elikah River section, Central Alborz Mountains, North of Iran, (Forel et al. 2015). Khachik Formation U (samples A. 192 and A. 200), Guadalupian, Ali-Bashi section, Iran (this study).

DIMENSIONS. – L= 87µm, H= 50µm, H/L= 0.55.

DISCUSSION. – The carapace exhibits a shape ranging from subelliptical to rectangular. The RV is larger than the LV and extends along the entire free edge. At the dorsal edge, both valves share equal height. The anterior margin is straight, with a slight convergence towards the dorsal margin as we move towards the posterior. The hind edge is rounded, forming a point in the upper third and displaying a pronounced bevel at its lower part.

Order RETICULOCOPIDA Kozur, 1993

Suborder PUNCIOCOPINA Schallreuter, 1968

Superfamily KIRKBYACEA Ulrich & Bassler, 1906

Family Kirkbyidae Ulrich & Bassler, 1906

Genus *Reviya* Sohn, 1961

Reviya sp.

(Plate 4.4 F1-F2)

MATERIAL. – 2 complete carapaces.

OCCURRENCES. – Khachik Formation (sample A. 156), Guadalupian, Ali-Bashi section, Iran (this study).

DIMENSIONS. – L= 69 – 74µm; H= 37 – 40µm; H/L= 0.53 – 0.54

REMARKS. – BD long and straight; no shoulder more than nodes; presence of a long and elongated kirkbyan pit; deep sulcus all along free margins, cardinal angles at 90°, presence of a ridge above pit; extremities compressed laterally; surface pitted.

Order PLATYCOPIDA Sars, 1866

Suborder PLATYCOPINA Sars, 1866

Superfamily CAVELLINOIDEA Egorov, 1950

Family CAVELLINIDAE Egorov, 1950

Genus *Sulcella* Coryell & Sample, 1932

Sulcella sulcata Coryell & Sample, 1932

(Plate 4.4 G)

Sulcella sulcata: Coryell & Sample 1932: Plate XXVI (26), fig. 18. – Lethiers et al. 1989: Plate 2, figure 3. – Crasquin-Soleau et al. 2004: Plate 4, figures 5-7.

MATERIAL. – 3 complete carapaces.

OCCURRENCES. – Pennsylvanian East Mountain Shale, Texas, USA (Coryell & Sample, 1932). Uppermost Wordain (Murghabian), Marls of Merbah el Oussif, Jebel Tebaga, Tunisia, (Lethiers et al. 1989). Permian - Triassic boundary of the Çürük dag section, Taurus, Antalya Nappes, Turkey (Crasquin-Soleau et al. 2004). Khachik Formation (sample A. 151), Guadalupian, Ali-Bashi section, Iran (this study).

DIMENSIONS. – L= 97 – 98µm, H=38 – 40µm, H/L= 0.39 – 0.40.

DISCUSSION. – The carapace is small and subovate shape when viewed from the lateral. Anterior margin approximately 1.8 of the height of the carapace. The dorsal margin is slight convexity, while the anterior margin is a consistently rounded contour. The connection between the anterior margin and the dorsal margin follows a curved path. In the posterior, the margin becomes narrowly rounded, and the ventral margin is either straight or slightly convex. The carapace's surface is finely granulated (Coryell & Sample, 1932).

4.5. CONCLUSION

Utilizing the various extraction method for ostracods facilitated the recognition of 67 ostracod forms from over 240 samples obtained from the Khachik Formation in the Ali-Bashi section. I have methodically identified and categorized these 67 species, which belong to 15 genera. The application of the CH₂O₂ method produced results that allowed me to pinpoint the distinct characteristics of each species. These are: *Bairdia deducta deducta* (Zalanyi, 1974); *Bairdia hungarica* Zalanyi, 1974; *Bairdia* sp.; *Fabalitypris parva* Wang, 1978, *Fabalitypris* sp. 1; *Fabalitypris* sp. 2; *Fabalitypris* sp. 3; *Fabalitypris* sp. 4; *Hollinella* (*Hollinella*) *herrickana* (Girty 1909), *Hollinella* sp., *Sargentina transita* (Kozur 1985); and *Silenites* sp.

The utilization of the hot acetolysis method enabled me to identify the following species: *Acratia changxingensis* (Shi, 1987); *Acratia* sp.; *Bairdia deducta deducta* (Zalanyi, 1974); *Bairdia elcapitanensis* Forel 2021; *Bairdia* cf. *fangnianqiao* Crasquin, 2010; *Bairdia grotei* Chitnarin, 2017 *Bairdia hungarica* Zalanyi, 1974; *Bairdia khaokanaensis* Chitnarin, 2017; *Bairdia radlerae* Kellett, 1934; *Bairdia rhomboidalis* Hamilton, 1942; *Bairdia* cf. *songthami* Chitnarin et al. 2017; *Bairdia* sp.30 sensu Chitnarin, 2009; *Bairdia* sp. 1; *Bairdia* sp. 2; *Bairdia* sp. 3; *Bairdia* sp. 4; *Bairdia* sp. 5; *Bairdia* sp. 6; *Bairdia* sp. 7; *Bairdia* sp. 8; *Bairdia* sp. 9; *Bairdia* ? sp.; *Bairdiacypris longirobusta* Chen, 1958; *Bairdiacypris* sp. 6 sensu Zazzali et al., 2015; *Bairdiacypris* sp. B sensu Tarnac et al., 2021; *Bairdiacypris* sp. 1; *Bairdiacypris* sp. 2; *Bairdiacypris* sp. 3; *Bairdiacypris* sp. 4; *Bairdiacypris* sp. 5; *Bairdiacypris* sp. 6; *Bairdiacypris* sp. 7; *Bairdiacypris* sp. 8; *Bairdiacypris* sp. 9; *Bairdiacypris* sp.; *Ceratobairdia sexagintaduella* Forel, 2021; *Ceratobairdia*? cf. *crenata* Chen, 1982; *Fabalitypris acetalata* (Coryell & Billings, 1932); *Fabalitypris glennensis* (Harlton, 1927); *Fabalitypris parva* Wang, 1978; *Fabalitypris reniformis* (Chen, 1958) sensu Wang, 1978; *Fabalitypris* sp. 5; *Fabalitypris* sp. 6; *Fabalitypris* sp. 7; *Hollinella* (*Hollinella*) *martensiformis* Crasquin et al., 2010 ; *Hollinella* sp. ; *Indivisia* sp. 1 sensu Forel et al. 2015; *Kempfina qinglaili* (Crasquin, 2008); *Kempfina* sp. 1 ; *Liuzhinia julfensis* Gliwa, 2021; *Praezabythocypris pulchra* Kozur, 1985; *Praezabythocypris* sp. 1; *Pseudacanthoscapha striatula* (Shi, 1982); *Reviya* sp. A; *Sargentina minuta* Wang, 1978; *Sargentina* sp.; and *Sulcella sulcata* Coryell & Sample, 1932.

Meanwhile, some of the identified species of the *Bairdia*, *Bairdiacypris* and *Fabalitypris* genus present promising opportunities for defining new species through further studies.

Furthermore, the successful identification of a large volume of ostracod's species from Middle and Upper Permian sequences highlights the significant potential for exploring this fossil-group in Iran.

PLATE 4.1

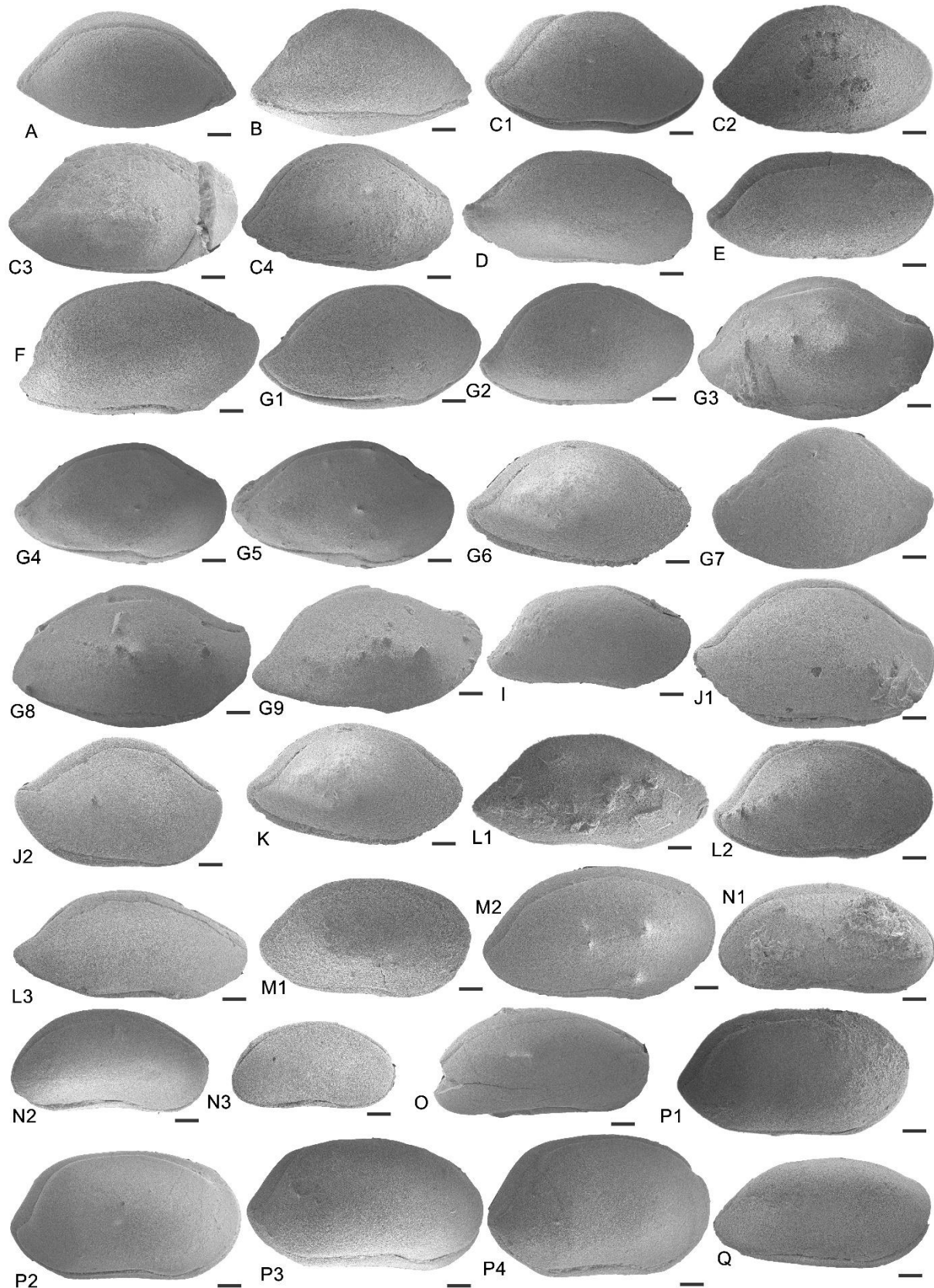


PLATE 4.1. SEM micrographs of ostracod from the Khachik Formation of Ali-Bashi section, NW Iran extracted by hot acetolysis preparation protocol. Scale bars: 100 µm. Specimens are stored in the MNHN (Muséum national d'Histoire naturelle) Paris France collections.

A. *Acratia changxingensis* (Shi, 1987). Right lateral view, sample A. 183, MNHN.F.F72039.

B. *Acratia* sp. Right lateral view, sample A. 188, MNHN.F.F72040.

C1-C4. *Bairdia deducta deducta* Zalanyi, 1974. C1: right lateral view, sample A. 152, MNHN.F.F72041; C2: right lateral view, sample A. 156, MNHN.F.F72042; C3: right lateral view, sample A. 244, MNHN.F.F72043; C4: right lateral view, sample A. 278, MNHN.F.F72044.

D. *Bairdia elcapitanensis* Forel in Trance et al. 2021. Right lateral view, sample A. 170, MNHN.F.F72045.

E. *Bairdia* cf. *fangnianqiao* Crasquin, 2010. Right lateral view, sample A. 132, MNHN.F.F72046.

F. *Bairdia grotei* Chitnarin et al. 2017. Right lateral view, sample A. 294, MNHN.F.F72047.

G1-G9. *Bairdia hungarica* Zalanyi, 1974. G1: right lateral view, sample A. 192, MNHN.F.F72048; G2: right lateral view, sample A. 192, MNHN.F.F72049; G3: right lateral view, sample A. 207, MNHN.F.F72050; G4: right lateral view, sample A. 210, MNHN.F.F72051; G5: right lateral view, sample A. 210, MNHN.F.F72052; G6: right lateral view, sample A. 279, MNHN.F.F72053; G7: left lateral view, sample A. 301, MNHN.F.F72054; G8: left lateral view, sample A. 322, MNHN.F.F72054; G9: right lateral view, sample A. 322, MNHN.F.F72055.

H. *Bairdia khaokanaensis* Chitnarin et al. 2017. Right lateral view, sample A. 294, MNHN.F.F72056.

I1-I2. *Bairdia radlerae* Kellett, 1934. I1: right lateral view, sample A. 203, MNHN.F.F72057; I2: right lateral view, sample A. 279, MNHN.F.F72058.

J. *Bairdia rhomboidalis* Hamilton, 1942. Right lateral view, sample A. 204, MNHN.F.F72059.

K1-K3. *Bairdia* Cf. *songthami* Chitnarin et al. 2017. J1: right lateral view, sample A. 111, MNHN.F.F72060; J2: right lateral view, sample A. 157, MNHN.F.F72061; J3: right lateral view, sample A. 204, MNHN.F.F72062.

L1-L2. *Bairdia* sp.30 *sensu* Chitnarin, 2009. L1: right lateral view, sample A. 327, MNHN.F.F72063; L2: right lateral view, sample A. 330, MNHN.F.F72064.

M1-M3. *Bairdia* sp. 1 M1: right lateral view, sample A. 202, MNHN.F.F72065; M2: right lateral view, sample A. 204, MNHN.F.F72066; M3: right lateral view, sample A. 207, MNHN.F.F72067

N. *Bairdia* sp. 2. Right lateral view, sample A. 301, MNHN.F.F72068.

O1-O4. *Bairdia* sp. 3. O1: right lateral view, sample A. 156, MNHN.F.F72069; O2: right lateral view, sample A. 167, MNHN.F.F72070; O3: right lateral view, sample A. 192, MNHN.F.F72071; O4: right lateral view, sample A. 192, MNHN.F.F72072.

P. *Bairdia* sp. 5. Right lateral view, sample A. 301, MNHN.F.F72073.

PLATE 4.2

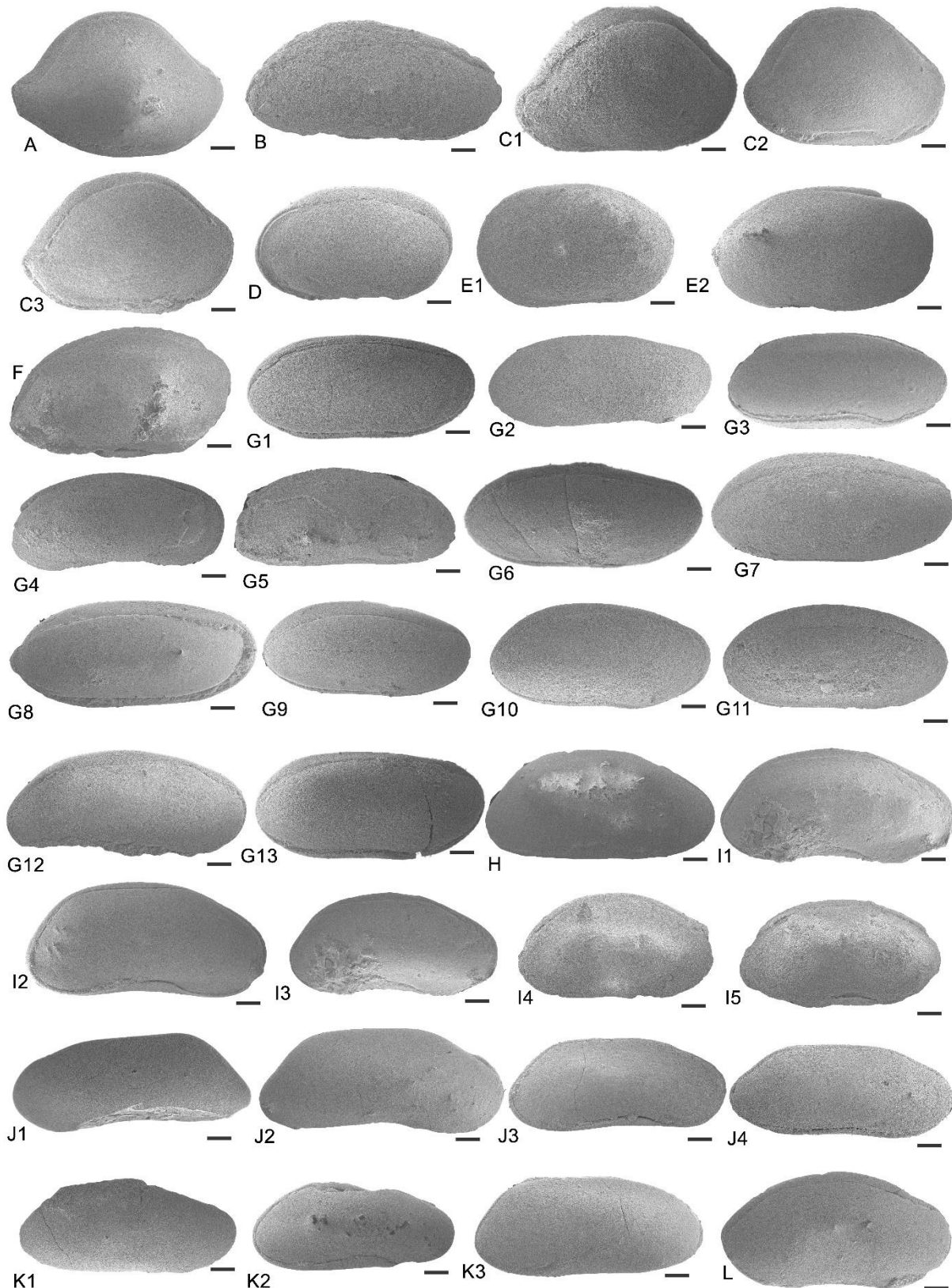


PLATE 4.2. SEM micrographs of ostracod from the Khachik Formation of Ali-Bashi section, NW Iran extracted by hot acetolysis preparation protocol. Scale bars: 100 μm . Specimens are stored in the MNHN (Muséum national d'Histoire naturelle) Paris France collections.

A. *Bairdia* sp. 5. Right lateral view, sample A. 204, MNHN.F.F72074.

B. *Bairdia* sp. 6. Right lateral view, sample A. 327, MNHN.F.F72075.

C1-C3. *Bairdia* sp. 7. C1: right lateral view, sample A. 118, MNHN.F.F72076; C2: right lateral view, sample A. 163, MNHN.F.F72077; C3: right lateral view, sample A. 192, MNHN.F.F72078.

D. *Bairdia* sp. 8. Right lateral view, sample A. 161, MNHN.F.F72079.

E1-E2. *Bairdia* sp. 9. E1: right lateral view, sample A. 192, MNHN.F.F72080; E2: right lateral view, sample A. 200, MNHN.F.F72081.

F. *Bairdia?* sp. Left lateral view, sample A. 330, MNHN.F.F72082.

G1-G13. *Bairdiacypris longirobusta* Chen, 1958. G1: right lateral view, sample A. 156, MNHN.F.F72083; G2: Right lateral view, sample A. 167, MNHN.F.F72084; G3: right lateral view, sample A. 287, MNHN.F.F72085; G4: Right lateral view, sample A. 290, MNHN.F.F72086; G5: left lateral view, sample A. 332, MNHN.F.F; G6: left lateral view, sample A. 191, MNHN.F.F72087; G7: left lateral view, sample A. 301, MNHN.F.F72088; G8: left lateral view, sample A. 157, MNHN.F.F72089; G9: left lateral view, sample A. 159, MNHN.F.F72090; G10: left lateral view, sample A. 159, MNHN.F.F72091; G11: right lateral view, sample A. 167, MNHN.F.F72092; G12: left lateral view, sample A. 192, MNHN.F.F72093; G13: left lateral view, sample A. 200, MNHN.F.F72094.

H. *Bairdiacypris* sp. 6 *sensu* Zazzali et al., 2015. Left lateral view, sample A. 330, MNHN.F.F72095.

I1-I5. *Bairdiacypris* sp. B *sensu* Tarnac et al., 2021. I1: left lateral view, sample A. 210, MNHN.F.F72096; I2: left lateral view, sample A. 210, MNHN.F.F72097; I3: left lateral view, sample A. 210, MNHN.F.F72098; I4: right lateral view, sample A. 322, MNHN.F.F72099; I5: right lateral view, sample A. 325, MNHN.F.F72100.

J1-J4. *Bairdiacypris* sp. 1. J1: left lateral view, sample A. 140, MNHN.F.F72101; J2: left lateral view, sample A. 152, MNHN.F.F72102; J3: right lateral view, sample A. 158, MNHN.F.F72103; J4: left lateral view, sample A. 188, MNHN.F.F72104.

K1.K3. *Bairdiacypris* sp. 2. K1: left lateral view, sample A. 157, MNHN.F.F72105; K2-K3: left lateral view, sample A. 159, MNHN.F.F72106.

L. *Bairdiacypris* sp.3. Left lateral view, sample A. 332, MNHN.F.F72107.

PLATE 4.3

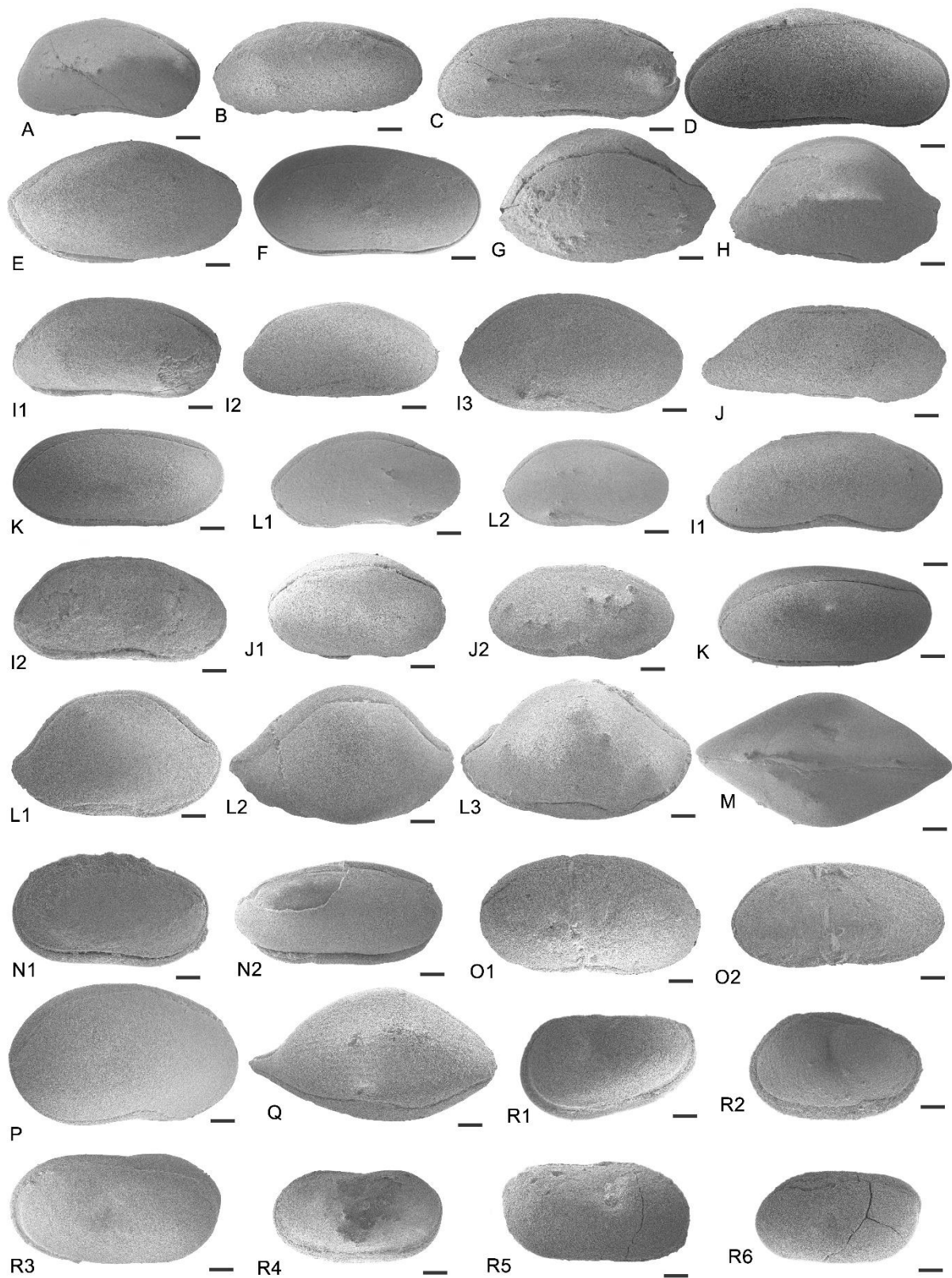


PLATE 4.3. SEM micrographs of ostracod from the Khachik Formation of Ali-Bashi section, NW Iran extracted by hot acetolysis preparation protocol. Scale bars: 100 μm . Specimens are stored in the MNHN (Muséum national d'Histoire naturelle) Paris France collections.

- A.** *Bairdiacypris* sp. 4. Left lateral view, sample A. 207, MNHN.F.F72108.
- B.** *Bairdiacypris* sp. 5. Left lateral view, sample A. 207, MNHN.F.F72109.
- C.** *Bairdiacypris* sp. 6. Left lateral view, sample A. 207, MNHN.F.F72110.
- D.** *Bairdiacypris* sp. 7. Right lateral view, sample A. 191, MNHN.F.F72111.
- E.** *Bairdiacypris* sp. 8. Right lateral view, sample A. 191, MNHN.F.F72112.
- F.** *Bairdiacypris* sp. 9. Right lateral view, sample A. 207, MNHN.F.F72113.
- G.** *Ceratobairdia sexagintaduella* Forel, 2021. Right lateral view, sample A. 207, MNHN.F.F72114.
- H.** *Ceratobairdia?* cf. *crenata* Chen, 1982. Left lateral view, sample A. 294, MNHN.F.F72115.
- I1-I3.** *Fabalitypris acetalata* (Coryell & Billings, 1932). I1: right lateral view, sample A. 202, MNHN.F.F72116; I2: right lateral view, sample A. 262, MNHN.F.F72117; I3: right lateral view, sample A. 329, MNHN.F.F72118.
- J.** *Fabalitypris glennensis* (Harlton, 1927). Right lateral view, sample A. 276, MNHN.F.F72119.
- K.** *Fabalitypris parva* Wang, 1978. Right lateral view, sample A. 151, MNHN.F.F2120.
- L1-L2.** *Fabalitypris reniformis* (Chen, 1958) *sensu* Wang, 1978. L1: right lateral view, sample A. 332, MNHN.F.F72121; L2: left lateral view, sample A. 332, MNHN.F.F72122.
- M1-M2.** *Fabalitypris* sp. 5. M1: left lateral view, sample A. 204, MNHN.F.F72123; M2: left lateral view, sample A. 210, MNHN.F.F72124.
- N1-N2.** *Fabalitypris* sp. 6. N1: right lateral view, sample A. 151, MNHN.F.F72125; N2: left lateral view, sample A. 210, MNHN.F.F72126.
- O.** *Fabalitypris* sp. 7. Right lateral view, sample A. 151, MNHN.F.F72127.
- P1-P3.** *Kempfina qinglaili* (Crasquin, 2008). P1: right lateral view, sample A. 167, MNHN.F.F72128; P2: right lateral view, sample A. 207, MNHN.F.F72129; P3: right lateral view, sample A. 284, MNHN.F.F72130.
- Q.** *Kempfina* sp. 1. Dorsal view, sample A. 200, MNHN.F.F72131.
- R1-R2.** *Liuzhinia julfensis* Gliwa et al. 2021. R1: right lateral view, sample A. 157, MNHN.F.F72132; R2: left lateral view, sample A. 161, MNHN.F.F72133.

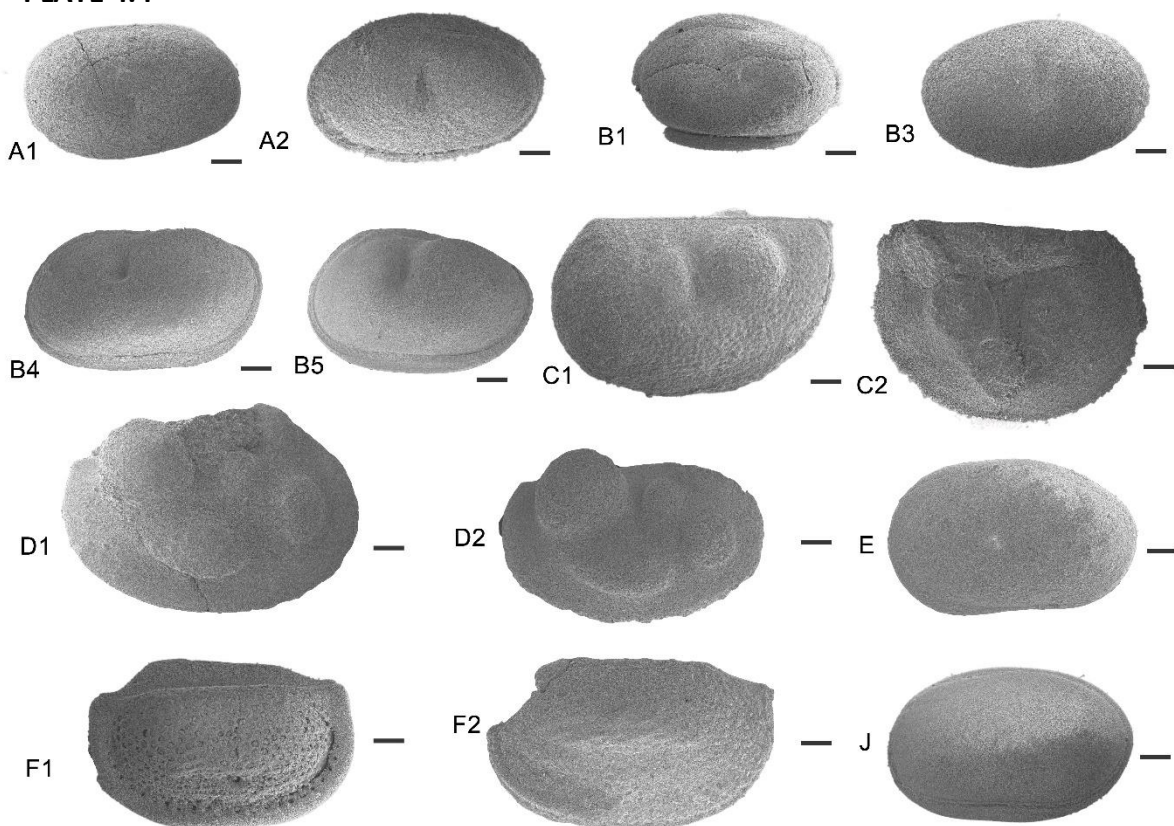
S1-S2. *Praezabythocypris pulchra* Kozur, 1985. S1: right lateral view, sample A. 207, MNHN.F.F72134; S2: left lateral view, sample A. 302, MNHN.F.F72135.

T. *Praezabythocypris* sp. 1. Right lateral view, sample A. 167, MNHN.F.F72136.

U. *Pseudacanthoscapha striatula* (Shi, 1982). Right lateral view, sample A. 274, MNHN.F.F72137.

V1-V5. *Sargentina minuta* Wang, 1978. V1: left lateral view, sample A. 144, MNHN.F.F72138; V2: left lateral view, sample A. 151, MNHN.F.F72139; V3: right lateral view, sample A. 153, MNHN.F.F72140; V4: right lateral view, sample A. 128, MNHN.F.F72141; V5: right lateral view, sample A. 207, MNHN.F.F72142.

PLATE 4.4



A1-A2. *Sargentina minuta* Wang, 1978. A1: Left lateral view, sample A. 168, MNHN.F.F.; A2: left lateral view, sample A. 192, MNHN.F.F72143

B1-B5. *Sargentina* sp. B1: right lateral view, sample A. 125, MNHN.F.F72144; B2: right lateral view, sample A. 154, MNHN.F.F72145; B3: right lateral view, sample A. 156, MNHN.F.F72146; B5: right lateral view, sample A. 191, MNHN.F.F72147; B5: right lateral view, sample A. 194, MNHN.F.F72148.

C1-C2. *Hollinella (Hollinella) martensiformis* Crasquin et al. 2010. I1: left lateral view, sample A. 153, MNHN.F.F72149; I2: right lateral view, sample A. 154, MNHN.F.F72150.

D1-D2. *Hollinella* sp. D1: left lateral view, sample A. 188, MNHN.F.F72151; D2: right lateral view, sample A. 194, MNHN.F.F72152.

E. *Indivisia* sp. 1 *sensu* Forel et al., 2015. Right lateral view, sample A. 200, MNHN.F.F72153.

F1-F2. *Reviya* sp. F1: Right lateral view, sample A. 156, MNHN.F.F72154; F2: lateral view, sample A. 244, MNHN.F.F72155.

G. *Sulcella sulcata* Coryell & Sample, 1932. Left lateral view, sample A. 151, MNHN.F.F72156

PLATE 4.5

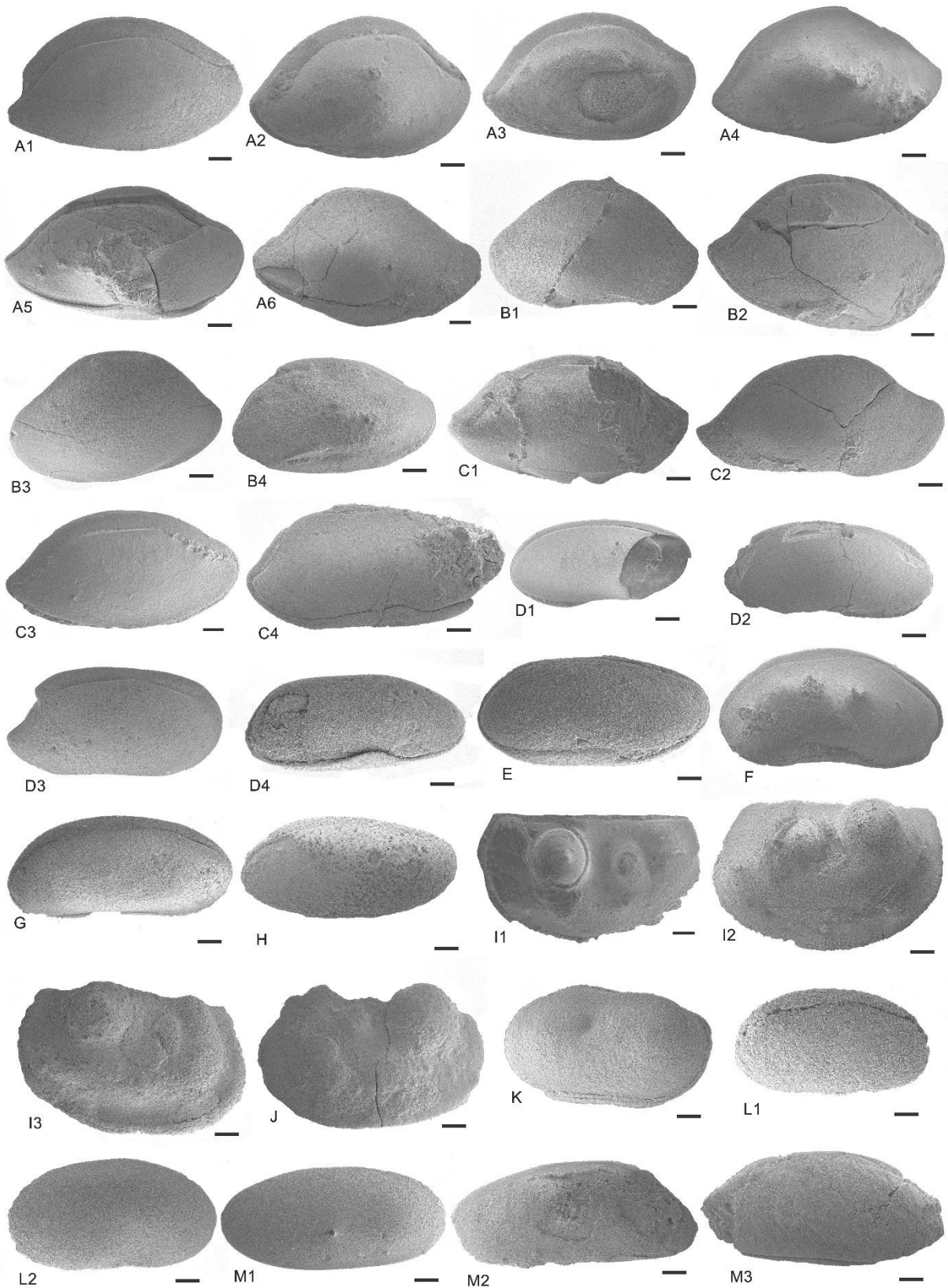


PLATE 4.5. SEM micrographs of ostracod from the Khachik Formation of Ali-Bashi section, NW Iran extracted by extracted by CH₂H₂ technique (**A1 - L2**) and by CH₃COOH technique (**M1 - M3**). Scale bars: 100 µm. Specimens are stored in the MNHN (Muséum national d'Histoire naturelle) Paris France collections.

A1-A6. *Bairdia deducta deducta* (Zalanyi, 1974). A1: right lateral view, sample A. 197, MNHN.F.F72157; A2 - A4: right lateral view, sample A. 210, MNHN.F.F7(2158-2160); A5: right lateral view, sample A. 189, MNHN.F.F72161; A6: right lateral view, sample A. 207, MNHN.F.F72162.

B1-B4. *Bairdia hungarica* Zalanyi, 1974. B1: left lateral view, sample A. 189, MNHN.F.F72163; B2: right lateral view, sample A. 189, MNHN.F.F72164; B3: left lateral view, sample A.170, MNHN.F.F72165; B4: right lateral view, sample A. 176, MNHN.F.F72166.

C1-C4. *Bairdia* sp. C1: left lateral view, sample A. 189, MNHN.F.F72167; C2: right lateral view, sample A. 189, MNHN.F.F72168; C3: left lateral view, sample A.170, MNHN.F.F72169; C4: right lateral view, sample A. 176, MNHN.F.F72170.

D1-D4. *Fabalitypris parva* Wang, 1978. D1: right lateral view, sample A. 194, MNHN.F.F72171; D2: right lateral view, sample A. 151, MNHN.F.F72172; D3: right lateral view, sample A. 192, MNHN.F.F72174; D4: right lateral view, sample A. 210 MNHN.F.F72176.

E. *Fabalitypris* sp. 1. Right lateral view, sample A. 207, MNHN.F.F72177.

F. *Fabalitypris* sp. 2. Right lateral view, sample A. 210, MNHN.F.F72178.

G: *Fabalitypris* sp. 3. Right lateral view, sample A. 158, MNHN.F.F72173

H: *Fabalitypris* sp. 4. Right lateral view, sample A. 210, MNHN.F.F72175

I1-I3. *Hollinella (Hollinella) herrickana* (Girty, 1909). G1:left lateral view, sample A. 15, MNHN.F.F72179; G2: left lateral view, sample A. 238, MNHN.F.F72180; G3: right lateral view, sample A. 238, MNHN.F.F72181.

J. *Hollinella* sp. left lateral view, sample A. 188, MNHN.F.F72182.

K. *Sargentina transita* (Kozur, 1985). Left lateral view, sample A. 176, MNHN.F.F72183.

L1-L2. *Silenites* sp. J1: right lateral view, sample A. 238, MNHN.F.F72184; J2: ventral view, sample A. 238, MNHN.F.F72185.

M1 – M3. Ostracods indet, MNHN.F.F7(2186-2188).

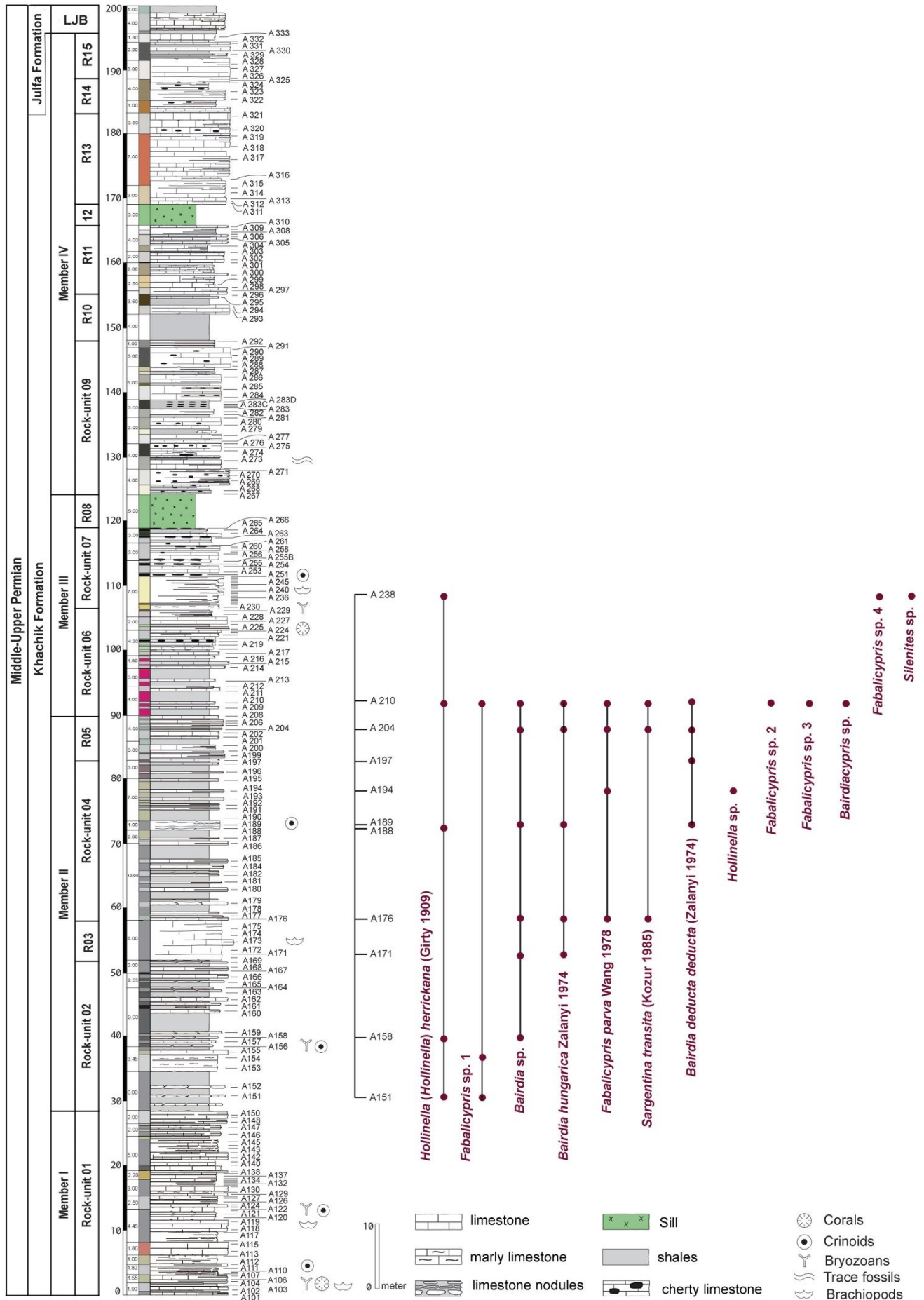


Fig. 4.5. Stratigraphic log and vertical distribution of ostracods (obtained from CH₂O₂ protocol) in the Khachik Formation from the Ali-Bashi section. The abbreviation of LJB is: lower Julfa Beds

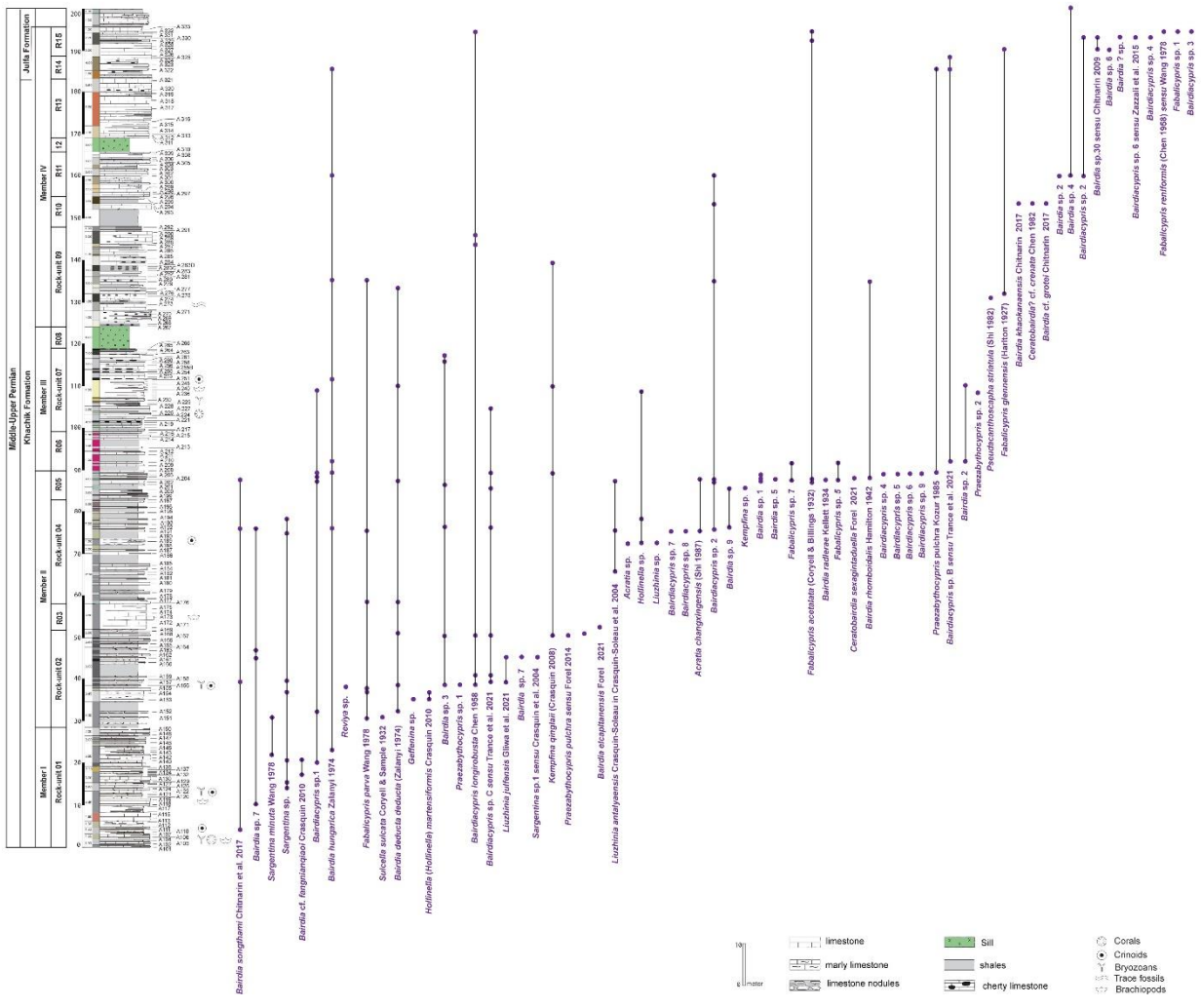


Fig. 4.6. Stratigraphic log and vertical distribution of ostracods (obtained from hot acetolysis protocol) in the Khachik Formation from the Ali-Bashi section.

4.7. REFERENCES

- Armstrong, W., and Brasier, M., 2005. *Microfossils*. (2nd ed.). Malden: Blackwell Pub.
- Bassler, R.S. and Kellett, B., 1934. *Bibliographic index of Paleozoic ostracoda* (Vol. 1). Geological Society of America.
- Belousova, Z.D., 1965. Evolution and succession of organisms at Paleozoic-Mesozoic boundary. *Trudy Paleontologicheskogo Instituta Akademii Nauk SSSR*, 108, pp.245-265.
- Bless, M.J.M. and Jordan, H., 1972. Ostracodes of the family Hollinellidae. *Meded. Rijks Geol. Dienst, Netherlands, Ser. C*.
- Bradfield, H.H., 1935. Pennsylvanian Ostracoda of the Ardmore Basin, Oklahoma. *Bulletins of American Paleontology*, 22, pp.1-173.
- Chen, d., & Shi, C., 1982. Latest Permian ostracoda from Nantong, Jiangsu and from Miannyang, Hubei. *Bulletin of Nanjing Institute of Geology and Palaeontology Academia Sinica* 4: pp. 105-152.
- Chen, T.C., 1958. Permian ostracods from the Chihsia limestone of Lungtan, Nanking. *Acta Palaeontologica Sinica*, 6, pp.215-257.
- Chitnarin, A., 2009. *Taxonomy of permian ostracods from central, northeastern, and western Thailand: implication for paleoenvironment and paleobiogeography* (Doctoral dissertation, School of Biology Institute of Science Suranaree University of Technology).
- Chitnarin, A., Crasquin, S., Charoentitirat, T., Tepnarong, P. and Thaneer, N., 2012. ostracods (Crustacea) of the early-Middle Permian from Central thailand (indochina block). Part i. order Palaeocopida. *Geodiversitas*, 34(4), pp.801-835.
- Chitnarin, A., Crasquin, S., Forel, M.B. and Tepnarong, P., 2017. Ostracods (Crustacea) of the Early-Middle Permian (Cisarulian-Guadalupean) from Central Thailand (Indochina Block): Part II, Orders Podocopida, Platycopida and Myodocopida. *Geodiversitas*, 39(4), pp.651-690. DOI: [10.5252/g2017n4a1](https://doi.org/10.5252/g2017n4a1)
- Cooper, C.L., 1946, Pennsylvanian ostracodes of Illinois. *Illinois State Geological Survey Bulletin* 70, pp. 1–177.
- Coryell, H.N. and Billings, G.D., 1932. Pennsylvanian Ostracoda of the Wayland shale of Texas. *American Midland Naturalist*, 13(4), pp.170-189.
- Coryell, H.N. and Booth, R.T., 1933. Pennsylvanian Ostracoda; a continuation of the study of the Ostracoda Fauna from the Wayland Shale, Graham, Texas. *American Midland Naturalist*, 14(3), pp.258-279.
- Coryell, H.N. and Johnson, S.C., 1939. Ostracoda of the Clore Limestone, Upper Mississippian, of Illinois. *Journal of Paleontology*, pp.214-224.

- Coryell, H.N. and Sample, C.H., 1932. Pennsylvanian Ostracoda. A study of the ostracoda fauna of the East Mountain shale, Mineral Wells formation, Mineral Wells, Texas. *American Midland Naturalist*, 13(5), pp.245-281.
- Coryell, H.N. and Sohn, I.G., 1938. Ostracoda from the Mauch Chunk (Mississippian) of West Virginia. *Journal of Paleontology*, pp.596-603.
- Coryell, H.N., 1928. Some new Pennsylvanian ostracoda. *Journal of Paleontology*, pp.87-94.
- Crasquin, S. and Forel, M.B., 2014. Ostracods (Crustacea) through Permian–Triassic events. *Earth-Science Reviews*, 137, pp.52-64.
- Crasquin, S., Forel, M.B., Qinglai, F., Aihua, Y., Baudin, F. and Collin, P.Y., 2010. Ostracods (Crustacea) through the Permian-Triassic boundary in South China: the Meishan stratotype (Zhejiang Province). *Journal of Systematic Palaeontology*, 8(3), pp.331-370.
- Crasquin, S., Perri, M.C., Nicora, A. and De Wever, P., 2008. Ostracods across the Permian-Triassic boundary in Western Tethys: the Bulla parastratotype (Southern Alps, Italy). *Rivista Italiana di Paleontologia e Stratigrafia*, 114(2).
- Crasquin-Soleau, S. and Baud, A., 1998. New Permian ostracods from Greece (Hydra Island). *Journal of Micropalaeontology*, 17(2), pp.131-152.
- Crasquin-Soleau, S. and Kershaw, S., 2005. Ostracod fauna from the Permian–Triassic boundary interval of South China (Huaying Mountains, eastern Sichuan Province): palaeoenvironmental significance. *Palaeogeography, Palaeoclimatology, Palaeoecology*, 217(1-2), pp.131-141.
- Crasquin-Soleau, S., Broutin, J., Roger, J., Platel, J.P., Al Hashmi, H., Angiolini, L., Baud, A., Bucher, H. and Marcoux, J., 1999. First Permian ostracode fauna from the Arabian plate (Khuff Formation, sultanate of Oman). *Micropaleontology*, pp.163-182.
- Crasquin-Soleau, S., Marcoux, J., Angiolini, L., Richoz, S., Nicora, A., Baud, A. and Bertho, Y., 2004. A new ostracode fauna from the Permian-Triassic boundary in Turkey (Taurus, Antalya Nappes). *Micropaleontology*, 50(3), pp.281-295. DOI: [10.2113/50.3.281](https://doi.org/10.2113/50.3.281)
- Crasquin-soleau, s., Vaslet, D. and Le Nindre, Y.M., 2005. Ostracods as markers of the Permian/Triassic boundary in the Khuff Formation of Saudi Arabia. *Palaeontology*, 48(4), pp.853-868. DOI: [10.1111/j.1475-4983.2005.00476.x](https://doi.org/10.1111/j.1475-4983.2005.00476.x)
- Egorov, V.G., 1950. Frasnian ostracods from Russian platform. I. Kloedenellitidae. *VNIGRI (All Russia Petroleum Research Exploration Institut)*, 175.
- Egorov, V.G., 1954. Ostracodes from the Frasnian of the Russian Platform; II–Bairdiidae, Hollinidae, Kirkbyidae. *VNIGRI (All Russia Petroleum Research Exploration Institut)*, Moscow, 133 pp. [in Russian]
- Forel, M.B. and Crasquin, S., 2011. In the aftermath of Permian-Triassic boundary mass-extinction: new ostracod (Crustacea) genus and species from South Tibet. *Geodiversitas*, 33(2), pp.247-263.

- Forel, M.B., 2012. Ostracods (Crustacea) associated with microbialites across the Permian-Triassic boundary in Dajiang (Guizhou Province, south China). *European Journal of Taxonomy*, (19). DOI: [10.5852/ejt.2012.19](https://doi.org/10.5852/ejt.2012.19).
- Forel, M.B., Crasquin, S., Hips, K., Kershaw, S., Collin, P.Y. and Haas, J., 2013. Biodiversity evolution through the Permian—Triassic boundary event: Ostracods from the Bükk Mountains, Hungary. *Acta Palaeontologica Polonica*, 58(1), pp.195-219.
- Forel, M.B., 2014. Heterochronic growth of ostracods (Crustacea) from microbial deposits in the aftermath of the end-Permian extinction. *Journal of Systematic Palaeontology*, 13(4), pp.315-349.
- Forel, M.B., Crasquin, S., Chitnarin, A., Angiolini, L. and Gaetani, M., 2015. Precocious sexual dimorphism and the Lilliput effect in Neo-Tethyan Ostracoda (Crustacea) through the Permian—Triassic boundary. *Palaeontology*, 58(3), pp.409-454.
- Geis, H.L., 1933. *Microcheilinella*, a new name for the ostracode genus *Microcheilus*. *Journal of Paleontology*, 7, p.112.
- Girty, G.H., 1909. [1908]. The Guadalupian Fauna. *US Geol. Sur. Prof. Pap.*, 58, p.627.
- Gliwa, J., Forel, M.B., Crasquin, S., Ghaderi, A. and Korn, D., 2021. Ostracods from the end-Permian mass extinction in the Aras Valley section (north-west Iran). *Papers in Palaeontology*, 7(2), pp.1003-1042. DOI: [10.1002/spp2.1330](https://doi.org/10.1002/spp2.1330)
- Gründel, J. and Zeissler, H., 1962. *Zur Taxionomie der Ostracoden der Gattendorfia-Stufe Thüringens*. Akad.-Verlag.
- Hamilton, B., 1942. Ostracodes from the Upper Permian of Texas. *Journal of Paleontology* 16 (6): pp. 712–718.
- Harlton, B.H., 1927. Some Pennsylvanian Ostracoda of the Glenn and Hoxbar Formations of Southern Oklahoma and of the upper part of the Cisco Formation of Northern Texas. *Journal of Paleontology* 1, pp. 203–212.
- Henningsmoen, G., 1953. Classification of Paleozoic straight hinged Ostracoda. *Norsk Geologisk Tidsskrift*, 31, pp.185-288.
- Honigstein, A., Rosenfeld, A. and Derin, B., 2005. Late Permian ostracodes: new subsurface material from Israel. *Micropaleontology*, 51(5), pp.405-422.
- Horne, D.J., 2003. Key events in the ecological radiation of the Ostracoda. *The Paleontological Society Papers*, 9, pp.181-202.
- Horne, D.J., 2005. Homology and homoeomorphy in ostracod limbs. *Hydrobiologia*, 538(1-3), pp.55-80.
- Horne, D.J., Cohen, A. and Martens, K., 2002. Taxonomy, morphology and biology of Quaternary and living Ostracoda. *Washington DC American Geophysical Union Geophysical Monograph Series*, 131, pp.5-36.

- Ikeya, N., Tsukagoshi, A. and Horne, D.J., 2005. Preface: The phylogeny, fossil record and ecological diversity of ostracod crustaceans. *Hydrobiologia*, 538, pp.vii-xiii.
- Jain, S., 2020. *Fundamentals of Invertebrate Palaeontology*. Springer India.
- Kellett, B., 1929. The ostracode genus *Hollinella*, expansion of the genus and description of some Carboniferous species. *Journal of Paleontology*, pp.196-217.
- Kellett, B., 1934. Ostracodes from the Upper Pennsylvanian and the Lower Permian strata of Kansas: II. The genus *Bairdia*. *Journal of Paleontology*, pp.120-138.
- Kellett, B., 1935. Ostracodes of the Upper Pennsylvanian and the Lower Permian strata of Kansas: III. Bairdiidae (concluded), Cytherellidae, Cypridinidae, Entomoconchidae, Cytheridae and Cypridae. *Journal of Paleontology*, pp.132-166.
- Kempf, E.K., 1996. Index and Bibliography of Marine Ostracoda, vols. 1-9. *Geologisches Institut der Universität Koeln, Sonderveröffentlichungen (2002, 2004, 2008, CD version)*, pp.50-53.
- Kempf, E.K., 1997. Index and bibliography of non-marine Ostracoda, vols. 1–6. *Geologisches Institut der Universität zu Koeln, Sonderveröffentlichungen (2001, 2006, CD version)*, pp. 35–38, 77, 109–112.
- Kozur, H., 1985a. Biostratigraphic evaluation of the Upper Paleozoic conodonts, ostracods and holothurian sclerites of the Bükk Mts. Part II: Upper Paleozoic ostracods. *Acta Geologica Hungarica*, 28(3-4), pp.225-256.
- Kozur, H., 1985b. *Neue Ostracoden-Arten aus dem oberen Mittelkarbon (höheres Moskovian), Mittel-und Oberperm des Bükk-Gebirges (N-Ungarn)*. Institut für Geologie und Paläontologie.
- Kozur, H., 1991. Permian deep-water ostracods from Sicily (Italy). Part 1: taxonomy. *Geologisch-Paläontologische Mitteilungen Innsbruck*, 3, pp.1-24.
- Kozur, H., 1993. Relation between Late Paleozoic-Triassic Kirkbyacea and Cretaceous-Recent Punciacea (Ostracoda). In *International symposium on ostracoda*. 11 (pp. 91-106).
- Kozur, H.W. and Mette, W., 2006. *Iranokirkbya brandneri* n. gen. n. sp., a new kirkbyid ostracod from the Late Permian (Dorashamian) of Zal, NW Iran. *Geo. Alp*, 3, pp.85-91.
- Latreille, P.A., 1802. *Histoire naturelle générale et particulière des crustacés et des insectes: ouvrage faisant suite aux Oeuvres de Leclerc de Buffon, et partie du Cours complet d'histoire naturelle rédigé par CS Sonnini* (Vol. 73). de l.
- Lethiers, F., S. Razgallah, J. P. Colin, and D. Vachard. "Micropalaeontology of the Permian Marls of Merbah el Oussif (Jebel Tebaga, Tunisia) with special emphasis on the Ostracods." *Journal of Micropalaeontology* 8, no. 2 (1989): 227-238. DOI: [10.1144/jm.8.2.227](https://doi.org/10.1144/jm.8.2.227)
- Maddocks, R.F., 1969. Revision of Recent Bairdiidae (Ostracoda). *Bulletin of the United States National Museum*.

- Martens, K. and Schon, I., 2008. Ancient asexuals: darwinulids not exposed. *Nature*, 453(7195), pp.587-587.
- Martens, K., Schön, I., Meisch, C. and Horne, D.J., 2008. Global diversity of ostracods (Ostracoda, Crustacea) in freshwater. *Freshwater animal diversity assessment*, pp.185-193.
- McCoy, F., 1844. A Synopsis of the characters of the Carboniferous limestone fossils of Ireland. *University Press, Dublin* 207.
- Mette, W., 2008. Upper Permian and lowermost Triassic stratigraphy, facies and ostracods in NW Iran-implications for the P/T extinction event. *Stratigraphy*, 5(2), pp.205-219.
- Mette, W., 2010. Ostracods from the Upper Permian and Permian/Triassic boundary interval of Northwest Iran. *Revista española de micropaleontología*, 42(1), pp.11-35.
- Moore, R.C., (Ed.). 1961. *Treatise on Invertebrate Paleontology, Part Q, Arthropoda 3* (PP. 74–92). Boulder Colorado and Lawrence, Kansas: Geological Society of America and University of Kansas Press.
- Rodriguez-Lazaro, J. and Ruiz-Munoz, F., 2012. A general introduction to ostracods: morphology, distribution, fossil record and applications. In *Developments in Quaternary Sciences* (Vol. 17, pp. 1-14). Elsevier.
- Salas, M.J., Vannier, J. and Williams, M., 2007. Early Ordovician ostracods from Argentina: their bearing on the origin of binodicope and palaeocope clades. *Journal of Paleontology*, 81(6), pp.1384-1395.
- Sars, G.O., 1866. Oversigt af Norges marine ostracoder. *Det Norske Videnskaps-Akademi Forhandlingar*, pp.1-130.
- Sars, G.O., 1866. Oversigt af Norges marine Ostracoder. *Forhandlingar i Videnskabs-Selskabet i Christiania*. 1865 (1). pp.1-130.
- Sars, G.O., 1888. Nye bidrag til kundskaben om Middelhavets invertebratfauna. 4. Ostracoda mediterranea. *Archiv for Mathematik og Naturvidenskab*. 12, pp.173–324. DOI: [10.5962/bhl.title.10252](https://doi.org/10.5962/bhl.title.10252)
- Schallreuter, R., 1968. Zur taxonomie und phylogenie der Eridostraca (Ostracoda). *Paläontologische Zeitschrift*, 42, pp.105-119.
- Scott, H.W., 1959. Type species of Paraparchites Ulrich & Bassler. *Journal of Paleontology*, pp.670-674.
- Scott, H.W., 1961. Shell morphology of Ostracoda. *Arthropoda 3*: 21-37.
- Shaver, R., 1961. "Family Bairdiocyprididae, Q364–Q367." *Treatise on Invertebrate Paleontology. Part Q. Arthropoda 3*.
- Shi, C.G., & Chen, D.Q., 1987. The Changhsingian ostracodes from Meishan, Chanxing, Zhejiang. *Stratigraphy and palaeontology of Systemic boundary in China, Permian and Triassic Boundary 5*: pp. 23-80.

- Shi, C.G., & Chen, D.Q., 2002. Late Permian ostracodes from Heshan and Yishan of Guangxi. *Bulletin of Nanjing Institute Geology and Paleontology, Academia Sinica* 15: pp. 47-129 (in Chinese with English abstract).
- Siveter, D.J., Sutton, M.D., Briggs, D.E. and Siveter, D.J., 2003. An ostracode crustacean with soft parts from the Lower Silurian. *Science*, 302(5651), pp.1749-1751.
- Sohn, I.G., 1954. Ostracoda from the Permian of the Glass Mountains, Texas. *United States Geological Survey Professional Paper* 264-A: 1–24. DOI: 10.3133/pp264a
- Sohn, I.G., 1960. Paleozoic species of *Bairdia* and related genera. *United States Geological Survey Professional Paper* 330-A: 1–105. DOI: 10.3133/pp330a
- Sohn, I.G., 1971. *New Late Mississippian ostracode genera and species from northern Alaska; a revision of the Paraparchitacea* (No. 711-A).
- Swartz, F.M., 1936. Revision of the Primitiidae and Beyrichiidae, with new Ostracoda from the Lower Devonian of Pennsylvania. *Journal of Paleontology*, pp.541-586.
- Tarnac, A., Forel, M.B., Nestell, G., Nestell, M. and Crasquin, S., 2021. Middle Permian ostracods (Crustacea) from the Guadalupe Mountains, West Texas, USA. *European Journal of Taxonomy*, 770, pp.1-60. DOI: [10.5852/ejt.2021.770](https://doi.org/10.5852/ejt.2021.770)
- Ulrich, E.O. and Bassler, R.S., 1906. New American Paleozoic Ostracoda. Notes and descriptions of Upper Carboniferous genera and species. *Proceedings of the United States National Museum*.
- Ulrich, E.O. and Bassler, R.S., 1908. New American Paleozoic Ostracoda. Preliminary revision of the Beyrichiidae, with descriptions of new genera. *Proceedings of the United States National Museum*.
- Wang, S., 1978. Late Permian and Early Triassic ostracods of Western Guizhou and Northeastern Yunnan. *Acta Palaeontologica Sinica* 17: pp. 277-308.
- Williams, M., Siveter, D.J., Salas, M.J., Vannier, J., Popov, L.E. and Ghobadi Pour, M., 2008. The earliest ostracods: the geological evidence. *Senckenbergiana lethaea*, 88, pp.11-21.
- Zalányi, B., 1974. Die oberpermischen ostracoden des Bükkgebirges, in sidÓ m. zAlányi b. & schréter z. (eds), Neue paläontologische Ergebnisse aus dem Oberpaläozoikum des Bükk-Gebirgrs. *Akadémiai Kiado Budapest*: pp. 95-251.
- Zheng, S., 1976. Early Mesozoic ostracods from some localities in South West China. *Acta Palaeontologica Sinica*, 15(1), pp.77-93.

CHAPTER 5

Microfacies and palaeoenvironmental analysis

5.1. INTRODUCTION.....	148
5.2. CARBONATE MICROFACIES OF KHCHIK FORMATION	153
5.2.1. INNER RAMP MICROFACIES ASSEMBLAGES	153
5.2.1.1. LAGOON MICROFACIES	155
5.2.1.2. RESTRICTED MICROFACIES	160
5.2.1.3. OPEN-MARINE MICROFACIES	167
5.2.2. MIDDLE RAMP MICROFACIES ASSEMBLAGES.....	173
5.2.3. OUTER RAMP MICROFACIES ASSEMBLAGES	178
5.3. DEPOSITIONAL MODEL OF KHCHIK FORMATION	186
5.4. CONCLUSION	188
5.5. REFERENCES.....	189

5.1. INTRODUCTION

Facies analysis stands as a fundamental technique for sedimentological investigations globally, and this approach has been applied within the scope of this study. Process-based facies analysis within a sedimentary sequence heavily relies on identifying a litho-unit's unique physical, chemical, and biological characteristics, distinguishing it from neighboring litho-units (Sarwary et al. 2022). The recognition and examination of alterations in facies, along with their perpendicular and parallel dispersions, play a crucial role in discerning the sedimentary settings of carbonate formations. The configuration of facies groupings can act as a pointer to nuanced and substantial shifts in environmental structures. Climatic conditions impact these fluctuations, the intensity of water currents, and changes in the relative sea level (Bachmann & Hersch 2006).

During the evaluation of the sedimentary environment of the Khachik Formation in the Ali-Bashi section, I used the petrographic analysis and classification of carbonate rocks of Dunham (1962) and Embry & Klovan (1971) (fig. 5.1).

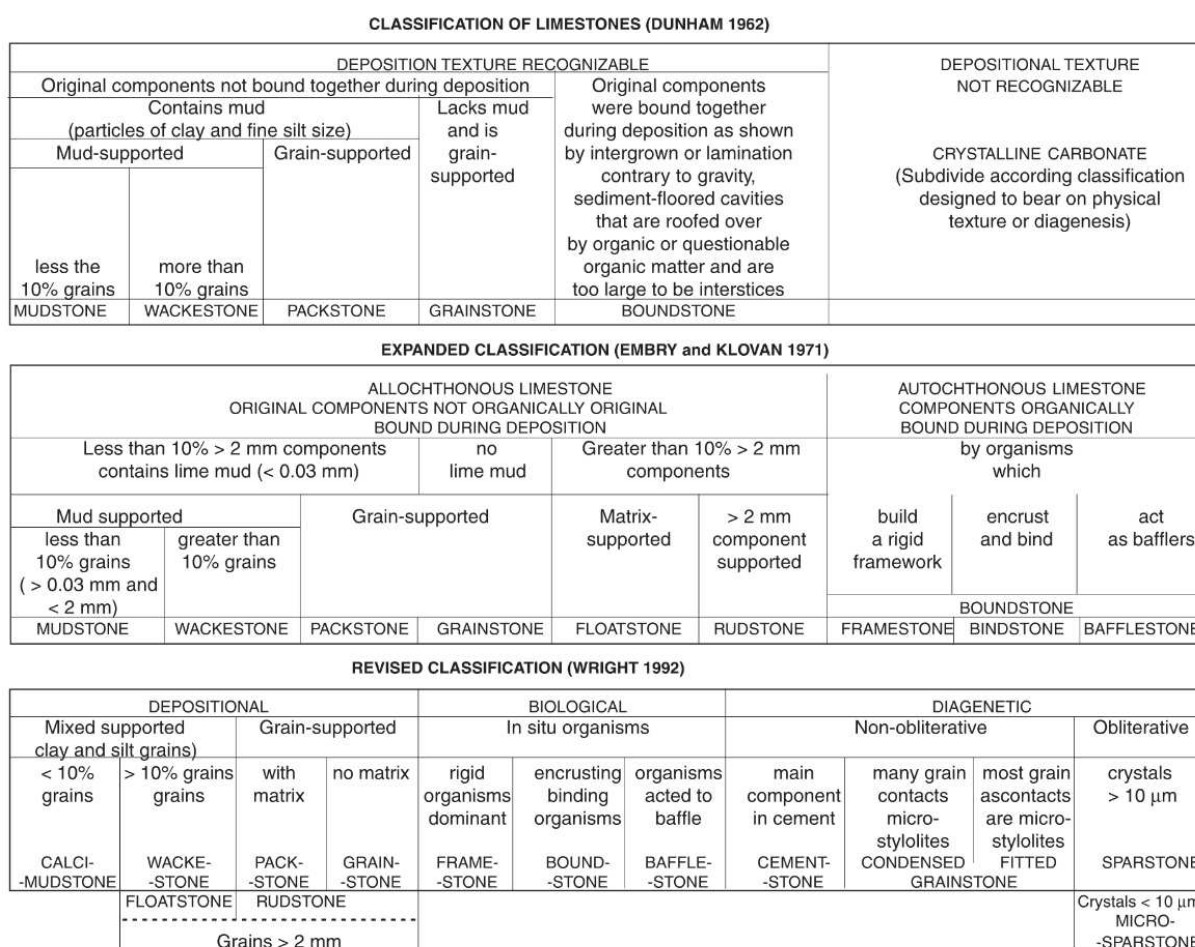


Fig. 5.1. Illustration of three significant classifications for the nomenclature of carbonate rocks from top to bottom: by Dunham (1962), by Klovan & Embry (1971) and by Wright (1992).

The identified microfacies have been compared with the conventional Standard Microfacies Types (SMF) and Ramp Microfacies Types (RMF) patterns, as evidenced by previous works (e.g., [Wilson 1975](#); [Wright 1992](#); [Flügel 2010](#)).

In [figures 5.2 and 5.3](#), the microfacies types depicted are presented and evaluations of the depositional environment of the carbonate facies have been done primarily based on their petrographic attributes ([Flügel 2010](#)). Furthermore, the application of [Wilson \(1975\)](#) standard facies belt model has aided in proposing a comprehensive depositional environment ([fig. 5.4](#)).

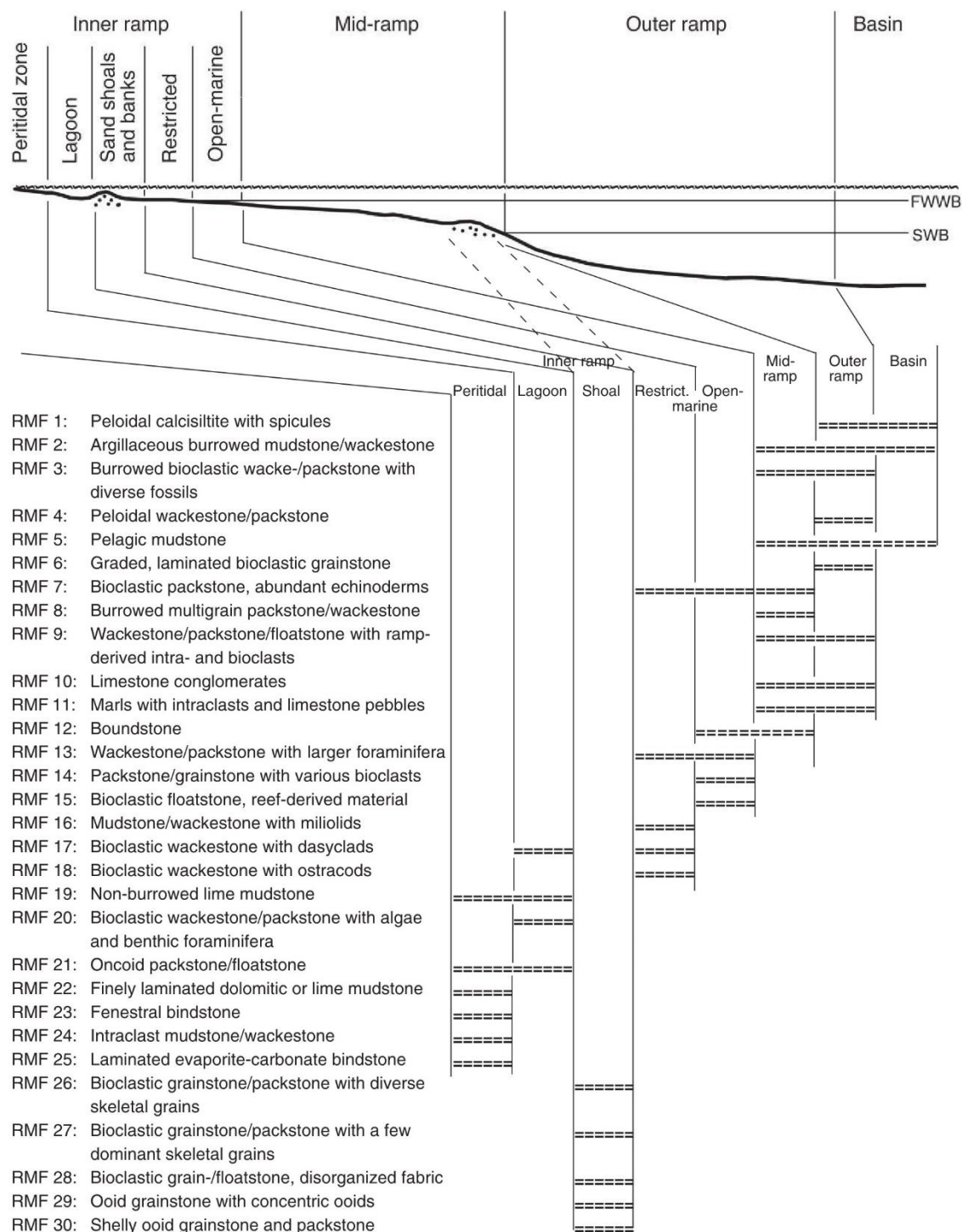


Fig. 5.2. General distribution of microfacies types on carbonate ramp ([Flügel 2010](#)).

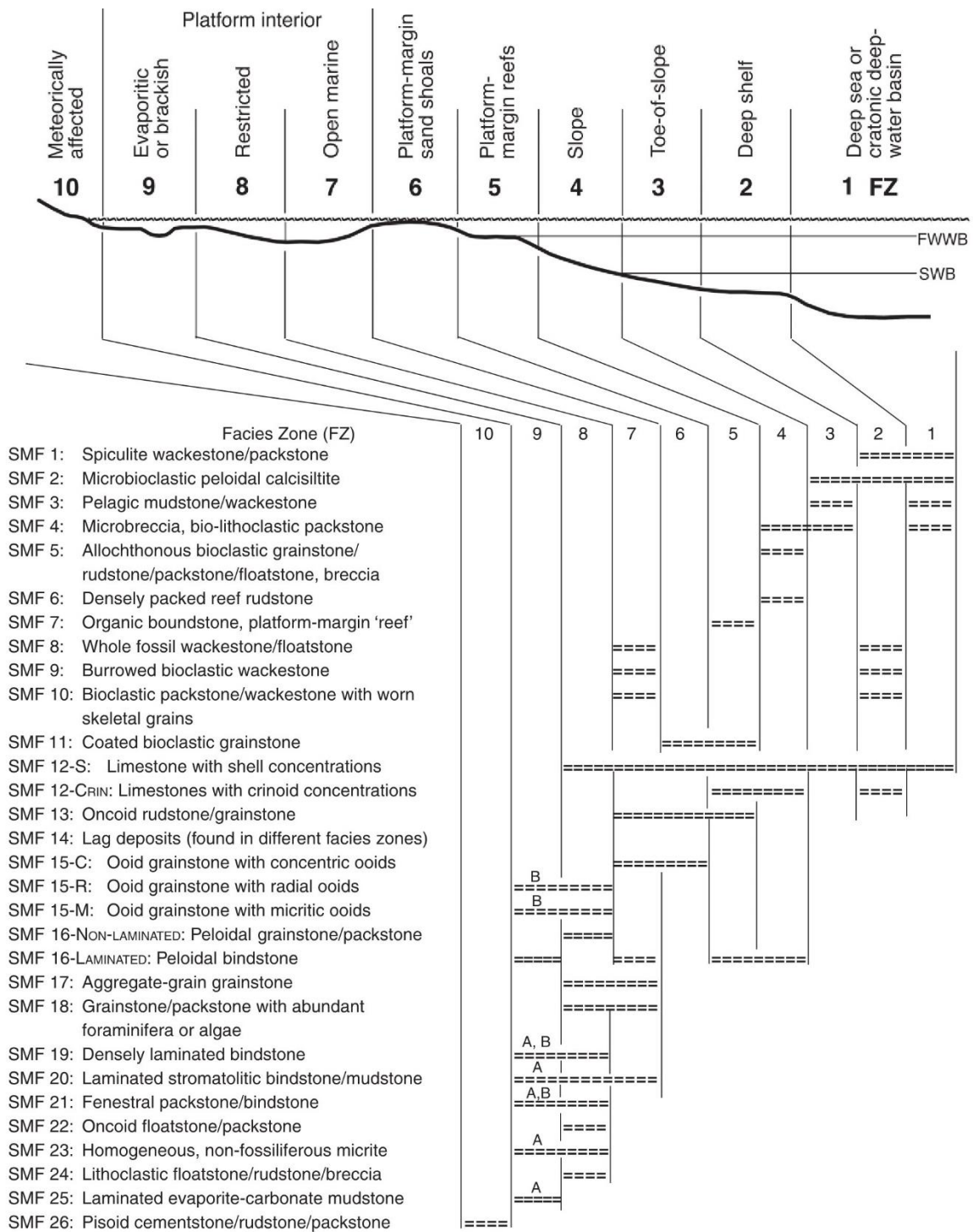


Fig. 5.3. SMF types Distribution across Facies Zones (FZ) in the Rimmed Carbonate Platform Model (Flügel 2010).

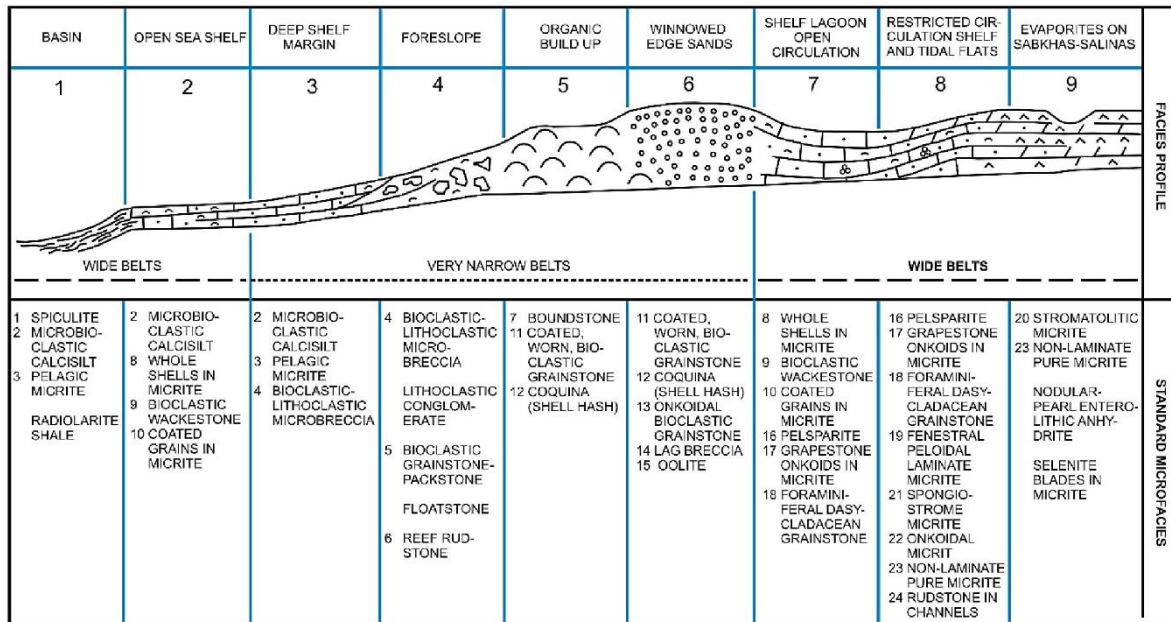


Fig. 5.4. Representation of Wilson's (1975) FZs (Facies Belts) and the corresponding SMF types (Mattern 2022).

The Khachik Formation strata in the Ali-Bashi section comprise a range of skeletal constituents, including bivalves, benthic foraminifers, brachiopods, bryozoans, calcareous algae, crinoid fragments, gastropods, ostracods, trilobite fragments, and bioturbation traces. Additionally, the recognized non-skeletal components encompass peloids and rarely intraclast in the upper part of the section, as illustrated in fig. 5.5.

The abbreviations employed for the allochems in the microfacies plates descriptions are as follows: Bi: bivalves, Fr: benthic foraminifers, Ba: brachiopod, Br: bryozoans, Ca: calcareous algae, Cr: crinoid fragments, Ga: gastropods, Os: ostracod, Tr: trilobite fragments, Bt: bioturbation traces, Pl: peloids.

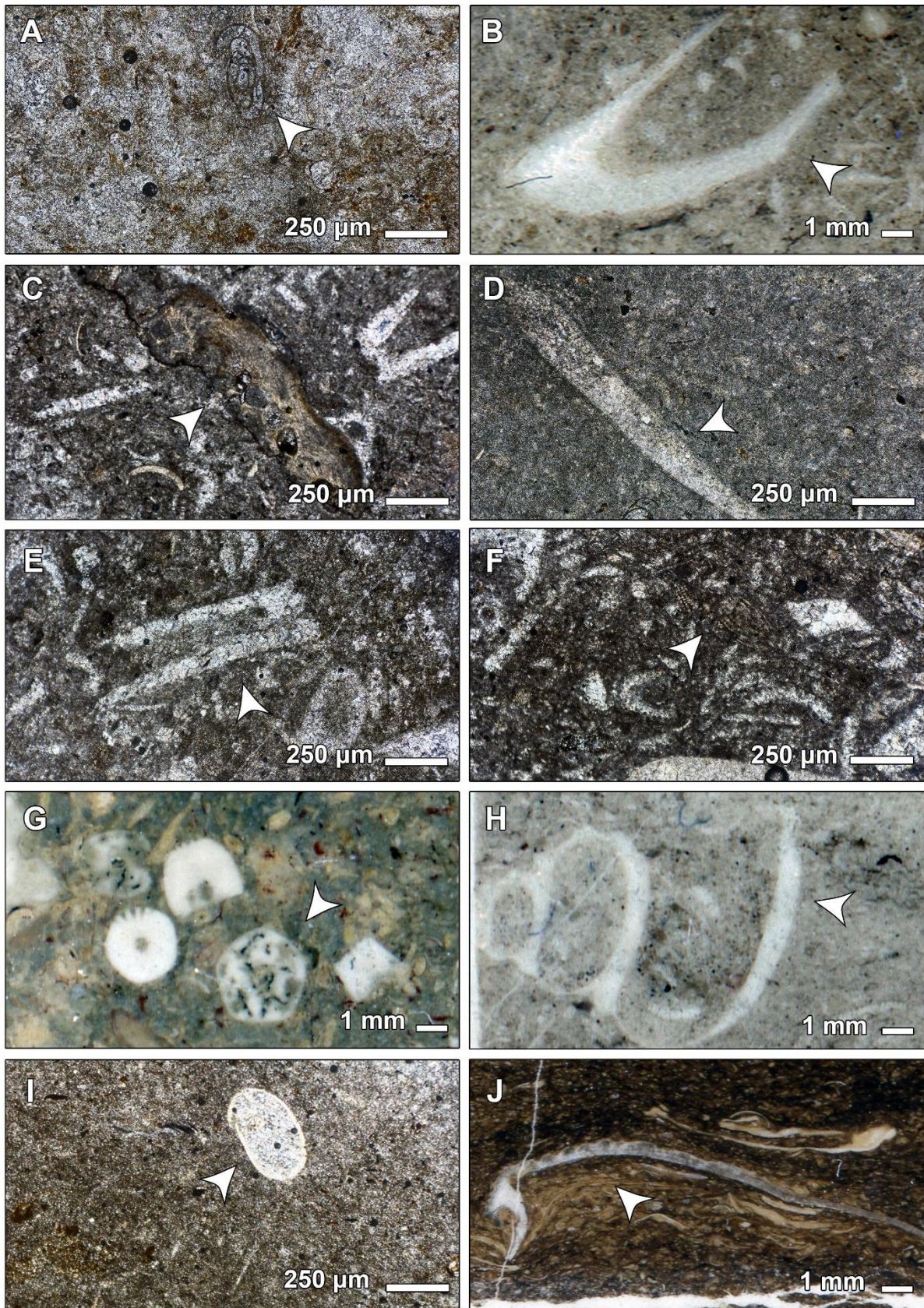


Fig. 5.5. Illustration of identified skeletal allochems (marked by the white arrows): A. Transverse section of benthic foraminifer, Transverse section of trilobite fragment, B. Oblique section of bivalve shell, C. bryozoan fragment, D. Longitudinal-oblique section of brachiopods shell, E and F. longitudinal and oblique sections of calcareous algae, G. Transverse section of crinoid, H. Longitudinal section of the gastropod, I. Longitudinal section of the ostracod, J. Longitudinal section of trilobite fragment.

5.2. CARBONATE MICROFACIES OF KHCHIK FORMATION

Analysis of carbonate rock microfacies of Khachik formation at the Ali-Bashi section led to the identification of 28 sub-microfacies that can be attributed to the 15 microfacies found in the [Flügel \(2010\)](#) ramp zones. These were further categorized into three main segments: the inner ramp, with sub-parts such as lagoon, restricted, and open-marine; the middle ramp; and finally, the outer ramp. Each microfacies (under the designation "MK" = Microfacies of Khachik Formation) has been classified according to [Embry & Klovan \(1971\)](#) classification.

To distinguish the facies categories, their first English initials have been utilized. Based on the standard microfacies introduced by [Flügel \(2010\)](#), ten microfacies of the RMF type and their equivalent 4 SMFs have been proposed for the studied strata. By the standard facies zones (FZ) presented by [Wilson \(1975\)](#), three FZs with a shallowing-upward trend, namely FZ8, FZ7, and FZ3, have been identified. Based on these explanations, the identified microfacies from the Ali-Bashi section from the coastal regions to the marine areas are described below ([table 5.1](#)).

5.2.1. INNER RAMP MICROFACIES ASSEMBLAGES

The sediments in the inner ramp are arranged in thin sequences with distinct layers of limestones and dolomites. Marls play a minor role in this area. The inner ramp encompasses a variety of environments, including open-marine areas with high water circulation, sheltered regions with restricted water movement, sandy shoals and banks characterized by oolitic and bioclastic grainstones and packstones, lagoons situated behind shoals or islands, and peritidal zones. The back-ramp environments are distinct from other parts of the inner ramp. Bioclastic packstones and wackestones are common texture types in open and protected inner ramp areas ([Flügel 2010](#)).

Table 5.1. The recognized microfacies within the Khachik Formation in the Ali-Bashi section

Ramp Zones		Microfacies		Plates	RMF	SMF	Facies Zones (Wilson 1975)		
		This study						(Flugel 2010)	
Inner ramp	Lagoon	MKL1		Pl. 5.1	A	19	23	8	
		MKL2	MKL2		B	20	18		
			MKL2-FORAM		C		18-FOR		
			MKL2-GYMNO		D		18-GYMNO		
	Restricted	MKR1	MKR1		Pl. 5.2	A	17	18	8,7
			MKR1-GYMNO			B		18-GYMNO	
			MKR1-DOIOM			C			
			MKR1-FUSUL			D			
			MKR1-MILIO			E		13	
		MKR2		Pl. 5.3	A	17	18-GYMNO		
		MKR3	MKR3		B	16	18-For		
			MKR3-BIOCL		C				
	MKR3-FUSUL		D						
	Open-marine	MKO1	MKO1		Pl. 5.4	A	14	10	7
			MKO1-BIOCL			B			
			MKO1-PEL/BIO			C			
		MKO2		D		18-GYMNO			
		MKO3	MKO3	E				7	
			MKO3-CRINO	F					
		MKO4	MKO4	G					
MKO4-CRINO			H						
Middle ramp	MKM1	MKM1		Pl. 5.5	A	3	8	7	
		MKM1-BIOCL			B				
		MKM1-PEL/BIO			C				
	MKM2	MKM2			D				9
		MKM2-BRACH			E				
	MKM3		F						
Outer ramp	MKT1	MKT1		Pl. 5.6	A	2	3	3	
		MKT1-BIOTU			B				
	MKT2		C						

	MKT2	MKT2-BIOCL		D			
		MKT2-FLOTS		E			
	MKT3			F			

5.2.1.1. LAGOON MICROFACIES

According to the studies, two distinct microfacies types have been identified with this specific environment's ramp zone.

5.2.1.1.1. MKL1: NON-FOSSILIFEROUS MUDSTONE

The MKL1 identified from various sections of the rock units: the upper parts of rock unit 1 (samples no. A. 144-147) and rock unit 2 (A.192); the lower part of rock unit 7 (samples no. A. 230, A. 234, A. 239, A. 241, and A. 246-247); the transition from the end of rock unit 7 to the beginning of rock-unit 9 (samples no. A. 264-268); the lower segment of rock-unit 13 (samples no. A. 313-314); and the middle part of rock-unit 15 (samples no. A. 327-328).

Also, in the field observation, the alternating thin-bedded limestones with shales, marly and nodular limestones stand out as the primary lithological feature linked to this microfacies. This particular microfacies lacks any skeletal allochems and traces of bioturbation and in the thin sections, non-skeletal elements are not present within the micritic texture (plate 5.1 A). The MKL1 microfacies corresponds with RMF19 and SMF23, as [Flugel \(2010\)](#) outlined, demonstrating the carbonate sequence sedimentation in the early sections of the inner ramp zone (lagoon). This aligns with the standard FZ8 as proposed by [Wilson \(1975\)](#).

5.2.1.1.1.1. INTERPRETATION OF MKL1

The microfacies were deposited in a shallow, inner ramp setting, with a notable absence of fossils indicating supratidal conditions within this inner ramp environment. Mudstones, clayey limestones, and shales probably settled in a low-energy setting, showing a characteristic environment of calm, sheltered brackish lagoons, as [Hips & Haas \(2009\)](#) and [Flugel \(2010\)](#) indicated.

5.2.1.1.2. MKL2

Generally, MKL2 represents a packstone microfacies; however, in some samples, the diverse content of allochems has identified three sub-microfacies.

5.2.1.1.2.1. MKL2: BIOCLASTIC PACKSTONE

The MKL2 has been identified in various sections of the rock units, including the following: the initial segments of rock unit 3 (samples no. A. 169-170); the middle part of rock unit 6 (samples no. A. 215, A. 217); the lower part (sample no. A. 236) and the terminus of rock-unit 7 (sample no. A. 262); the lower segment of rock-unit 13 (samples no. A. 313-314); the upper part of rock-unit 10 (sample no. A. 295); and the upper part of rock-unit 15 (samples no. A. 326 and A. 330). Additionally, in terms of field characteristics, medium-bedded limestone, alternating thin-bedded limestone with shale, and thin to medium-bedded limestone are the prominent lithological features associated with this microfacies.

With its abundance of skeletal allochems associated with packstone facies, this microfacies contains allochems, such as calcareous algae from the Gymnocoliaceae family, embedded within micrite pastes. Furthermore, the microfauna comprises foraminifera and small carapaces of ostracods with rare bivalves. Crinoids have also been identified as part of the skeletal grains, while no bioturbation was observed (plate 5.1 B). The MKL2 microfacies corresponds with RMF20 and SMF18 (FOR&GYMNO) as described by [Flügel \(2010\)](#), signifying the sedimentation of carbonate sequences in the initial sections of the inner ramp zone (lagoon). This is in accordance with the standard FZ8,7, as [Wilson \(1975\)](#) suggested.

5.2.1.1.2.2. MKL2-FORAM: FORAMINIFERAL/ALGAL BIOCLASTIC PACKSTONE

The rock units associated with this sub-microfacies include the middle portion of rock unit 3 (sample no. A. 121) and the upper segment of rock-unit 6 (sample no. A. 259), characterized by the lithological feature of thin-bedded limestone in relation to MKL2-FORAM.

The allochems present resemble those in MKL2, although benthic foraminifera are more abundant than calcareous algae. Additionally, the thin section and photo scans of the rock samples have revealed the presence of brachiopod shells and trilobite fragments (plate 5.1

C). The correspondence of RMF and FZ for MKL2-FORAM is the same as that for MKL2. However, due to the prevalence of foraminifers in this sub-microfacies, the SMF18-FOR, as described by [Flügel \(2010\)](#), was selected.

5.2.1.1.2.3. MKL2-GYMNO: ALGAL BIOCLASTIC PACKSTONE

Among the sub-microfacies, this particular one boasts the highest number of rock samples in the Khachik Formation strata and the rock units linked with MKL2-GYMNO are the upper of rock-unit 1 (samples no. A. 139-143); rock unit 4 (samples no. A. 176, A. 178, A. 180, A. 189-191 and A. 197); rock-unit 5 (samples no. A. 198-204 and A. 207-208); rock unit 6 (samples no. A. 210 and A. 213); the middle of rock unit 7 (samples no. A. 257-258); rock units 11 (samples no. A. 296-304 and A. 308); rock units 13, 14 and end of 15 (samples no. A. 315-325 and A. 329). The field-lithological character of MKL2-GYMNO includes the alternation of thin-bedded limestones with shales that, in some rock units, the shales are dominating and thin to medium-bedded limestones.

The allochems in MKL2-GYMNO closely resemble those in MKL2, with a notable abundance of calcareous algae (occasionally comprising up to 50 percent) from the family Gymnocyodiaceae, encompassing species like *Gymnocodium bellerophontis*, *Gymnocodium* sp., and *Permocalculus* sp. Dasycladaceae, notably the species *Mizzia* sp., are also present. These entities are embedded within a micritic matrix and are highly condensed in specific beds. Other elements of the microfauna include foraminifera such as *Nankinella* sp., *Glomomidiella nestellorum*, and *Agathammina* sp., with rare brachiopods, ostracods, and bivalves (plate 5.1 D). The correspondence of RMF and FZ for MKL2-GYMNO is identical to that of MKL2 and MKL2-FORAM. Considering the prominence of calcareous algae in this sub-microfacies, the SMF18-GYMNO, as outlined by [Flügel \(2010\)](#), was chosen.

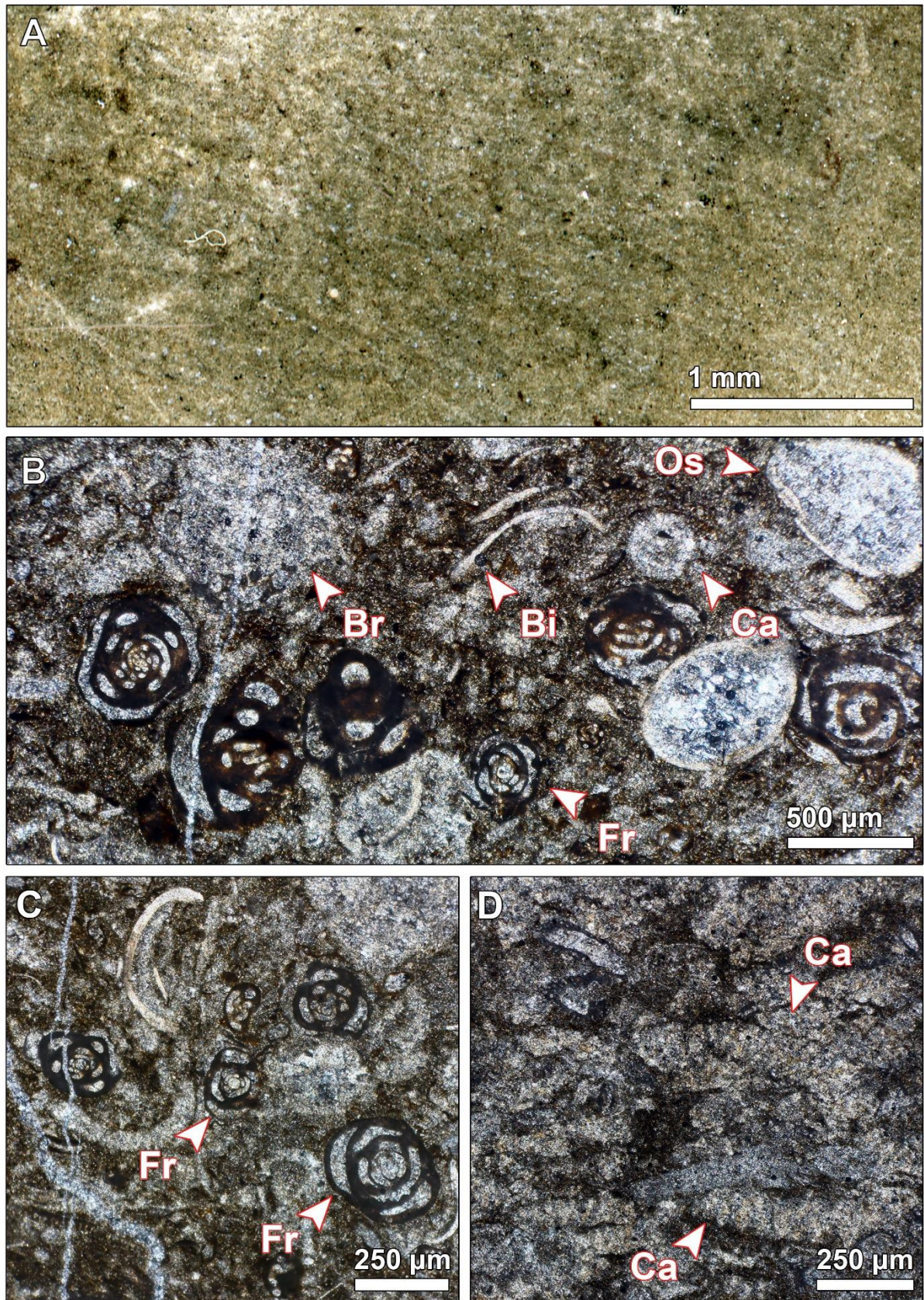


PLATE 5.1

Plate 5.1. Illustrations of the identified microfacies: A. Photo of MKL1 revealing the absence of skeletal allochems, B. MKL2 displayed with a variety of skeletal allochems: bryozoans, foraminifers, calcareous algae and ostracods, C. MKL2-FORAM exhibiting benthic foraminifers (Miliolidae family), D. Longitudinal-oblique sections of compact calcareous algae within the MKL2-GYMNO sub-microfacies.

5.2.1.1.2.4. INTERPRETATION OF MKL2

The high presence of calcareous algae in these samples, particularly the family Gymnocodiaceae, may indicate their favorable living conditions (Flugel 2010). The proliferation and substantial algae in MKL2 indicate their adaptation to the most favorable temperature range within the shallow, sunlit layer of the water. According to Oertli (1964), these algae belong to the euhaline type and typically thrive in marine environments with salinities ranging from 33 to 40‰. The sedimentological and palaeontological features, including the distribution of smaller and larger miliolids and agglutinated conical foraminifera (Geel 2000; Romero et al. 2002; Vecchio & Hottinger 2007, Afzal et al. 2011 and Spanicek et al. 2017) in the MFL 2 microfacies, indicate deposition in low to moderate-energy environments of the inner ramp. The simultaneous presence of green algae, foraminifera and large-size bioclasts such as bivalves and brachiopod shells suggests the existence of a dynamic lagoon zone. This lagoon would have had shallow waters, ample nutrients, and an ideal water temperature, as shown by Chatalov (2007), Westphal et al. (2010), Nebelsick et al. (2012) and Abasaghi et al. (2020). In the MKL2 micro-environment groups, a diverse range of heterozoan fauna, including echinoderms and brachiopods, was observed. The presence of currents and upwelling processes can elevate the nutrient levels in the surroundings, thereby promoting the prevalence of the heterozoan community (Westphal et al. 2010; James & Jones 2015; Michel et al. 2018; Abasaghi et al. (2020). Additionally, Ghaderi (2014) reported significant compaction in packstone beds of algal debris in the thin sections of Khachik Formation succession from the Main Valley section of the Ali-Bashi Mountain, likely influenced by internal displacement and transporting within the environment. The deformation of these microfossils is speculated to be the result of fluctuations in energy levels, which are associated with intrabasinal currents. This phenomenon may also be observed in microfacies.

5.2.1.2. RESTRICTED MICROFACIES

Three microfacies have been distinguished based on the presence of various allochems, such as total abundance of benthic foraminifers (miliolids and fusulinids), calcareous algae (primarily Gymnodiaceae), brachiopod, bryozoan, and crinoid fragments within a delineated area of the restricted ramp.

5.2.1.2.1. MKR1

In general, MKR1 indicates wackestone microfacies; nevertheless, the diverse presence of allochems in specific samples has resulted in the recognition of five sub-microfacies.

5.2.1.2.1.1. MKR1: BIOCLASTIC WACKESTONE

The rock units associated with this microfacies are rock unit 2 (samples no. A. 151 and A. 162); the lower part of rock unit 4 (samples no. A. 177 and A. 179); rock unit 6 (samples no. A. 216); rock unit 7 (samples no. A. 232, A. 222, A. 225-227 A. 240 and A. 253-256); the upper of rock unit 9 (sample no. A. 290). The field-lithological character of this sub-microfacies is an alternative of thin-bedded limestones with shales; in some rock units, the shales dominate and thin to medium-bedded limestones.

In this sub-microfacies of MKR1, the prevalence of calcareous algae is moderate. Some samples exhibit some foraminifers. Also, in the thin sections of MKR1 (plate 5.2 A), ostracod, brachiopod and unidentifiable shell fragments have been discovered. The microfacies MKR1 aligns with RMF17 and SMF18 (FOR&GYMNO) as outlined in [Flugel \(2010\)](#) description, indicating the deposition of carbonate sequences within the midsections of the inner ramp zone (restricted). This conforms to the recognized FZ8,7 standard, as proposed by [Wilson \(1975\)](#).

5.2.1.2.1.2. MKR1-GYMNO: ALGAL BIOCLASTIC WACKESTONE

The rock units related to MKR1-GYMNO are rock unit 1 (samples no. A. 110-111, A. 116-117, A. 120, A. 123-124); the lower part of rock unit 7 (samples no. A. 243-244); rock unit 9

(samples no. A. 269-270, A. 289 and A. 291). Field-lithological characteristics are thin-bedded limestones, an alternative to thin-bedded limestones with shales; some rock unit shales dominate with thin to medium-bedded limestones with nodular chert. Like MKR1, the prevalence of calcareous algae is moderate. In some samples, a foraminifer, crinoid fragments and rare bryozoan are the other skeletal allochems (plate 5.2 B). Within the thin sections, some samples of MKR1-GYMNO exhibit the presence of peloids alongside rarely intraclast fragments. The RMF, ramp zone and FZ of the MKR1-GYMNO, like MKR1 and the SMF18-GYMNO, were delineated for comparative analysis.

5.2.1.2.1.3. MKR1-DOLOM: DOLOMITIZED BIOCLASTIC WACKESTONE

The observed sub-microfacies is in the medium-bedded limestones of the lower part of rock unit R1 (sample A. 114). Rare fragments of crinoids, calcareous algae and brachiopods constitute the allochems in MKR1-DOLOM, embedded within the highly deteriorated and compacted dolomitized micrite matrix (plate 5.2 C). The RMF, SMF, ramp zone, and FZ of the MKR1-DOLOM are the same as those of the MKR1-GYMNO.

5.2.1.2.1.4. MKR1-FUSUL: FUSULINID BIOCLASTIC WACKESTONE

Samples A. 228-229 represent this specific sub-microfacies, characterized by thin-bedded limestones located towards the top of rock unit 6, as observed on the outcrop. Fusulinids are the most frequent skeletal allochem in MKR1-FUSUL. Fragments of brachiopods, bryozoans and families of textulariidae constitute the additional allochems (plate 5.2 D). The MKR1-FUSUL aligns with RMF16 and SMF18-FOR of the [Flügel \(2010\)](#), indicating the deposition of carbonate sequences within the confined section of the inner ramp zone, consistent with [Wilson \(1975\)](#) FZ8,7 standard.

5.2.1.2.1.5. MKR1-MILIO: MILIOLID BIOCLASTIC WACKESTONE

Sample A. 193 presents distinct sub-microfacies in the middle of rock unit 6. It is distinguished by thinly bedded limestone observed at the outcrop site. The key skeletal allochems in the MKR1-MILIO is miliolid, a small-size benthic foraminifer. In this context, destroyed calcareous

algae are among the other allochems (plate 5.2 E). The MKR1-MILIO aligns with RMF13 and SMF18-FOR of the [Flugel \(2010\)](#), indicating the deposition of carbonate sequences within the confined section of the inner ramp zone, consistent with [Wilson's \(1975\)](#) FZ8,7 standard.

5.2.1.2.1.6. INTERPRETATION OF MKR1

During the Permian, Gymnodiaceans were abundant and commonly found as fragments of sand and gravel size fragments in the non-reefal limestone of ramp and outer-shelf environments ([Riding & Guo 1991](#); [Abasaghi et al. 2020](#)). The abundance of fusulinids in this microfacies indicates shallow, warm to temperate water environments. Typically, they thrive in tropical and subtropical regions, predominantly within shelves, platforms, and reefs. They lived in normal marine, well-oxygenated environments on subtidal open shelves, depths between a few to tens of meters. Middle to Late Permian verbeekinid and neoschwagerinid fusulinids are often associated with platform margin reefs. Some species of fusulinids are restricted to back-reef lagoons ([Flugel 2010](#)). The sedimentological and paleontological characteristics suggest that deposition occurred in an extremely shallow, low-energy, restricted marine setting, fostering the thriving of small epiphytic foraminifera (small miliolids) and discorbids ([Spanicek et al. 2017](#)). In addition, the presence of calcareous algae signifies an ethaline environment and a symbiotic relationship between fusulinid foraminifera and algae. The abundant presence of algae and large fusulinids suggests deposition within a euphotic zone, typically at depths of less than 150 meters ([Vachard et al. 2004](#); [Saitoh et al. 2013](#); [Abasaghi et al. 2020](#)).

5.2.1.2.2. MKR2: ALGAL BIOCLASTIC WACKESTONE/PACKSTONE

The outcrops of the medium-bedded limestones of rock unit 1 (Samples no. A. 118 and A. 122), thin-bedded limestones of the upper part of rock units R5 and rock units R5 and R9 (Samples no. A. 205 and A. 286) linked with this microfacies. The allochems in MKR2 are relatively abundant in calcareous algae. Also, trilobite fragments, crinoid segments and unidentifiable shell fragments have been discovered in this microfacies (plate 5.3 A). The MKR2 aligns with RMF17 and SMF18-GYMNO of the [Flugel \(2010\)](#), indicating the deposition

of carbonate sequences in the restricted section of the inner ramp zone, consistent with [Wilson's \(1975\)](#) FZ8,7 standard.

5.2.1.2.2. INTERPRETATION OF MKR2

Similar to MKR1, calcareous algae dominate in the MKR2 environment; however, the prevalence of allochems is even more pronounced. This characteristic indicates that the conditions remain conducive to the survival of these organisms. Additionally, the presence of calcareous algae signifies euhaline conditions.

5.2.1.2.3. MKR3

The MKR3 shows packstone microfacies. However, the varied presence of allochems (in particular of benthic foraminifers) in some samples has led to the identification of three sub-microfacies

5.2.1.2.3.1. MKR3: MILIOLID PACKSTONE

The rock units related to MKR3 are rock unit 2 (samples no. A. 165 and A. 167-168). Lithological characters of this sub-microfacies are alternations of thin-bedded limestones with shales that dominated in some rock-unit. The key skeletal allochem found in the MKR3 is Miliolid, a small-size benthic foraminifer. Additionally, destroyed calcareous algae are among the other allochems (plate 5.3 B).

The MKR3 aligns with RMF16 and SMF18-FOR of the [Flügel \(2010\)](#), indicating the deposition of carbonate sequences within the confined part of the inner ramp zone, consistent with [Wilson's \(1975\)](#) FZ8,7 standard.

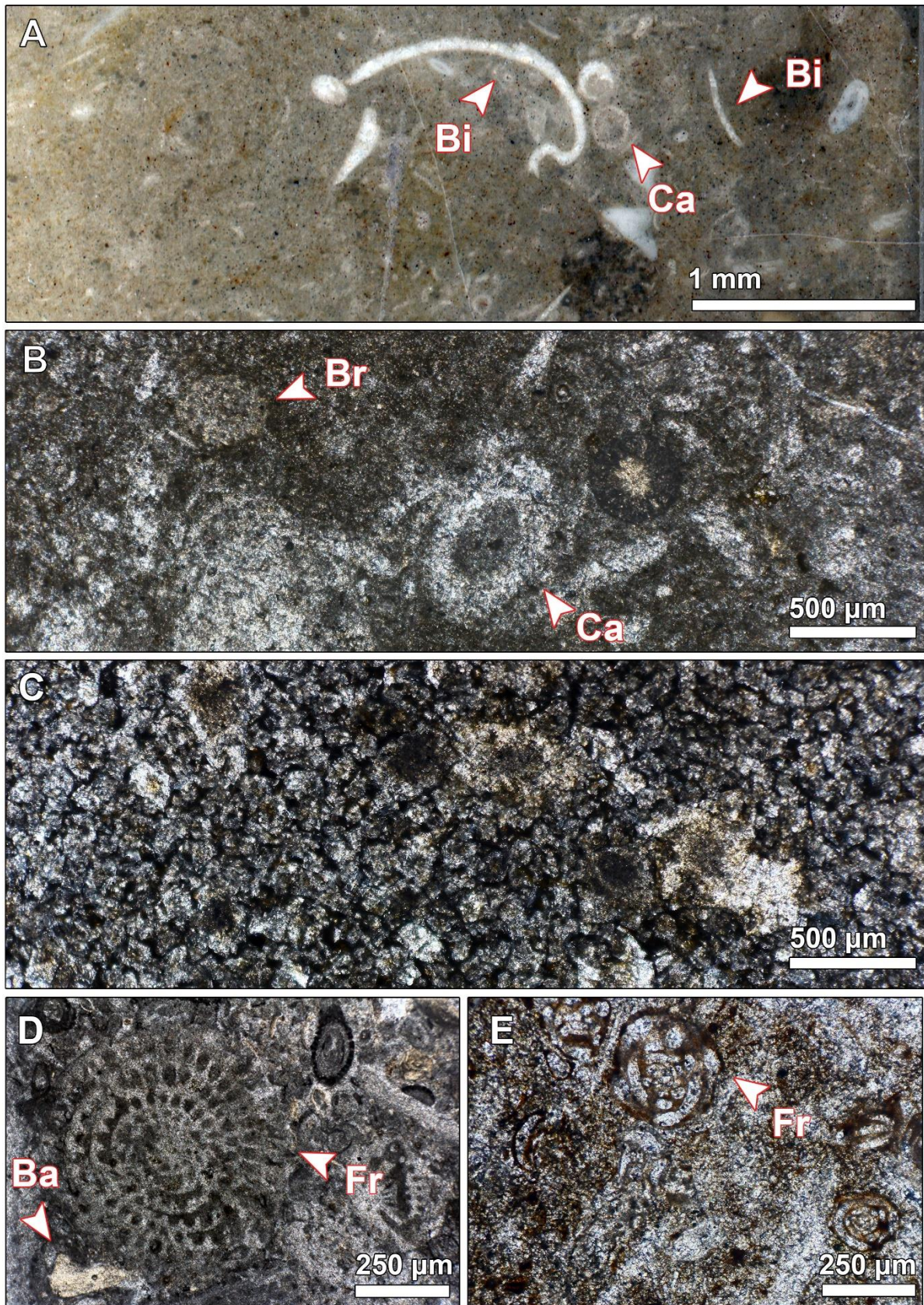


PLATE 5.2

Plate 5.2. Illustrations of microfacies: A. Photo-scan related to MKR1 with different cutting sections of skeletal allochems, B. MKR1-GYMNO displayed with a variety of skeletal allochems: bryozoans with cross section and calcareous algae fragments assemblages with different cutting sections, C. MKR1-DOLOMO where skeletal elements have been heavily affected by dolomitization and have been destroyed, D. MKR1-FUSUL with large-size longitudinal section of fusulinid, E. MKR1-MILIO cross section of miliolida with undefined shell fragments.

5.2.1.2.3.2. MKR3-BIOCL: BIOCLASTIC MILIOLID PACKSTONE

Samples A. 173-175 of the of rock-unit R3; samples A. 181 and A. 185 of the lower part of the rock-unit R4, A. 260 of the rock-unit R7 and A. 278-280 of the middle part of rock-unit R9 linked with MKR3-BIOCL. The outcrops display for this sub-microfacies is alternation of thin-bedded limestone with shale and thin-bedded limestone and the main skeletal allochem found in the MKR3-BIOCL is miliolid. Additionally, calcareous algae and crinoid fragments are the other allochems in this context (plate 5.3 C).

The RMF, SMF, ramp zone and FZ of the MKR3-BIOCL are the same as those of the MKR3.

5.2.1.2.3.3. MKR3-FUSUL: FUSULINID MILIOLID PACKSTONE

The outcrops display of this sub-microfacies is an alternation of thin-bedded limestone with shale and samples A. 171-172 of the rock unit R3 and samples A. 180 of the lower part of the rock-unit R4 linked with MKR3-FUSUL. Furthermore, in this sub-microfacies, there is a higher abundance of fusulinids than miliolids, the primary skeletal allochems found in the MKR3-FUSUL. Additionally, calcareous algae have been observed in certain parts of the samples (plate 5.3 D).

The RMF, SMF, ramp zone, and FZ of the MKR3-FUSUL are similar to those of the MKR3 and MKR3-BIOCL.

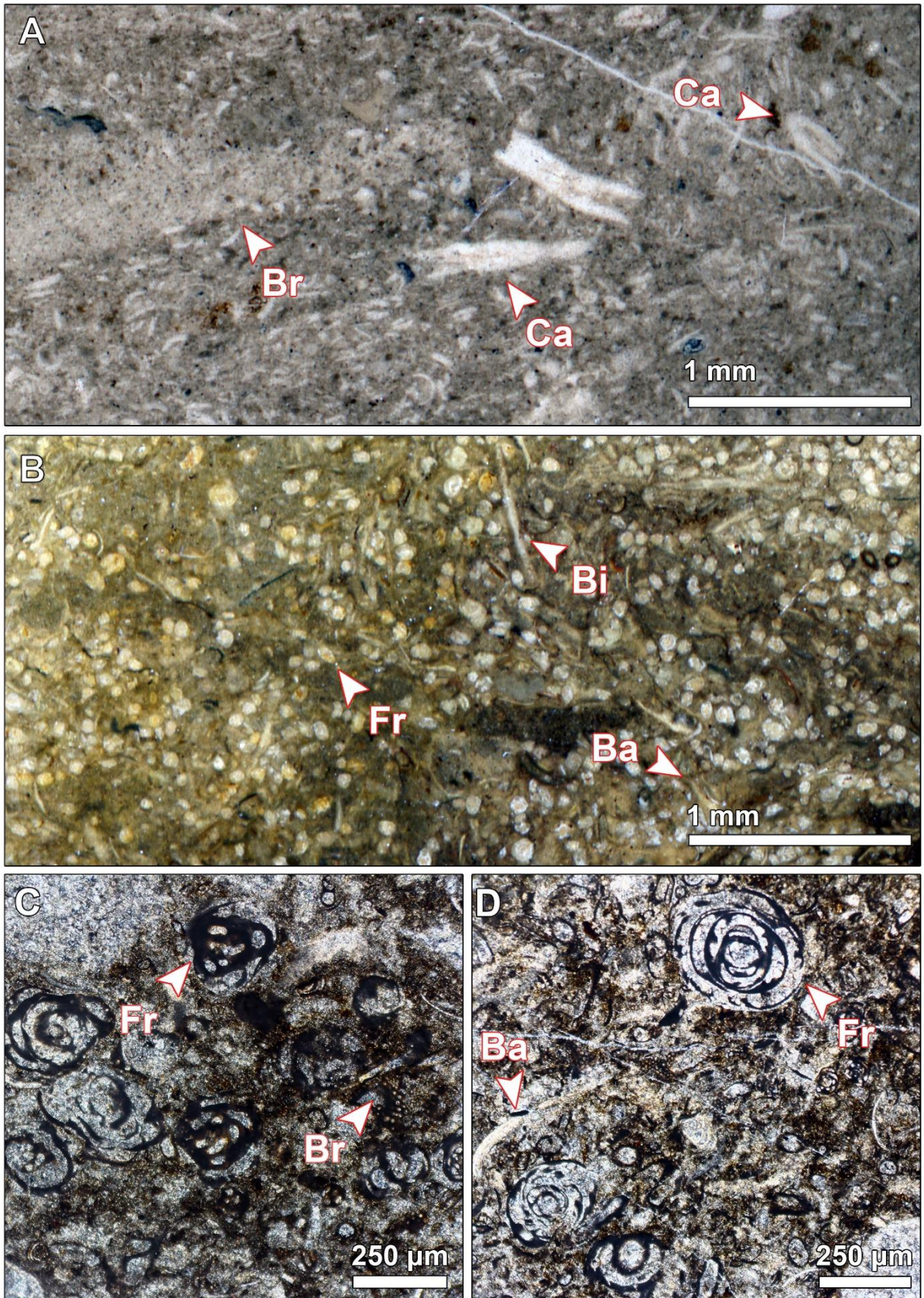


PLATE 5.3

Plate 5.3. Illustrations of the microfacies A. photo-scan MKR2 with different cutting sections *permocalculus* species and bryozoan fragment, B. photo-scan of MKR3 displayed with a variety of skeletal allochems: bivalves shell, high assemblage of miliolida families, C. MKR3-BIOCL with cross section of the miliolids, bryozoan fragments and undefined shell fragments, D. MKR3-FUSUL with large-size longitudinal section of fusulinid, brachiopod shell fragment and undefined shell pieces.

5.2.1.2.3.4. INTERPRETATION OF MKR3

In this microfacies group, the calcareous algae are rare and almost destroyed. The state of preservation of these microfossils might plausibly be linked to transportation into this environment. Alternatively, this microfossil deformation could result from fluctuations in energy levels associated with intrabasinal currents. The profusion of fusulinids in this micro-environment suggests the presence of a setting in shallow, warm, and mildly temperate waters in the restricted zone ([Flugel 2010](#)). Furthermore, foraminifera with dark test walls points to heightened containment and hypersaline conditions ([Frontalini et al. 2011](#); [Abasaghi et al. 2020](#)). The occurrence of crinoids in specific samples up to 30 percent might demonstrate normal marine euhaline environments ([Oertli 1964](#)).

5.2.1.3. OPEN-MARINE MICROFACIES

Four microfacies have been distinguished on the presence of various allochems, such as total abundance of benthic foraminifers (miliolids and fusulinids), calcareous algae (mainly Gymnocodiacea), brachiopod, bryozoan, and crinoid fragments within the restricted ramp. Peloids in this ramp zone serve as the primary non-skeletal allochems, playing a significant role in certain sub-microfacies to the extent that they contribute to the terms of the microfacies.

5.2.1.3.1. MKO1

The MKO1 demonstrates packstone microfacies similar to MKR1 (but the allochems's content, it is slightly different).

Due to the diverse presence of allochems, particularly peloids, three sub-microfacies have been identified.

5.2.1.3.1.1. MKO1: PELOIDAL PACKSTONE

Samples A. 331-333 from rock-unit R15 exhibit lithological characteristics typical of MKO1, characterized by thin-bedded limestone outcrops. Peloids in MKO1 play a significant role as the primary non-skeletal allochems. Calcareous algae are infrequent, and benthic foraminifers with brachiopod shell fragments are the skeletal allochems observed in certain parts of this sub-microfacies (plate 5.4 A).

The MKO1 aligns with RMF14 and SMF10 of [Flugel \(2010\)](#), representative of the deposition of carbonate sequences in the open-marine part of the inner ramp zone, consistent with [Wilson's \(1975\)](#) 7 standard.

5.2.1.3.1.2. MKO1-BIOCL: BIOCLASTIC PELOID PACKSTONE

The rock units related to MKO1-BIOCL are rock unit 1 (samples no. A. 105-106), the lower part of rock unit 9 (samples no. A. 281, A. 284-285 and A. 290), the upper part of the rock unit 9 (sample no. A. 305). The outcrops composed of this sub-microfacies are thin-bedded limestones and the allochem contexts are: peloids remain the main allochems in this sub-microfacies; however, the diversity of bioclastic allochems surpasses that of peloids. Calcareous algae are uncommon, while brachiopod fragments, ostracods, undefined bioclastic shells, and benthic foraminifers are missing (plate 5.4 B).

The RMF, SMF, ramp zone, and FZ of the MKO1-BIOCL are similar to those of the MKO1.

5.2.1.3.1.3. MKO1-PEL/BIO: PELOIDAL/BIOCLASTIC PACKSTONE

The rock units associated with MKO1-PEL/BIO can be identified as follows: rock-unit 1, including samples A. 109, A. 136, and A. 138; the lower part of rock-unit 7, with samples A. 243-244; and the upper part of rock-unit 9, involving sample A. 307. Thinly stratified limestones characterize these particular sub-microfacies. In contrast to the MKO1-BIOCL, the main emphasis of this sub-microfacies lies on peloids. Although bioclastic allochems have a

high diversity, their quantity is lesser than that of peloids. Calcareous algae are not common, and the skeletal composition of the MKO1-BIOCL predominantly comprises brachiopods, ostracods, and indistinct bioclastic shells, with a noticeable absence of benthic foraminifers (as depicted in plate 5.4 C). Moreover, the RMF, SMF, ramp zone, and FZ of the MKO1-PEL/BIO are the same as those observed in the MKO1 and MKO1-BIOCL.

5.2.1.3.1.4. INTERPRETATION OF MKO1

The peloids exhibit a round to elliptical shape with sub-rounded features. They are commonly regarded as by-products of ooids or the micritization process of bioclast fragments (Zadeh et al. 2019; Ahmad et al. 2021; Yousef et al. 2023). Furthermore, the high occurrence of peloids in this microfacies suggests that sedimentation occurred in an open marine environment below the fair-weather wave base, characterized by low-energy conditions. As a result, the formation of numerous peloids is thought to have occurred through the micritization of smaller foraminifera deposited within the interior of a ramp platform characterized by moderate water circulation and a confined marine environment, as well as inner ramp settings (Flugel 2010). The presence of these peloids in this section suggests that they might have been transported from the restricted zone to the initial part of the open marine environment.

5.2.1.3.2. MKO2: ALGAL BIOCLASTIC PELOID PACKSTONE

The rock units linked with MKO2 can be discerned as follows: rock-unit 1, encompassing samples A. 107-108 and A. 130-135; the middle part of rock-unit 2, involving sample A. 160. These sub-microfacies are distinguished by alternating thin-bedded limestones with shales and thinly stratified limestones. The prevalence of calcareous algae, particularly within the Gymnodiaceae, is registered within this microfacies. There is a notable diversity of other bioclastic allochems, such as benthic foraminifers, brachiopods, and ostracods (as illustrated in plate 5.4 D).

MKO2 corresponds to RMF14 and SMF18-GYMNO of Flugel classification (2010), representing the deposition of carbonate sequences in the open-marine part of the inner ramp zone, in accordance with Wilson (1975) 7 facies zone.

5.2.1.3.3. INTERPRETATION OF MKO2

The depositional environment conditions for MKO2 resembled those of the previous microfacies (MKO1). However, the presence of calcareous algae suggests that the environmental conditions have somewhat improved for living them. However, the presence of their fragments could also be attributed to transportation.

5.2.1.3.3. MKO3

MKO3 characterizes a wackestone/packstone microfacies. This classification is attributed to the diverse presence of various allochems, notably fragments of crinoids. Consequently, two sub-microfacies have been identified:

5.2.1.3.3.1. MKO3: BIOCLASTIC WACKESTONE/PACKSTONE

The rock units associated with MKO3 can be identified as follows: rock-unit 1, with samples A. 103-104 and A. 129; the middle part of rock-unit 2, with sample A. 161; rock-unit 6, with samples A. 211-212, A. 214, and A. 218; the lower part of rock-unit 9, with samples A. 271-273; and the upper part of rock-unit 10, with samples A. 293-294. These sub-microfacies are characterized by alternating thin-bedded limestones with shales and thinly stratiform limestones. In terms of the allochems, identifiable components include fragments of brachiopod, crinoid, calcareous algae, ostracods, and unidentified shells, as indicated in plate 5.4 E. MKO3 links to RMF7 and SMF10 of [Flügel \(2010\)](#), representing the deposition of carbonate sequences in the open-marine part of the inner ramp zone, in accordance with [Wilson \(1975\)](#) seven facies zone.

5.2.1.3.3.2. MKO3-CRINO: CRINOID BIOCLASTIC WACKESTONE/PACKSTONE

The samples A. 237 and A. 245 from the thin-bedded limestone outcrops of rock unit seven are associated with MKO3-CRINO. The allochems are characterized by the significant presence of relatively large crinoid and brachiopod, accompanied by fragments of calcareous

algae (plate 5.4 F). Moreover, The RMF, SMF, ramp zone, and FZ of the MKO3-CRINO are the same as those detected in the MKO3.

5.2.1.3.3. INTERPRETATION OF MKO3

Crinoids exist in both warm and cold-water environments, representing a minor component of carbonate rocks (Wilson 1975; Flugel 2010). Some sections of the Khachik beds indicate their exposure to diagenetic processes, as evidenced by the dissolution of their remains. Thin-section microphotographs of the equatorial sections exhibit a round or oval appearance and are prone to micritization, followed by calcite-filling processes (Flugel 2010). Additionally, the presence of echinoderms and algae suggests that the depositional environment of the shoal facies' association maintains typical oxygenation and salinity conditions (Yusef et al. 2023).

5.2.1.3.4. MKO4

A packstone/rudstone microfacies characterize MKO4. This classification is based on the diverse presence of various allochems, particularly fragments of crinoids, large-sized brachiopods, and ostracods. Consequently, two distinct sub-microfacies have been identified:

5.2.1.3.4.1. MKO4: BIOCLASTIC PACKSTONE/RUDSTONE

Sample A. 209 from the alternative of thin-bedded limestones with shaly outcrops in the lower part of the rock unit six is linked with MKO4. The most skeletal allochems are large-size brachiopod shells, fragments of calcareous algae and ostracods (plate 5.4 G). Besides, the RMF, SMF, ramp zone and FZ of this sub-microfacies are the same as those detected in the MKO3 and MKO3-CRINO.

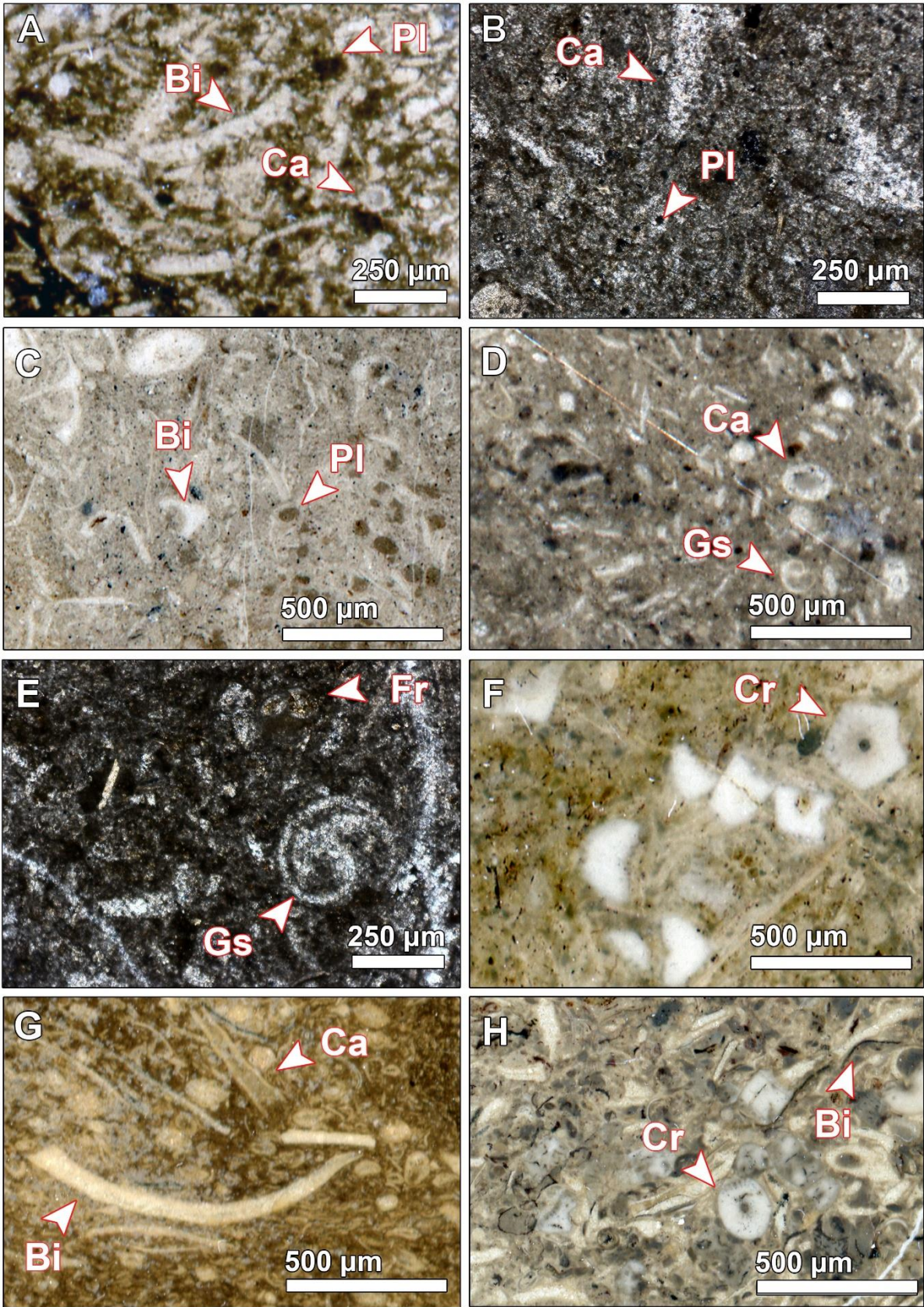


PLATE 5.4

Plate 5.4. Illustrations of the identified microfacies: A. MKO1 with different allochems, B. MKO1-BIOCL with a longitudinal-oblique section of *permocalculus*, with peloids, C. MKO1-PEL/BIO with peloids and bivalve fragments, D. MKO2 with longitudinal section of *permocalculus*, gastropod fragment and undefined bioclastic elements, E. MKO3 gastropod fragment with foraminifers and undefined bioclastic elements, F. MKO3-CRINO large-sized of crinoid in the various cutting section with undefined bioclastic elements, G. MKO4 longitudinal section of *permocalculus* with bivalves fragment and undefined bioclastic elements, H. MKO4-CRINO large-sized of crinoid in the various cutting section with bivalve fragment and undefined bioclastic elements.

5.2.1.3.4.2. MKO4-CRINO: CRINOID BIOCLASTIC PACKSTONE/RUDSTONE

Samples A. 154-158 from the alternative of thin-bedded limestones with shale outcrops of the middle part of rock unit 2 are associated with MKO4. MKO4-CRINO is characterized by the significant presence of relatively large crinoid fragments and large-size brachiopod shells, accompanied by pieces of compacted calcareous algae and ostracods (plate 5.4 H). The RMF, SMF, ramp zone, and FZ of the MKO4-CRINO are the same as those detected in the MKO3, MKO3-CRINO and MKO4.

5.2.1.3.4.3. INTERPRETATION OF MKO4

The presence of crinoids in this area indicates that the environmental conditions continue to suit them, although their relative abundance is slightly lower than the previous facies. It has also become evident that there have been changes in the environmental conditions for their presence.

5.2.2. MIDDLE RAMP MICROFACIES ASSEMBLAGES

This area has medium-bedded, fine-grained bioclastic limestones and marls, frequently showing signs of burrowing. The skeletal grains are often eroded, and echinoderms are a common feature. The sediment composition includes mudstones, wackestones, packstones, and some grainstones. Farther away from the shore, where the incline becomes steeper,

there is evidence of slumps and various indications of the reworking and transportation of fine-grained ramp material (Flügel 2010).

Three distinct microfacies have been identified based on various allochems in the thin sections of Khachik Formation strata in the Ali-Bashi section, including brachiopod shells and crinoid fragments in a specified area of the middle ramp.

5.2.2.1. MKM1

MKM1 is considered a wackestone microfacies, and due to the presence of various allochems, particularly peloids, three distinct sub-microfacies have been identified.

5.2.2.1.1. MKM1: PELOIDAL WACKESTONE

Samples A. 186-187 from the alternative of thin-bedded limestones with shale outcrops of the middle part of the rock unit 4 are included in MKM1. MKM1 is characterized by the significant presence of peloids and rare fragments of the brachiopod, ostracods and undefined shell fragments (plate 5.5 A). MKM1 links to RMF3 and SMF8 of Flügel (2010), representing the deposition of carbonate sequences in the middle ramp zone in accordance with FZ 7 of Wilson (1975).

5.2.2.1.2. MKM1-BIOCL: BIOCLASTIC PELOID WACKESTONE

Sample A. 127 from thin-bedded limestone outcrops of the middle part of the rock unit 1 is included in MKM1-BIOCL. This sub-microfacies is characterized by the significant presence of peloids and bioclastic fragments such as crinoid, brachiopod, destroyed calcareous algae that have probably been transported and undefined shell fragments (plate 5.5 B). However, the volume of bioclastic allochems is more than that of peloids and the RMF, SMF, ramp zone, and FZ of the MKM1-BIOCL are the same as those detected in the MKM1.

5.2.2.1.3. MKM1-PEL/BIO: PELOIDAL/BIOCLASTIC WACKESTONE

Sample A. 128, obtained from the thinly bedded limestone outcrops in the middle of rock-unit 1, is associated with the MKM1-PEL/BIO. The allochems characteristics of this particular sub-microfacies closely resemble those of MKM1-BIOCL, but there are fewer peloids (as shown in plate 5.5 C). Additionally, RMF, SMF, ramp zone, and FZ of the MKM1-PEL/BIO are consistent with those observed in MKM1 and MKM1-BIOCL.

5.2.2.1.4. INTERPRETATION OF MKM1

The facies association is notably characterized by marine bioclasts such as bivalves, brachiopods, and certain foraminifera. These species, identified through thin-section petrography, reside in the micritic matrix. Their presence signifies circulation in open marine environments and is frequently associated with normal oxygen and salinity conditions (Read 1985; Flugel 2010). The prevalent mudstone texture commonly illustrates a low-energy depositional environment (Zhao et al. 2017). The presence of peloids in this area could also result from their transportation from the adjacent section. In the association of open marine fossil facies, larger or intact fossil fragments are observed, believed to have originated from adjacent shoals (Flugel 2010). The higher energy levels in the open marine environment of the middle ramp setting frequently result in storm waves breaking off sections of the shoals, leading to the transportation of larger or whole fossil components into the open marine environment (Yusef et al. 2023).

5.2.2.2. MKM2

MKM2 is considered a floatstone microfacies. Due to the diverse presence of various allochems, particularly high-volume large brachiopod and crinoid fragments, two sub-microfacies have been divided.

5.2.2.2.1. MKM2: BIOCLASTIC FLOTSTONE

Rock unit 1 comprises samples A. 126 and A. 150, while the lower part of rock unit 7 includes samples A. 223-224. The presence of thin-bedded limestones characterizes the outcrops. Allochems in this sub-microfacies include fragments of brachiopod and relatively large crinoid fragments, accompanied by poorly preserved calcareous algae, ostracod, and unedified shell fragments (plate 5.5 D). The RMF, SMF, ramp zone and FZ detected in MKM2 align with those identified in MKM1.

5.2.2.2.2. MKM2-BRACH: BRACHIOPOD FLOTSTONE

Sample A. 233, obtained from the thinly bedded limestone outcrops in the middle rock-unit 7, is associated with the MKM2. The allochems characteristics of this particular sub-microfacies consist of the large-sized brachiopod, ostracod, and undefined shell fragments (plate 5.5 E). Additionally, RMF, SMF, ramp zone, and FZ of the MKM2-BRACH are consistent with those observed in MKM2 and MKM1.

5.2.2.2.3. INTERPRETATION OF MKM2

The occurrence of bioclastic floatstone may be attributed to a decrease in allochems and an abundance of calcareous mud within the rock. This characteristic suggests a reduction in environmental energy and potentially a relative deepening of the basin ([Ghaderi 2014](#)). Sedimentological characteristics identified in the thin sections of the thinly bedded strata and the relatively well-preserved brachiopod fragments indicate a depositional environment marked by low energy, corroborating the earlier assertions ([Haas et al. 2007](#)). Brachiopods are known to inhabit typical marine euhaline environments, constituting up to 30 percent, according to [Oertli \(1964\)](#).

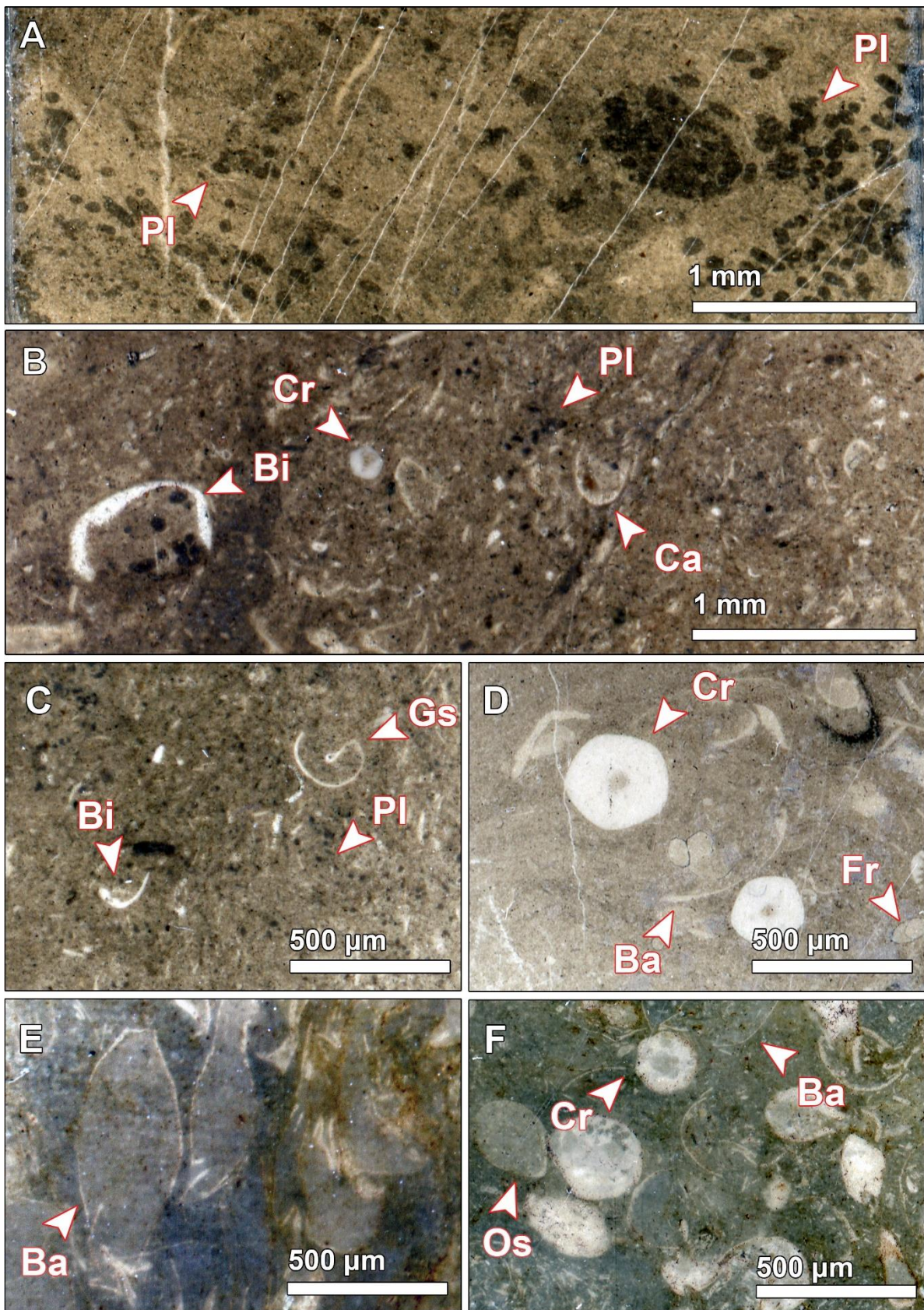


PLATE 5.5

Plate 5.5. Illustrations of the identified microfacies (all of the figures are the photo-scan): A. MKM1 with peloid allochems, B. MKM1-BIOCL with variety of skeletal allochems: bivalves, crinoid fragments, destroyed calcareous algae and peloids, C. MKM1-PEL/BIO with destroyed bivalves, depressed gastropod and undefined shell fragments, D. MKM2 with large-size cross section of the crinoids, brachiopod fragment, benthic foraminifers and undefined shell pieces. E. MKM2-BRACH large-size of the brachiopods in micritic matrix. F. MKM3 with various allochems: brachiopod fragments, cross section of the crinoids, ostracods and undefined shell pieces.

5.2.2.3. MKM3: BIOCLASTIC WACKESTONE/FLOTSTONE

Samples A. 221 of the upper part of rock unit 6 and A. 238 in the middle rock unit 7 obtained from the thinly bedded limestones are attributed to MKM3.

The allochem characteristics include large-sized brachiopod, ostracod, and unedified shell fragments with destroyed and poorly persevered calcareous algae (plate 5.5 F). Additionally, RMF, SMF, ramp zone, and FZ of the MKM3 are consistent with those observed in MKM2 and MKM1.

5.2.2.3.1. INTERPRETATION OF MKM3

The sedimentary environment interpretation for MKM3 aligns with the earlier findings (MKM2), given that fossil traces indicate a decrease in the influx of skeletal allochems and a decline in environmental energy.

5.2.3. OUTER RAMP (TOE-OF-SLOPE) MICROFACIES ASSEMBLAGES

The sedimentary layers consist of thin to medium-bedded, fine-grained limestones and marls, frequently exhibiting traces of burrowing. Laminated marls alternate with lime mudstones, while the skeletal grains are typically well-preserved and show no sign of erosion. The sediment composition also includes mudstones, wackestones and packstones. Additionally, occasional tempestite beds are composed of grainstones ([Flugel 2010](#)).

Three distinct microfacies have been identified within the Khachik Formation layers at the Ali-Bashi section. Different allochems characterize these microfacies, notably infrequent benthic

foraminifer families (miliolids). Notably the absent of some microfossils such as: calcareous algae, brachiopod, crinoid fragments, ostracod, and bioturbation traces in a specific area of the outer ramp corresponding to the base of the slope.

5.2.3.1. MKT1

MKT1 is considered a mudstone microfacies, and due to the diverse presence of various allochems, particularly bioturbation traces, two sub-microfacies have been divided.

5.2.3.1.1. MKT1: MUDSTONE WITH RARE FOSSILS AND BIOTURBATIONS

Samples A. 163-164 of the upper part of rock unit 2, alternating the thin-bedded limestones with shales, are associated with the MKT1. The allochem characteristics of this particular sub-microfacies comprise deteriorated and inadequately preserved calcareous algae (transfer of algae occurs from the photic zone) and a trace of bioturbations (plate 5.6 A). MKT1 links to RMF2 and SMF3 of [Flugel \(2010\)](#), representing the deposition of carbonate sequences in the outer ramp zone in accordance with FZ3 (the toe-of-slope) of [Wilson \(1975\)](#).

5.2.3.1.2. MKT1-BIOTU: MUDSTONE WITH BIOTURBATIONS

The rock units related to MKT1-BIOTU exhibit an alternating of thin-bedded limestones with shales and thin-bedded limestone outcrops. These units consist of samples, including A. 149, A. 153, and A. 150 in rock-unit 1 and samples A. 183-184 lower part of rock unit 6. Trace of bioturbations and rarely interaolast evidence origin from the restricted ramp zone (plate 5.6 B). The RMF, SMF, ramp zone and FZ of the MKT1-BIOTU are consistent with those observed in MKT1.

5.2.3.1.3. INTERPRETATION OF MKT1

This particular group of microfacies lacks shallow-marine fossils, such as corals, fusulinds and calcareous algae. The absence of fossils from photosynthetic organisms indicates a sedimentary environment potentially at a depth exceeding 150 meters, as referenced in

Saitoh et al. (2013). The presence of microscopic bioturbations supports a quiet basin, a relative oxygen abundance, decreased suspended food material in the water, and the benthic organisms' need to forage in the sediments (Ghaderi 2014).

5.2.3.2. MKT2

MKT2 is considered as a fossiliferous mudstone up to wackestone microfacies and due to the presence of various allochems (brachiopods, some benthic foraminifers and ostracods), three sub-microfacies have been divided.

5.2.3.2.1. MKT2: FOSSILIFEROUS MUDSTONE

Samples A. 101-102 and A. 115 from the lower section of rock unit 1 exhibit thin to medium-bedded limestones. Sample A. 152 from the initial part of rock unit 2 shows an alternation between thin-bedded limestones and shales. Sample A. 188 from the middle part of rock unit 4 also demonstrates an alternation between thin-bedded limestones and shales. Sample A. 220, extracted from the lower part of rock unit 7, showcases the presence of thinly bedded limestones. Additionally, samples A. 234-235, taken from the lower section of rock unit 7, reveal an alternating sequence of thin-bedded limestone and shale layers. These samples are all linked to MKT2. The allochem features of this sub-microfacies containing benthic foraminifers (milliolid family), brachiopods fragments, small pieces of crinoids that filled and cemented with calcite spray, ostracods and tiny filaments of the bivalve (plate 5.6 C). The RMF, SMF, ramp zone and FZ of the MKT2 are consistent with those observed in MKT1.

5.2.3.2.2. MKT2-BIOCL: FOSSILIFEROUS MUDSTONE/BIOCLASTIC WACKESTONE

The rock units related to MKT2-BIOCL exhibit an alternation of thin to medium-bedded and thin-bedded limestones with shale outcrops. These units consist of samples, including A. 112-113 and A. 137; sample A. 306, upper part of the rock unit 11; and sample A. 312, lower part of the rock unit 13. Brachiopod fragments, small pieces of the crinoids, ostracods and tiny filaments of the bivalves (all the skeletal elements are less than 10 percent frequency) are all

linked to MKT2-BIOCL (plate 5.5 D). The RMF, SMF, ramp zone and FZ of the MKT2-BIOCL are consistent with those observed in MKT2 and MKT1.

5.2.3.2.3. MKT2-FLOTS: FOSSILIFEROUS MUDSTONE/FLOTSTONE

Sample A. 125, obtained from the thinly bedded limestone outcrops in the middle of rock unit 1, is associated with the MKT2-FLOTS. The allochems of this sub-microfacies include large-sized brachiopod and unedified shell fragments with destroyed and poorly persevered calcareous algae transferred from the other ramp zone part (as shown in plate 5.6 E). The RMF, SMF, ramp zone, and FZ of the MKT2- FLOTS are consistent with those observed in MKT2, MKT2-BIOCL and MKT1.

5.2.3.2.4. INTERPRETATION OF MKT2

Like MKT2, in this microfacies also the lack of photosynthetic and shallow-marine fossils suggests a deposition at a depth considerably beneath the euphotic zone. The presence of brachiopod and undefined shell components displaying transitional effects indicate their transfer from the middle ramp zone during this zone.

5.2.3.3. MKT3: MUDSTONE/BIOCLASTIC WACKESTONE

The rock units associated with MKT3 can be identified as rock unit 7, comprising samples A. 248-251, and the lower part of rock unit 9 (samples A. 276-277 and A. 282). These specific sub-microfacies are characterized by alternating thin-bedded limestones with shales and thinly stratiform limestones in some parts of the Ali-Bashi section. Calcareous algae in a state of destruction and poor preservation, large-sized fragments of crinoids showing signs of transportation, carapaces of ostracods, and fragments of undefined shells are the allochems identified in MKT3 (plate 5.6 F). The RMF, SMF, ramp zone and FZ of the MKT3 are consistent with those observed in MKT2 and MKT1.

5.2.3.3.1. INTERPRETATION OF MKT3

The presence of some bioclastic (e.g., destroyed bivalves and undefined shells) in the MKT3 that indicates transportation to this area, along with the absence of bioturbation traces, could result from increased environmental energy compared to the previous microfacies. Crinoids are found in the Khachik sediments, with some parts indicating the influence of diagenetic processes as their remnants have dissolved. This suggests that at the end of the Khachik Formation in this section, the sedimentary energy in the depositional environment has increased.

To enhance observations and a more accurate assessment of microfacies and their related sedimentary environments in the studied section, the facies column illustrates the prevalence of allochemical content (including skeletal and non-skeletal components) and the sediment accumulation environment (see fig 5.6). Moreover, as a consequence of Ghaderi et al. (2016) report and the subdivision of the Khachik Formation into nine informal units (Chapter 3), a broad overview of the microfacies within the Main Valley section located in the Kuh-e-Ali Bashi (Ali Bashi Mountains) was provided. To facilitate a more comprehensive comprehension and assessment of the microfacies identified in this current study, in conjunction with the research above, a comparison of the microfacies in the stratigraphic column of both studies is presented (fig. 5.7).

Plate 5.6. Illustrations of the identified microfacies (all of the figures are the photo-scan): A. MKT1 with peloid allochems and destroyed bivalve fragments, B. MKT1-BIOTU shown bioturbations traces, C. MKT2 with recrystallized crinoid fragment, D. MKT2-BIOCL with large-size bivalve fragment, E. MKT2-FLOTS large-size of crinoid fragment which are seen as floats in a micritic matrix with undefined shells, F. MKT3 with bivalve shell fragments and undefined shell pieces.

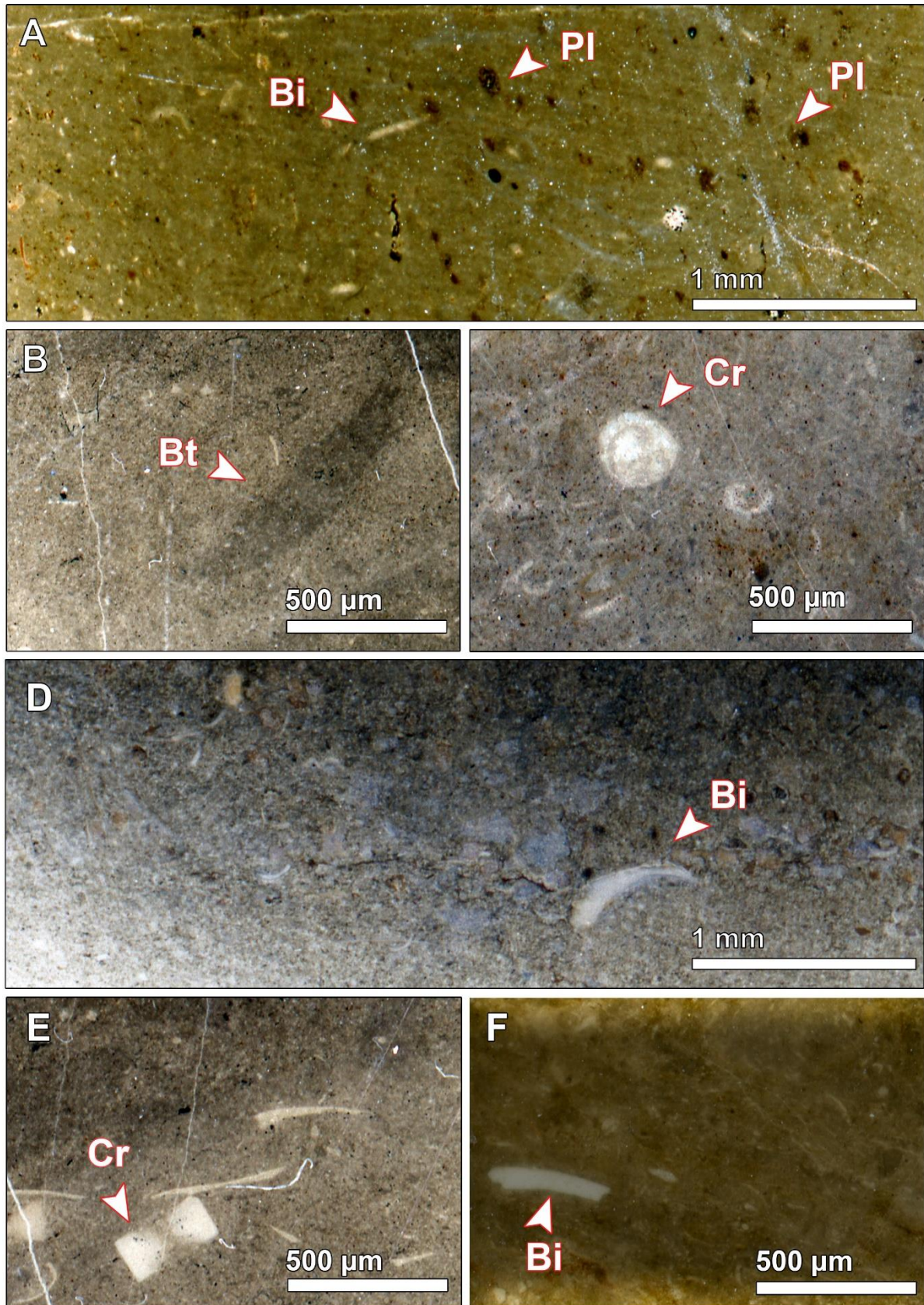


PLATE 5.6

This study

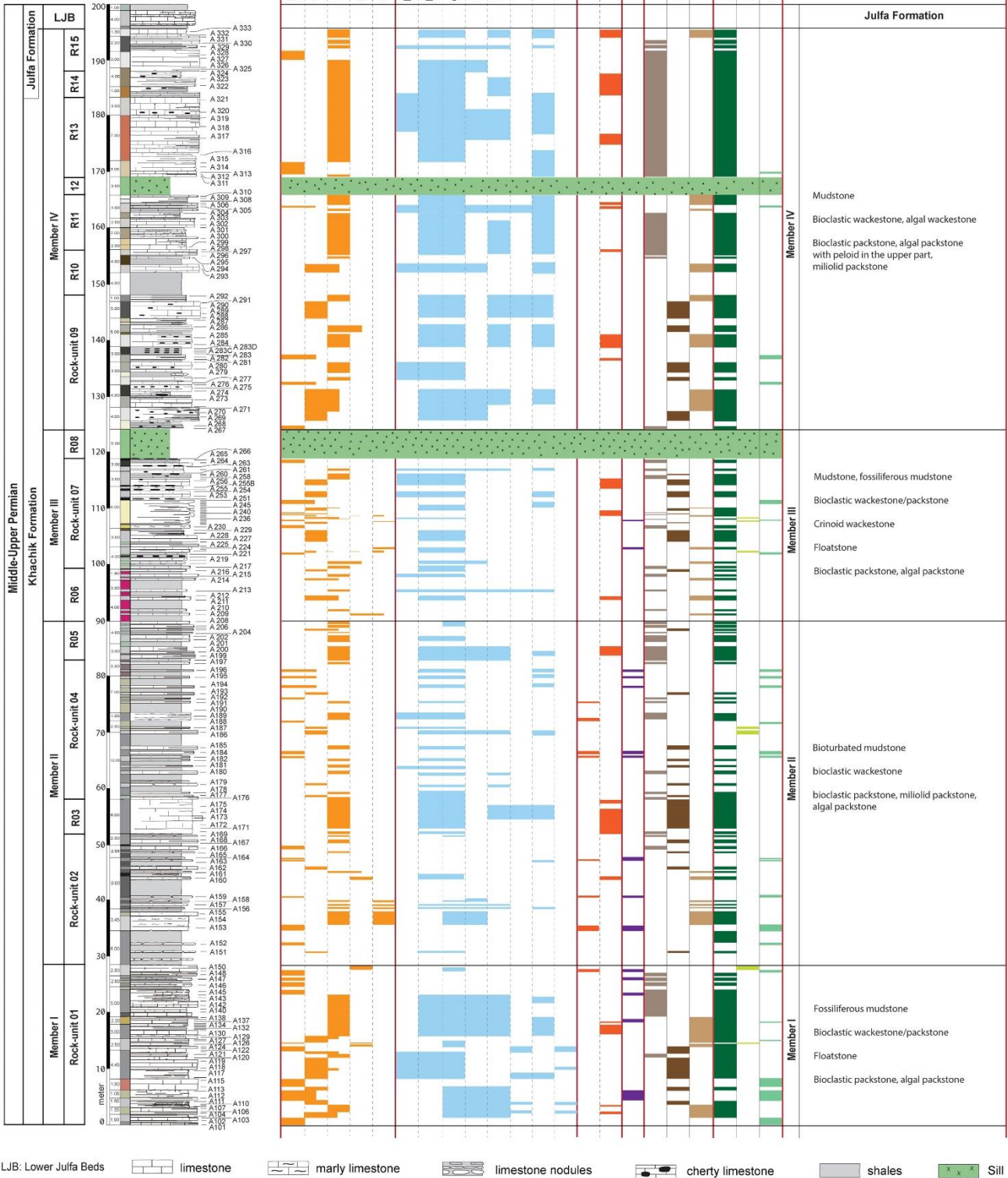


Fig. 5.6. Composite log detailing the carbonate microfacies attributes in the Khachik Formation in the Ali-Bashi section.

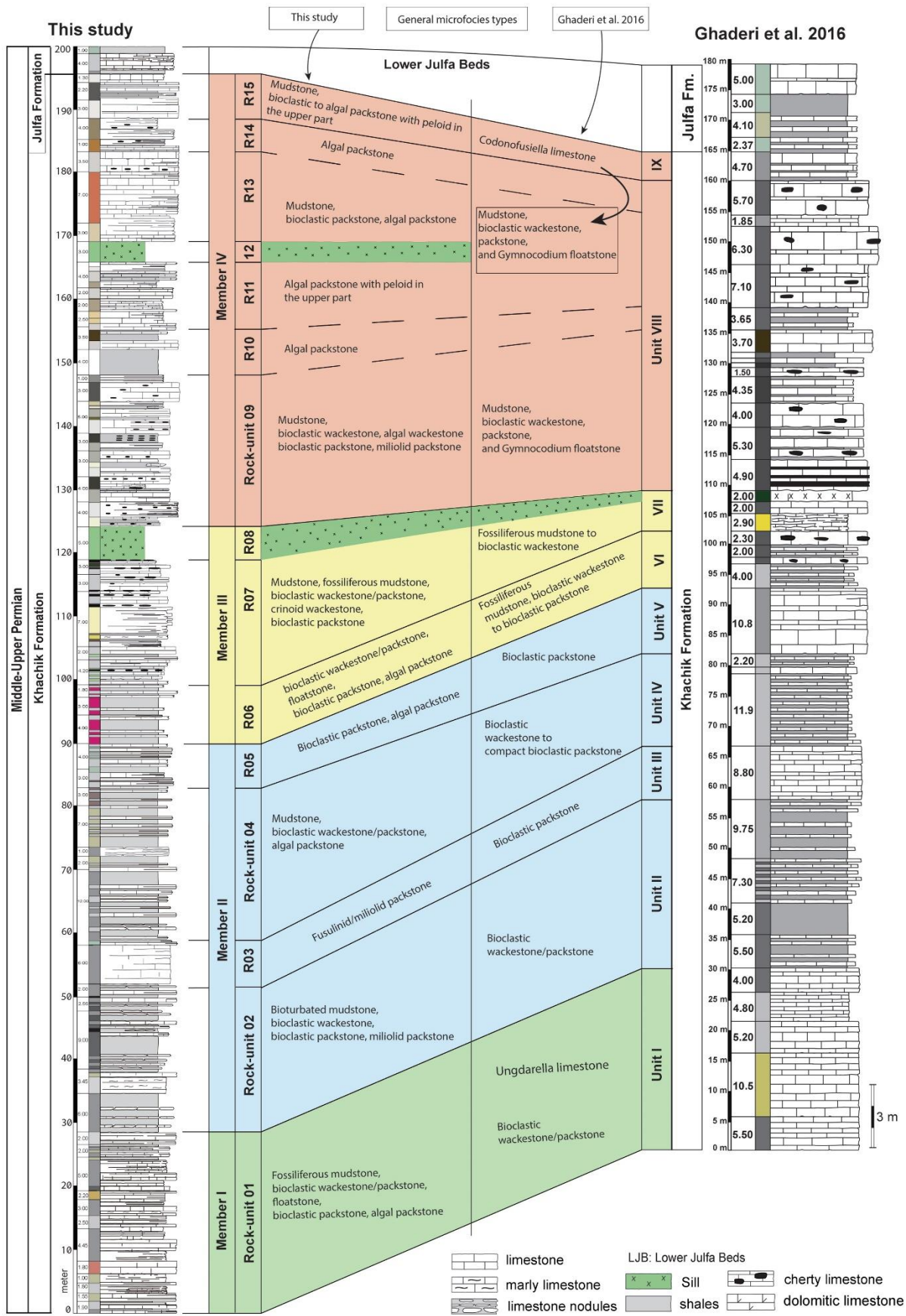


Fig. 5.7. Correlating the general microfacies characteristics of each rock unit on the stratigraphic log of this research with those identified by Ghaderi et al. (2016) in the main valley section of the Kuh-e-Ali Bashi.

5.3. DEPOSITIONAL MODEL OF KHCHIK FORMATION

Depositional models provide sedimentary system investigations, with the initial information gathered from historical local research and its amalgamation with contemporary events (Flügel, 2010). According to the analysis of microfacies and following Walter's law in 1894 (Middleton, 1973; Lopez 2014), the depositional environment of the Khachik Formation in the Ali-Bashi section in the ramp carbonate platform ranges from the initial parts of the inner ramp to the outer ramp. The position of the microfacies group assemblages, from MKL1 to MKL2, indicates a lagoonal environment, while the sedimentary microfacies from MKR2 to MKR3 exhibit characteristics of the restricted inner ramp environment.

The position of the microfacies group, MKO1 to MKO4, was restricted after the limited microfacies and developed in the inner ramp's final parts within an open marine environment. The microfacies groups, MKM1 to MKM3, were deposited after the open marine environment and in the mid-ramp zones. In contrast, MKT1 to MKT3 were deposited in the initial parts of the outer ramp, equivalent to the Toe-of-slope of the carbonate shelf setting (figs 5.6-5.7).

There was no evidence of any sedimentary deposits belonging to deltaic, coastal, or continental environments in the Khachik Formation, indicating that the deposition of the Khachik Formation sequences took place at least in a sedimentary environment away from the shoreline and the marginal basin deposits. So, it is better to attribute the sedimentation of the Khachik Formation to the offshore region and its direct connection to the open sea, where in some areas of the basin, its depth has even increased to the extent of deep-water regions. Additionally, based on the standard facies belt (FZ) presented by Wilson (1975), three FZs with the transition shallow to the deeper part were identified, including FZ8, FZ7, and FZ3, which are depicted in figure 5.8 of the reconstructed sedimentary model of the Khachik Formation in the Ali-Bashi section. In this model, each microfacies' position and expansion are introduced along with their allochems content.

Furthermore, in the analysis by Hips & Haas (2009), during the latest Permian, sediment deposition occurred in a shallow subtidal environment where normal salinity and well-oxygenated, euphotic conditions supported rich biota.

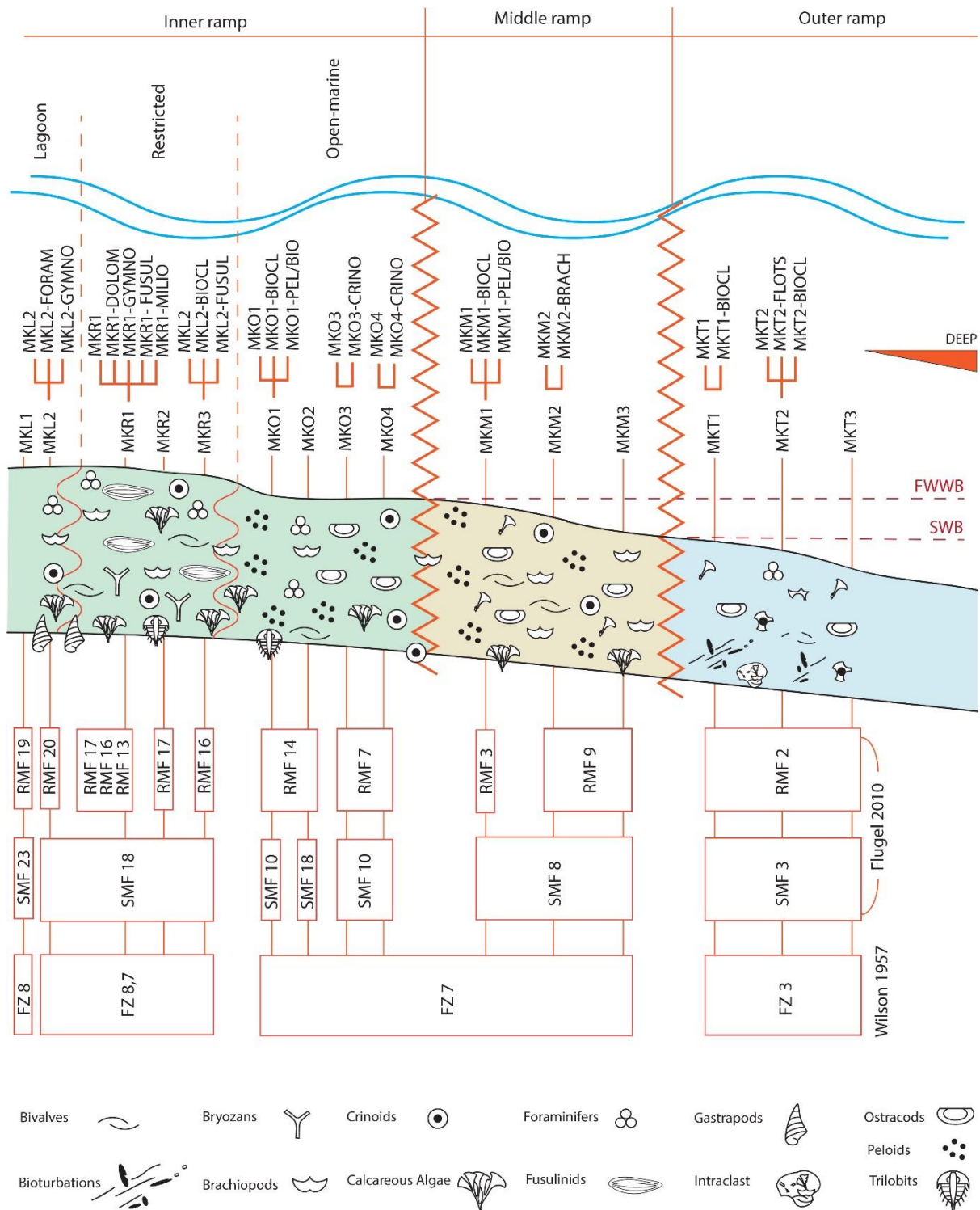


Fig. 5.8. The depositional pattern of the Khacik Formation in the Ali-Bashi section is delineated in accordance with [Flugel's \(2010\)](#) framework. Abbreviations used include FWWB for Fair-weather wave base and SWB for Storm wave base.

Changes in the sedimentary conditions were marked by abundant peloids, most likely derived from bioclasts of the topmost sediments. This character could be followed in the upper part of the Khachik Formation in the Ali-Bashi section. Based on the results of [Hips & Haas \(2009\)](#), a substantial decline in skeletal carbonate production triggered the formation of oolites. This process effectively removed carbonates from the supersaturated, warm, and turbulent shallow-marine water in the inner ramp zone, potentially accounting for the extensive spread of an oolite horizon in the periphery of the western Tethys. However, the absence of oolite formation within the sequences of the Khachik Formation in the Ali-Bashi section suggests that, at the very least, there were no pronounced indications of a significant reduction in skeletal carbonate production. The continuous deposition of carbonate sediment appears to have persisted without substantial interruption.

5.4. CONCLUSION

The comprehensive sedimentological analysis points to the deposition of the Khachik Formation strata across the entire extent of the inner to outer carbonate ramp. We recognize 15 distinct microfacies within this formation, categorized into 28 sub-microfacies. These microfacies, delimited by allochem content, are distributed across a range of environments, including the lagoon (MKL1 and MKL2 microfacies group), restricted (MKR1 microfacies group; MKR2 and MKR3 microfacies group), and open-marine settings (MKO1 microfacies group; MKO2; MKO3 microfacies group and MKO4 microfacies group). These settings covered the inner ramp zone and the MKM1 microfacies group; the MKM2 microfacies group and MKM3 were recognized for the middle ramp zone. Correspondingly, the outer ramp zone contains the MKT1 microfacies group, MKT2 microfacies group, and MKT3.

These strata revealed the presence of 10 RMF14 and 5 SMF, following the [Flügel](#) standard classification ([2010](#)). Based on Wilson's standard facies belt (FZ) framework ([1975](#)), three distinct FZs indicating a transition from terrestrial to marine conditions were identified, namely FZ8, FZ7, and FZ3. Besides, the correlation between the identified microfacies in this study and those documented by [Ghaderi et al. \(2016\)](#) demonstrates that these microfacies are identifiable and closely align with other geological sections during the same time frame.

In conclusion, notable features of the Khachik Formation in the Ali-Bashi section encompass the absence of tidal sediments, the lack of oolitic deposits, the prevalence of microfacies rich in calcareous algae, and the alternating presence of shales with thin-bedded limestones.

5.5. REFERENCES

- Abasaghi, F., Mahboubi, A., Gharaie, M.H.M. and Khanehbad, M., 2020. Occurrence of Zoophycos in the Ruteh Formation, Middle Permian (Guadalupian), Central Alborz, Iran: palaeoenvironmental and sequence stratigraphy implications. *Neues Jahrbuch für Geologie und Paläontologie-Abhandlungen*, pp.285-309.
- Afzal, J., Williams, M., Leng, M.J. and Aldridge, R.J., 2011. Dynamic response of the shallow marine benthic ecosystem to regional and pan-Tethyan environmental change at the Paleocene–Eocene boundary. *Palaeogeography, Palaeoclimatology, Palaeoecology*, 309(3-4), pp.141-160.
- Ahmad, F., Quasim, M.A. and Ahmad, A.H.M., 2021. Microfacies and diagenetic overprints in the limestones of Middle Jurassic Fort Member (Jaisalmer Formation), Western Rajasthan, India: Implications for the depositional environment, cyclicity, and reservoir quality. *Geological Journal*, 56(1), pp.130-151.
- Bachmann, M. and Hirsch, F., 2006. Lower Cretaceous carbonate platform of the eastern Levant (Galilee and the Golan Heights): stratigraphy and second-order sea-level change. *Cretaceous Research*, 27(4), pp.487-512.
- Chatalov, A.G., 2007. Physicochemical precipitation of fine-grained carbonate in seawater-an example of Triassic marine micrites from the Western Balkanides, Bulgaria. *Neues Jahrbuch für Geologie und Paläontologie-Abhandlungen*, pp.149-167.
- Dunham, R.J., 1962. Classification of carbonate rocks according to depositional textures. In: Ham, W.E. (ed.): *Classification of Carbonate Rocks – A Symposium*, 1: 108–121; Tulsa (American Association of Petroleum Geologists).
- Flügel, E. and Munnecke, A., 2010. *Microfacies of carbonate rocks: analysis, interpretation and application* (Vol. 976, p. 2004). Berlin: Springer.
- Frontalini, F. and Coccioni, R., 2011. Benthic foraminifera as bioindicators of pollution: a review of Italian research over the last three decades. *Revue de micropaléontologie*, 54(2), pp.115-127.
- Geel, T., 2000. Recognition of stratigraphic sequences in carbonate platform and slope deposits: empirical models based on microfacies analysis of Palaeogene deposits in southeastern Spain. *Palaeogeography, palaeoclimatology, palaeoecology*, 155(3-4), pp.211-238.

- Ghaderi, A., 2014. Stratigraphy and paleoecology of the Upper Permian to Permian–Triassic boundary in the northwest of Iran based on biostratigraphic data of conodonts and brachiopods. *Ferdowsi University of Mashhad, Mashhad*.
- Ghaderi, A., Taherpour Khalil Abad, M., Ashouri, A.R. and Korn, D., 2016. Permian calcareous algae from the Khachik Formation at the Ali Bashi Mountains, NW of Iran. *Arabian Journal of Geosciences*, 9, pp.1-11.
- Hips, K. and Haas, J., 2009. Facies and diagenetic evaluation of the Permian–Triassic boundary interval and basal Triassic carbonates: shallow and deep ramp sections, Hungary. *Facies*, 55, pp.421-442.
- James, N.P. and Jones, B.G., 2015. The cool-water neritic realm in. *Origin of Carbonate Rocks*, pp.135-149.
- Klovan, J.E. and Embry, A.F., 1971. Upper Devonian stratigraphy, northeastern Banks Island, NWT. *Bulletin of Canadian Petroleum Geology*, 19(4), pp.705-729.
- López, G.I., 2014. Walther's law of facies. *Encyclopedia of scientific dating methods. Springer (Dordrecht)*, pp.957-958.
- Mattern, F., 2022. A Compiled Synoptic Table of the Standard Microfacies and Facies Zone System of Flügel (2010): A Practical Tool. *Sultan Qaboos University Journal for Science [SQUJS]*, 27(1), pp.74-76.
- Michel, L., Ehlers, T.A., Glotzbach, C., Adams, B.A. and Stübner, K., 2018. Tectonic and glacial contributions to focused exhumation in the Olympic Mountains, Washington, USA. *Geology*, 46(6), pp.491-494.
- Middleton, G.V., 1973. Johannes Walther's law of the correlation of facies. *Geological Society of America Bulletin*, 84(3), pp.979-988.
- Nebelsick, J.H., Bassi, D. and Lempp, J., 2013. Tracking paleoenvironmental changes in coralline algal-dominated carbonates of the Lower Oligocene Calcareniti di Castelgomberto formation (Monti Berici, Italy). *Facies*, 59, pp.133-148.
- Oertli, H.J., 1964. The Venice System for the classification of marine waters according to salinity. *Pubblicazioni della Stazione Zoologica di Napoli*, 33, p.611.
- Read, J.F., 1985. Carbonate platform facies models. *AAPG Bulletin*, 69(1), pp.1-21.
- Riding, R. and Guo, L., 1991. Permian marine calcareous algae. In *Calcareous algae and stromatolites* (pp. 452-480). Berlin, Heidelberg: Springer Berlin Heidelberg.
- Romero, J., Caus, E. and Rosell, J., 2002. A model for the palaeoenvironmental distribution of larger foraminifera based on late Middle Eocene deposits on the margin of the South Pyrenean basin (NE Spain). *Palaeogeography, Palaeoclimatology, Palaeoecology*, 179(1-2), pp.43-56.
- Saitoh, M., Isozaki, Y., Yao, J., Ji, Z., Ueno, Y. and Yoshida, N., 2013. The appearance of an oxygen-depleted condition on the Capitanian disphotic slope/basin in South China: Middle–Upper Permian stratigraphy at Chaotian in northern Sichuan. *Global and Planetary Change*, 105, pp.180-192.

- Sarwary, M.N., Alamy, C.S., Rahimi, M.L. and Kumar, P., 2022. Interpretation of Depositional Environment of Fusulinid Bearing Middle Permian Succession of Bolula and Khaja Ghar Formation, Bamian Zone, Central Afghanistan. *International Journal of Geosciences*, 13(7), pp.499-530.
- Spanicek, J., Cosovic, V., Mrinjek, E. and Vlahovic, I., 2017. Early Eocene evolution of carbonate depositional environments recorded in the Cikola Canyon (North Dalmatian Foreland Basin, Croatia). *Geologia Croatica*, 70(1), p.11.
- Vachard, D., de Dios, A.F. and Buitrón, B., 2004. Guadalupian and Lopingian (Middle and Late Permian) deposits from Mexico and Guatemala, a review with new data. *Geobios*, 37(1), pp.99-115.
- Vecchio, E. and Hottinger, L., 2007. Agglutinated conical foraminifera from the Lower-Middle Eocene of the Trentinara Formation (southern Italy). *Facies*, 53(4), pp.509-533.
- Walther, J., 1894. Einleitung in die Geologie als historische Wissenschaft. In *Lithogenesis der Gegenwart*. Jena: G. Fischer, Bd. 3, pp. 535–1055.
- Westphal, H., Halfar, J. and Freiwald, A., 2010. Heterozoan carbonates in subtropical to tropical settings in the present and past. *International Journal of Earth Sciences*, 99, pp.153-169.
- Wilson, J.L., 1975. Principles of carbonate sedimentation. *Carbonate Facies in Geologic History*, pp.1-19.
- Wright, V.P., 1992. A revised classification of limestones. *Sedimentary geology*, 76(3-4), pp.177-185.
- Yousef, I., Morozov, V.P., Kolchugin, A.N., Sudakov, V., Idrisov, I. and Leontev, A., 2023. Microfacies analysis and depositional environment of the upper Devonian dankovo-lebedyansky sediments, Tatarstan, Volga-Ural Basin, Russia. *Petroleum Research*, 8(2), pp.244-255.
- Zadeh, P.G., Adabi, M.H. and Sadeghi, A., 2019. Microfacies, geochemistry and sequence stratigraphy of the Sarvak Formation (Mid Cretaceous) in the Kuh-e Siah and Kuh-e Mond, Fars area, southern Iran. *Journal of African Earth Sciences*, 160, p.103634.
- Zhao, J., Jin, Z., Jin, Z., Wen, X., Geng, Y., Yan, C. and Nie, H., 2017. Depositional environment of shale in Wufeng and Longmaxi Formations, Sichuan Basin. *Petroleum Research*, 2(3), pp.209-221.

CHAPTER 6

Discussion, results and topic suggestions for research

6.1. DISCUSSION.....	192
6.2. RESULTS.....	196
6.2. TOPIC SUGGESTIONS FOR RESEARCH	199

6.1. DISCUSSION

Following persistent efforts and systematic experimentation involving various extraction protocols, such as formic acids and acetic acids, aimed at retrieving conodont microfossils from the strata of the Khachik Formation in the Ali-Bashi section and the Jamal Formation in the Bagh-e-Vangh section, recognized for their significant geological research backgrounds and considered as having high potential for tracing the Guadalupian-Lopingian boundary (GLB) within the Permian strata in Iran, the outcome of this research project revealed the absence of conodont microfossils in these sections.

In light of the extensive geological investigations and the anticipated high potential of these stratigraphic sections for identifying the GLB within the middle and upper Permian sequences in Iran, it can be concluded that the pursuit of conodont specimens in these specific areas will not be fruitful. Despite the initial expectations, the absence of conodont microfossils in the Khachik Formation in the Ali-Bashi section and the Jamal Formation in the Bagh-e-Vangh section suggests that alternative approaches or locations may need to be explored in future research endeavors to achieve success in delineating the Guadalupian-Lopingian boundary within the Permian sequences of Iran.

In light of the extensive geological investigations and the anticipated high potential of these stratigraphic sections for identifying the GLB within the middle and upper Permian sequences in Iran, it can be concluded that the pursuit of conodont specimens in these specific areas will not be fruitful. Despite the initial expectations, the absence of conodont microfossils in the Khachik Formation in the Ali-Bashi section and the Jamal Formation in the Bagh-e-Vangh section suggests that alternative approaches or locations may need to be explored in future research endeavors to achieve success in delineating the Guadalupian-Lopingian boundary within the Permian sequences of Iran.

Consequently, the findings underscore the complexity of the geological history and depositional environments in these particular sections, challenging conventional expectations regarding the presence of conodont microfossils. This revelation prompts a reevaluation of the prevailing assumptions about the distribution of conodonts in Permian strata within the region. The absence of these microfossils in the targeted formations raises intriguing questions about the environmental conditions, sedimentary processes, or taphonomic factors that may have influenced the preservation or formation of conodonts in this specific

geological context. To move forward in the quest to delineate the Guadalupian-Lopingian boundary, future research efforts might consider broadening the scope of investigation to encompass adjacent formations or exploring alternative techniques for fossil extraction. Employing advanced methodologies, such as high-resolution imaging or geochemical analyses, could provide insights into subtle variations in sedimentary conditions that might have influenced the preservation of conodonts. Additionally, collaboration with experts in related fields, including paleoecology and sedimentology, could offer a holistic understanding of the paleoenvironmental dynamics and aid in refining the search strategy for conodont specimens in Permian sequences. In conclusion, while the current endeavor did not yield the expected results, it serves as a stepping stone for refining future research strategies. The pursuit of scientific understanding often involves adapting and evolving methodologies in response to unexpected outcomes, and the absence of conodont microfossils in the Khachik and Jamal formations presents an opportunity to refine hypotheses, explore alternative avenues, and deepen our understanding of the geological history of the Permian strata in Iran. Extending our exploration beyond conodonts to include other microfossils, particularly ostracods, presents an intriguing avenue for future studies. Ostracods, characterized by their widespread distribution and sensitivity to environmental changes, hold immense potential for contributing valuable insights into the paleoenvironmental dynamics of the Permian strata in Iran. Given their diverse ecological preferences and rapid evolutionary responses, ostracods can serve as sensitive indicators of subtle variations in water chemistry, temperature, and other environmental parameters.

Incorporating ostracod analysis into our research framework offers a holistic approach to deciphering the complex interplay between biotic assemblages and environmental conditions during the Guadalupian-Lopingian transition. Their fossilized remains, if present in the Khachik and Jamal formations, could provide crucial information about paleoclimate, paleosalinity, and sedimentary regimes. The absence or presence of ostracods, along with a detailed examination of their species composition and abundance, could enhance our understanding of the paleoecological context and help refine our interpretations of the depositional settings.

Moreover, a comprehensive study encompassing various microfossil groups will contribute to a more nuanced reconstruction of the Permian paleoenvironment, addressing the limitations encountered in the quest for conodonts. Collaborative efforts involving paleontologists,

stratigraphers, and micropaleontologists will be essential in designing a multidisciplinary approach that integrates diverse datasets and methodologies. This inclusive strategy not only widens the scope of our investigation but also ensures a more comprehensive and robust interpretation of the geological history in the targeted Permian sequences.

In essence, the exploration of alternative microfossil groups, with a specific focus on ostracods, promises to enrich our understanding of the paleoenvironmental complexities during the critical Guadalupian-Lopingian transition. As we navigate these uncharted research territories, embracing a diverse array of microfossils will undoubtedly contribute to the advancement of Permian stratigraphy and paleoenvironmental reconstruction in Iran.

Moreover, the absence of conodonts not only impedes the creation of accurate biostratigraphic models but also hinders the establishment of a chronological framework essential for understanding the sequence of biological events and crises that unfolded during the mid-to-late Permian in Iran. Conodonts, being reliable chronostratigraphic markers, play a pivotal role in precisely dating geological boundaries, and their scarcity in these sections complicates efforts to delineate the GLB with temporal accuracy. This limitation reverberates through subsequent studies, affecting the ability to correlate events and species turnover with precision. The absence of a well-defined GLB in the Permian sequences of Iran inhibits the establishment of a robust foundation for studying evolutionary patterns, biodiversity changes, and potential environmental factors influencing ecosystems during this critical geological interval.

To address this challenge, future research endeavors should explore alternative methodologies and collaborate across disciplines to uncover alternative stratigraphic markers or proxies that can compensate for the absence of conodonts. Additionally, a concerted effort to expand the geographical scope of investigation to include neighboring regions may provide a broader context for understanding the regional variations in fossil assemblages and environmental conditions during the mid-to-late Permian.

Acknowledging the crucial role of biostratigraphic models in pinpointing the Guadalupian-Lopingian boundary, particularly in the early stages, it is advisable to turn to alternative microfossils. Microfossils that are traditionally considered of secondary importance in biostratigraphy, such as fusulinds, can prove valuable for dating, establishing standard biozones, and precisely determining the location of this boundary. Therefore, the exploration

of additional microfossil groups becomes imperative to improve the precision of the biostratigraphic framework when studying the Permian sequences in Iran.

Although, there have been prior investigations into fusulinds microfossils and the demarcation of this boundary based on the observed range of these Permian microfossils in Iran, a notable limitation exists. Regrettably, a majority of these studies rely on tethyan biozone nomenclatures. The absence of adherence to the international standard zoning of the Permian poses a significant challenge, making the results less reliable and incompatible with broader biostratigraphic frameworks. Hence, it is imperative to undertake new research that adheres to contemporary standards, utilizing the Permian standard nomenclature system. This approach should be applied to selected stratigraphic sections, aligning with the fossil content, to ensure a more accurate and standardized assessment.

Moreover, in relation to the identified cherty layers within these stratigraphic sections, despite dedicated endeavors, conclusive results remain elusive. Unfortunately, this research refrains from proposing a specific theory regarding the nature of these layers. This observation is significant, especially given the repeated application of the siliceous microfossil extraction protocol, which, despite efforts, did not result in the retrieval of microfossil species from these particular layers. It is noteworthy to highlight that within the cherty sediments, discernible signs of sponge spines have been observed, suggesting the biological origin of these layers. Nevertheless, given the time limitations of this project, a comprehensive understanding of the origin of the cherty layers demands further investigation, particularly through geochemical analyses. It is hoped that the outcomes of such research will capture the attention of scholars in this field.

The noteworthy aspect of this project lies in the successful extraction of diverse species of ostracods. Limited studies on these species in the middle and upper Permian of Iran, along with scarce reports, indicate the potential for further exploration. With additional studies, a more comprehensive understanding of the Permian ostracods in Iran can be achieved. Moreover, among these extracted species, instances exist where the systematic characteristics for identification differ from those previously identified. This suggests the possibility of discovering new species of ostracods from the Permian of Iran through further studies.

The precise location of the Guadalupian-Lopingian boundary has consistently stirred debate within the scientific community and remains, to this day, an enigma. Despite rigorous efforts

made in this project, the paleontological placement of this boundary remained an unsolved puzzle. As I continue to unravel the mysteries of this boundary and its implications for the Permian era in Iran, my efforts promise to provide a lasting knowledge for upcoming projects.

6.2. RESULTS

The focused study on GLB issues within this project involved investigating three high-precision selected sections. To begin, the Ali-Bashi section played a pivotal role in I research, involving the meticulous collection of over 240 rock samples from a precisely measured thickness of 189 meters within the Kachik Formation. Moving on, the Bagh-e-Vang section demanded painstaking efforts, resulting in the acquisition of more than 160 rock samples from an outcrop spanning 260 meters in thickness in the Jamal Formation. Lastly, the Baghuk section presented unique challenges, hampering our progress due to adverse climatic conditions, Iran's economic crisis, and the disruptive impact of the COVID-19 pandemic. Moreover, I assessed a range of extraction techniques, encompassing CH_2O_2 , CH_3COOH , hot acetolysis, and HF protocols, in order to isolate microfossils like conodonts, ostracods, foraminifers, and radiolarians from samples gathered at both the Ali-Bashi and Bagh-e-Vang sections.

These endeavors ultimately produced the following outcomes.

- After conducting a comprehensive sampling and high-detailed lithostratigraphical investigation of the Khachik Formation in the Ali-Bashi section, led to identified 15 distinct rock units within the four main members. This discovery has the potential to stimulate the creation of a new lithostratigraphic inventory for these sequences, which can be aligned with the existing background research on the Khachik Formation in this particular section. Furthermore, in the Bagh-e-Vang section, 10 rock units from Jamal Formation strata's belonging to the three members have also been identified, and they exhibit coherence with the previously gathered data.
- Following extensive preparation and meticulous adherence to a carefully crafted protocol for conodont element identification, a comprehensive analysis was conducted on more than 240 samples sourced from the Khachik Formation in the Ali-Bashi section. Despite employing both the CH_2O_2 and CH_3COOH techniques, these endeavors proved

unsuccessful in uncovering any traces of conodonts, pivotal markers for microfossil analysis via high-performance microscopic sediment examination. Regrettably, the anticipated outcomes were not achieved. In the case of the Bagh-e-Vang section, a similar approach was taken, utilizing the diluted CH_3COOH technique to search for conodonts. Despite several months of dedicated effort and meticulous examination of over 150 sediment samples under a microscope, the definitive conclusion was reached that conodonts were indeed absent in this second section.

- In this study, I explored three alternative techniques (Hot and cold CH_3COOH ; cold CH_2O_2 acid) for extracting ostracods from over 240 samples collected from Khachik Formation at the Ali-Bashi section and 67 specimens of the ostracods were extracted from those samples. To prepare the samples, I employed a cold solution comprising 10% formic acid (CH_2O_2) and 15% acetic acid (CH_3COOH). The CH_2O_2 method proved to be highly effective, yielding well-preserved ostracods and enabling the identification of twelve distinct taxa including: *Bairdia deducta deducta* (Zalanyi, 1974), *Bairdia hungarica* Zalanyi, 1974, *Bairdia* sp., *Fabalitypris parva*, Wang 1978, *Fabalitypris* sp. 1, *Fabalitypris* sp. 2, *Fabalitypris* sp. 3, *Fabalitypris* sp. 4, *Hollinella (Hollinella) herrickana* (Girty, 1909), *Hollinella* sp., *Sargentina transita* (Kozur, 1985) and *Silenites* sp. Amongst these assemblages, *Bairdia* sp, *Hollinella (Hollinella) herrickana* (Girty, 1909), *Fabalitypris* sp. 1, *Fabalitypris* sp. 2, *Fabalitypris* sp. 3, *Fabalitypris* sp. 4, *Sargentina transita* (Kozur, 1985) and *Silenites* sp., were obtained exclusively through the diluted CH_2O_2 protocol from the hard dolomitized limestones, while the other cold CH_3COOH procedures were unsuccessful.
- The implementation of the hot acetolysis protocol yielded favourable results by extracting a substantial number of superbly preserved ostracods, resulting in the identification of various species, including: *Acratia changxingensis* (Shi, 1987); *Acratia* sp.; *Bairdia deducta deducta* (Zalanyi, 1974); *Bairdia elcapitanensis* Forel 2021; *Bairdia* cf. *fangnianqiaoi* Crasquin, 2010; *Bairdia grotei* Chitnarin, 2017 *Bairdia hungarica* Zalanyi, 1974; *Bairdia khaokanaensis* Chitnarin, 2017; *Bairdia radlerae* Kellett, 1934; *Bairdia rhomboidalis* Hamilton, 1942; *Bairdia* cf. *songthami* Chitnarin et al. 2017; *Bairdia* sp.30 sensu Chitnarin, 2009; *Bairdia* sp. 1; *Bairdia* sp. 2; *Bairdia* sp. 3; *Bairdia* sp. 4; *Bairdia* sp. 5; *Bairdia* sp. 6; *Bairdia* sp. 7; *Bairdia* sp. 8; *Bairdia* sp. 9; *Bairdia* ? sp.; *Bairdiacypris longirobusta* Chen,

1958; *Bairdiacypris* sp. 6 sensu Zazzali et al., 2015; *Bairdiacypris* sp. B sensu Tarnac et al., 2021; *Bairdiacypris* sp. 1; *Bairdiacypris* sp. 2; *Bairdiacypris* sp. 3; *Bairdiacypris* sp. 4; *Bairdiacypris* sp. 5; *Bairdiacypris* sp. 6; *Bairdiacypris* sp. 7; *Bairdiacypris* sp. 8; *Bairdiacypris* sp. 9; *Bairdiacypris* sp.; *Ceratobairdia sexagintaduella* Forel, 2021; *Ceratobairdia?* cf. *crenata* Chen, 1982; *Fabalitypris acetalata* (Coryell & Billings, 1932); *Fabalitypris glennensis* (Harlton, 1927); *Fabalitypris parva* Wang, 1978; *Fabalitypris reniformis* (Chen, 1958) sensu Wang, 1978; *Fabalitypris* sp. 5; *Fabalitypris* sp. 6; *Fabalitypris* sp. 7; *Hollinella* (*Hollinella*) *martensiformis* Crasquin et al., 2010 ; *Hollinella* sp. ; *Indivisia* sp. 1 sensu Forel et al. 2015; *Kempfina qinglaili* (Crasquin, 2008); *Kempfina* sp. 1 ; *Liuzhinia julfensis* Gliwa, 2021; *Praezabythocypris pulchra* Kozur, 1985; *Praezabythocypris* sp. 1; *Pseudacanthoscapha striatula* (Shi, 1982); *Reviya* sp. ; *Sargentina minuta* Wang, 1978; *Sargentina* sp.; and *Sulcella sulcata* Coryell & Sample, 1932. Meanwhile, certain species within the Bairdia, Bairdiacypris, and Fabalitypris genera show potential for the discovery of new species through additional research. Additionally, the effective identification of numerous ostracod's species in Middle and Upper Permian sequences underscores the considerable opportunities for investigating this Fossil-Group in Iran.

- Despite my steadfast dedication and meticulous devotion to the prescribed protocol, my attempt to utilize the HF technique in the processing of 12 cherty samples collected from both the Ali-Bashi and Bagh-e-Vang sections yielded a discouraging result. Regrettably, no discernible radiolarian specimens were found within the sediment of either sample set.
- Furthermore, a thorough analysis (involving at least five randomly selected fields) of the microfacies in thin sections obtained from the Khachik Formation's carbonate rocks at the Ali-Bashi section has revealed 28 sub-microfacies. These sub-microfacies, derived from the classification system established by Embry & Klovan (1971) and documented in Flugel (2010)'s ramp zones, have been correlated with 15 distinct microfacies. The assemblage of microfacies groups, ranging from MKL1 to MKL2, indicates a lagoonal environment, while the sedimentary microfacies from MKR2 to MKR3 exhibit features characteristic of a restricted inner ramp setting. The placement of microfacies groups, MKO1 to MKO4, suggests a confined setting subsequent to the limited microfacies development, occurring within the final segments of the inner ramp under an open marine environment.

Microfacies groups MKM1 to MKM3 are inferred to have been deposited after the open marine environment, within the mid-ramp zones, whereas MKT1 to MKT3 were identified in the initial segments of the outer ramp, corresponding to the Toe-of-slope position within the carbonate shelf setting. Additionally, adhering to the standard microfacies designated by [Flügel \(2010\)](#), the study proposes 10 microfacies of the RMF type, along with their corresponding 4 SMFs for the studied strata. According to the evaluation of the collected information from the identified microfacies, the depositional environment of the Khachik Formation in the Ali-Bashi section in the ramp carbonate platform ranges from the initial parts of inner ramp to the outer ramp. Furthermore, there was no evidence of any sedimentary deposits belonging to deltaic, coastal, or continental environments in the Khachik Formation, indicating that the deposition of the Khachik Formation sequences took place at least in a sedimentary environment away from the shoreline and the marginal basin deposits. Moreover, based on the standard facies zones (FZ) introduced by [Wilson \(1975\)](#), three FZs exhibiting a shallowing-upward trend, namely FZ8, FZ7, and FZ3, have been successfully delineated.

6.3. TOPIC SUGGESTIONS FOR RESEARCH

By delving into the findings and results obtained from the research in this study, the opportune moment has now arrived for the author of this doctoral thesis to propose suggestions based on the knowledge and discoveries gained along this path. These suggestions can serve as solutions to address the existing challenges in the field of Permian geology in Iran and contribute to formulating a novel perspective on the boundaries between the Middle and Late Permian. These proposals, derived from the precise outcomes of this research, can be pursued in the following areas and introduced as topics for future research.

- 1. Ongoing endeavors to procure additional ostracod specimens from alternative Permian sections identified as potential candidates.**
- 2. Developing a meticulously detailed biostratigraphic model based on the composition of benthic foraminifers.**
- 3. Investigating the absence of conodonts in these sections through the lens of paleoenvironmental perspectives to uncover plausible explanations.**

These proposals, grounded in the exact findings of this research, can be further explored and expanded upon in various domains. Firstly, an in-depth investigation into the geological formations specific to the Permian period in Iran can provide valuable insights. Additionally, a comprehensive analysis of the environmental factors influencing these formations would enhance our understanding of the geological processes at play. Moreover, the suggested solutions can be extended to include collaborative studies with interdisciplinary fields such as paleontology, climatology, and tectonics. By integrating knowledge from these diverse areas, a more holistic comprehension of Permian geology in Iran can be achieved, facilitating a nuanced approach to addressing the identified challenges. Furthermore, the proposed perspectives on the Middle and Upper Permian boundaries could be validated through advanced geological mapping and stratigraphic analysis. Employing cutting-edge technologies and methodologies in these endeavors may lead to more accurate delineations of these boundaries, refining our comprehension of the geological history in the region. In conclusion, the recommendations stemming from this research not only offer solutions to current geological challenges but also pave the way for future investigations. Through targeted studies and interdisciplinary collaborations, the scientific community can gain a deeper understanding of Permian geology in Iran, contributing to the broader knowledge of Earth's geological evolution.

APPENDIX: ALPHABETICAL SPECIES INDEX
IDENTIFIED SPECIES IN THIS THESIS

A

<i>Acratia changxingensis</i> (Shi, 1987)	98
<i>Acratia</i> sp.	99

B

<i>Bairdia deducta deducta</i> (Zalanyi, 1974)	99
<i>Bairdia elcapitanensis</i> Forel, 2021	100
<i>Bairdia</i> cf. <i>fangnianqiao</i> Crasquin, 2010.....	100
<i>Bairdia</i> cf. <i>grotei</i> Chitnarin, 2017	101
<i>Bairdia hungarica</i> Zalanyi, 1974	101
<i>Bairdia khaokanaensis</i> Chitnarin, 2017	102
<i>Bairdia radlerae</i> Kellett, 1934	102
<i>Bairdia rhomboidalis</i> Hamilton, 1942	103
<i>Bairdia</i> cf. <i>songthami</i> Chitnarin, 2017	103
<i>Bairdia</i> sp.30 <i>sensu</i> Chitnarin, 2009	104
<i>Bairdia</i> sp. 1.....	104
<i>Bairdia</i> sp. 2	105
<i>Bairdia</i> sp. 3	105
<i>Bairdia</i> sp. 4	105
<i>Bairdia</i> sp. 5	106
<i>Bairdia</i> sp. 6	106
<i>Bairdia</i> sp. 7	106
<i>Bairdia</i> sp. 8	107
<i>Bairdia</i> sp. 9	107
<i>Bairdia?</i> sp.	107
<i>Bairdia</i> sp.	108
<i>Bairdiacypris longirobusta</i> Chen, 1958	108
<i>Bairdiacypris</i> sp. 6 <i>sensu</i> Zazzali et al., 2015	109
<i>Bairdiacypris</i> sp. B <i>sensu</i> Tarnac et al., 2021	109

<i>Bairdiacypris</i> sp. 1	110
<i>Bairdiacypris</i> sp. 2	110
<i>Bairdiacypris</i> sp. 3	110
<i>Bairdiacypris</i> sp. 4	111
<i>Bairdiacypris</i> sp. 5	111
<i>Bairdiacypris</i> sp. 6	111
<i>Bairdiacypris</i> sp. 7	112
<i>Bairdiacypris</i> sp. 8	112
<i>Bairdiacypris</i> sp. 9	112
<i>Bairdiacypris</i> sp.	113

C

<i>Ceratobairdia sexagintaduella</i> Forel, 2021.....	113
<i>Ceratobairdia?</i> cf. <i>crenata</i> Chen, 1982	113

F

<i>Fabalitypris acetalata</i> (Coryell & Billings, 1932)	114
<i>Fabalitypris glennensis</i> (Harlton, 1927).....	114
<i>Fabalitypris parva</i> Wang, 1978.....	115
<i>Fabalitypris reniformis</i> (Chen, 1958) sensu Wang, 1978.....	116
<i>Fabalitypris</i> sp. 1.....	117
<i>Fabalitypris</i> sp. 2.....	117
<i>Fabalitypris</i> sp. 3.....	108
<i>Fabalitypris</i> sp. 4.....	117
<i>Fabalitypris</i> sp. 5.....	118
<i>Fabalitypris</i> sp. 6.....	118
<i>Fabalitypris</i> sp. 7.....	119

H

<i>Hollinella</i> (<i>Hollinella</i>) <i>herrickana</i> (Girty, 1909)	124
---	-----

Hollinella (Hollinella) martensiformis Crasquin, 2010 125

Hollinella sp. 126

I

Indivisia sp. 1 *sensu* Forel et al., 2015..... 126

K

Kempfina qinglaili (Crasquin, 2008)..... 119

Kempfina sp. 1..... 119

L

Liuzhinia julfensis Gliwa et al., 2021 120

M

Microcheilinella sp. F *sensu* Chitnarin et al. 2017..... 120

P

Praezabythocypris pulchra Kozur, 1985..... 121

Praezabythocypris sp. 122

Pseudacanthoscapha striatula (Shi, 1982)..... 122

R

Reviya sp. 127

S

Sargentina minuta Wang, 1978 123

Sargentina sp. 118

*Sargentina transit*a (Kozur, 1985)..... 123

Silenites sp..... 120

Sulcella sulcata Coryell & Sample, 1932 128

Soheil HEMMATI

Docteur en cotutelle à Sorbonne Université
et Ferdowsi Université de Mashhad

Centre de Recherche en Paléontologie - Paris

Campus Pierre & Marie Curie

4 place Jussieu

Tour 46-56, 5ème étage

75005 Paris

France

soheil.hemmati@sorbonne-universite.fr

Soheilhemmati@gmail.com

Research Ethics Oath

"In the presence of my peers"

With the completion of my doctorate in «Geology», in my quest for knowledge, I have carried out demanding research, demonstrated intellectual rigor, ethical reflection, and respect for the principles of research integrity. As I pursue my professional career, whatever my chosen field, I pledge, to the greatest of my ability, to continue to maintain integrity in my relationship to knowledge, in my methods and in my results."

Serment d'éthique de la recherche

"En Présence De Mes Pairs"

Parvenu à l'issue de mon doctorat en «Géologie», et ayant ainsi pratiqué, dans ma quête du savoir, l'exercice d'une recherche scientifique exigeante, en cultivant la rigueur intellectuelle, la réflexivité éthique et dans le respect des principes de l'intégrité scientifique, je m'engage, pour ce qui dépendra de moi, dans la suite de ma carrière professionnelle quel qu'en soit le secteur ou le domaine d'activité, à maintenir une conduite intègre dans mon rapport au savoir, mes méthodes et mes résultats."

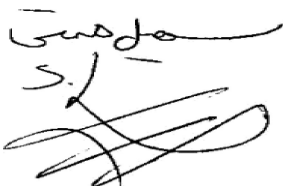
سوگندنامه اخلاق پژوهشی

"در حضور همتایانم"

با اخذ دکتری در رشته «زمین‌شناسی»، در تلاش برای افزایش دانش، تحقیقات پرچالشی را انجام داده‌ام. اصرار فکری، تفکر اخلاقی و احترام به اصول اخلاقی تحقیقات را در این مسیر ارائه داده‌ام. در پی پیشرفت حرفه‌ای خود، در هر زمینه‌ای که انتخاب کنم، به بهترین توانم تعهد می‌کنم که انصاف در ارتباط با دانش، روش‌هایم و نتایجم را حفظ کنم.

Soheil HEMMATI

10/01/2024



In numerous languages, dreams bear different appellations:

In Persian, call it 'رویا' (Royā).

The French refer to it as 'Rêve.'

Azerbaijanis say 'Yuxu.'

Turks say 'Rüya.'

Arabs call it 'حلم' (Hulm).

But the best definition comes from Paulo Coelho, who says: 'A **personal legend**.'

"This thesis is dedicated to those whose nickname is the pursuer of **personal legends."**

END.